

**DEUTSCHES ELEKTRONEN-SYNCHROTRON**  
in der HELMHOLTZ-GEMEINSCHAFT

DESY 06-037

April 2006

**Statistical Optics approach to the design of  
beamlines for Synchrotron Radiation**

Gianluca Geloni, Evgeni Saldin, Evgeni Schneidmiller and  
Mikhail Yurkov

*Deutsches Elektronen-Synchrotron DESY, Hamburg*

ISSN 0418-9833

**NOTKESTRASSE 85 - 22607 HAMBURG**

# Statistical Optics approach to the design of beamlines for Synchrotron Radiation

Gianluca Geloni <sup>a</sup> Evgeni Saldin <sup>a</sup> Evgeni Schneidmiller <sup>a</sup>  
Mikhail Yurkov <sup>a</sup>

<sup>a</sup>*Deutsches Elektronen-Synchrotron (DESY), Hamburg, Germany*

---

## Abstract

In this paper we analyze the image formation problem for undulator radiation through an optical system, accounting for the influence of the electron beam emittance. On the one hand, image formation with Synchrotron Radiation is governed by the laws of Statistical Optics. On the other hand, the widely used Gaussian-Shell model cannot be applied to describe the coherence properties of X-ray beams from third generation Synchrotron Radiation sources. As a result, a more rigorous analysis of coherence properties is required. We propose a technique to explicitly calculate the cross-spectral density of an undulator source, that we subsequently propagate through an optical imaging system. At first we focus on the case of an ideal lens with a non-limiting pupil aperture. Our theory, which makes consistent use of dimensionless analysis, also allows treatment and physical understanding of many asymptotes of the parameter space, together with their applicability region. Particular emphasis is given to the asymptotic situation when the horizontal emittance is much larger than the radiation wavelength, which is relevant for third generation Synchrotron Radiation sources. First principle calculations of undulator radiation characteristics (i.e. ten-dimensional integrals) are then reduced to one-dimensional convolutions of analytical functions with universal functions specific for undulator radiation sources. We also consider the imaging problem for a non-ideal lens in presence of aberrations and a limiting pupil aperture, which increases the dimension of the convolution from one to three. In particular we give emphasis to cases when the intensity at the observation plane can be presented as a convolution of an impulse response function and the intensity from an ideal lens. Our results may be used in practical cases as well as in benchmarks for numerical methods.

### *Key words:*

X-ray beams, Undulator radiation, Transverse coherence, Image formation, Emittance effects

*PACS:* 41.60.m, 41.60.Ap, 41.50 + h, 42.50.Ar

---

## Contents

1	Introduction	6
2	Elements and definitions of image formation theory	13
2.1	Wave propagation in free space	13
2.2	Image formation with coherent light	17
2.2.1	Large non-limiting aperture	20
2.2.2	Effect of aperture size	22
2.3	Propagation of partially coherent light in free space	25
2.4	Image formation with partially coherent light	28
2.4.1	Large non-limiting aperture	29
2.4.2	Effect of aperture size	30
3	Image formation with a perfectly coherent undulator source	32
3.1	Large non-limiting aperture	38
3.2	Effect of aperture size	43
4	Image formation with partially coherent undulator source	46
4.1	Coherence properties of undulator source in the presence of electron beam emittance	46
4.2	Large non-limiting aperture	53
4.3	Effect of aperture size	54
5	Imaging of quasi-homogeneous Gaussian undulator sources by a lens with large non-limiting aperture	56
5.1	Evolution of the cross-spectral density function in free space	56
5.2	Evolution of the cross-spectral density function behind the lens	60
6	Imaging of quasi-homogeneous non-Gaussian undulator sources by a lens with large non-limiting aperture	63
6.1	Source with non-Gaussian angular distribution in the vertical direction	64

6.2	Source with non-Gaussian intensity distribution in the vertical direction	67
7	Analysis of the image formation mechanism for quasi-homogeneous undulator sources in terms of Geometrical Optics	73
8	Imaging of quasi-homogeneous undulator sources: effect of aperture size	86
8.1	Quasi-homogeneous Gaussian undulator sources	86
8.2	Quasi-homogeneous non-Gaussian undulator sources	96
8.2.1	Source with non-Gaussian angular distribution in the vertical direction	96
8.2.2	Source with non-Gaussian intensity distribution in the vertical direction	98
9	Aberrations and imaging of quasi-homogeneous sources	100
9.1	Aberrations and the effect of aperture size	101
9.2	Severe aberrations	108
9.2.1	Physical Optics prediction of the line spread function	108
9.2.2	Physical Optics and Geometrical Optics	111
9.2.3	Geometrical Optics prediction of the line spread function	115
10	Pinhole optics	119
11	Imaging in the focal plane	135
12	A unified theory of incoherent imaging by a single lens	140
13	Depth of focus	142
13.1	Large non-limiting aperture	144
13.1.1	Far zone	145
13.1.2	Near zone	146
13.2	Effect of aperture size	147
14	Solutions to the image formation problem for non-homogeneous undulator sources	149

14.1	Horizontally quasi-homogenous and vertically non-homogeneous source	150
14.1.1	Large non-limiting aperture	150
14.1.2	Effect of aperture size	156
14.2	Horizontally non-homogeneous and vertically diffraction limited source	159
14.3	General imaging considerations	161
15	Supplementary remarks on quasi-homogeneous undulator source asymptotes	164
16	Conclusions	169

## 1 Introduction

The majority of experiments based on the use of X-rays are carried out at Synchrotron Radiation facilities, as very high brilliance is achievable by means of undulator devices installed in storage rings. Guiding the photons from the exit of an undulator to the specimen position requires the development of optical beamlines whose main task is to re-image the undulator source to any plane of interest. To deal with the image formation problem, one should account for the fact that Synchrotron Radiation constitutes a random stochastic process. In fact, the shot noise in the electron beam causes fluctuations of the electron beam current density. These fluctuations are random both in space and time. As a result, the radiation field produced by the electron beam can be described in terms of a phasor with random amplitudes and phases and, in all generality, the laws of Statistical Optics must be applied to solve the image formation problem. In this paper we study the image formation problem with undulator radiation beams based on Statistical Optics. In this framework, the basic quantity characterizing Synchrotron Radiation sources is the second order correlation function of the fields at two observation points on a given transverse plane identified by the coordinate  $z_o$  along the optical beamline. Once such a plane is fixed, the two points,  $P_1$  and  $P_2$ , are fully characterized by their transverse coordinates  $\vec{r}_{\perp 1}$  and  $\vec{r}_{\perp 2}$  respectively. Our presentation will be given in the frequency domain. Due to the limited temporal resolution of detectors in Synchrotron Radiation experiments, the analysis in frequency domain is much more natural than that in the time domain. As a consequence of this choice, and without restrictive assumptions on the system, we study the spatial correlation between Fourier transforms of the electric field <sup>1</sup> at a fixed frequency  $\omega$ , that is the cross-spectral density

$$G = \left\langle \bar{E}(z_o, \vec{r}_{\perp 1}, \omega) \bar{E}^*(z_o, \vec{r}_{\perp 2}, \omega) \right\rangle . \quad (1)$$

In Eq. (1)  $\bar{E}$  is the complex amplitude of the Fourier transform of a given Cartesian component of the electric field at the space-frequency point  $(z_o, \vec{r}_{\perp}, \omega)$ , the asterisk denotes complex conjugation, and brackets  $\langle \dots \rangle$  indicate an ensemble average over electron bunches. Since we study an ultra-relativistic system, the paraxial approximation can always be enforced so that, here, the electric field is understood to obey the paraxial wave equation [1]. The cross-spectral density carries all information about the transverse characteristics of undulator radiation. A fully general study of the cross-spectral density is not a trivial one. Difficulties arise when one tries to include simultaneously the effect of intrinsic divergence of the radiation, due to the presence of the undulator, of

---

<sup>1</sup> Since our analysis deals with the electric field in frequency domain, we will sometimes refer to the "Fourier transform of the electric field" simply as "the field", when this does not generate confusion.

the electron beam size and of the electron beam divergence. In [2] a technique was described, based on Statistical Optics, to calculate the cross-spectral density from undulator sources in the most general case <sup>2</sup>, at any position after the undulator but still without optical elements (i.e. in free space). Although self-contained, the present study relies on that work. Expressions from [2] will be taken as a starting point to proceed along the optical beamline towards the specimen position.

In general, as we will see, undulator radiation can be thought as originating from an equivalent source localized on a transverse plane at a given longitudinal position. By definition, such source has the following property: it produces a field which coincides with that from the undulator at any distance from the exit of the undulator. In particular, we localize the equivalent source in the center of the undulator, that will be conventionally taken as the beamline origin  $z = 0$ . Since in this case the equivalent source does not reproduce the real electromagnetic field distribution in the center of the undulator, we refer to it as *virtual source*. Further on, throughout this paper we assume that the beta functions of the electron beam have their minimal value in the center of the undulator. By this, as we will see, the virtual source exhibits particular properties which simplify our treatment. Once the concept of virtual source is introduced, the problem of describing radiation characteristics at a certain observation plane after a given optical element is twofold. First, one has to characterize the cross-spectral density at the virtual source and, second, one has to propagate the cross-spectral density along the optical beamline to the observation plane.

Let us first consider the problem of characterizing the source. An important simplified model which admits an analytical description without loss of essential information about the source features is obtained by letting both horizontal and vertical electron beam emittances be much larger than the radiation wavelength ( $\epsilon_{x,y} \gg \lambda/(2\pi)$ ). This is a good assumption for second generation Synchrotron Radiation sources. The kind of virtual source obtained for  $\epsilon_{x,y} \gg \lambda/(2\pi)$  belongs to the wider class of quasi-homogeneous ones. These are characterized by the fact that the cross-spectral density at the virtual source plane (i.e. at  $z = 0$ ) can be written as:

$$G(\vec{r}_{\perp 1}, \vec{r}_{\perp 2}, \omega) = I(\vec{r}_{\perp 1}, \omega) g(\vec{r}_{\perp 2} - \vec{r}_{\perp 1}, \omega) , \quad (2)$$

where

$$I(\vec{r}_{\perp 1}, \omega) = \langle |E(\vec{r}_{\perp 1}, \omega)|^2 \rangle \quad (3)$$

---

<sup>2</sup> With the point of view of the source parameters.

is the field intensity distribution and  $g(\vec{r}_{\perp 2} - \vec{r}_{\perp 1}, \omega)$  is the spectral degree of coherence (normalized, by definition, so that  $g(0, \omega) = 1$ ). The definition of quasi-homogeneity amounts to a factorization of the cross-spectral density as the product of the field intensity distribution and the spectral degree of coherence, which contains information about the spatial correlation. A set of necessary and sufficient conditions for such factorization to be possible follows: (a) the radiation intensity at the virtual source varies very slowly with the position across the source on the scale of the field correlation length and (b) the spectral degree of coherence depends on the positions across the source only through the difference  $\vec{r}_{\perp 2} - \vec{r}_{\perp 1}$ .

There are situations when the Statistical Optics description is not the only one possible. The asymptotic limit for large electron beam emittances ( $\epsilon_{x,y} \gg \lambda/(2\pi)$ ) is one of these. In this limit, the Statistical Optics description of the source coincides with the Geometrical Optics (or Hamiltonian) description of the source, where a photon-beam phase space is defined and can be described in terms of rays specified by position-angle coordinates. In the Geometrical Optics approach, based on the uncertainty principle, only the radiation originating by a photon-beam phase space area of order  $[\lambda/(2\pi)]^2$  is spatially coherent. When the emittance is much larger than the wavelength,  $2\pi\epsilon_{x,y}/\lambda \gg 1$ , the divergence of the electron beam is much larger than the diffraction angle of undulator radiation, and the transverse size of the electron beam is much larger than the diffraction size of undulator radiation. As a result one can completely neglect diffraction effects, and the Geometrical Optics approach can always be applied. Since Geometrical Optics describes a limiting situation of Statistical Optics there must be a relation between the fundamental Geometrical Optics quantity, the phase space distribution, and the fundamental Statistical Optics quantity, the cross-spectral density. It can be shown [3] that the radiant intensity of the field generated in free space by a quasi-homogeneous source in the direction of a unit vector  $\vec{s}$  can be expressed as

$$\mathcal{I}(\vec{s}, \omega) \propto \Gamma(\vec{s}, \omega) , \quad (4)$$

$\Gamma(\vec{s}, \omega)$  being the two-dimensional spatial Fourier transform of the degree of transverse coherence  $g(\vec{r}_{\perp 2} - \vec{r}_{\perp 1}, \omega)$ :

$$\Gamma(\vec{s}, \omega) = \int g(\vec{\rho}', \omega) \exp \left[ \frac{i\omega}{c} \vec{s} \cdot \vec{\rho}' \right] d\vec{\rho}' . \quad (5)$$

The expression for the phase space distribution is given by the product of the intensity distribution of the source and the radiant intensity

$$\Phi(\vec{s}, \vec{r}_{\perp}) = I(\vec{r}_{\perp}, \omega) \mathcal{I}(\vec{s}, \omega) \propto I(\vec{r}_{\perp}, \omega) \Gamma(\vec{s}, \omega) , \quad (6)$$

where the variables  $(\vec{r}_\perp, \vec{s})$  characterize a ray in phase space. A comparison between Eq. (6) and Eq. (2) shows that cross-spectral density and phase space distribution contain the same information in the limiting case  $\epsilon_{x,y} \gg \lambda/(2\pi)$ .

In other words, if a source has a large angular divergence (compared with the diffraction angle) and a large transverse size (compared with the diffraction size), one can completely neglect diffraction effects and treat the problem of the characterization of the source by means of Geometrical Optics<sup>3</sup>.

Despite the previous discussion, the possibilities of using Geometrical Optics to describe undulator sources are quite limited in many realistic situations. Applications of Synchrotron Radiation make use of a very wide range of wavelengths which span over four order of magnitude, from 0.1Å to 10<sup>3</sup>Å. For third generation light sources, either planned or in operation, the horizontal electron beam emittance  $\epsilon_x = \sigma_x \sigma_{x'}$  is of order of 1 ÷ 3 nm. The vertical emittance is given by  $\epsilon_y = \sigma_y \sigma_{y'} = \chi \epsilon_x$ ,  $\chi$  being the so called coupling factor. Typical values of  $\chi$  for third generation light sources are of order  $\chi \sim 0.01$ , corresponding to vertical emittances of order 0.1 ÷ 0.3Å. These values are always near or within the diffraction limit for wavelength ranges up to the hard X-rays in the vertical direction, and Geometrical Optics descriptions fail. In particular, in the VUV wavelength range, both vertical and horizontal emittances are much smaller than the radiation wavelength ( $\epsilon_{x,y} \ll \lambda/(2\pi)$ ). One recovers, then, the perfectly coherent situation when the source is diffraction limited in both horizontal and vertical directions. This is another situation when the Statistical Optics description is not the only one possible. In this case, deterministic Wave Optics may be used as well. As the wavelength becomes shorter, in the soft X-ray range, one obtains  $\epsilon_y \ll \lambda/(2\pi)$ , but  $\epsilon_x \gg \lambda/(2\pi)$ . At wavelengths of about 1Å the vertical emittance reaches the same order of magnitude of the wavelength  $\epsilon_y \sim \lambda/(2\pi)$ , while  $\epsilon_x \gg \lambda/(2\pi)$ . Finally, in the hard X-ray region, at a wavelength of about 0.1Å, both emittances are much larger than

---

<sup>3</sup> Condition  $2\pi\epsilon_{x,y}/\lambda \gg 1$  is sufficient, but not necessary. In general, we cannot say that Geometrical Optics is never applicable for electron beam emittances smaller than the radiation wavelength  $\lambda$ . We will treat this subject in a more extensive fashion in Section 7. There we will see that there are situations when Geometrical Optics can be applied to describe the (virtual) source even when the electron beam emittance is smaller than  $\lambda$ . We will find that a sufficient (less restrictive, but still not necessary) condition for the applicability of Geometrical Optics to the description of a given undulator source is that such source can be characterized in terms of a quasi-homogeneous virtual source. Moreover, as it will also be discussed in Section 7, our comparison of the emittance with the radiation wavelength is done under the assumption that the electron beam beta function is comparable with the radiation formation length at wavelength  $\lambda$ . This is often, but not always, the case for undulator sources, since the radiation formation length is the undulator length, which is at least a few meters. However, it is not the case for bending magnet radiation.

the wavelength ( $\epsilon_{x,y} \gg \lambda/(2\pi)$ ), and Geometrical Optics can be used alongside Statistical Optics. It follows that, for third generation light sources, only the limiting cases for wavelengths around 100 nm and 0.1Å can be treated, respectively, by means of Wave Optics or Geometrical Optics. The intermediate situation can be treated in a rigorous way only with the help of Statistical Optics, which includes both Wave Optics and Geometrical Optics as asymptotic cases.

Strictly related to the problem of source characterization, but separate from it, is the issue of propagating the photon beam through the optical beamline to the observation plane. In the case of quasi-homogeneous virtual sources, if diffraction effects from the optical elements can be neglected, Geometrical Optics can be taken advantage of. The virtual source can be described in terms of phase space distribution, and interactions with optical media can be conveniently modelled in terms of symplectic transformations, very much like electron beams in storage rings optics. Several computer codes (e.g. SHADOW [4]), usually referred to as ray-tracing codes, have been developed and are standard tools used to carry out Geometrical Optics-based calculations. However, this approach is not always possible as the virtual source may not be quasi-homogeneous or diffraction effects may not be neglected in the optical beamline. A rigorous analysis of the object-image coherence relationship is of fundamental importance in the context of several coherence-based techniques like fluctuation correlation dynamics, phase imaging, coherent X-ray diffraction and X-ray holography, whose development has been fostered by the high flux of coherent X-rays provided by state-of-the-art third generation facilities. It should be noted that, in the case of partially coherent wavefronts, even the calculation of the intensity distribution at the specimen position should involve Statistical Optics techniques. In fact, to obtain the intensity at the specimen position as some optical element is present one first needs to track the cross-spectral density through the beamline i.e. one needs to study the evolution of the partially coherent wavefront.

Computer codes have been written [5] in order to deal with beamline design in the case of partially coherent radiation. These are devoted to the solution of the image formation problem starting from first principles. Results may in fact be obtained using numerical techniques alone, starting from the Lienard-Wiechert expressions for the electromagnetic field and applying the definition of the field correlation function without any analytical manipulation. Yet, a first-principle calculation of the field correlation function between two generic points or, in particular, calculation of the intensity at a single point involves very complicated and time-expensive numerical evaluations. To be specific, one needs to perform two integrations along the undulator device and four integrations over the electron-beam phase space distribution to solve the problem in free space. Then, modelling the optical beamline as a single convergent lens, other four integrations are needed to characterize coherence

properties on the image plane, for a total of ten integrations. The development of a universal code for any experimental setup is then likely to be problematic. A more conservative approach may suggest the use of computer codes based on some analytical manipulation of first principle equations suited for specific experimental setups. From this viewpoint our most general expressions may be used as reliable basis for the development of numerical methods. Yet, computer codes can calculate properties for a given set of parameters, but can hardly improve physical understanding, which is particularly important in the stage of planning experiments. Our theory will allow treatment and physical understanding of many asymptotes of the parameter space and their applicability region with the help of a consistent use of dimensional analysis. In the most general asymptotic cases treated here, this will allow to reduce first principle calculations (i.e. ten-dimensional integrals) to one-dimensional convolutions of analytical functions with universal functions specific for the undulator source case, and still to retain a certain degree of generality. It is also worth to underline that our asymptotic results may also be used as a benchmark for numerical methods.

One of the main difficulties in applying a Statistical Optics approach to Synchrotron Radiation sources stems from the fact that Statistical Optics has principally developed in connection with problems involving thermal light. Solutions to all these problems share approximations that allow major simplifications, but are specific of thermal sources only. For instance, thermal sources can be modelled as perfectly incoherent, and the cross-spectral density assumes the form

$$G(\vec{r}_{\perp 1}, \vec{r}_{\perp 2}, \omega) \propto I(\vec{r}_{\perp 1}, \omega) \delta(\vec{r}_{\perp 2} - \vec{r}_{\perp 1}) \quad , \quad (7)$$

where  $I$  is the source intensity distribution and  $\delta$  is the two-dimensional Dirac  $\delta$ -function. However, there is a close connection between the state of coherence of the source and the angular distribution of the radiant intensity (see Eq. (4)). The physical interpretation of Eq. (7) is that the source is correlated over the minimal possible distance (which is of order of the wavelength). This has the consequence that the radiant intensity is distributed over a solid angle of order  $2\pi$ . This is correct for thermal sources, but is in contradiction with the fact that any Synchrotron Radiation source is confined within a narrow cone in the forward direction. The high directionality of Synchrotron Radiation rules out the use of Eq. (7) as a model for Synchrotron Radiation sources. However, such high directionality is not in contrast with the poor coherence which characterizes the quasi-homogeneous limit. Quasi-homogeneous sources are only locally coherent over a distance of many wavelengths but, by definition of quasi-homogeneity, the linear dimension of the source is much larger than the correlation distance. Even though a quasi-homogeneous source can be described with Geometrical Optics techniques, a coherence distance of many

wavelengths rules out the use of Eq. (7) as a model for Synchrotron Radiation sources. A more precise knowledge of the cross-spectral density (that is equivalent to the knowledge of the correct phase space density) is necessary to solve the image formation problem. For instance, suppose that a light source is placed at arbitrary distance in front of a lens. If the source is perfectly incoherent (thermal light case) the area of the light incident on the lens is always the area of the lens. In the case of Synchrotron Radiation source though, such area may be smaller than the lens. Even in the limit for a large beam emittance (compared with the radiation wavelength), information about the small angular distribution must be printed in the wavefront at the exit of the undulator leading once more to the same conclusion: Eq. (7) cannot be used in order to model Synchrotron Radiation sources. In [2] we treated, among other cases, the asymptote for a large electron beam size and divergence. The expression for the cross-spectral density of the source in free space simplifies and a particular quasi-homogeneous model can be given. In the same work, we specified also the region of applicability of such model, and we showed that it cannot be applied outside the limit for a large electron beam size and divergence.

In relation with these remarks it should be mentioned that an attempt to follow the path proposed in this paper is described in [6]. To our knowledge, [6] constitutes the first remarkable attempt to use Statistical Optics techniques in order to characterize the evolution of partially coherent X-ray beams through optical systems. In that work, as well as in [7], the beamline optics from the undulator to the specimen can be modelled as a critical illumination system [8], the beamline behaving as the condenser. After this, Statistical Optics techniques are consistently used to calculate coherent properties on the image plane. However, the authors of [6] reduced the general ten-dimensional integrals to four-dimensional integrals by postulating that the cross-spectral density distribution at the exit of the undulator can be written as Eq. (7), i.e. a perfectly incoherent source is assumed at the exit of the undulator. As we have just seen though, this assumption is always inconsistent in the case of Synchrotron Radiation, even in the Geometrical Optics limit and, *a fortiori*, in the case treated by the authors (the undulator beamline 12 at ALS), where  $\epsilon_y \simeq 0.1\lambda/(2\pi)$  and  $\epsilon_x \simeq 3\lambda/(2\pi)$ , which is highly spatially coherent.

We organize our work as follows. Besides this Introduction, in Section 2 we describe the optical system under study and some concepts from Statistical Optics that will be widely used in the following Sections. In Section 3 we review some general expressions pertaining undulator radiation from a single particle. In particular, following [2] we present an analytical expression for the Fourier transform of the electric field generated by a single electron with offset and deflection which is valid at any distance from the exit of the undulator. We also present the analytical solution of the imaging problem for a deterministic model of undulator radiation (absence of electron beam emittance). In Section

4 we give a derivation of the cross-spectral density for undulator radiation based sources. Subsequently we analyze the evolution of the cross-spectral density function through the optical system with particular attention to the focal and to the image plane. The following two Sections 5 and 6 describe quasi-homogeneous sources, respectively Gaussian and non-Gaussian, in the ideal case when the lens is aberration-free and the pupil aperture is non-limiting. A digression is then taken in Section 7, where we analyze in detail the relation between Geometrical Optics and quasi-homogeneous sources. Such Section may therefore be skipped in a first reading, without interrupting the main logical stream of our work. The next Section 8 describes the effects of a finite aperture size on the radiation characteristics from quasi-homogeneous sources at the image plane, and is followed by Section 9 that assumes a quasi-homogeneous source as well and deals with the consequences of lens aberration on the intensity at the image plane. In Section 10 we introduce a particular setup, a pinhole camera, capable of producing images of the sources in the absence of lenses. The study of this particular setup is of particular interest because it allows the reader to recognize mathematical analogies between cases otherwise physically different and serves as a junction between the previous Section 9 and Section 11 treating physical cases when one obtains, surprisingly, the image of the source on the focal plane. In the following Section 12 we extend the treatment for the focal plane to any plane of interest. In Section 13 we discuss the depth of focus, including the case of a large non-limiting aperture and the effects of aperture size. In the next Section 14 solutions for the image formation problem in non-homogeneous cases relevant for third generation Synchrotron Radiation sources are given. Before conclusions, in Section 15, we discuss the accuracy of quasi-homogeneous source asymptotes. Finally, in Section 16, we come to conclusions.

## 2 Elements and definitions of image formation theory

### 2.1 Wave propagation in free space

Let us indicate with  $E_{\perp}(z, \vec{r}_{\perp}, t)$  any fixed polarization component (along the direction  $x$  or  $y$ ) of the electric field at time  $t$  calculated on a plane at position  $z$  down the beamline at a certain transverse location  $\vec{r}_{\perp}$ .  $E_{\perp}(z, \vec{r}_{\perp}, t)$  obeys, in free space, the homogeneous wave equation:

$$c^2 \nabla^2 E_{\perp} - \frac{\partial^2 E_{\perp}}{\partial t^2} = 0 . \quad (8)$$

Let us now introduce the Fourier transform  $\bar{E}_\perp(z, \vec{r}_\perp, \omega)$  of the electric field  $E_\perp(z, \vec{r}_\perp, t)$ :

$$\bar{E}_\perp(\omega) = \int_{-\infty}^{\infty} dt E_\perp(t) e^{i\omega t} , \quad (9)$$

so that

$$E_\perp(t) = \frac{1}{2\pi} \int_{-\infty}^{\infty} d\omega \bar{E}_\perp(\omega) e^{-i\omega t} . \quad (10)$$

As already remarked in footnote 1, we will sometimes refer to  $\bar{E}_\perp$  as "the field", understanding that we are working in the frequency domain.

Let us consider the field propagation problem. To this purpose, we first introduce the complex envelope of the field:

$$\tilde{E} = \bar{E}_\perp \exp[-i\omega z/c] . \quad (11)$$

It is always possible to give such a definition. However, its utility is restricted to the case when  $\tilde{E}$  is a slowly varying function of  $z$  with respect to the radiation wavelength  $\lambda$ . When the paraxial approximation is applicable (i.e. always, for Synchrotron Radiation sources), this condition is fulfilled [1].

In paraxial approximation and in free space, the following parabolic equation holds for the complex envelope  $\tilde{E}$  of the Fourier transform of the electric field along a fixed polarization component:

$$\left( \nabla_\perp^2 + \frac{2i\omega}{c} \frac{\partial}{\partial z} \right) \tilde{E} = 0 . \quad (12)$$

The derivatives in the Laplacian operator  $\nabla_\perp^2$  are taken with respect to the transverse coordinates. One has to solve Eq. (12) with a given initial condition at  $z$ , which is a Cauchy problem. Indicating with  $\vec{r}_o$  the transverse coordinate of an observation point on a plane at longitudinal position  $z_o$  we have

$$\tilde{E}(z_o, \vec{r}_o) = \frac{i\omega}{2\pi c(z_o - z)} \int d\vec{r}^j \tilde{E}(z, \vec{r}^j) \exp \left[ \frac{i\omega |\vec{r}_o - \vec{r}^j|^2}{2c(z_o - z)} \right] , \quad (13)$$

where the integral is performed over the transverse plane.

Next to the propagation equation for the field in free space, Eq. (13), we can discuss a propagation equation for the spatial Fourier transform of the field, which can also be derived from Eq. (12) and will be useful in the following parts of this work. We will indicate the spatial Fourier transform of  $\tilde{E}(z, \vec{r}')$  with  $F(z, \vec{u})$ <sup>4</sup>:

$$F(z, \vec{u}) = \int d\vec{r}' \tilde{E}(z, \vec{r}') \exp [i\vec{r}' \cdot \vec{u}] . \quad (14)$$

Eq. (12) can be rewritten in terms of  $F$  as

$$\left( \nabla_{\perp}^2 + \frac{2i\omega}{c} \frac{\partial}{\partial z} \right) \left\{ \int d\vec{u} F(z, \vec{u}) \exp [-i\vec{r}' \cdot \vec{u}] \right\} = 0 . \quad (15)$$

Eq. (15) requires that

$$\left( -|\vec{u}|^2 + \frac{2i\omega}{c} \frac{\partial}{\partial z} \right) F(z, \vec{u}) = 0 . \quad (16)$$

Solution of Eq. (16) can be presented as

$$F(z, \vec{u}) = F(0, \vec{u}) \exp \left[ -\frac{ic|\vec{u}|^2 z}{2\omega} \right] . \quad (17)$$

It should be noted that the definition of  $F(0, \vec{u})$  is a matter of initial conditions. In many practical cases, including the totality of the situation treated in this paper,  $F$  (or  $\tilde{E}$ ) may have no direct physical meaning at  $z = 0$ . For instance, in

---

<sup>4</sup> For the sake of completeness we explicitly write the definitions of the two-dimensional Fourier transform and inverse transform of a function  $g(\vec{r})$  in agreement with the notations used in this paper. The Fourier transform and inverse transform pair reads:

$$\tilde{g}(\vec{k}) = \int d\vec{r} g(\vec{r}) \exp [i\vec{r} \cdot \vec{k}] ; \quad g(\vec{r}) = \frac{1}{4\pi^2} \int d\vec{k} \tilde{g}(\vec{k}) \exp [-i\vec{r} \cdot \vec{k}] ,$$

the integration being understood over the entire plane. If  $g$  is circular symmetric we can introduce the Fourier-Bessel transform and inverse transform pair:

$$\tilde{g}(k) = 2\pi \int_0^{\infty} dr r g(r) J_0(kr) ; \quad g(r) = \frac{1}{2\pi} \int_0^{\infty} dk k \tilde{g}(k) J_0(kr) ,$$

$r$  and  $k$  indicating the modulus of the vectors  $\vec{r}$  and  $\vec{k}$  respectively, and  $J_0$  being the zero-th order Bessel function of the first kind.

all cases considered in this paper,  $z = 0$  is in the center of the undulator, well within the radiation formation length. However,  $F(0, \vec{u})$  can be considered as the spatial Fourier transform of the field produced by a *virtual* source. Such a source is defined by the fact that, supposedly placed at  $z = 0$ , it would produce, at any distance from the undulator, the same field as the real source does. The result in Eq. (17) is very general. On the one hand, the spatial Fourier transform of the electric field exhibits an almost trivial behavior in  $z$ , since  $|F(z)|^2 = \text{const}$ . On the other hand, the behavior of the electric field itself is not trivial at all (see Section 2.4 and Figs 3-6). These properties follow directly from the propagation equation for the field and its Fourier transform.

Let us now discuss the physical meaning of Eq. (17). The spatial Fourier transform of the field,  $F(z, \vec{u})$ , may be interpreted as a superposition of plane waves (the so-called *angular spectrum*). Once the frequency  $\omega$  is fixed, the wave number  $k = \omega/c$  is fixed as well, and a given value of the transverse component of the wave vector  $\vec{k}_\perp = \vec{u}$  corresponds to a given angle of propagation of a plane wave. Different propagation directions correspond to different distances travelled to get to a certain observation point. Therefore, they also correspond to different phase shifts, which depend on the position along the  $z$  axis (see, for example, reference [9] Section 3.7). Free space basically acts as a Fourier transformation. This means that the field in the far zone is, phase factor and proportionality factor aside, the spatial Fourier transform of the field at any position  $z$ . To show this fact, we first recall that if we know the field at a given position  $(z, \vec{r}')$  we may use Eq. (13) to calculate the field at another position  $(z_o, \vec{r}_o)$ . Let us now consider the limit  $z_o \rightarrow \infty$ , with finite ratio  $\vec{r}_o/z_o$ . In this case, the exponential function in Eq. (13) can be expanded giving

$$\tilde{E}(z_o, \vec{r}_o) = \frac{i\omega}{2\pi c z_o} \int d\vec{r}' \tilde{E}(z, \vec{r}') \exp \left[ \frac{i\omega |\vec{r}_o|^2}{2c z_o} - \frac{i\omega (\vec{r}_o \cdot \vec{r}')}{c z_o} + \frac{i\omega z |\vec{r}_o|^2}{2c z_o^2} \right]. \quad (18)$$

Letting  $\vec{\theta} = \vec{r}_o/z_o$  we have

$$\tilde{E}(z_o, \vec{r}_o) = \frac{i\omega}{2\pi c z_o} \exp \left[ \frac{i\omega |\vec{\theta}|^2}{2c} (z_o + z) \right] F \left( z, -\frac{\omega \vec{\theta}}{c} \right). \quad (19)$$

With the help of Eq. (17), Eq. (19) may be presented as

$$\tilde{E}(z_o, \vec{r}_o) = \frac{i\omega}{2\pi c z_o} \exp \left[ \frac{i\omega |\vec{\theta}|^2}{2c} z_o \right] F \left( 0, -\frac{\omega \vec{\theta}}{c} \right). \quad (20)$$

Eq. (20) shows what we wanted to demonstrate: free space basically acts as a Fourier transformation.

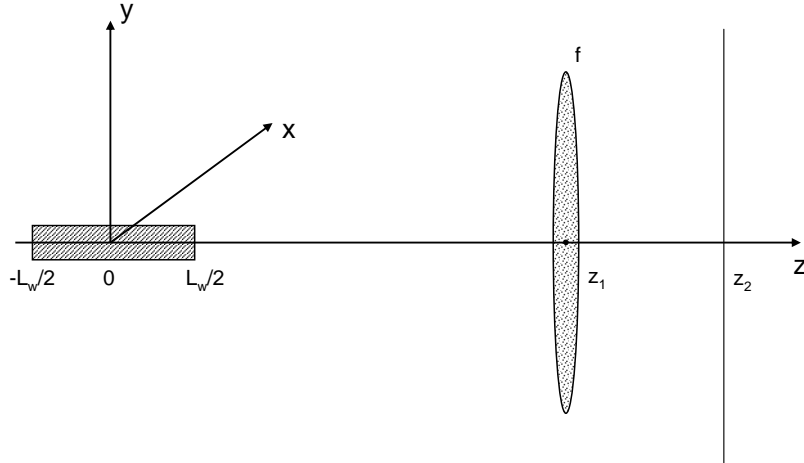


Fig. 1. Single lens imaging system with an undulator source as object.

## 2.2 Image formation with coherent light

As has been remarked in [6], any beamline optics used to re-image undulator radiation to an observation plane of interest can be modelled as a critical illumination system [8]. Therefore, the setup considered in this paper can be sketched as in Fig. 1. It consists of an undulator of length  $L_w$  centered at  $z = 0$ , a convergent lens positioned at  $z = z_1$ , characterized by a focusing strength  $f$ , and a plane of observation at position  $z = z_2$ . In principle,  $z_1$ ,  $z_2$  and  $f$  are unrelated parameters. However our main case of interest is a critical illumination system. Therefore, a given source plane at coordinate  $z = z_s$  - the object - is imaged at a particular observation position  $z = z_2$ , that defines the image plane. Using Ray Optics we can calculate the distance  $z_2$  along the axis behind the lens where the image is formed. This gives the well-known lens-maker equation

$$\frac{1}{f} = \frac{1}{z_1 - z_s} + \frac{1}{z_2 - z_1} . \quad (21)$$

The size of the image is magnified by a factor  $|M|$  and a real image is inverted with respect to the object because

$$M = -\frac{z_2 - z_1}{z_1 - z_s} < 0 , \quad (22)$$

as expected from Ray Optics. We also define a scale factor  $m$ , that is the inverse of the magnification power  $|M|$  of the lens:

$$m = \frac{1}{|M|} = \frac{z_1 - z_s}{z_2 - z_1} . \quad (23)$$

Once the lens position is fixed at  $z = z_1$ , the position  $z_s$  of the source is a matter of choice. Such a choice fixes the position  $z_i = z_2$  of the image plane in agreement with Eq. (21). For instance, with [6] and [7], one may set the critical illumination system to image the radiation at the undulator exit, in which case the choice  $z_s = L_w/2$  is made. However, one is not obliged to do so. In particular, in this paper, we will make the choice  $z_s = 0$ . Then, the critical illumination system images the center of the undulator, in the sense that the image plane  $z_i = z_2$  obeys Eq. (21) with  $z_s = 0$ .

From a mathematical viewpoint, specifying the source is equivalent to fixing the initial conditions for Maxwell equations in terms of a field distribution on a certain transverse plane. When a certain field distribution (in the frequency domain) is fixed on a plane at position  $z$ , Maxwell equations automatically set the way radiation propagates in free space, and the source is univocally defined. The choice made in [6] and [7] corresponds to the choice of a real source. The denomination "real" is justified by the fact that the initial condition for Maxwell equations amounts to the specification of a field distribution which is actually present, and in principle measurable, at the exit of the undulator. On the contrary, our choice  $z_s = 0$  corresponds to the position down the z-axis in the middle of the undulator, well within the radiation formation length. Although it makes sense to talk about the distribution of the electromagnetic field in the middle of the undulator, it does not make any sense to identify such distribution with the initial condition for Maxwell equations, i.e. with the source. However, it makes sense to define a *virtual* source as in Section 2.1. There is a particular reason for the choice  $z = 0$  as the position for the virtual source. In the case of a coherent undulator source (that is being treated in the present Section), the wavefront of the radiation at a virtual source located at  $z = 0$  is plane. In other words, the far zone field from an undulator has spherical wavefronts centered in the middle of the undulator. This fact alone makes the center of the undulator a privileged point with respect to others. Moreover, in the more general case of partially coherent radiation we will assume (as it is often verified in practice) that the beta functions of the electron beam have their minima (in both horizontal and vertical directions) in the center of the undulator. Subject to this assumption, as we will see, the center of the undulator constitutes a privileged point of interest in this case as well. As a result of the previous discussion we set

$$z_s = 0 . \tag{24}$$

Let us assume that the position  $z_1$  and the focal length  $f$  of the lens are set. Throughout this paper we will be particularly interested in the radiation characteristics at two privileged positions down the beamline:

- the image plane, at position  $z_2$  identified by Eq. (21).
- the focal plane, at position  $z_2$  identified by the equation  $z_2 - z_1 = f$ .

As it will be seen in the next Sections, both image and focal planes have special properties that can be expressed in terms of Fourier Optics. These properties are valid for any wavefront. We will first take advantage of them in Section 3, where we will deal with wavefronts generated by an electron beam with zero emittance and further on in Section 4, where emittance effects will be discussed in the realm of Statistical Optics. In the present Section, after having set the configuration under study, we will limit ourselves to describe these properties and to define basic quantities to be used in the Statistical Optics formulation of the image formation problem.

Consider the problem of mapping the plane *immediately in front* of the lens onto the plane at longitudinal position  $z_2 > z_1$  *behind* the lens (see Fig. 1). If one knows  $\tilde{E}$  at position  $z = z_1$  *immediately in front* of the lens, one can also obtain the expression for  $\tilde{E}$  *immediately behind* the lens multiplying by the transmission function:

$$T(\vec{r}') = P(\vec{r}') \exp \left[ -i\omega \frac{|\vec{r}'|^2}{2cf} \right]. \quad (25)$$

For simplicity of notation we consider here identical focal distances in the horizontal and in the vertical direction, i.e.  $f = f_x = f_y$ . Results for more complicated optical systems (e.g. a combination of cylindrical mirrors) are found substituting consistently Eq. (25) with its straightforward generalization. We assume with [8] that the complex pupil function  $P$  is zero outside the lens aperture. Its phase accounts for aberrations and its modulus may vary along the lens to describe apodizations: the simplest possible study case is for  $|P| = 1$  and  $\arg(P) = 0$  within the lens aperture. Accounting for Eq. (25), the propagation equation for any field  $\tilde{E}(z_1, \vec{r}')$  *immediately in front* of the lens to the point  $(z_2, \vec{r}_2)$  on the observation plane *behind* the lens can be written as:

$$\begin{aligned} \tilde{E}(z_2, \vec{r}_2) = & \frac{i\omega}{2\pi c(z_2 - z_1)} \exp \left[ \frac{i\omega |\vec{r}_2|^2}{2c(z_2 - z_1)} \right] \int d\vec{r}' \left\{ \tilde{E}(z_1, \vec{r}') P(\vec{r}') \right. \\ & \left. \times \exp \left[ \frac{i\omega}{c} \left( \frac{1}{2(z_2 - z_1)} - \frac{1}{2f} \right) |\vec{r}'|^2 \right] \right\} \exp \left[ -\frac{i\omega(\vec{r}_2 \cdot \vec{r}')}{c(z_2 - z_1)} \right]. \quad (26) \end{aligned}$$

Since Synchrotron Radiation is highly collimated, it is practically relevant to discuss the case when the area of the spot of the incident radiation is small compared with the area of the lens. It is also simpler and more natural to start with this situation. Then, effects from a finite pupil dimension can be neglected. Note that this is not the case for thermal sources: since these are emitting into a solid angle of  $2\pi$  (they are perfectly incoherent) the finite pupil dimensions cannot be ignored and result in the so-called *vignetting* effect [8]. Considering a perfect lens with no aberrations too, Eq. (26) assumes a

particularly simple form at the focal and on the image plane. Initially we will consider situations when the pupil presence can be neglected. Later on we discuss how to include the effects due to the presence of the pupil.

### 2.2.1 Large non-limiting aperture

We will now specialize the result in Eq. (26) in the asymptote for a large non-limiting aperture and in the case of the focal and of the image plane. Let us denote with  $(z_f, \vec{r}_f)$  a point on the focal plane, and with  $(z_i, \vec{r}_i)$  a point on the image plane. From Eq. (26), on the focal plane we have

$$\tilde{E}(z_f, \vec{r}_f) = \frac{i\omega}{2\pi cf} \exp\left[\frac{i\omega|\vec{r}_f|^2}{2cf}\right] \int d\vec{r}' \tilde{E}(z_1, \vec{r}') \exp\left[-\frac{i\omega(\vec{r}_f \cdot \vec{r}')}{cf}\right]. \quad (27)$$

With the help of Eq. (14) we can write Eq. (27) as

$$\tilde{E}(z_f, \vec{r}_f) = \frac{i\omega}{2\pi cf} \exp\left[\frac{i\omega|\vec{r}_f|^2}{2cf}\right] F\left(z_1, -\frac{\omega\vec{r}_f}{cf}\right). \quad (28)$$

Substitution of Eq. (17) in Eq. (28) gives

$$\tilde{E}(z_f, \vec{r}_f) = \frac{i\omega}{2\pi cf} \exp\left[\frac{i\omega|\vec{r}_f|^2}{2cf}\right] \exp\left[-\frac{i\omega z_1 |\vec{r}_f|^2}{2cf^2}\right] F\left(0, -\frac{\omega\vec{r}_f}{cf}\right). \quad (29)$$

For the image plane, remembering that

$$\frac{1}{f} = \frac{1}{z_1} + \frac{1}{z_i - z_1} \quad (30)$$

and that

$$d_i = z_i - z_1 = \frac{z_1}{m}, \quad (31)$$

we obtain, from Eq. (26)

$$\tilde{E}(z_i, \vec{r}_i) = \frac{i\omega m}{2\pi cz_1} \exp\left[\frac{i\omega m |\vec{r}_i|^2}{2cz_1}\right] \int d\vec{r}' \left\{ \tilde{E}(z_1, \vec{r}') \exp\left[-\frac{i\omega |\vec{r}'|^2}{2cz_1}\right] \right\} \exp\left[-\frac{i\omega m (\vec{r}_i \cdot \vec{r}')}{cz_1}\right]. \quad (32)$$

On the image plane, according to Eq. (32), we have to calculate the Fourier transform of the product of two factors:  $\exp[-i\omega|\vec{r}'|^2/(2cz_1)]$ , representing the phase of a spherical wave in paraxial approximation, and  $\tilde{E}(z_1, \vec{r}')$ . A direct calculation shows that the Fourier transform of the phase factor is

$$\int d\vec{r}' \exp\left[-\frac{i\omega|\vec{r}'|^2}{2cz_1}\right] \exp\left[-\frac{i\omega\mathbf{m}(\vec{r}_i \cdot \vec{r}')}{cz_1}\right] = -4iz_1 \exp\left[\frac{im^2\omega|\vec{r}_i|^2}{2cz_1}\right]. \quad (33)$$

Since the Fourier transform of a product is equal to the convolution of the Fourier transforms of each separate factor, from Eq. (32) one obtains

$$\begin{aligned} \tilde{E}(z_i, \vec{r}_i) &= \frac{\mathbf{m}}{4\pi^2} \exp\left[\frac{i\omega\mathbf{m}|\vec{r}_i|^2}{2cz_1}\right] \\ &\times \int d\vec{u} F(z_1, \vec{u}) \exp\left[\frac{icz_1}{2\omega} \left(-\frac{\mathbf{m}\omega\vec{r}_i}{cz_1} - \vec{u}\right)^2\right]. \end{aligned} \quad (34)$$

Substitution of Eq. (17) in Eq. (34) gives

$$\begin{aligned} \tilde{E}(z_i, \vec{r}_i) &= \frac{\mathbf{m}}{4\pi^2} \exp\left[\frac{i\omega\mathbf{m}|\vec{r}_i|^2}{2cz_1}\right] \exp\left[\frac{i\omega\mathbf{m}^2|\vec{r}_i|^2}{2cz_1}\right] \\ &\times \int d\vec{u} F(0, \vec{u}) \exp[i\mathbf{m}\vec{r}_i \cdot \vec{u}], \end{aligned} \quad (35)$$

that is

$$\tilde{E}(z_i, \vec{r}_i) = \mathbf{m} \exp\left[\frac{i\omega\mathbf{m}|\vec{r}_i|^2}{2cz_1}\right] \exp\left[\frac{i\omega\mathbf{m}^2|\vec{r}_i|^2}{2cz_1}\right] \tilde{E}(0, -\mathbf{m}\vec{r}_i). \quad (36)$$

The phase factor in the Fourier transform of the electric field, given in Eq. (17), cancels the quadratic phase factor in  $|\vec{u}|^2$  in Eq. (34). Therefore, the convolution integral in Eq. (34) transforms to a Fourier integral. As a result, in the image plane we always obtain (aside for a scaling and a net phase factor) the inverted field distribution in the virtual source plane. More in general, at any observation plane located at  $z = z_2$  behind the lens and the focal plane, one observes (aside, again, for a scaling and a net phase factor) the inverted field distribution on an object plane located at  $z = z_s$ , where  $z_s$  satisfies the lens condition Eq. (21).

Eq. (29) and Eq. (36) are reflections of well-known theorems of Fourier Optics. Neglecting the effects from a finite pupil dimension and assuming a perfect lens with no aberrations, the focal plane has the following property [9]:

- For any position of the object in front of the lens, the field distribution (amplitude and phase) on the focal plane differs from the spatial Fourier transform of the field distribution on the object plane by a scale factor  $-\omega/(cf)$  and a net phase factor.

At the image plane, instead, the following property applies [9]:

- For any position of the object in front of the lens, the field distribution (amplitude and phase) on the image plane differs from the field distribution on the object plane by a scale factor  $-m$  and a net phase factor <sup>5</sup>.

These properties can be interpreted in terms of intensity distributions. The first tells that the intensity profile on the focal plane has the same shape of that on a distant plane and is obtained taking, essentially, the square modulus of the Fourier transform of the field on the object plane. The second tells that the intensity profile of the object is inverted and magnified by the lens on the image plane. For the image plane we just obtained, for perfectly coherent light, the same result which is obtained in Geometrical Optics in the perfectly incoherent limit.

### 2.2.2 Effect of aperture size

Pupil effects are taken into account, from a general standpoint, in Eq. (26). Eq. (26) takes a specific form in the focal and in the image plane. One has

$$\tilde{E}(z_f, \vec{r}_f) = \frac{i\omega}{2\pi cf} \exp\left[\frac{i\omega|\vec{r}_f|^2}{2cf}\right] \int d\vec{r}' \tilde{E}(z_1, \vec{r}') P(\vec{r}') \exp\left[-\frac{i\omega(\vec{r}_f \cdot \vec{r}')}{cf}\right] \quad (37)$$

and

$$\begin{aligned} \tilde{E}(z_i, \vec{r}_i) &= \frac{i\omega m}{2\pi cz_1} \exp\left[\frac{i\omega m|\vec{r}_i|^2}{2cz_1}\right] \int d\vec{r}' \left\{ \tilde{E}(z_1, \vec{r}') P(\vec{r}') \exp\left[-\frac{i\omega|\vec{r}'|^2}{2cz_1}\right] \right\} \\ &\times \exp\left[-\frac{i\omega m(\vec{r}_i \cdot \vec{r}')}{cz_1}\right]. \end{aligned} \quad (38)$$

Eq. (37) and Eq. (38) are formal extensions of Eq. (27) and Eq. (32), respectively. Use of the convolution theorem on Eq. (37) and Eq. (38) allows to write analogous extensions of Eq. (29) and Eq. (36). To this purpose we define

<sup>5</sup> The prefactor  $m(z_i)$  is a consequence of the conservation of the total energy associated with the propagating field.

$$\mathcal{P}(\vec{u}) = \int d\vec{r}' P(\vec{r}') \exp[-i\vec{r}' \cdot \vec{u}] . \quad (39)$$

Then, indicating with  $\tilde{E}_P$  the field in the presence of the pupil, on the focal plane we have

$$\begin{aligned} \tilde{E}_P(z_f, \vec{r}_f) = & \exp\left[\frac{i\omega|\vec{r}_f|^2}{2cf}\right] \\ & \times \int d\vec{u} \mathcal{P}\left(\frac{\omega\vec{r}_f}{cf} - \vec{u}\right) \cdot \exp\left[-\frac{icf|\vec{u}|^2}{2\omega}\right] \tilde{E}\left(z_f, \frac{cf\vec{u}}{\omega}\right) \end{aligned} \quad (40)$$

and on the image plane

$$\begin{aligned} \tilde{E}_P(z_i, \vec{r}_i) = & \exp\left[\frac{i\omega m|\vec{r}_i|^2}{2cz_1}\right] \\ & \times \int d\vec{u} \mathcal{P}\left(\frac{\omega m\vec{r}_i}{cz_1} - \vec{u}\right) \cdot \exp\left[-\frac{icz_1|\vec{u}|^2}{2\omega m}\right] \tilde{E}\left(z_i, \frac{cz_1\vec{u}}{\omega m}\right) . \end{aligned} \quad (41)$$

One may apply the following mnemonic rule to include the effects of the pupil in Eq. (29) or Eq. (36). First, divide Eq. (29) or Eq. (36) by the first phase factor, corresponding to the phase factor outside the integral sign in Eq. (26). Second, convolve with  $\mathcal{P}$ . Third, put the phase factor back.

It should be noted that, in the limit for large apertures,  $\mathcal{P}$  can be substituted by a  $\delta$ -Dirac function in both Eq. (40) and Eq. (41). In this case, from Eq. (40) we recover  $\tilde{E}_P(z_f, \vec{r}_f) = \tilde{E}(z_f, \vec{r}_f)$ , given in Eq. (29). From Eq. (41) instead, we have  $\tilde{E}_P(z_i, \vec{r}_i) = \tilde{E}(z_i, \vec{r}_i)$ , given in Eq. (36).

Unless particular conditions are met, the phase factors under the integral signs in Eq. (40) and Eq. (41) compensate only partially the phase of  $\tilde{E}$ , which can be found in Eq. (29) and Eq. (36) respectively. This fact complicates the evaluation of the convolution integrals. Let us restrict our attention to the image plane. We can treat analytically the case when the phase factors under integral in Eq. (41) completely compensate the phase factor in Eq. (36), i.e. when we can neglect the second phase factor in Eq. (36). This happens when we are in the far field limit. The far field limit of Eq. (36) can be obtained by substitution of Eq. (20) in Eq. (32). After the inverse Fourier transform in Eq. (32) is calculated one obtains

$$\tilde{E}(z_i, \vec{r}_i) = m \exp\left[\frac{i\omega m|\vec{r}_i|^2}{2cz_1}\right] \tilde{E}(0, -m\vec{r}_i) , \quad (42)$$

that can also be obtained directly from Eq. (36) neglecting the second phase

factor on the right hand side. This is possible when

$$\frac{\omega m^2 |\vec{r}_i|^2}{2cz_1} \ll 1 \quad (43)$$

for any point  $\vec{r}_i$  on the image pattern.

Let us indicate with  $\sigma_i$  the characteristic size of the image. Condition (43) can be interpreted as the following requirement for  $z_1$ :

$$z_1 \gg \frac{\omega m^2 \sigma_i^2}{c} . \quad (44)$$

Since we are interested in the parametric dependence only, a factor 2 has been neglected in Eq. (44). From Eq. (36) follows that  $m\sigma_i$  is the characteristic size of the virtual source. As such it is independent of the position of the lens and of the magnification factor  $|M| = m^{-1}$  as well. Condition (44) is often met in practice and means that the radiation spot size on the lens,  $cz_1/(\omega m\sigma_i)$ , is much larger than the characteristic size of the virtual source,  $m\sigma_i$ . Then, the lens is placed in the far zone with respect to the virtual undulator source by definition of far zone  $\lambda z_1/(2\pi\sigma_o) \gg \sigma_o$ ,  $\sigma_o$  being the source size. We conclude that the condition for the lens to be placed in the far zone is equivalent to the condition that Eq. (36) can be reduced to Eq. (42). This result will be of importance in what follows. However, this kind of reasoning is only valid on the image plane. On the focal plane the second phase factor in Eq. (29) follows directly from the phase factor in Eq. (17), that is related with the propagation of the angular spectrum: in this case one concludes that plane waves with different directions of propagation lead to an increasing phase difference as the distance  $z_1$  increases. Therefore, in the focal plane, some simplification may be obtained in the near field only, as  $z_1$  is small enough that the phase difference between different plane wave components is negligible. We will not investigate this situation further. Going back to the image plane one can see that a term of the expansion of the phase factor under the integral sign in Eq. (34) cancels the phase factor in Eq. (17). It follows that the second phase factor in Eq. (36) is not related with the propagation of the angular spectrum. Therefore, in the far field region, when condition (44) holds, we have that the pupil effects can be accounted for by means of a simpler convolution. In the following parts of this paper we will restrict to this particular case when treating pupil effects. It is interesting to remark that pupil effects due to finite pupil dimension are especially important in the far region. In this limit the radiation spot size on the lens is much larger than the size of the radiation spot at the virtual source, and is often larger than the size of the pupil. In the near field instead, the radiation spot size on the lens is of order of the radiation spot size at the virtual source. Therefore, in this limit, one can neglect effects

from any finite pupil aperture larger than the radiation spot size at the virtual source.

In conclusion, explicit substitution of Eq. (42) in Eq. (41) yields the following far field limit expression on the image plane:

$$\tilde{E}_P(z_i, \vec{r}_i) = \exp \left[ \frac{i\omega m |\vec{r}_i|^2}{2cz_1} \right] \int d\vec{u} \mathcal{P} \left( \frac{\omega m \vec{r}_i}{cz_1} - \vec{u} \right) \cdot \tilde{E} \left( 0, -\frac{cz_1 \vec{u}}{\omega} \right) . \quad (45)$$

### 2.3 Propagation of partially coherent light in free space

Let us now consider the stochastic nature of the Synchrotron Radiation field in general terms. Synchrotron Radiation is a Gaussian stochastic process. As has been discussed in detail in reference [2], the electromagnetic signal at any position down the beamline is completely characterized, from a statistical viewpoint, by the knowledge of the second order field correlation function in space-frequency domain

$$\Gamma_\omega(z_o, \vec{r}_{o1}, \vec{r}_{o2}, \omega, \omega') = \left\langle \bar{E}_\perp(z_o, \vec{r}_{o1}, \omega) \bar{E}_\perp^*(z_o, \vec{r}_{o2}, \omega') \right\rangle . \quad (46)$$

In this paper, the averaging brackets  $\langle \dots \rangle$  will always indicate an ensemble average over bunches. As it will be better explained in the following Section 3, we will restrict ourselves to the treatment of radiation from planar undulators in resonance with the fundamental harmonic. Therefore we can neglect vertically polarized radiation components and consider  $\bar{E}$  as a scalar quantity. The shot noise in the electron beam is responsible for random fluctuations of the beam density, both in space and time. As a result, the temporal Fourier transform of the Synchrotron Radiation pulse at a fixed frequency and a fixed point in space is a sum of a great many independent contributions:

$$\bar{E}_\perp(z_o, \vec{r}_o, \omega) = \sum_{k=1}^N \bar{E}_{s\perp}(\vec{\eta}_k, \vec{l}_k, z_o, \vec{r}_o, \omega) \exp(i\omega t_k) , \quad (47)$$

where  $N$  is the number of electrons in the bunch. Here  $\vec{\eta}_k, \vec{l}_k$  and  $t_k$  are random variables describing random angular direction, position and arrival time of an electron at the reference position  $z_o = 0$ . As has been demonstrated in [2], under the assumption - generally verified for X-ray beams and third generation light sources - that the radiation wavelengths of interest is much shorter than the bunch length we can write Eq. (46) as

$$\Gamma_\omega(z_o, \vec{r}_{o1}, \vec{r}_{o2}, \omega, \omega') = N F_\omega(\omega - \omega')$$

$$\times \left\langle \bar{E}_{s\perp}(\vec{\eta}, \vec{l}, z_o, \vec{r}_{o1}, \omega) \bar{E}_{s\perp}^*(\vec{\eta}, \vec{l}, z_o, \vec{r}_{o2}, \omega') \right\rangle_{\vec{\eta}, \vec{l}}, \quad (48)$$

where  $F(\omega)$  is the Fourier transform of the bunch longitudinal profile function  $F_t(t_k)$ , that is

$$\langle \exp(i\omega t_k) \rangle_t = \int_{-\infty}^{\infty} dt_k F_t(t_k) e^{i\omega t_k} = F_\omega(\omega). \quad (49)$$

Note that the ensemble average on the right hand side of Eq. (48) is done over the product of the electric field produced by the same electron. In other words each electron is correlated only with itself.

If the dependence of  $\bar{E}_{s\perp}$  on  $\omega$  and  $\omega'$  is slow enough, so that  $\bar{E}_{s\perp}$  does not vary appreciably on the characteristic scale of  $F_\omega$  we can substitute  $\bar{E}_{s\perp}^*(\vec{\eta}, \vec{l}, z_o, \vec{r}_{o2}, \omega')$  with  $\bar{E}_{s\perp}^*(\vec{\eta}, \vec{l}, z_o, \vec{r}_{o2}, \omega)$  in Eq. (48) thus obtaining:

$$\Gamma_\omega(z_o, \vec{r}_{o1}, \vec{r}_{o2}, \omega, \omega') = N F_\omega(\omega - \omega') G(z_o, \vec{r}_{o1}, \vec{r}_{o2}, \omega) \quad (50)$$

where

$$G(z_o, \vec{r}_{o1}, \vec{r}_{o2}, \omega) = \left\langle \bar{E}_{s\perp}(\vec{\eta}, \vec{l}, z_o, \vec{r}_{o1}, \omega) \bar{E}_{s\perp}^*(\vec{\eta}, \vec{l}, z_o, \vec{r}_{o2}, \omega) \right\rangle_{\vec{\eta}, \vec{l}}. \quad (51)$$

As has been shown in [2] this assumption is by no means a restrictive one.

From now on we will be concerned with the calculation of the correlation function  $G(z_o, \vec{r}_{o1}, \vec{r}_{o2}, \omega)$ , while the correlation in frequency (which may be complicated by other factors describing, for instance, the presence of a monochromator) can be dealt with separately.

On the one hand, the cross-spectral density as is defined in Eq. (51) includes the product of fields which obey the free space propagation relation Eq. (13). On the other hand, the averaging over random variables commutes with all operations involved in the calculation of the field propagation. More explicitly, introducing the notation  $\tilde{E}(z_o) = \mathcal{O}[\tilde{E}(z)]$  as a shortcut for Eq. (13) one can write

$$\begin{aligned} G(z_o) &= \left\langle \bar{E}_{s\perp}(z_o) \bar{E}_{s\perp}^*(z_o) \right\rangle = \left\langle \mathcal{O} \left[ \bar{E}_{s\perp}(z) \right] \mathcal{O}^* \left[ \bar{E}_{s\perp}^*(z) \right] \right\rangle = \\ &= \mathcal{O} \cdot \mathcal{O}^* \left[ \left\langle \bar{E}_{s\perp}(z) \bar{E}_{s\perp}^*(z) \right\rangle \right] = \mathcal{O} \cdot \mathcal{O}^* [G(z)]. \end{aligned} \quad (52)$$

Note that  $\mathcal{O}$  may represent, more in general, any linear operator.

As a result, one can obtain a law for the propagation of the cross-spectral density in free space in analogy with Eq. (13) from position  $z$  to position  $z_o$ :

$$G(z_o, \vec{r}_{o1}, \vec{r}_{o2}) = \frac{\omega^2}{4\pi^2 c^2 (z_o - z)^2} \int d\vec{r}'_1 d\vec{r}'_2 G(z, \vec{r}'_1, \vec{r}'_2) \times \exp \left[ \frac{i\omega}{2c(z_o - z)} \left( |\vec{r}'_{o1} - \vec{r}'_1|^2 - |\vec{r}'_{o2} - \vec{r}'_2|^2 \right) \right], \quad (53)$$

where the integral is performed in four dimensions. We may now proceed in parallel with Section 2.1. In analogy with Eq. (14) let us first define

$$\mathcal{G}(z, \vec{u}_1, \vec{u}_2) = \int d\vec{r}'_1 d\vec{r}'_2 G(z, \vec{r}'_1, \vec{r}'_2) \exp \left[ i \left( \vec{u}_1 \cdot \vec{r}'_1 - \vec{u}_2 \cdot \vec{r}'_2 \right) \right]. \quad (54)$$

Eq. (54) is a second-order correlation function between spatial Fourier transforms of the field. In the following, for simplicity, and with some abuse of language, we will denote  $\mathcal{G}$  as the "Fourier transform of  $G$ ". The spatial Fourier transform of  $\tilde{E}$  depends on the position along the beamline through a phase factor only. Moreover, as already said, the operation of ensemble average commutes with the operation of Fourier transform. It follows that also  $\mathcal{G}$  depends on the position along the beamline through a phase factor only. To be specific, the analogous of Eq. (17) is given by

$$\mathcal{G}(z, \vec{u}_1, \vec{u}_2) = \mathcal{G}(0, \vec{u}_1, \vec{u}_2) \exp \left[ -\frac{ic}{2\omega} \left( |\vec{u}_1|^2 - |\vec{u}_2|^2 \right) z \right]. \quad (55)$$

Continuing in analogy with Section 2.1 we find Eq. (20), which relates the far field expression for  $\tilde{E}(z_o, \vec{r}_o)$  (in the limit  $z_o \rightarrow \infty$  and for a finite ratio  $\vec{r}_o/z_o$ ) to the spatial Fourier transform  $F$ . We can take advantage of Eq. (20) to obtain, with the help of Eq. (51) and Eq. (54), a useful relation between the cross-spectral density in the far field and the Fourier transform of  $G$  at the virtual-source position. In the limit  $z_o \rightarrow \infty$  and for finite ratios  $\vec{\theta}_1 = \vec{r}_{o1}/z_o$ ,  $\vec{\theta}_2 = \vec{r}_{o2}/z_o$  we have

$$G(z_o, \vec{r}_{o1}, \vec{r}_{o2}) = \frac{\omega^2}{4\pi^2 c^2 z_o^2} \exp \left[ \frac{i\omega z_o}{2c} \left( |\vec{\theta}_1|^2 - |\vec{\theta}_2|^2 \right) \right] \mathcal{G} \left( 0, -\frac{\omega \vec{\theta}_1}{c}, -\frac{\omega \vec{\theta}_2}{c} \right). \quad (56)$$

This expression will be very useful later on. In [2] we obtained an explicit expression for the cross-spectral density of the undulator source in free space at any distance from the undulator. In particular we can calculate the cross-spectral density in the far field, which assumes a simplified form. Consequently,

the use of Eq. (56) allows to calculate the Fourier transform of the cross-spectral density at the virtual-source position. As a result we can characterize the virtual source and operate with it. Our starting point, here as in [2] is the electron beam in the undulator device. In contrast with this, previous literature dealing with application of Statistical Optics to undulator radiation assumes *a priori* the validity of a postulated expression for the cross-spectral density.

#### 2.4 Image formation with partially coherent light

In analogy with Section 2.2 we will now consider the problem of propagating the cross-spectral density *immediately in front* of the lens through the optical system up to the screen at  $z = z_2$  *behind* the lens. Suppose that we know  $G(z_1)$  *immediately in front* of the lens. The cross spectral density *immediately behind* the lens,  $G_l(z_1)$ , is related to  $G(z_1)$  by

$$G_l(z_1, \vec{r}'_1, \vec{r}'_2) = G(z_1, \vec{r}'_1, \vec{r}'_2) T(\vec{r}'_1) T^*(\vec{r}'_2) , \quad (57)$$

where the transmission function  $T$  is defined by Eq. (25). One can obtain a law for the propagation of the cross-spectral density in free space using Eq. (53), in agreement with [8], from position  $z_1$  *immediately behind* the lens to the image plane at position  $z_2$ , that is

$$G(z_2, \vec{r}_1, \vec{r}_2) = \frac{\omega^2}{4\pi^2 c^2 (z_2 - z_1)^2} \int d\vec{r}'_1 d\vec{r}'_2 G_l(z_1, \vec{r}'_1, \vec{r}'_2) \times \exp \left[ \frac{i\omega}{2c(z_2 - z_1)} \left( |\vec{r}_1 - \vec{r}'_1|^2 - |\vec{r}_2 - \vec{r}'_2|^2 \right) \right] . \quad (58)$$

Substituting Eq. (57) in Eq. (58) and remembering Eq. (25) one finds

$$G(z_2, \vec{r}_1, \vec{r}_2) = \frac{\omega^2}{4\pi^2 c^2 (z_2 - z_1)^2} \int d\vec{r}'_1 d\vec{r}'_2 G(z_1, \vec{r}'_1, \vec{r}'_2) P(\vec{r}'_1) P^*(\vec{r}'_2) \times \exp \left[ \frac{i\omega}{2cf} \left( |\vec{r}_2|^2 - |\vec{r}'_1|^2 \right) + \frac{i\omega}{2c(z_2 - z_1)} \left( |\vec{r}_1 - \vec{r}'_1|^2 - |\vec{r}_2 - \vec{r}'_2|^2 \right) \right] . \quad (59)$$

Manipulation of the argument in the exponential function under integral allows the more suggestive representation

$$\begin{aligned}
G(z_2, \vec{r}_1, \vec{r}_2) &= \frac{\omega^2}{4\pi^2 c^2 (z_2 - z_1)^2} \exp \left[ \frac{i\omega}{2c(z_2 - z_1)} (|\vec{r}_1|^2 - |\vec{r}_2|^2) \right] \\
&\times \int d\vec{r}'_1 d\vec{r}'_2 \left\{ G(z_1, \vec{r}'_1, \vec{r}'_2) P(\vec{r}'_1) P^*(\vec{r}'_2) \right. \\
&\times \exp \left[ \frac{i\omega}{c} \left( \frac{1}{2f} - \frac{1}{2(z_2 - z_1)} \right) (|\vec{r}'_2|^2 - |\vec{r}'_1|^2) \right] \left. \right\} \\
&\times \exp \left[ \frac{i\omega}{c(z_2 - z_1)} (-\vec{r}_1 \cdot \vec{r}'_1 + \vec{r}_2 \cdot \vec{r}'_2) \right], \tag{60}
\end{aligned}$$

that is analogous to Eq. (26). The quantity in brackets  $\{\dots\}$  is basically Fourier-transformed. As mentioned before, similarities between the way  $G$  and  $\tilde{E}$  evolve through the beamline have to be ascribed to the fact that the average over random variables commutes with all other operations in the calculation of the cross-spectral density. As a result, the reason why Eq. (60) is basically a Fourier transformation is due to the particular way  $\tilde{E}$  evolves.

Similarly as has been explained above for the fields, the image and the focal plane are privileged planes for which the cross-spectral density assumes particularly simple forms, that can be found in terms of Fourier Optics.

#### 2.4.1 Large non-limiting aperture

We will now proceed in analogy with Section 2.2.1. On the focal plane, similarly to Eq. (28) we have

$$\begin{aligned}
G(z_f, \vec{r}_{1f}, \vec{r}_{2f}) &= \frac{\omega^2}{4\pi^2 c^2 f^2} \exp \left[ \frac{i\omega}{2cf} (|\vec{r}_{1f}|^2 - |\vec{r}_{2f}|^2) \right] \\
&\times \mathcal{G} \left( z_1, -\frac{\omega \vec{r}_{1f}}{cf}, -\frac{\omega \vec{r}_{2f}}{cf} \right), \tag{61}
\end{aligned}$$

while using Eq. (55) we obtain, similarly to Eq. (29),

$$\begin{aligned}
G(z_f, \vec{r}_{1f}, \vec{r}_{2f}) &= \frac{\omega^2}{4\pi^2 c^2 f^2} \exp \left[ \frac{i\omega}{2cf} (|\vec{r}_{1f}|^2 - |\vec{r}_{2f}|^2) \right] \\
&\times \exp \left[ -\frac{i\omega z_1}{2cf^2} (|\vec{r}_{1f}|^2 - |\vec{r}_{2f}|^2) \right] \mathcal{G} \left( 0, -\frac{\omega \vec{r}_{1f}}{cf}, -\frac{\omega \vec{r}_{2f}}{cf} \right). \tag{62}
\end{aligned}$$

In analogy with Eq. (32), for the image plane we can write

$$G(z_i, \vec{r}_{1i}, \vec{r}_2) = \left( \frac{m\omega}{2\pi c z_1} \right)^2 \exp \left[ \frac{i\omega m}{2c z_1} (|\vec{r}_{1i}|^2 - |\vec{r}_2|^2) \right]$$

$$\begin{aligned}
& \times \int d\vec{r}'_1 d\vec{r}'_2 G(z_1, \vec{r}'_1, \vec{r}'_2) \exp \left[ \frac{i\omega}{2cz_1} \left( |\vec{r}'_2|^2 - |\vec{r}'_1|^2 \right) \right] \\
& \times \exp \left[ -\frac{im\omega}{cz_1} \left( \vec{r}_{1i} \cdot \vec{r}'_1 - \vec{r}_{2i} \cdot \vec{r}'_2 \right) \right] . \tag{63}
\end{aligned}$$

Using the convolution theorem in analogy with Eq. (34) we obtain

$$\begin{aligned}
G(z_i, \vec{r}_{1i}, \vec{r}_{2i}) &= \left( \frac{m}{4\pi^2} \right)^2 \exp \left[ \frac{i\omega m}{2cz_1} \left( |\vec{r}_{1i}|^2 - |\vec{r}_{2i}|^2 \right) \right] \int d\vec{u} d\vec{v} \mathcal{G}(z_1, \vec{u}, \vec{v}) \\
& \times \exp \left\{ \frac{icz_1}{2\omega} \left[ \left( \frac{m\omega\vec{r}_{1i}}{cz_1} + \vec{u} \right)^2 - \left( \frac{m\omega\vec{r}_{2i}}{cz_1} + \vec{v} \right)^2 \right] \right\} . \tag{64}
\end{aligned}$$

Finally, taking advantage of Eq. (55) we have

$$\begin{aligned}
G(z_i, \vec{r}_{1i}, \vec{r}_{2i}) &= \left( \frac{m}{4\pi^2} \right)^2 \exp \left[ \frac{i\omega m}{2cz_1} \left( |\vec{r}_{1i}|^2 - |\vec{r}_{2i}|^2 \right) \right] \\
& \times \exp \left[ \frac{im^2\omega}{2cz_1} \left( |\vec{r}_{1i}|^2 - |\vec{r}_{2i}|^2 \right) \right] \\
& \times \int d\vec{u} d\vec{v} \mathcal{G}(0, \vec{u}, \vec{v}) \exp [im(\vec{r}_{1i} \cdot \vec{u} - \vec{r}_{2i} \cdot \vec{v})] , \tag{65}
\end{aligned}$$

that can be rewritten as the analogous of Eq. (36):

$$\begin{aligned}
G(z_i, \vec{r}_{1i}, \vec{r}_{2i}) &= m^2 \exp \left[ \frac{im\omega}{2cz_1} \left( |\vec{r}_{1i}|^2 - |\vec{r}_{2i}|^2 \right) \right] \\
& \times \exp \left[ \frac{im^2\omega}{2cz_1} \left( |\vec{r}_{1i}|^2 - |\vec{r}_{2i}|^2 \right) \right] G(0, -m\vec{r}_{1i}, -m\vec{r}_{2i}) . \tag{66}
\end{aligned}$$

#### 2.4.2 Effect of aperture size

Effects of aperture size can be included in strict analogy with Section 2.2.2. Similarly to Section 2.2.2 the following mnemonic rule can be applied to include the effects of the pupil in Eq. (62) or Eq. (66). First, divide Eq. (62) or Eq. (66) by the first phase factor, corresponding to the phase factor outside the integral sign in Eq. (60). Second, convolve twice with  $\mathcal{P}$  and  $\mathcal{P}^*$ ,  $\mathcal{P}$  having already been defined in Eq. (39). Third, put the phase factor back. We will denote with  $G_P$  the cross-spectral density including the effects due to the presence of the pupil. On the focal plane, in analogy with Eq. (40), one obtains

$$\begin{aligned}
G_P(z_f, \vec{r}_{1f}, \vec{r}_{2f}) &= \exp \left[ \frac{i\omega}{2cf} \left( |\vec{r}_{1f}|^2 - |\vec{r}_{2f}|^2 \right) \right] \\
&\times \int d\vec{u} d\vec{v} \mathcal{P} \left( \frac{\omega\vec{r}_{1f}}{cf} - \vec{u} \right) \mathcal{P}^* \left( \frac{\omega\vec{r}_{2f}}{cf} - \vec{v} \right) \\
&\times \exp \left[ \frac{icf}{2\omega} \left( |\vec{v}|^2 - |\vec{u}|^2 \right) \right] G \left( z_f, \frac{cf\vec{u}}{\omega}, \frac{cf\vec{v}}{\omega} \right) \quad (67)
\end{aligned}$$

while on the image plane, in analogy with Eq. (41), one has

$$\begin{aligned}
G_P(z_i, \vec{r}_{1i}, \vec{r}_{2i}) &= \exp \left[ \frac{im\omega}{2cz_1} \left( |\vec{r}_{1i}|^2 - |\vec{r}_{2i}|^2 \right) \right] \\
&\times \int d\vec{u} d\vec{v} \mathcal{P} \left( \frac{\omega m \vec{r}_{1i}}{cz_1} - \vec{u} \right) \mathcal{P}^* \left( \frac{\omega m \vec{r}_{2i}}{cz_1} - \vec{v} \right) \\
&\times \exp \left[ \frac{icz_1}{2\omega m} \left( |\vec{v}|^2 - |\vec{u}|^2 \right) \right] G \left( z_i, \frac{cz_1\vec{u}}{\omega m}, \frac{cz_1\vec{v}}{\omega m} \right) . \quad (68)
\end{aligned}$$

In the limit for large apertures,  $\mathcal{P}$  and  $\mathcal{P}^*$  can be substituted by  $\delta$ -Dirac functions in both Eq. (67) and Eq. (68). In this case, from Eq. (67) we recover  $G_P(z_f, \vec{r}_{1f}, \vec{r}_{2f}) = G(z_f, \vec{r}_{1f}, \vec{r}_{2f})$ , that is given by Eq. (62). From Eq. (68) instead, we have  $G_P(z_i, \vec{r}_{1i}, \vec{r}_{2i}) = G(z_i, \vec{r}_{1i}, \vec{r}_{2i})$ , that is given by Eq. (66).

Similarly to the case analyzed in Section 2.2, unless particular conditions are met, the phase factor under the integrals in Eq. (67) and Eq. (68) compensate only partially the phase in Eq. (62) and Eq. (66). In the following we will restrict our attention to the image plane. In this case, complete phase compensation is achieved when the lens is in the far field.

The far field limit of Eq. (66) can be obtained by substitution of Eq. (56) in Eq. (63). After calculating the inverse transformation of Eq. (54) one obtains:

$$G(z_i, \vec{r}_{1i}, \vec{r}_{2i}) = m^2 \exp \left[ \frac{im\omega}{2cz_1} \left( |\vec{r}_{1i}|^2 - |\vec{r}_{2i}|^2 \right) \right] G(0, -m\vec{r}_{1i}, -m\vec{r}_{2i}) . \quad (69)$$

Eq. (69) can also be obtained directly from Eq. (66) neglecting the second phase factor on the right hand side, that is possible when

$$\frac{m^2\omega}{2cz_1} \left( |\vec{r}_{1i}|^2 - |\vec{r}_{2i}|^2 \right) \ll 1 \quad (70)$$

for any pair of points  $(\vec{r}_{1i}, \vec{r}_{2i})$  on the image pattern. When the coherence length on the image plane is much smaller than the characteristic size of the image, condition (70) constitutes, similarly to condition (43) before (that holds in the case of coherent light), the requirement to be satisfied for the lens to

be in the far zone. When condition (70) is satisfied, Eq. (69) holds instead of Eq. (66). As explained in Section 2.2, in this paper we will study pupil effects only under this assumption.

Explicit substitution of Eq. (69) in Eq. (68) yields, the following far field limit expression:

$$G_P(z_i, \vec{r}_{1i}, \vec{r}_{2i}) = \exp \left[ \frac{i m \omega}{2 c z_1} (|\vec{r}_{1i}|^2 - |\vec{r}_{2i}|^2) \right] \int d\vec{u} d\vec{v} \mathcal{P} \left( \frac{\omega m \vec{r}_{1i}}{c z_1} - \vec{u} \right) \\ \times \mathcal{P}^* \left( \frac{\omega m \vec{r}_{2i}}{c z_1} - \vec{v} \right) G \left( 0, -\frac{c z_1 \vec{u}}{\omega}, -\frac{c z_1 \vec{v}}{\omega} \right), \quad (71)$$

that is the analogous of Eq. (45) in Section 2.2.2.

### 3 Image formation with a perfectly coherent undulator source

In order to give an explicit expression for the cross-spectral density at position  $z_2$  we need to know an explicit expression for the cross-spectral density  $G(z_1, \vec{r}'_1, \vec{r}'_2)$  *immediately in front* of the lens. This was the subject of our previous work [2]. In this and in the following Sections we will present the image formation problem and its solution with the help of that reference. In particular, in the present Section 3 we will begin with the simpler deterministic case of zero electron beam emittance. One may think of a filament electron beam or equivalently, as concerns the cross-spectral density, of a single electron. We will start neglecting the presence of the pupil. At the end we will generalize our results to account for it. In the following parts of this paper we will then generalize the results obtained in the present Section 3 to include emittance effects, thus taking full advantage of the Statistical Optics formulation.

Our starting point is an expression, derived in reference [2], for the complex envelope  $\tilde{E}_{s\perp}$  of the Fourier transform of the electric field produced by a single electron moving through a planar undulator at any distance from the exit of the undulator. That expression accounts for a given offset and deflection angle of the particle trajectory with respect to the undulator axis. Referring to Fig. 2 we found

$$\tilde{E}_{s\perp} = -\frac{K \omega e A_{JJ}}{c^2 \gamma} \int_{-L_w/2}^{L_w/2} dz' \frac{1}{z_o - z'} \\ \times \exp \left\{ i \left[ \left( C + \frac{\omega |\vec{\eta}|^2}{2c} \right) z' + \frac{\omega (\vec{r}_{\perp o} - \vec{l} - \vec{\eta} z')^2}{2c(z_o - z')} \right] \right\}. \quad (72)$$

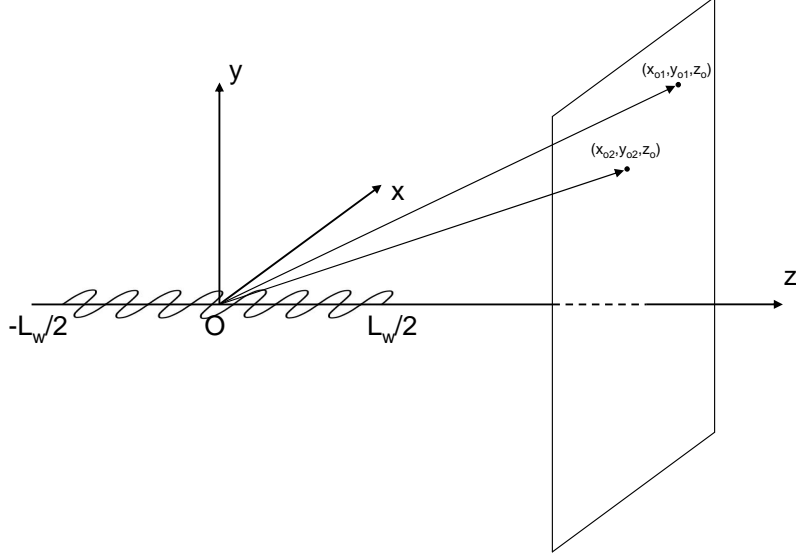


Fig. 2. Illustration of the undulator geometry and of the observation plane after the undulator.

Here  $K$  is the undulator parameter,  $L_w$ , as before, is the undulator length,  $(-e)$  is the electron charge and  $\gamma$  is the relativistic Lorentz factor. Moreover

$$A_{JJ} = J_0 \left( \frac{K^2}{4 + 2K^2} \right) - J_1 \left( \frac{K^2}{4 + 2K^2} \right), \quad (73)$$

$J_n$  being the Bessel function of the first kind of order  $n$ . Also,

$$\omega_o = \frac{4\pi c \gamma^2}{\lambda_w (1 + K^2/2)} \quad (74)$$

is the fundamental frequency of the undulator,  $\lambda_w$  being the undulator period. Finally,

$$C = \frac{2\pi}{\lambda_w} \frac{\omega - \omega_o}{\omega_o} \quad (75)$$

is the detuning parameter, which accounts for small deviations in frequency from resonance.

Eq. (72) is valid for frequencies about the fundamental harmonic  $\omega_o$ . This means that we are considering a large number of undulator periods  $N_w \gg 1$  and that we are looking at frequencies near the fundamental at angles within the main lobe of the directivity diagram of the radiation. In this situation one can neglect the vertical  $y$ -polarization component of the field with an accuracy  $(4\pi N_w)^{-1}$ . This constitutes a great simplification of the problem. At

any position of the observer, we may consider the temporal Fourier transform of the electric field as a complex scalar quantity corresponding to the surviving  $x$ -polarization component of the original vector quantity. Moreover it should be noted that, in deriving Eq. (72), we assumed that no influence of focusing is present inside the undulator.  $\vec{\eta}$  and  $\vec{l}$  are to be understood as deflection angles and offset of the electron at the position  $z = 0$ .

Let us introduce normalized units <sup>6</sup>

$$\begin{aligned}
\hat{E}_{s\perp} &= -\frac{c^2\gamma\tilde{E}_{s\perp}}{K\omega eA_{JJ}}, \\
\vec{\hat{\eta}} &= \vec{\eta}\sqrt{\frac{\omega L_w}{c}}, \\
\hat{C} &= L_w C = 2\pi N_w \frac{\omega - \omega_o}{\omega_o}, \\
\vec{\hat{r}}_{\perp o} &= \vec{r}_{\perp o} \sqrt{\frac{\omega}{L_w c}}, \\
\vec{\hat{l}} &= \vec{l} \sqrt{\frac{\omega}{L_w c}}, \\
\hat{z} &= \frac{z}{L_w}.
\end{aligned} \tag{76}$$

As shown in Appendix B of [2], after some algebraic manipulation, Eq. (72) can be rewritten in normalized units as

$$\hat{E}_{s\perp} = \int_{-1/2}^{1/2} \frac{d\hat{z}'}{\hat{z}_o - \hat{z}'} \exp \left\{ i \left[ \Phi_U + \hat{C}\hat{z}' + \frac{\hat{z}_o\hat{z}'}{2(\hat{z}_o - \hat{z}')} \left( \vec{\hat{\theta}} - \frac{\vec{\hat{l}}}{\hat{z}_o} - \vec{\hat{\eta}} \right)^2 \right] \right\}, \tag{77}$$

where

$$\vec{\hat{\theta}} = \frac{\vec{\hat{r}}_{\perp o}}{\hat{z}_o} \tag{78}$$

---

<sup>6</sup> The relation between  $\hat{E}_{s\perp}$  and  $\tilde{E}_{s\perp}$  in Eq. (76) differs from the analogous one in Eq. (25) of reference [2] for a factor  $\hat{z}_o = z_o/L_w$ . The reason for this discrepancy is related to the different subjects treated. In [2] we considered only the free space case, while in this paper we extend our considerations to an optical element, thus introducing another privileged longitudinal position (the lens position) other than the observation plane. The definition of  $\tilde{E}_{s\perp}$  in [2] is no more a convenient one here and would lead to artificial complications in the following parts of this paper. Therefore it has been slightly modified as in Eq. (76). This leads to slight changes (related with the factor  $\hat{z}_o$ ) in some of the following equations when compared to the analogous quantities in [2].

represents the observation angle and  $\Phi_U$  is given by

$$\Phi_U = \left( \vec{\theta} - \frac{\vec{l}}{\hat{z}_o} \right)^2 \frac{\hat{z}_o}{2} . \quad (79)$$

Eq. (77) is of the form

$$\hat{E}_{s\perp} \left( \hat{C}, \hat{z}_o, \vec{\theta} - \frac{\vec{l}}{\hat{z}_o} - \vec{\eta} \right) = \exp(i\Phi_U) S \left[ \hat{C}, \hat{z}_o, \left( \vec{\theta} - \frac{\vec{l}}{\hat{z}_o} - \vec{\eta} \right)^2 \right] . \quad (80)$$

It is possible to show that the expression for the function  $S(\cdot)$  reduces to a  $\text{sinc}(\cdot)$  function as  $\hat{z}_o \gg 1$ . In this limiting case, the expression for the electric field from a single particle, Eq. (77), is simplified to

$$\hat{E}_{s\perp} = \exp(i\Phi_U) \int_{-1/2}^{1/2} \frac{d\hat{z}'}{\hat{z}_o} \exp \left\{ i\hat{z}' \left[ \hat{C} + \frac{1}{2} \left( \vec{\theta} - \frac{\vec{l}_x}{\hat{z}_o} - \vec{\eta} \right)^2 \right] \right\} . \quad (81)$$

Eq. (81) can be integrated analytically giving

$$\hat{E}_{s\perp} = \exp(i\Phi_U) \frac{1}{\hat{z}_o} \text{sinc} \left( \frac{\hat{C}}{2} + \frac{\zeta^2}{4} \right) , \quad (82)$$

where

$$\zeta = \vec{\theta} - \frac{\vec{l}}{\hat{z}_o} - \vec{\eta} \quad (83)$$

and where the sinc function has been defined as

$$\text{sinc}(x) = \frac{\sin(x)}{x} . \quad (84)$$

For simplicity, in this paper we will restrict our attention to the case  $\hat{C} = 0$ . In the particular case  $\hat{C} = 0$ , the function  $S$  can be represented in terms of the exponential integral function  $\text{Ei}(\cdot)$  as

$$S(0, \hat{z}_o, \zeta^2) = \exp(-i\hat{z}_o\zeta^2/2) \left[ \text{Ei} \left( \frac{i\hat{z}_o^2\zeta^2}{-1 + 2\hat{z}_o} \right) - \text{Ei} \left( \frac{i\hat{z}_o^2\zeta^2}{1 + 2\hat{z}_o} \right) \right] . \quad (85)$$

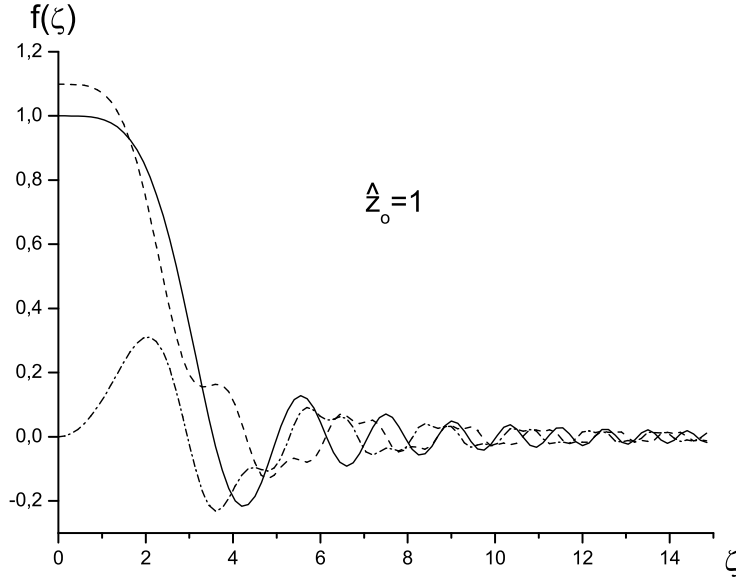


Fig. 3. Comparison between  $f(\zeta) = \text{sinc}(\zeta^2/4)$  (solid line), the real (dashed line) and the imaginary (dash-dotted line) parts of  $f(\zeta) = \hat{z}_o S(0, \hat{z}_o, \zeta^2)$  at  $\hat{z}_o = 1$ .

It is interesting to study the behavior of the  $S$  function as the distance from the undulator center  $\hat{z}_o$  increases. This gives an idea of how good the asymptotic approximation of the  $S$  function for  $\hat{z}_o \gg 1$  (that is a sinc function) is. A comparison between  $\text{sinc}(\zeta^2/4)$  and the real and imaginary parts of  $\hat{z}_o S(0, \hat{z}_o, \zeta^2)$  for  $\hat{z}_o = 1$ ,  $\hat{z}_o = 2$ ,  $\hat{z}_o = 5$  and  $\hat{z}_o = 10$  is given respectively in Fig. 3, Fig. 4, Fig. 5 and Fig. 6.

When the electron beam has zero emittance we are dealing with a perfectly coherent wavefront. The evolution of the radiation wavefront through our optical system can be obtained with the help of Eq. (80). In the following we will study such evolution assuming  $\hat{C} = 0$ ,  $\vec{\hat{l}} = 0$  and  $\vec{\hat{\eta}} = 0$ . These assumptions mean that the radiation frequency is perfectly tuned to the fundamental frequency of the undulator and that the electron beam is moving on the  $z$  axis. In this case Eq. (82) describes, in the far field region, a spherical wave with the source in the center of the undulator. This remark allows one to consider the undulator center as a privileged point. In other words, the phase factor in Eq. (82) represents, in paraxial approximation, the phase difference (characterizing a spherical wave) between the point  $(\hat{x}_o, \hat{y}_o, \hat{z}_o)$  and the point  $(0, 0, \hat{z}_o)$  on the observation plane.

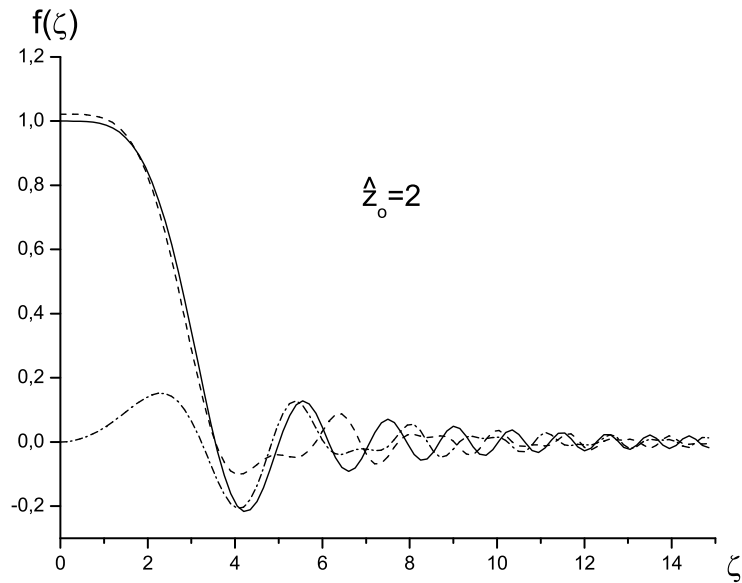


Fig. 4. Comparison between  $f(\zeta) = \text{sinc}(\zeta^2/4)$  (solid line), the real (dashed line) and the imaginary (dash-dotted line) parts of  $f(\zeta) = \hat{z}_o S(0, \hat{z}_o, \zeta^2)$  at  $\hat{z}_o = 2$ .

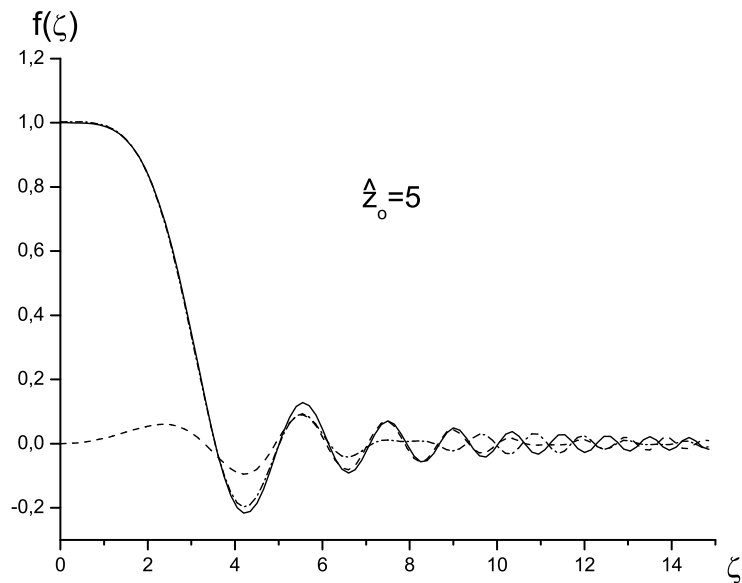


Fig. 5. Comparison between  $f(\zeta) = \text{sinc}(\zeta^2/4)$  (solid line), the real (dashed line) and the imaginary (dash-dotted line) parts of  $f(\zeta) = \hat{z}_o S(0, \hat{z}_o, \zeta^2)$  at  $\hat{z}_o = 5$ .

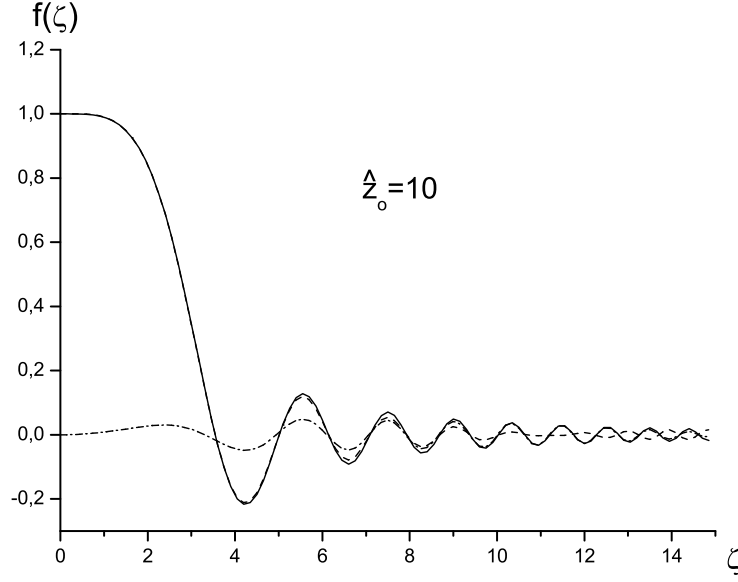


Fig. 6. Comparison between  $f(\zeta) = \text{sinc}(\zeta^2/4)$  (solid line), the real (dashed line) and the imaginary (dash-dotted line) parts of  $f(\zeta) = \hat{z}_o S(0, \hat{z}_o, \zeta^2)$  at  $\hat{z}_o = 10$ .

### 3.1 Large non-limiting aperture

We will first study the case when the pupil function can be neglected. Let us introduce a normalized version of the spatial Fourier transform of the field, analogous to Eq. (14), that is

$$\hat{F}(\hat{z}, \vec{u}) = \int d\vec{r}' \hat{E}(\hat{z}, \vec{r}') \exp[i\vec{r}' \cdot \vec{u}] . \quad (86)$$

The spatial Fourier transform  $\hat{F}(\hat{z}, \vec{u})$  can be calculated directly from Eq. (77) (compare also with Eq. (184) of reference [2]) and gives

$$\hat{F}(\hat{z}, \vec{u}) = -2\pi i \text{sinc}\left(\frac{|\vec{u}|^2}{4}\right) \exp\left[-\frac{i|\vec{u}|^2 \hat{z}}{2}\right] . \quad (87)$$

Eq. (28) and Eq. (34) can be respectively rewritten in normalized units as

$$\hat{E}_\perp(\hat{z}_f, \vec{r}_f) = \frac{i}{2\pi \hat{f}} \exp\left[\frac{i|\vec{r}_f|^2}{2\hat{f}}\right] \hat{F}\left(\hat{z}_1, -\frac{\vec{r}_f}{\hat{f}}\right) \quad (88)$$

and

$$\hat{E}_\perp(\hat{z}_i, \vec{r}_i) = \frac{m}{4\pi^2} \exp\left[\frac{im|\vec{r}_i|^2}{2\hat{z}_1}\right] \int d\vec{u} \hat{F}(\hat{z}_1, \vec{u}) \exp\left[\frac{i\hat{z}_1}{2} \left(-\frac{m\vec{r}_i}{\hat{z}_1} - \vec{u}\right)^2\right], \quad (89)$$

where  $\hat{f} = f/L_w$ . Substitution of Eq. (87) in Eq. (88) and in Eq. (89) yields results respectively for the focal and the image plane. In the focal plane we have

$$\hat{E}_\perp(\hat{z}_f, \vec{r}_f) = \frac{1}{\hat{f}} \exp\left[\frac{i|\vec{r}_f|^2}{2\hat{f}}\right] \exp\left[-\frac{i\hat{z}_1|\vec{r}_f|^2}{2\hat{f}^2}\right] \text{sinc}\left(\frac{|\vec{r}_f|^2}{4\hat{f}^2}\right). \quad (90)$$

Note that the relative distribution of intensity in the focus reproduces the angular distribution of intensity in the far field, that is

$$\hat{I}(\hat{r}_f) = \text{sinc}^2\left(\frac{|\vec{r}_f|^2}{4\hat{f}^2}\right). \quad (91)$$

A plot of the universal function  $\text{sinc}^2(\alpha^2/4)$  is given in Fig. 7. Note that all expressions pertaining undulator radiation from a single electron are azimuthal symmetric but do not admit factorization in the product of functions separately depending on the  $x$  and the  $y$  coordinates. As we have shown in [2], the absence of factorization leads to an influence of the presence of the horizontal emittance on the coherent properties of undulator radiation in the vertical direction. As a result, even in the case of zero vertical emittance one cannot have perfect coherence in the vertical direction.

For the image plane we obtain:

$$\begin{aligned} \hat{E}_\perp(\hat{z}_i, \vec{r}_i) &= -\frac{im}{2\pi} \exp\left[\frac{im|\vec{r}_i|^2}{2\hat{z}_1}\right] \exp\left[\frac{im^2|\vec{r}_i|^2}{2\hat{z}_1}\right] \\ &\times \int d\vec{u} \text{sinc}\left(\frac{|\vec{u}|^2}{4}\right) \exp\left[im\vec{r}_i \cdot \vec{u}\right]. \end{aligned} \quad (92)$$

As already seen in Eq. (190) of [2] (Appendix C), the Fourier transform in Eq. (92) can be calculated in terms of a Fourier-Bessel transform:

$$\int d\vec{u} \text{sinc}\left(\frac{|\vec{u}|^2}{4}\right) \exp\left[im\vec{r}_i \cdot \vec{u}\right] = 2\pi \int_0^\infty du u J_0(m|\vec{r}_i|u) \text{sinc}\left(\frac{u^2}{4}\right)$$

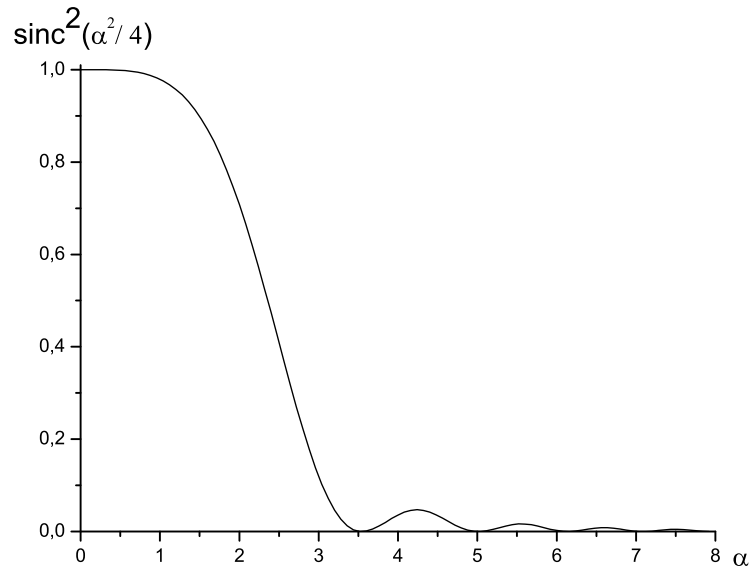


Fig. 7. Universal function  $\text{sinc}^2(\alpha^2/4)$  used to calculate (according to Eq. (91)) the focal intensity of a single electron at the fundamental harmonic at perfect resonance.

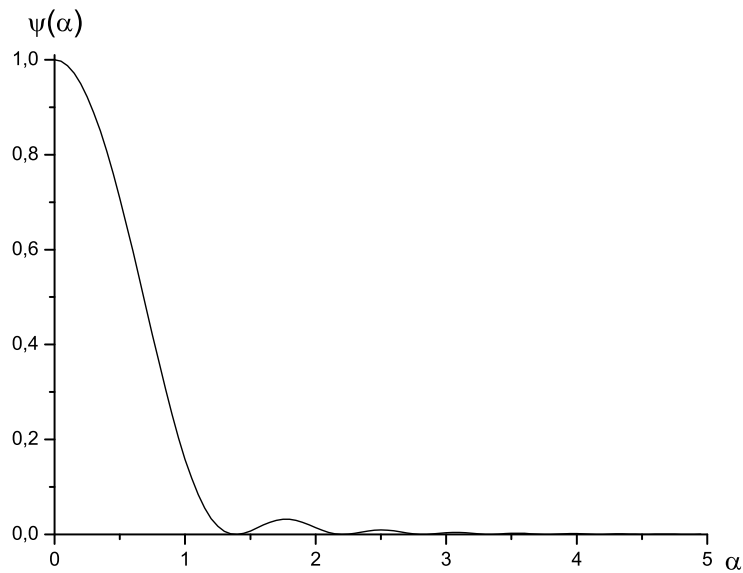


Fig. 8. Universal function  $\Psi(\alpha)$  used to calculate (according to Eq. (96)) the intensity distribution on the image plane from a single electron at the fundamental harmonic at perfect resonance.

$$= 2\pi \left[ \pi - 2\text{Si} \left( m^2 |\vec{r}_i|^2 \right) \right] . \quad (93)$$

Eq. (92) can now be written as

$$\hat{E}_\perp(\hat{z}_i, \vec{r}_i) = -im \exp \left[ \frac{im |\vec{r}_i|^2}{2\hat{z}_1} \right] \exp \left[ \frac{im^2 |\vec{r}_i|^2}{2\hat{z}_1} \right] \cdot \left[ \pi - 2\text{Si} \left( m^2 |\vec{r}_i|^2 \right) \right] . \quad (94)$$

It is convenient to introduce the following universal function normalized to unity:

$$\Psi(\alpha) = \frac{1}{\pi^2} \left[ \pi - 2\text{Si} \left( \alpha^2 \right) \right]^2 \quad (95)$$

The relative intensity on the image plane is related to the universal function  $\Psi$  through the scaling factor  $m$ :

$$\hat{I} \left( |\vec{r}_i| \right) = \Psi \left( m |\vec{r}_i| \right) . \quad (96)$$

A plot of the universal function  $\Psi(\alpha)$  is given in Fig. 8.

Comparison of Eq. (94) with Eq. (36) allows one to conclude that the equivalent source for a single electron moving on the  $z$  axis is a source characterized by a plane wavefront and an intensity distribution related to the universal function  $\Psi$ , that can be written as

$$\hat{E}_\perp(0, \vec{r}) = -i \left[ \pi - 2\text{Si} \left( |\vec{r}|^2 \right) \right] . \quad (97)$$

By means of an inverse Fourier transformation it follows that

$$\hat{F} \left( 0, \vec{u} \right) = -2\pi i \text{sinc} \left( \frac{|\vec{u}|^2}{4} \right) , \quad (98)$$

in agreement with Eq. (87). Comparison of Eq. (97) with a normalized version of Eq. (20) show that the phase of the field of the virtual source is shifted of a quantity  $-\pi/2$  with respect to the spherical wave in the far zone. Such phase shift is the analogous of the Guoy phase shift in laser physics. A single electron produces a laser-like radiation beam that has a (virtual) waist much larger than the radiation wavelength located in the center of the undulator.

The intensity distribution from the most elementary undulator source, i.e. the radiation from a single electron (or, equivalently, from an electron beam with

zero emittance) was just described analytically. Such analytical description, Eq. (96), can immediately be applied in situations of practical relevance. In [10, 11] a characterization of the vertical emittance in Spring-8 is reported. It is based on the measurement of the X-Ray beam coherence length in the far zone. The experiment was performed at the beamline BL29XU. Based on the assumption of validity of the van Cittert-Zernike theorem, it was found that the rms electron beam size at the undulator center (corresponding to the minimal value of the beta function) was  $s_y \simeq 4.5 \mu\text{m}$ , and that the coupling factor between horizontal and vertical emittance was down to the value  $\chi \simeq 0.12\%$ , which corresponds to an extremely small vertical emittance  $\epsilon_y = 3.6 \text{ pm}\cdot\text{rad}$ . A resolution limit of this method was also discussed, based on numerical calculations of the radiation size from a single electron  $s_p \simeq 1.6 \mu\text{m}$  at  $E_p = 14.41 \text{ keV}$  for the 4.5 m long undulator used in the experiment. The resolution limit of the measurement of  $s_y$  was estimated to be about  $1 \mu\text{m}$ .

Based on Eq. (96), we can determine the virtual source size of undulator radiation from a single electron. Let us consider the case when the single electron is emitting photons at the fundamental harmonic with energy  $E = 14.41 \text{ keV}$ . The angular frequency of light oscillations is given, in this case, by  $\omega = 2.2 \cdot 10^{19} \text{ Hz}$ . For an undulator length  $L_w = 4.5 \text{ m}$ , the normalization factor for the transverse size introduced in Eq. (76),  $(L_w c/\omega)^{1/2}$ , is about  $8 \mu\text{m}$ . From Fig. 8 obtain the dimensionless Half Width Half Maximum (HWHM) radiation size from a single electron (i.e. the HWHM width of the intensity distribution at the virtual source, located at the center of the undulator). This HWHM dimensionless value is about 0.7. It follows that the HWHM value of the radiation spot size from a single electron is about  $0.7 \cdot (cL_w/\omega)^{1/2} \simeq 6 \mu\text{m}$ . Therefore, the rms value  $s_p \simeq 1.6 \mu\text{m}$  in [10, 11], which was calculated numerically [12], is an underestimation of the correct value.

Note that the HWHM radiation spot size from a *single electron* is larger than the *rms electron beam size*  $s_y \simeq 4.5 \mu\text{m}$  found by means of coherence measurements. One concludes that the uncertainty due to finite resolution is larger than the measured electron beam size. This suggests that the method used in [10, 11] may be inconsistent. Such inconsistency may be traced to the fact that authors of [10, 11] assume the validity of the van Cittert-Zernike theorem in the vertical direction. If one assumes their result of a vertical emittance  $\epsilon_y \simeq 0.3\lambda/(2\pi)$ , it follows *a posteriori* that the van Cittert-Zernike theorem could not have been applied in first instance (in this experiment the value of the beta function was  $\beta \simeq L_w$ ). Hence the inconsistency of the method follows. Analysis of experimental results should have been based, instead, on the study of transverse coherence for non-homogeneous undulator sources in free space made in [2].

### 3.2 Effect of aperture size

The effects due to the presence of the pupil can be included in the treatment by means of a normalized version of Eq. (40) and Eq. (41) on the focal plane

$$\begin{aligned} \hat{E}_P(\hat{z}_f, \vec{r}_f) = & \exp \left[ \frac{i|\vec{r}_f|^2}{2\hat{f}} \right] \\ & \times \int d\vec{u} \hat{\mathcal{P}} \left( \frac{\vec{r}_f}{\hat{f}} - \vec{u} \right) \cdot \exp \left[ -\frac{i\hat{f}|\vec{u}|^2}{2} \right] \hat{E}_\perp(\hat{z}_f, \hat{f}\vec{u}) , \end{aligned} \quad (99)$$

and on the image plane

$$\begin{aligned} \hat{E}_P(\hat{z}_i, \vec{r}_i) = & \exp \left[ \frac{im|\vec{r}_i|^2}{2\hat{z}_1} \right] \\ & \times \int d\vec{u} \hat{\mathcal{P}} \left( \frac{m\vec{r}_i}{\hat{z}_1} - \vec{u} \right) \cdot \exp \left[ -\frac{i\hat{z}_1|\vec{u}|^2}{2m} \right] \hat{E}_\perp \left( z_i, \frac{\hat{z}_1\vec{u}}{m} \right) , \end{aligned} \quad (100)$$

where

$$\hat{\mathcal{P}}(\vec{u}) = \int d\vec{r}' P(\vec{r}') \exp \left[ -i\vec{r}' \cdot \vec{u} \right] . \quad (101)$$

Eq. (100) is valid independently of the position of the lens. However, as explained in Section 2.2 and in Section 2.4 we will limit ourselves to the case when the lens is in the far zone. From Eq. (96) we see that the characteristic size of the source is of order unity, because  $\Psi$  is a universal function. As a result, the far field zone for a single particle is defined by the condition

$$\hat{z}_1 \gg 1 . \quad (102)$$

By substitution of Eq. (20) in Eq. (26), followed by use of the lens equation Eq. (30) and normalization, one obtains an expression for the field valid in the case the lens is placed in the far zone. Such expression is equivalent, in that limit, to Eq. (100). If the pupil function is not set to unity, we have

$$\begin{aligned} \hat{E}_P(\hat{z}_i, \vec{r}_i) = & -\frac{m}{4\pi^2\hat{z}_1^2} \exp \left[ \frac{im|\vec{r}_i|^2}{2\hat{z}_1} \right] \\ & \times \int d\vec{r}' \hat{F} \left( 0, -\frac{\vec{r}'}{\hat{z}_1} \right) P(\vec{r}') \exp \left[ -\frac{im(\vec{r}_i \cdot \vec{r}')}{\hat{z}_1} \right] . \end{aligned}$$

(103)

Eq. (103) can also be obtained by substitution of Eq. (89) in Eq. (100) followed by application of the convolution theorem.

In the far field case Eq. (100) (or Eq. (103)) can be more easily used to calculate the effects of the pupil on the intensity. A natural example to study is the case of a lens with azimuthal symmetry and no aberrations. Consider a pupil of radius  $a$ . After introduction of the normalized pupil radius:

$$\hat{a} = a \sqrt{\frac{\omega}{L_w c}} \quad (104)$$

we set the pupil function:

$$P(\vec{r}) = \begin{cases} 1 & \text{if } |\vec{r}| < \hat{a} \\ 0 & \text{otherwise .} \end{cases} \quad (105)$$

Using the Fourier-Bessel transform one obtains

$$\hat{\mathcal{P}}(\vec{u}) = \frac{2\pi\hat{a}}{|\vec{u}|} J_1(\hat{a}|\vec{u}|) . \quad (106)$$

Substitution of Eq. (94) in Eq. (100) and use of the far zone assumption leads to

$$\begin{aligned} \hat{E}_P(\hat{z}_i, \vec{r}_i) &= -2\pi i m \hat{a} \exp \left[ \frac{i m |\vec{r}_i|^2}{2\hat{z}_1} \right] \\ &\times \int d\vec{u} \left| \frac{m\vec{r}_i}{\hat{z}_1} - \vec{u} \right|^{-1} J_1 \left( \hat{a} \left| \frac{m\vec{r}_i}{\hat{z}_1} - \vec{u} \right| \right) \left[ \pi - 2\text{Si}(\hat{z}_1^2 |\vec{u}|^2) \right] . \end{aligned} \quad (107)$$

Eq. (107) is, essentially, the convolution product of the Fourier transform of two known functions with circular symmetry. Therefore, recalling Eq. (93) and Eq. (105), Eq. (107) can be written in terms of the following Fourier-Bessel transform:

$$\hat{E}_P(\hat{z}_i, \vec{r}_i) = -i \exp \left[ \frac{i m |\vec{r}_i|^2}{2\hat{z}_1} \right] \int_0^{\hat{a}/\hat{z}_1} d\hat{u} \hat{u} J_0(m|\vec{r}_i|\hat{u}) \text{sinc} \left( \frac{\hat{u}^2}{4} \right) . \quad (108)$$

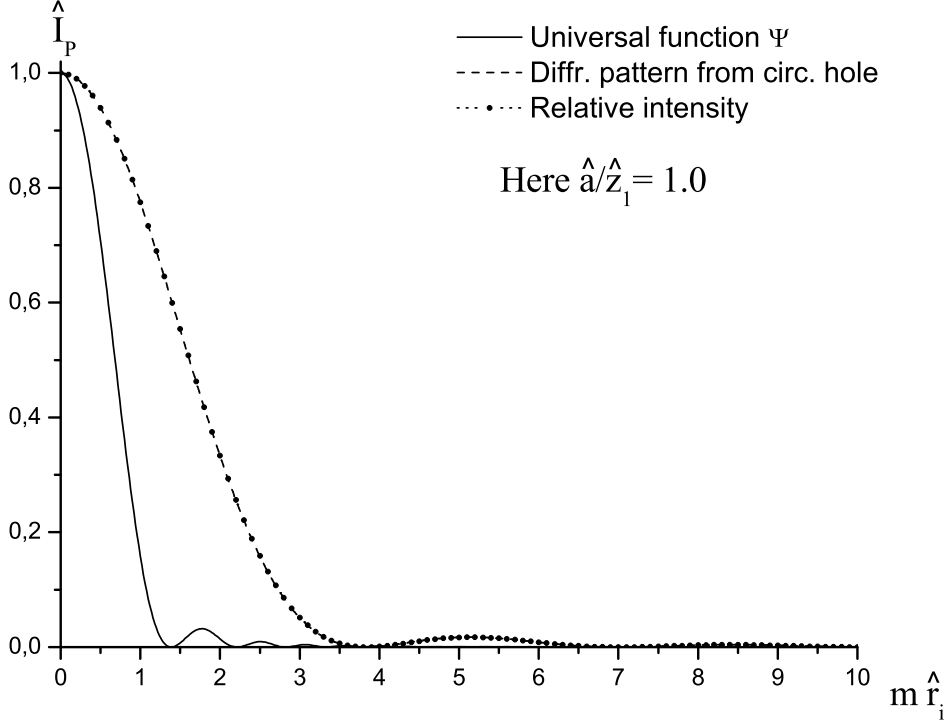


Fig. 9. Comparison between the relative intensity for a single electron at the image plane  $\hat{I}_P$ , Eq. (109), the universal function  $\Psi$ , Eq. (96), and the (Airy) diffraction pattern from a circular hole, Eq. (110), as a function of  $m\hat{r}_i$ . Here  $\hat{a}/\hat{z}_1 = 1$ .

Eq. (108) can also be directly obtained using the Fourier-Bessel integration formula and Eq. (103). Eq. (108) corresponds to a relative intensity

$$\hat{I}_P(|\vec{r}_i|) = \frac{1}{4} \left[ \text{Si} \left( \frac{\hat{a}^2}{4\hat{z}_1^2} \right) \right]^{-2} \left| \int_0^{\hat{a}/\hat{z}_1} d\hat{u} \hat{u} J_0(m|\vec{r}_i|\hat{u}) \text{sinc} \left( \frac{\hat{u}^2}{4} \right) \right|^2. \quad (109)$$

In the limit  $\hat{a}/\hat{z}_1 \gg 1$  Eq. (108) gives back Eq. (94) without the second phase factor, and Eq. (109) gives back Eq. (96) as it should be.

When  $\hat{a}/\hat{z}_1 \ll 1$  the  $\text{sinc}(\cdot)$  drops out of the integral in Eq. (109) giving the diffraction pattern from a circular hole:

$$\hat{I}_P(|\vec{r}_i|) = \frac{4\hat{z}_1^4}{\hat{a}^4} \left| \int_0^{\hat{a}/\hat{z}_1} d\hat{u} \hat{u} J_0(m|\vec{r}_i|\hat{u}) \right|^2 = \frac{4\hat{z}_1^2}{\hat{a}^2 m^2 |\vec{r}_i|^2} J_1^2 \left( \frac{\hat{a} m \hat{r}_i}{\hat{z}_1} \right). \quad (110)$$

Further, analysis of Fig. 9 actually shows that Eq. (110) retains its validity

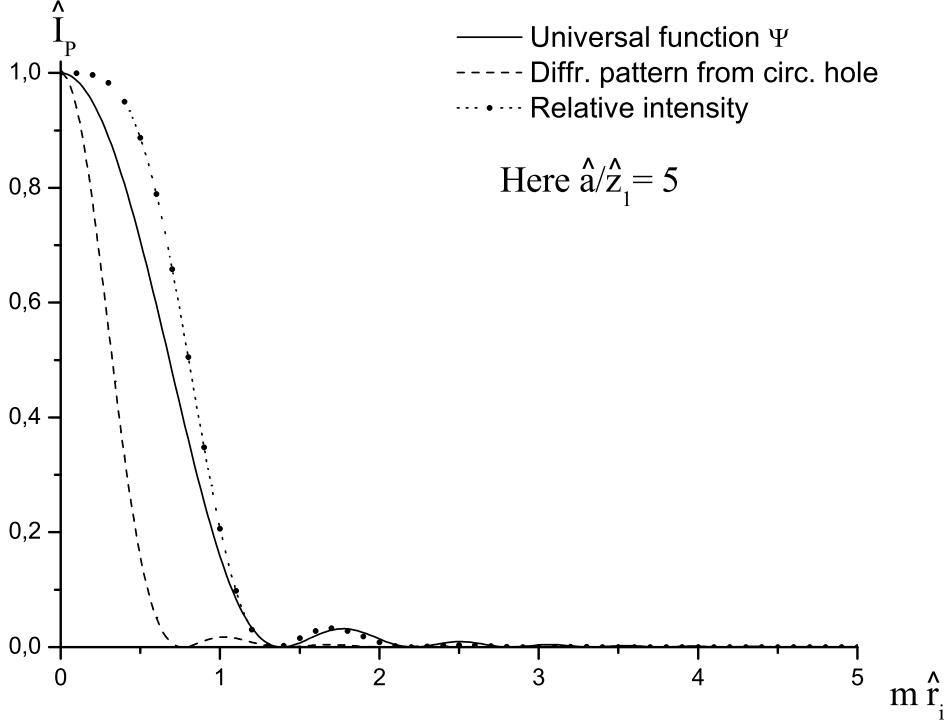


Fig. 10. Comparison between the relative intensity for a single electron at the image plane  $\hat{I}_P$ , Eq. (109), the universal function  $\Psi$ , Eq. (96), and the (Airy) diffraction pattern from a circular hole, Eq. (110), as a function of  $m\hat{r}_i$ . Here  $\hat{a}/\hat{z}_1 = 5$ .

also for  $\hat{a}/\hat{z}_1 \lesssim 1$ .

Comparisons between the relative intensity  $\hat{I}_P$ , Eq. (109), the universal function  $\Psi$ , Eq. (96), and the diffraction pattern from a circular hole, Eq. (110), are plotted as a function of  $m\hat{r}_i$  in Fig. (9) for  $\hat{a}/\hat{z}_1 = 1$ , in Fig. (10) for  $\hat{a}/\hat{z}_1 = 5$  and in Fig. (11) for  $\hat{a}/\hat{z}_1 = 10$ .

## 4 Image formation with partially coherent undulator source

### 4.1 Coherence properties of undulator source in the presence of electron beam emittance

In the last Section we dealt with the image formation problem in the case of a filament beam, i.e. when the electron beam emittance is zero. In this Section we will generalize the previous results to the case when the electron beam has finite emittance. In this situation, methods from Statistical Optics must

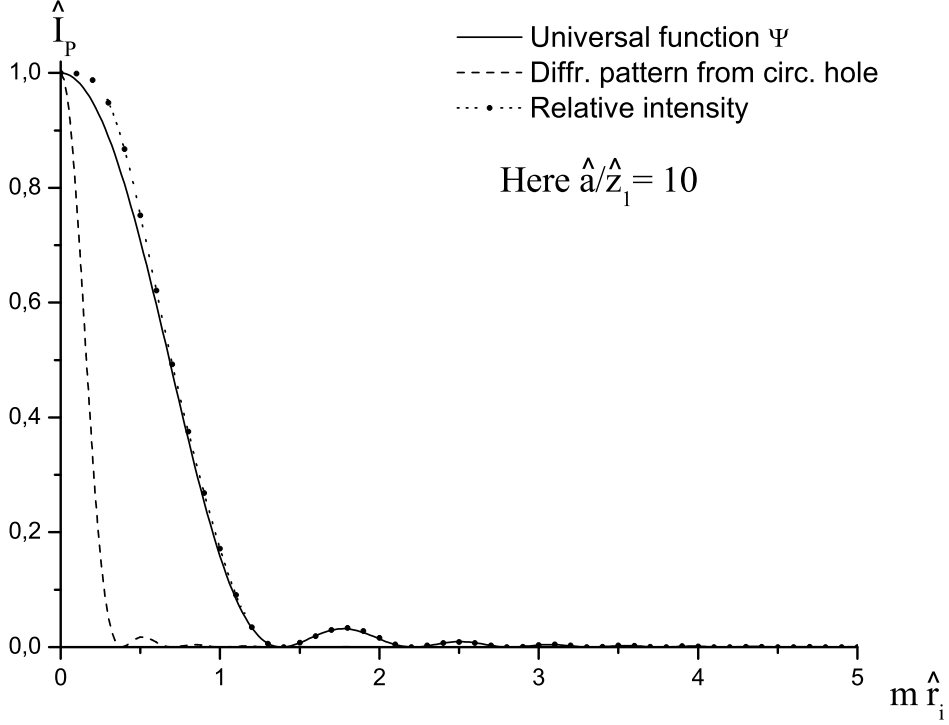


Fig. 11. Comparison between the relative intensity for a single electron at the image plane  $\hat{I}_P$ , Eq. (109), the universal function  $\Psi$ , Eq. (96), and the (Airy) diffraction pattern from a circular hole, Eq. (110), as a function of  $m\hat{r}_i$ . Here  $\hat{a}/\hat{z}_1 = 10$ .

be applied in order to solve the image formation problem. As discussed before, the cross-spectral density of an undulator source must first be calculated at the lens position and subsequently propagated through the lens and the forthcoming optical beamline up to the experimental plane.

In [2] we proposed a method, based on Eq. (77), to calculate the cross-spectral density from undulator sources at any position in free space after the undulator. Let us follow [2] and use Eq. (77) to calculate the cross-spectral density. The cross-spectral density  $G$  is given, in dimensional units and as a function of dimensional variables, by Eq. (51). Since the field in Eq. (77) is given in normalized units and as a function of normalized variables  $\hat{z}_o$ ,  $\vec{\hat{\theta}}_{x,y}$  and  $\hat{C}$ , it is convenient to introduce a version of  $G$  defined by means of the field in normalized units

$$\hat{G}(\hat{z}_o, \vec{\hat{\theta}}_1, \vec{\hat{\theta}}_2, \hat{C}) = \left\langle \hat{E}_{s\perp} \left( \hat{C}, \hat{z}_o, \vec{\hat{\theta}}_1 - \frac{\vec{\hat{l}}}{\hat{z}_o} - \vec{\hat{\eta}} \right) \right\rangle$$

$$\times \hat{E}_{s\perp}^* \left( \hat{C}, \hat{z}_o, \vec{\theta}_2 - \frac{\vec{l}}{\hat{z}_o} - \vec{\eta} \right) \Bigg\rangle_{\vec{\eta}, \vec{l}}. \quad (111)$$

Transformation of  $G$  in Eq. (51) to  $\hat{G}$  (and viceversa) can be performed shifting from dimensional to normalized variables and multiplying  $G$  by an inessential factor

$$\hat{G} = \left( \frac{c^2 \gamma}{K w e A_{JJ}} \right)^2 G. \quad (112)$$

Substituting Eq. (80) in Eq. (111) we obtain

$$\begin{aligned} \hat{G}(\hat{z}_o, \vec{\theta}_1, \vec{\theta}_2, \hat{C}) = & \left\langle S \left[ \hat{C}, \hat{z}_o, \left( \vec{\theta}_1 - \frac{\vec{l}}{\hat{z}_o} - \vec{\eta} \right)^2 \right] S^* \left[ \hat{C}, \hat{z}_o, \left( \vec{\theta}_2 - \frac{\vec{l}}{\hat{z}_o} - \vec{\eta} \right)^2 \right] \right. \\ & \left. \times \exp \left\{ i \left[ \left( \vec{\theta}_1 - \frac{\vec{l}}{\hat{z}_o} \right)^2 - \left( \vec{\theta}_2 - \frac{\vec{l}}{\hat{z}_o} \right)^2 \right] \frac{\hat{z}_o}{2} \right\} \right\rangle_{\vec{\eta}, \vec{l}}. \quad (113) \end{aligned}$$

Expanding the exponent in the exponential factor in the right hand side of Eq. (113), one can see that terms in  $\hat{l}_{x,y}^2$  cancel out. Terms in  $\hat{\theta}_{x,y}^2$  contribute for a common factor, and only linear terms in  $\hat{l}_{x,y}$  remain inside the ensemble average sign. Substitution of the ensemble average with integration over the beam distribution function leads to

$$\begin{aligned} \hat{G}(\hat{z}_o, \vec{\theta}_1, \vec{\theta}_2, \hat{C}) = & \exp \left[ i \left( \vec{\theta}_1 - \vec{\theta}_2 \right) \frac{\hat{z}_o}{2} \right] \int d\vec{\eta} d\vec{l} F_{\vec{\eta}, \vec{l}}(\vec{\eta}, \vec{l}) \\ & \times \exp \left[ i (\vec{\theta}_2 - \vec{\theta}_1) \cdot \vec{l} \right] S \left[ \hat{C}, \hat{z}_o, \left( \vec{\theta}_1 - \frac{\vec{l}}{\hat{z}_o} - \vec{\eta} \right)^2 \right] \\ & \times S^* \left[ \hat{C}, \hat{z}_o, \left( \vec{\theta}_2 - \frac{\vec{l}}{\hat{z}_o} - \vec{\eta} \right)^2 \right]. \quad (114) \end{aligned}$$

Here integrals  $d\vec{\eta}$  and  $d\vec{l}$  are to be intended as integrals over the entire plane spanned by the  $\vec{\eta}$  and  $\vec{l}$  vectors. Eq. (114) is very general and can be used as a starting point for computer simulations.

We assume that the distribution in the horizontal and vertical planes are not correlated, so that  $F_{\vec{\eta}, \vec{l}} = F_{\hat{\eta}_x, \hat{l}_x} F_{\hat{\eta}_y, \hat{l}_y}$ . If the transverse phase-space is specified at the virtual-source position  $\hat{z}_o = 0$  corresponding to the minimal values of the beta functions, we can write  $F_{\hat{\eta}_x, \hat{l}_x} = F_{\hat{\eta}_x} F_{\hat{l}_x}$  and  $F_{\hat{\eta}_y, \hat{l}_y} = F_{\hat{\eta}_y} F_{\hat{l}_y}$  with

$$\begin{aligned}
F_{\hat{\eta}_x}(\hat{\eta}_x) &= \frac{1}{\sqrt{2\pi\hat{D}_x}} \exp\left(-\frac{\hat{\eta}_x^2}{2\hat{D}_x}\right), \\
F_{\hat{\eta}_y}(\hat{\eta}_y) &= \frac{1}{\sqrt{2\pi\hat{D}_y}} \exp\left(-\frac{\hat{\eta}_y^2}{2\hat{D}_y}\right), \\
F_{\hat{l}_x}(\hat{l}_x) &= \frac{1}{\sqrt{2\pi\hat{N}_x}} \exp\left(-\frac{\hat{l}_x^2}{2\hat{N}_x}\right), \\
F_{\hat{l}_y}(\hat{l}_y) &= \frac{1}{\sqrt{2\pi\hat{N}_y}} \exp\left(-\frac{\hat{l}_y^2}{2\hat{N}_y}\right).
\end{aligned} \tag{115}$$

From Eq. (76) and Eq. (78) it is possible to see that

$$\hat{D}_{x,y} = \sigma_{x',y'}^2 \frac{\omega L_w}{c} \tag{116}$$

$$\hat{N}_{x,y} = \sigma_{x,y}^2 \frac{\omega}{c L_w} \tag{117}$$

where  $\sigma_{x,y}$  and  $\sigma_{x',y'}$  are the rms transverse bunch dimension and angular spread. Parameters  $\hat{N}_{x,y}$  will be indicated as the beam diffraction parameters and are analogous to Fresnel numbers. They correspond to the normalized square of the electron beam sizes.  $\hat{D}_{x,y}$  represent the normalized square of the electron beam divergences instead. It is also convenient to introduce the square of the apparent angular size of the electron beam at the observer point position  $\hat{z}_o$ , that is

$$\hat{A}_{x,y} = \frac{\hat{N}_{x,y}}{\hat{z}_o^2}. \tag{118}$$

Substitution of relations (115) in Eq. (114) yields<sup>7</sup> at perfect resonance ( $\hat{C} = 0$ ):

$$\hat{G}(\hat{z}_o, \vec{\theta}_1, \vec{\theta}_2) = \frac{\exp\left[i\left(\vec{\theta}_1^2 - \vec{\theta}_2^2\right)\hat{z}_o/2\right]}{4\pi^2\sqrt{\hat{D}_x\hat{D}_y\hat{N}_x\hat{N}_y}} \int_{-\infty}^{\infty} d\hat{\eta}_x \exp\left(-\frac{\hat{\eta}_x^2}{2\hat{D}_x}\right)$$

<sup>7</sup> In Eq. (119), for notational simplicity we substituted the proper notation  $\hat{G}(\hat{z}_o, \vec{\theta}_1, \vec{\theta}_2, \hat{C})$  with the simplified dependence  $\hat{G}(\hat{z}_o, \vec{\theta}_1, \vec{\theta}_2)$ . This is justified because we will be treating the case  $\hat{C} = 0$  only. Consistently, also  $S[\hat{z}_o, (\vec{\theta} - \vec{l}/\hat{z}_o - \vec{\eta})^2]$  is to be understood as a shortcut notation for  $S[\hat{C}, \hat{z}_o, (\vec{\theta} - \vec{l}/\hat{z}_o - \vec{\eta})^2]$  calculated at  $\hat{C} = 0$ .

$$\begin{aligned}
& \times \int_{-\infty}^{\infty} d\hat{\eta}_y \exp\left(-\frac{\hat{\eta}_y^2}{2\hat{D}_y}\right) \int_{-\infty}^{\infty} d\hat{l}_x \exp\left(-\frac{\hat{l}_x^2}{2\hat{N}_x}\right) \\
& \times \int_{-\infty}^{\infty} d\hat{l}_y \exp\left(-\frac{\hat{l}_y^2}{2\hat{N}_y}\right) \exp\left[i(\vec{\theta}_2 - \vec{\theta}_1) \cdot \vec{l}\right] \\
& \times S\left[\hat{z}_o, \left(\vec{\theta}_1 - \frac{\vec{l}}{\hat{z}_o} - \vec{\eta}\right)^2\right] S^*\left[\hat{z}_o, \left(\vec{\theta}_2 - \frac{\vec{l}}{\hat{z}_o} - \vec{\eta}\right)^2\right]. \quad (119)
\end{aligned}$$

Let us now introduce<sup>8</sup>

$$\Delta\hat{\theta}_x = \frac{\hat{\theta}_{x1} - \hat{\theta}_{x2}}{2}, \quad \bar{\theta}_x = \frac{\hat{\theta}_{x1} + \hat{\theta}_{x2}}{2} \quad (120)$$

and

$$\Delta\hat{\theta}_y = \frac{\hat{\theta}_{y1} - \hat{\theta}_{y2}}{2}, \quad \bar{\theta}_y = \frac{\hat{\theta}_{y1} + \hat{\theta}_{y2}}{2}. \quad (121)$$

With this variables redefinition we obtain

$$\hat{G} = \hat{G}(\hat{z}_o, \bar{\theta}_x, \bar{\theta}_y, \Delta\hat{\theta}_x, \Delta\hat{\theta}_y) \quad (122)$$

and, explicitly,

$$\begin{aligned}
\hat{G} &= \frac{\exp\left[i2\hat{z}_o(\bar{\theta}_x\Delta\hat{\theta}_x + \bar{\theta}_y\Delta\hat{\theta}_y)\right]}{4\pi^2\sqrt{\hat{D}_x\hat{D}_y\hat{N}_x\hat{N}_y}} \int_{-\infty}^{\infty} d\hat{\eta}_x \exp\left(-\frac{\hat{\eta}_x^2}{2\hat{D}_x}\right) \\
& \times \int_{-\infty}^{\infty} d\hat{\eta}_y \exp\left(-\frac{\hat{\eta}_y^2}{2\hat{D}_y}\right) \int_{-\infty}^{\infty} d\hat{l}_x \exp\left(-\frac{\hat{l}_x^2}{2\hat{N}_x}\right) \\
& \times \int_{-\infty}^{\infty} d\hat{l}_y \exp\left(-\frac{\hat{l}_y^2}{2\hat{N}_y}\right) \exp\left[-2i(\Delta\hat{\theta}_x\hat{l}_x + \Delta\hat{\theta}_y\hat{l}_y)\right] \\
& \times S\left[\hat{z}_o, \left(\bar{\theta}_x + \Delta\hat{\theta}_x - \frac{\hat{l}_x}{\hat{z}_o} - \hat{\eta}_x\right)^2 + \left(\bar{\theta}_y + \Delta\hat{\theta}_y - \frac{\hat{l}_y}{\hat{z}_o} - \hat{\eta}_y\right)^2\right] \\
& \times S^*\left[\hat{z}_o, \left(\bar{\theta}_x - \Delta\hat{\theta}_x - \frac{\hat{l}_x}{\hat{z}_o} - \hat{\eta}_x\right)^2 + \left(\bar{\theta}_y - \Delta\hat{\theta}_y - \frac{\hat{l}_y}{\hat{z}_o} - \hat{\eta}_y\right)^2\right]. \quad (123)
\end{aligned}$$

<sup>8</sup> Note that the definition of  $\Delta\hat{\theta}_x$  and  $\Delta\hat{\theta}_y$  differ for a factor 2 and a sign with respect to notations in [8, 9].

A double change of variables  $\hat{\eta}_{x,y} \longrightarrow \hat{\eta}_{x,y} + \bar{\theta}_{x,y}$  followed by the substitution  $\hat{l}_{x,y}/\hat{z}_o \longrightarrow \hat{\phi}_{x,y} - \hat{\eta}_{x,y}$  and by analytical calculation of the integrals in  $d\hat{\eta}_{x,y}$  leads to

$$\begin{aligned}
\hat{G} = & \frac{1}{4\pi^2 \sqrt{\hat{A}_x \hat{D}_x \hat{A}_y \hat{D}_y}} \\
& \times \exp \left[ i2\bar{\theta}_x \hat{z}_o \Delta \hat{\theta}_x \right] \exp \left[ -\frac{\bar{\theta}_x^2 + 4\hat{A}_x \hat{z}_o^2 \Delta \hat{\theta}_x^2 \hat{D}_x + 4i\hat{A}_x \bar{\theta}_x \hat{z}_o \Delta \hat{\theta}_x}{2(\hat{A}_x + \hat{D}_x)} \right] \\
& \times \exp \left[ i2\bar{\theta}_y \hat{z}_o \Delta \hat{\theta}_y \right] \exp \left[ -\frac{\bar{\theta}_y^2 + 4\hat{A}_y \hat{z}_o^2 \Delta \hat{\theta}_y^2 \hat{D}_y + 4i\hat{A}_y \bar{\theta}_y \hat{z}_o \Delta \hat{\theta}_y}{2(\hat{A}_y + \hat{D}_y)} \right] \\
& \times \int_{-\infty}^{\infty} d\hat{\phi}_x \int_{-\infty}^{\infty} d\hat{\phi}_y \exp \left[ -\frac{\hat{\phi}_x^2 + 2\hat{\phi}_x (\bar{\theta}_x + 2i\hat{A}_x \hat{z}_o \Delta \hat{\theta}_x)}{2(\hat{A}_x + \hat{D}_x)} \right] \\
& \times \exp \left[ -\frac{\hat{\phi}_y^2 + 2\hat{\phi}_y (\bar{\theta}_y + 2i\hat{A}_y \hat{z}_o \Delta \hat{\theta}_y)}{2(\hat{A}_y + \hat{D}_y)} \right] \\
& \times S^* \left[ \hat{z}_o, (\hat{\phi}_x - \Delta \hat{\theta}_x)^2 + (\hat{\phi}_y - \Delta \hat{\theta}_y)^2 \right] \\
& \times S \left[ \hat{z}_o, (\hat{\phi}_x + \Delta \hat{\theta}_x)^2 + (\hat{\phi}_y + \Delta \hat{\theta}_y)^2 \right]. \tag{124}
\end{aligned}$$

Eq. (124) is a valid expression for the cross-spectral density in free space *after* the undulator device (i.e. for  $\hat{z}_o > 1/2$ ) and can be used together with equations from (60) to (66).

Let us now introduce the dimensionless version of Eq. (54) with the help of  $\vec{r} = \hat{z}_o \vec{\theta}$  and  $\Delta \vec{r} = \hat{z}_o \Delta \vec{\theta}$ <sup>9</sup>:

<sup>9</sup> A short digression about Eq. (125) is due here. As the reader may have noticed,  $\hat{\mathcal{G}}$  coincides with the Fourier transform, done with respect to  $\vec{r}'$ , of the Wigner distribution  $\hat{\Phi}(\hat{z}, \vec{r}, \vec{u}) = \int d\Delta \vec{r}' \hat{G}(\hat{z}, \vec{r}, \Delta \vec{r}') \exp[2i(\vec{u} \cdot \Delta \vec{r}')] ]$ . The knowledge of the Wigner distribution is mathematically equivalent to the knowledge of  $\hat{\mathcal{G}}$  or  $\hat{G}$ . A formalism based on the Wigner distribution may be thus developed, which is mathematically equivalent to the one developed here. In the case of quasi-homogeneous sources, the Wigner distribution amounts to Eq. (6), that is the phase space distribution. Interpretations of such a function as a sort of generalized phase space distribution in more generic cases for non-homogeneous sources have been proposed. However, there is no practical advantage in considering such an approach in our case. Moreover, the Wigner distribution is a quantity that cannot be directly measured. Therefore, we prefer to use a formalism based on the cross-spectral density which is a physically measurable quantity. The cross-spectral density may be directly measured by means of Young's double pinhole interferometer, whereas the Wigner function is a mathematical transformation of the cross-spectral density.

$$\hat{G}(\hat{z}, \vec{u}, \Delta\vec{u}) = \int d\vec{r}' d\Delta\vec{r}' \hat{G}(\hat{z}, \vec{r}', \Delta\vec{r}') \exp \left[ 2i (\vec{u} \cdot \Delta\vec{r}' + \Delta\vec{u} \cdot \vec{r}') \right] . \quad (125)$$

Its inverse is given by

$$\hat{G}(\hat{z}, \vec{r}, \Delta\vec{r}) = \frac{1}{(2\pi)^4} \int d\vec{u}' d\Delta\vec{u}' \times \hat{\mathcal{G}}(\hat{z}, \vec{u}', \Delta\vec{u}') \exp \left[ -2i (\vec{u}' \cdot \Delta\vec{r} + \Delta\vec{u}' \cdot \vec{r}) \right] . \quad (126)$$

Similarly as before, we consider coordinates  $\vec{\theta} = \vec{r}/\hat{z}_o$  and  $\Delta\vec{\theta} = \Delta\vec{r}/\hat{z}_o$  in the limit  $\hat{z}_o \rightarrow \infty$  but for finite ratios  $\vec{\theta}$  and  $\Delta\vec{\theta}$ . The dimensionless version of Eq. (56) then reads:

$$\hat{G}(\hat{z}_o, \vec{\theta}, \Delta\vec{\theta}) = \frac{1}{4\pi^2 \hat{z}_o^2} \exp \left[ 2i \hat{z}_o \vec{\theta} \cdot \Delta\vec{\theta} \right] \hat{\mathcal{G}}(0, -\vec{\theta}, -\Delta\vec{\theta}) . \quad (127)$$

This result will be widely used in what follows. Moreover an analogous of Eq. (55) is:

$$\hat{\mathcal{G}}(\hat{z}, \vec{\theta}, \Delta\vec{\theta}) = \hat{\mathcal{G}}(0, \vec{\theta}, \Delta\vec{\theta}) \exp \left[ -i 2 \hat{z} \vec{\theta} \cdot \Delta\vec{\theta} \right] . \quad (128)$$

This result means that, aside for a phase factor, the spatial Fourier transform of the cross-correlation function,  $\hat{\mathcal{G}}$ , does not depend on  $\hat{z}$ , as it follows from the analogous property of the Fourier transform of the electric field discussed in Section 2.

Before proceeding, let us introduce the spectral degree of coherence  $g$ , which can be presented as a function of  $\vec{r}$  and  $\Delta\vec{r}$ :

$$g(\vec{r}, \Delta\vec{r}) = \frac{\hat{G}(\vec{r}, \Delta\vec{r})}{\left\langle |\hat{E}_{s\perp}(\vec{r} + \Delta\vec{r})|^2 \right\rangle^{1/2} \left\langle |\hat{E}_{s\perp}(\vec{r} - \Delta\vec{r})|^2 \right\rangle^{1/2}} . \quad (129)$$

With reference to Fig. 12, the modulus of the spectral degree of coherence,  $|g|$ , mathematically describes the fringe visibility of the interference pattern from a Young's double-pinhole interferometric measure. The phase of the spectral degree of coherence is related, instead, to the position of the fringes. The cross-spectral density gives amplitude *and* position of the fringes. In general, the process may not be quasi-homogeneous. In this case, the result of Young's experiment varies with  $\vec{r}$ . In this case, the relation between the visibility  $V$  of the fringes and  $g(\vec{r}, \Delta\vec{r})$  reads

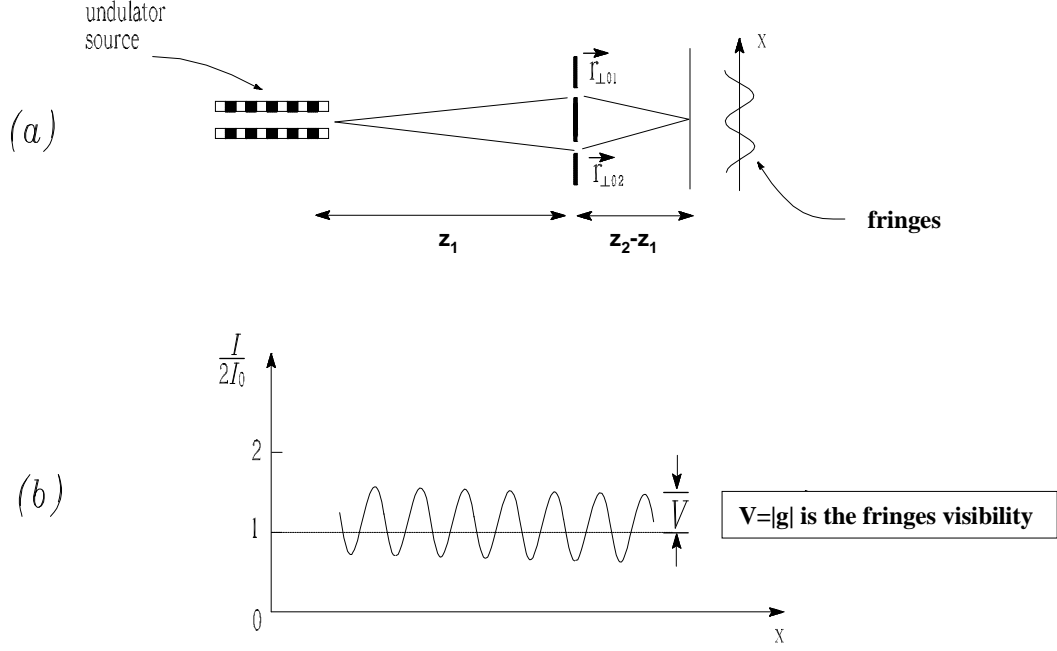


Fig. 12. Measurement of the cross-spectral density of an undulator source. (a) Young's double-pinhole interferometer demonstrating the coherence properties of undulator radiation. Radiation must be spectrally filtered by a monochromator or detector (not shown in figure). (b) In the quasi-homogeneous case the fringe visibility  $V$  of the resultant interference pattern is equal to the absolute value of the spectral degree of coherence:  $V = |g|$ .

$$V = 2 \frac{\left\langle \left| \hat{E}_{s\perp}(\vec{r} + \Delta\vec{r}) \right|^2 \right\rangle^{1/2} \left\langle \left| \hat{E}_{s\perp}(\vec{r} - \Delta\vec{r}) \right|^2 \right\rangle^{1/2}}{\left\langle \left| \hat{E}_{s\perp}(\vec{r} + \Delta\vec{r}) \right|^2 \right\rangle + \left\langle \left| \hat{E}_{s\perp}(\vec{r} - \Delta\vec{r}) \right|^2 \right\rangle} \left| g(\vec{r}, \Delta\vec{r}) \right|. \quad (130)$$

In the quasi-homogeneous limit  $V \rightarrow |g(\Delta\vec{r})|$ .

#### 4.2 Large non-limiting aperture

As explained before we start neglecting, at first, the effects from a finite pupil dimension, assuming a perfect lens with no aberrations. The imaging problem for an ideal lens is solved once we find the cross-spectral density of the equivalent virtual source for the undulator source. On the focal plane we can write Eq. (62) in normalized units as

$$\hat{G}(\hat{z}_f, \vec{r}_f, \Delta\vec{r}_f) = \frac{1}{4\pi^2 \hat{f}^2} \exp \left[ \frac{2i}{\hat{f}} \vec{r}_f \cdot \Delta\vec{r}_f \right]$$

$$\times \exp \left[ -\frac{2i\hat{z}_1}{\hat{f}^2} \vec{r}_f \cdot \Delta \vec{r}_f \right] \hat{G} \left( 0, -\frac{\vec{r}_f}{\hat{f}}, -\frac{\Delta \vec{r}_f}{\hat{f}} \right), \quad (131)$$

while on the image plane, Eq. (66) in normalized units reads

$$\begin{aligned} \hat{G}(\hat{z}_i, \vec{r}_i, \Delta \vec{r}_i) &= m \exp \left[ \frac{2im}{\hat{z}_1} \vec{r}_i \cdot \Delta \vec{r}_i \right] \\ &\times \exp \left[ \frac{2im^2}{\hat{z}_1} \vec{r}_i \cdot \Delta \vec{r}_i \right] \hat{G} \left( 0, -m\vec{r}_i, -m\Delta \vec{r}_i \right). \end{aligned} \quad (132)$$

In all cases considered in this paper the position  $\hat{z} = 0$  is well within the radiation formation length of the undulator. Therefore the cross-spectral density  $\hat{G}$ , calculated at  $\hat{z} = 0$  has no direct physical meaning, and must be considered as a quantity characterizing the virtual source only. From the definitions of virtual source and cross-spectral density follows that the virtual source produces not only the same field but also the same cross-spectral density of the real undulator source, at any distance from the exit of the undulator.

In the present study case of a radiation spot size smaller than the area of the lens and of a lens with no aberrations, Eq. (124) and Eq. (128), together with Eq. (131) and Eq. (132), solve the problem of characterizing the cross-spectral density on the focal plane (with the help of Eq. (131)) and on the image plane (with the help of Eq. (132)). The situation of a radiation spot size smaller than the area of the lens is practically achievable for Synchrotron Radiation due to its high directionality. In this case, vignetting effects are not present. However, even in this case, in order to use Eq. (131) and Eq. (132) one must further assume that aberrations can be neglected.

### 4.3 Effect of aperture size

Accounting for the presence of the pupil, in analogy with Eq. (60) one has the following normalized expression for the cross-spectral density on any observation plane at position  $\hat{z}_2$  along the beamline behind the lens:

$$\begin{aligned} \hat{G}(\hat{z}_2, \vec{r}, \Delta \vec{r}) &= \frac{1}{4\pi^2(\hat{z}_2 - \hat{z}_1)^2} \exp \left[ \frac{2i\vec{r} \cdot \Delta \vec{r}}{\hat{z}_2 - \hat{z}_1} \right] \\ &\times \int d\vec{r}' d\Delta \vec{r}' \left\{ \hat{G} \left( \hat{z}_1, \vec{r}', \Delta \vec{r}' \right) P \left( \vec{r}' + \Delta \vec{r}' \right) P^* \left( \vec{r}' - \Delta \vec{r}' \right) \right. \\ &\left. \times \exp \left[ 2i \left( -\frac{1}{\hat{f}} + \frac{1}{\hat{z}_2 - \hat{z}_1} \right) \vec{r}' \cdot \Delta \vec{r}' \right] \right\} \end{aligned}$$

$$\times \exp \left[ -\frac{2i}{\hat{z}_2 - \hat{z}_1} \left( \vec{r} \cdot \Delta \vec{r}' + \vec{r}' \cdot \Delta \vec{r} \right) \right]. \quad (133)$$

Let us consider, more specifically, the focal and the image plane. Results can be obtained directly from Eq. (133). Alternatively, in analogy with Eq. (67) and Eq. (68), one can use our previous results, Eq. (131) and Eq. (132), divide them by the first phase factor, convolve them twice with  $\hat{\mathcal{P}}$  and  $\hat{\mathcal{P}}^*$  and, finally, put the phase factor back. A normalized version of the cross-spectral density  $\hat{G}_P$  including pupil effects at the focal is then found and can be written as

$$\begin{aligned} \hat{G}_P(\hat{z}_f, \vec{r}_f, \Delta \vec{r}_f) &= \exp \left[ \frac{2i}{\hat{f}} \vec{r}_f \cdot \Delta \vec{r}_f \right] \\ &\times \int d\vec{u} d\Delta \vec{u} \exp \left[ -2i\hat{f}\vec{u} \cdot \Delta \vec{u} \right] \hat{G}(\hat{z}_f, \hat{f}\vec{u}, \hat{f}\Delta \vec{u}) \\ &\times \hat{\mathcal{P}} \left[ \frac{\vec{r}_f + \Delta \vec{r}_f}{\hat{f}} - \vec{u} - \Delta \vec{u} \right] \hat{\mathcal{P}}^* \left[ \frac{\vec{r}_f - \Delta \vec{r}_f}{\hat{f}} - \vec{u} + \Delta \vec{u} \right], \end{aligned} \quad (134)$$

while on the image plane one obtains

$$\begin{aligned} \hat{G}_P(\hat{z}_i, \vec{r}_i, \Delta \vec{r}_i) &= \exp \left[ \frac{2im}{\hat{z}_1} \vec{r}_i \cdot \Delta \vec{r}_i \right] \int d\vec{u} d\Delta \vec{u} \exp \left[ -\frac{2i\hat{z}_1}{m} \vec{u} \cdot \Delta \vec{u} \right] \\ &\times \hat{G} \left( \hat{z}_i, \frac{\hat{z}_1}{m} \vec{u}, \frac{\hat{z}_1}{m} \Delta \vec{u} \right) \hat{\mathcal{P}} \left[ \frac{m}{\hat{z}_1} (\vec{r}_i + \Delta \vec{r}_i) - \vec{u} - \Delta \vec{u} \right] \\ &\times \hat{\mathcal{P}}^* \left[ \frac{m}{\hat{z}_1} (\vec{r}_i - \Delta \vec{r}_i) - \vec{u} + \Delta \vec{u} \right]. \end{aligned} \quad (135)$$

As said before, we will treat particular situations in the image plane when the lens is in the far field. Using coordinates  $\vec{r}_i$  and  $\Delta \vec{r}_i$  the analog of condition (70) reads

$$\frac{2m^2}{\hat{z}_1} \vec{r}_i \cdot \Delta \vec{r}_i \ll 1 \quad (136)$$

for any pair of points on the image pattern.

Explicit substitution of Eq. (132) in Eq. (135) yields the following far field limit expression, which accounts for condition (136):

$$\begin{aligned} \hat{G}_P(\hat{z}_i, \vec{r}_i, \Delta \vec{r}_i) &= m \exp \left[ \frac{2im}{\hat{z}_1} \vec{r}_i \cdot \Delta \vec{r}_i \right] \int d\vec{u} d\Delta \vec{u} \hat{G} \left( 0, -\hat{z}_1 \vec{u}, -\hat{z}_1 \Delta \vec{u} \right) \\ &\times \hat{\mathcal{P}} \left[ \frac{m}{\hat{z}_1} (\vec{r}_i + \Delta \vec{r}_i) - \vec{u} - \Delta \vec{u} \right] \end{aligned}$$

$$\times \hat{\mathcal{P}}^* \left[ \frac{m}{\hat{z}_1} (\vec{r}_i - \Delta \vec{r}_i) - \vec{u} + \Delta \vec{u} \right]. \quad (137)$$

Eq. (137) is in analogy with Eq. (71) and Eq. (45).

## 5 Imaging of quasi-homogeneous Gaussian undulator sources by a lens with large non-limiting aperture

In this Section we specialize our discussion to the particular case of quasi-homogeneous Gaussian undulator sources, assuming a lens with large non-limiting aperture and no aberrations. A Statistical Optics treatment is not the only one possible in this particular study case. A Geometrical Optics approach can also be applied, practically consisting in ray-tracing techniques. In this Section we will consider the image formation problem from a Statistical Optics viewpoint. In Section 7 an analysis in terms of Geometrical Optics will be given, and agreement between these two methods will be demonstrated.

From this point on, we will systematically ignore unimportant pre-factors appearing in the expressions for the cross-spectral density. Moreover we will assume  $\hat{N}_x \gg 1$  and  $\hat{D}_x \gg 1$  which is a reasonable approximation for third generation light sources in the X-ray region. We will show that this assumption leads to a major simplification: namely, horizontal and vertical coordinates turn out to be factorized in the expression for the cross-spectral density in free space. As a consequence, Eq. (131) and (132) can also be factorized in the product of a factor depending on the horizontal coordinates and a factor depending on the vertical coordinates. These separate factors will be obtained from Eq. (131) and (132) substituting all vector quantities with scalar quantities (horizontal or vertical components).

### 5.1 Evolution of the cross-spectral density function in free space

Eq. (124) is a valid expression for the cross-spectral density in free space at perfect resonance, calculated under the only assumptions that the system is ultra-relativistic (and, therefore, the paraxial approximation can be applied) and that the insertion device is characterized by a large number of undulator periods. In this case the resonance approximation is enforced. Eq. (124) is quite generic and, with respect to first-principle calculations, it involves the computation of a two-dimensional integral, whereas the most generic calculations would require a total of six integrations, two over the undulator length and four over the electron beam transverse phase space (assuming that the cross-correlation terms between different electrons is neglected). From a computational viewpoint, the advantage of reducing the number of integration is

obvious and it can be appreciated even more after the cross-spectral density is propagated through an optical system with limiting apertures, which naturally increases the dimensions of the integration to be performed.

When  $\hat{N}_x \gg 1$  and  $\hat{D}_x \gg 1$  the cross-spectral in free space, Eq. (124), can be written as the product of factors separately depending on the  $x$  and on the  $y$  coordinate, as has been shown in [2]. In fact, analyzing the exponential factor outside the integral sign in Eq. (124) it is possible to see that the maximum value of  $\Delta\hat{\theta}_x^2$  is of order  $(\hat{A}_x + \hat{D}_x)/(\hat{A}_x\hat{D}_x\hat{z}_o^2) \ll 1$ , where we remember  $\hat{A}_x = \hat{N}_x^2/\hat{z}_o^2$ . As a result,  $\Delta\hat{\theta}_x$  can be neglected inside the  $S$  functions in Eq. (124). Moreover, since  $\hat{D}_x \gg 1$  one can also neglect the exponential factor in  $\hat{\phi}_x^2 + 2\hat{\phi}_x\bar{\theta}_x$  inside the integral. This leads to

$$\begin{aligned}
\hat{G} = & \exp [i2\bar{\theta}_x\hat{z}_o\Delta\hat{\theta}_x] \exp \left[ -\frac{\bar{\theta}_x^2 + 4\hat{A}_x\hat{z}_o^2\Delta\hat{\theta}_x^2\hat{D}_x + 4i\hat{A}_x\bar{\theta}_x\hat{z}_o\Delta\hat{\theta}_x}{2(\hat{A}_x + \hat{D}_x)} \right] \\
& \times \exp [i2\bar{\theta}_y\hat{z}_o\Delta\hat{\theta}_y] \exp \left[ -\frac{\bar{\theta}_y^2 + 4\hat{A}_y\hat{z}_o^2\Delta\hat{\theta}_y^2\hat{D}_y + 4i\hat{A}_y\bar{\theta}_y\hat{z}_o\Delta\hat{\theta}_y}{2(\hat{A}_y + \hat{D}_y)} \right] \\
& \times \int_{-\infty}^{\infty} d\hat{\phi}_x \exp \left[ i\hat{\phi}_x \frac{2\hat{A}_x\hat{z}_o\Delta\hat{\theta}_x}{\hat{A}_x + \hat{D}_x} \right] \\
& \times \int_{-\infty}^{\infty} d\hat{\phi}_y \exp \left[ -\frac{\hat{\phi}_y^2 + 2\hat{\phi}_y(\bar{\theta}_y + 2i\hat{A}_y\hat{z}_o\Delta\hat{\theta}_y)}{2(\hat{A}_y + \hat{D}_y)} \right] \\
& \times S^*[\hat{z}_o, \hat{\phi}_x^2 + (\hat{\phi}_y - \Delta\hat{\theta}_y)^2] S[\hat{z}_o, \hat{\phi}_x^2 + (\hat{\phi}_y + \Delta\hat{\theta}_y)^2] . \tag{138}
\end{aligned}$$

Following the same reasoning in [2], we can also neglect the phase factor in  $\hat{\phi}_x$  under the integral in  $d\hat{\phi}_x$  in Eq. (138). As a result, when  $\hat{N}_x \gg 1$  and  $\hat{D}_x \gg 1$  horizontal and vertical coordinates are factorized and we obtain the following equation for  $\hat{G}$ :

$$\hat{G}(\hat{z}_o, \bar{\theta}_x, \bar{\theta}_y, \Delta\hat{\theta}_x, \Delta\hat{\theta}_y) = \hat{G}_x(\hat{z}_o, \bar{\theta}_x, \Delta\hat{\theta}_x) \hat{G}_y(\hat{z}_o, \bar{\theta}_y, \Delta\hat{\theta}_y) , \tag{139}$$

where

$$\hat{G}_x = \exp [i2\bar{\theta}_x\hat{z}_o\Delta\hat{\theta}_x] \exp \left[ -\frac{\bar{\theta}_x^2 + 4\hat{A}_x\hat{z}_o^2\Delta\hat{\theta}_x^2\hat{D}_x + 4i\hat{A}_x\bar{\theta}_x\hat{z}_o\Delta\hat{\theta}_x}{2(\hat{A}_x + \hat{D}_x)} \right] \tag{140}$$

and

$$\hat{G}_y = \exp [i2\bar{\theta}_y\hat{z}_o\Delta\hat{\theta}_y] \exp \left[ -\frac{\bar{\theta}_y^2 + 4\hat{A}_y\hat{z}_o^2\Delta\hat{\theta}_y^2\hat{D}_y + 4i\hat{A}_y\bar{\theta}_y\hat{z}_o\Delta\hat{\theta}_y}{2(\hat{A}_y + \hat{D}_y)} \right]$$

$$\begin{aligned}
& \times \int_{-\infty}^{\infty} d\hat{\phi}_y \exp \left[ -\frac{\hat{\phi}_y^2 + 2\hat{\phi}_y (\bar{\theta}_y + 2i\hat{A}_y \hat{z}_o \Delta\hat{\theta}_y)}{2(\hat{A}_y + \hat{D}_y)} \right] \\
& \times \int_{-\infty}^{\infty} d\hat{\phi}_x S^* [\hat{z}_o, \hat{\phi}_x^2 + (\hat{\phi}_y - \Delta\hat{\theta}_y)^2] S [\hat{z}_o, \hat{\phi}_x^2 + (\hat{\phi}_y + \Delta\hat{\theta}_y)^2] . \quad (141)
\end{aligned}$$

To begin our investigation of quasi-homogeneous sources we will consider the limit  $\hat{N} \gg 1$  and  $\hat{D} \gg 1$ , when the photon-beam phase space in a certain (horizontal or both horizontal and vertical) direction is an exact replica of the electron-beam phase space. Calculations can be performed in one dimension, suppressing indexes  $x$  and  $y$ . In the case of Second Generation light sources the results that we are going to derive constitute a realistic description of the radiation characteristics in both horizontal and vertical directions. Then, Eq. (141) coincides with Eq. (140).

Let us present Eq. (140), i.e. the asymptotic expression for the cross-spectral density in the limit  $\hat{N} \gg 1$  and  $\hat{D} \gg 1$ , in terms of coordinates  $\bar{r} = \hat{z}\bar{\theta}$  and  $\Delta\hat{r} = \hat{z}\Delta\hat{\theta}$ . We have

$$\begin{aligned}
\hat{G}(\hat{z}, \bar{r}, \Delta\hat{r}) &= \exp \left[ -\frac{\bar{r}^2}{2(\hat{A} + \hat{D})\hat{z}^2} \right] \exp \left[ 2i\frac{\bar{r}\Delta\hat{r}}{\hat{z}} \right] \\
&\times \exp \left[ -2i\frac{\hat{A}\bar{r}\Delta\hat{r}}{\hat{z}(\hat{A} + \hat{D})} \right] \exp \left[ -2\frac{\hat{A}\hat{D}(\Delta\hat{r})^2}{(\hat{A} + \hat{D})} \right] , \quad (142)
\end{aligned}$$

where

$$\hat{A} = \frac{\hat{N}}{\hat{z}^2} . \quad (143)$$

Note that here, depending on the situation,  $r$  may assume the meaning of either variable  $x$  or  $y$ .

In the far field limit, when  $\hat{A} \ll \hat{D}$  one obtains the following limiting expression of Eq. (142):

$$\hat{G}(\hat{z}, \bar{r}, \Delta\hat{r}) = \exp \left[ 2i\frac{\bar{r}\Delta\hat{r}}{\hat{z}} \right] \exp \left[ -\frac{\bar{r}^2}{2\hat{D}\hat{z}^2} \right] \exp \left[ -2\hat{A}(\Delta\hat{r})^2 \right] . \quad (144)$$

With the help of Eq. (144) and using Eq. (127) one can find the expression for  $\hat{\mathcal{G}}$  and  $\hat{G}$  at the virtual source position in the center of the undulator. In the case under study ( $\hat{N} \gg 1$  and  $\hat{D} \gg 1$ ) the virtual source is a Gaussian quasi-homogeneous source. Aside for unessential multiplication constants we have

$$\hat{G}(0, \bar{\theta}, \Delta\hat{\theta}) = \exp[-2\hat{N}\Delta\hat{\theta}^2] \exp\left[-\frac{\bar{\theta}^2}{2\hat{D}}\right]. \quad (145)$$

Therefore, using Eq. (126) we also obtain

$$\hat{G}(0, \bar{r}, \Delta\hat{r}) = \exp\left[-\frac{\bar{r}^2}{2\hat{N}}\right] \exp[-2\hat{D}(\Delta\hat{r})^2]. \quad (146)$$

From Eq. (146) we conclude that the intensity distribution of the virtual source is a replica of the electron beam density distribution at the position of minimal beta function of the undulator (i.e. at the undulator center). Moreover, in this particular study case, if the position of the minimal beta function does not coincide with the undulator center, the virtual source corresponding to the description in Eq. (146) is simply translated, and is always located at the position where the beta function of the electron beam is minimal.

It should be noted that the far field limit  $\hat{A} \ll \hat{D}$  corresponds with the applicability region of the van Cittert-Zernike theorem. In virtue of the van Cittert-Zernike theorem the modulus of the spectral degree of coherence in the far field, i.e.  $\exp[-2\hat{A}(\Delta\hat{r})^2]$  from Eq. (144), forms a Fourier pair with the intensity distribution of the virtual source, i.e.  $\exp[-\bar{r}^2/2\hat{N}]$  from Eq. (146).

In particular one concludes that the rms width of the virtual source is  $\sqrt{\hat{N}}$ , as it can be seen directly from Eq. (146). In our study case for  $\hat{N} \gg 1$  and  $\hat{D} \gg 1$ , such a relation between the rms width of the spectral degree of coherence in the far field and the rms dimension of the virtual source is also a relation between the rms width of the cross-spectral density function in the far field and the rms dimension of the electron beam at the plane of minimal beta function in the center of the undulator. In dimensional units one can write the value  $\sigma_c$  of the rms width of the spectral degree of coherence  $g(\Delta\vec{r})$  in the far field as

$$\sigma_c = \frac{\lambda z}{2\pi\sigma}, \quad (147)$$

$\sigma$  being, as usual, the rms dimension of the electron beam. These few last remarks help to clarify what is the size of the source in the van Cittert-Zernike theorem, that is far from being a trivial question. For instance, assume that the van Cittert-Zernike theorem can be applied. Then, the rms electron beam size can be recovered from the measurement of the transverse coherence length. In this regard, in [10] Section V, one may find a statement according to which the rms electron beam size "is only the average value along the undulator" because "the beta function has a large variation along the undulator". However, as we have seen before, the concept of virtual source does not require a small variation of the beta function. In the most general case, any variation of the

beta function does not affect the virtual source size and, in our case of quasi-homogeneous Gaussian source, the virtual source size is also the transverse size of the electron beam at the position where the beta function is minimal. Another example dealing with the same issue is given in reference [13]. This paper (as well as reference [10]) reports experimental results. However, authors of [13] observe a disagreement between the electron beam rms size reconstructed from the van Cittert-Zernike theorem and beam diagnostics result of about a factor 2. They ascribe this variation to the variation of the electron beam size along the undulator. In footnote [25] of reference [13], one may read: "The precise shape and width of the x-ray intensity distribution in the source plane are directly connected to the properties of the electron beam. It would not be surprising if the limited depth of focus of the parabolically shaped electron beta function in the undulator translates into a virtually enlarged x-ray source size." At first glance it looks like if the Synchrotron Radiation source has a finite longitudinal dimension. However, based on the previous discussion we conclude that the virtual source size is equal to the electron beam size at the point where the beta functions have their minimum and that it is not affected by variations of the beta function along the undulator. As a result, one should not observe any virtually enlarged X-ray source size because of this reason.

## 5.2 Evolution of the cross-spectral density function behind the lens

If we neglect the effect of the pupil in the particular case under examination ( $\hat{N} \gg 1$  and  $\hat{D} \gg 1$ ), it is possible to find an analytical expression for the cross-spectral density for any observation plane, and not only for the focal or the image plane. This is due to the fact that, in this particular case, the virtual source is gaussian. In the most general case instead, one has to make use of Eq. (133).

As usual we will neglect, at first, the effect of the pupil function and group all the phase terms in  $\Delta\hat{r}'\bar{r}'$  in Eq. (133) with the help of the definition

$$\hat{Q} = \frac{1}{\hat{z}_1} - \frac{\hat{A}}{\hat{z}_1(\hat{A} + \hat{D})} - \frac{1}{\hat{f}} + \frac{1}{\hat{z}_2 - \hat{z}_1}, \quad (148)$$

where

$$\hat{A} = \frac{\hat{N}}{\hat{z}_1^2}. \quad (149)$$

With this in mind, after substitution of Eq. (142) calculated at  $\hat{z} = \hat{z}_1$  in Eq. (133), one obtains

$$\begin{aligned} \hat{G}(\hat{z}_2, \bar{r}, \Delta\hat{r}) = & \exp \left[ 2i \frac{\bar{r}\Delta\hat{r}}{\hat{z}_2 - \hat{z}_1} \right] \exp \left[ -\frac{2(\hat{A} + \hat{D})\hat{z}_1^2(\Delta\hat{r})^2}{(\hat{z}_2 - \hat{z}_1)^2} \right] \\ & \times \exp \left\{ -\frac{(\hat{A} + \hat{D}) \left[ \bar{r} + 2i\hat{Q}(\hat{A} + \hat{D})\hat{z}_1^2\Delta\hat{r} \right]^2}{\left[ 2\hat{A}\hat{D} + 2(\hat{A} + \hat{D})^2\hat{Q}^2\hat{z}_1^2 \right] (\hat{z}_2 - \hat{z}_1)^2} \right\}. \end{aligned} \quad (150)$$

which corresponds to a relative intensity

$$\hat{I}(\hat{z}_2, \bar{r}) = \exp \left\{ -\frac{(\hat{A} + \hat{D})\bar{r}^2}{\left[ 2\hat{A}\hat{D} + 2(\hat{A} + \hat{D})^2\hat{Q}^2\hat{z}_1^2 \right] (\hat{z}_2 - \hat{z}_1)^2} \right\}. \quad (151)$$

and to a modulus of the spectral degree of transverse coherence

$$|g(\hat{z}_2, \bar{r}, \Delta\hat{r})| = \exp \left\{ -\frac{2\hat{A}\hat{D}(\hat{A} + \hat{D})\hat{z}_1^2(\Delta\hat{r})^2}{\left[ \hat{A}\hat{D} + (\hat{A} + \hat{D})^2\hat{Q}^2\hat{z}_1^2 \right] (\hat{z}_2 - \hat{z}_1)^2} \right\}. \quad (152)$$

Letting  $\hat{Q} = -\hat{A}/[\hat{z}_1(\hat{A} + \hat{D})]$  the reader can specialize the results to the case of the image plane. For  $\hat{Q} = \hat{1}/\hat{z}_1 - \hat{A}/[\hat{z}_1(\hat{A} + \hat{D})]$  one gets the results for the focal plane. Also, the intensity and the modulus of the spectral degree of coherence on the image plane can be obtained from those on the focal plane exchanging  $\hat{A}$  with  $\hat{D}$ . This symmetry can be explained in terms of Fourier transforms. Phase factors aside, the cross-spectral density on the image plane is equal to the cross-spectral density on the object plane. The cross-spectral density on the focal plane instead, is equal (phase factors aside) to the Fourier transform of the cross-spectral density on the object plane.

As we have seen, in the case for a Gaussian electron beam with  $\hat{N} \gg 1$ ,  $\hat{D} \gg 1$  and for a perfect lens with non-limiting aperture and no aberrations, the Gaussian approximation for the cross-spectral density at the virtual source in Eq. (146) can be used, and the cross-spectral density in free space at any position  $\hat{z}$  can be calculated with the help of Eq. (142). Then, Eq. (133) can be simplified to recover both the intensity and the modulus of the spectral degree of coherence (Eq. (151) and Eq. (152) respectively), which are Gaussian functions for any value of  $\hat{z}_2$  and  $\hat{z}_1$ . Even for quasi-homogeneous sources though, there are a number of examples when it is difficult to obtain analytical results from Eq. (133) for any value of  $\hat{z}_2$ . Nevertheless it is possible to calculate the cross-spectral density at the image plane and at the focal plane (for any value of  $\hat{z}_1$ ) with the help of Eq. (131) and Eq. (132). This can be done relying on the calculation of the cross-spectral density at the virtual-source position (and its Fourier transform), which allows further use of Eq. (131) and Eq. (132). We will first use Eq. (131) and Eq. (132) to deal with the case that we just discussed when  $\hat{N} \gg 1$  and  $\hat{D} \gg 1$ . This is not a simple repetition of already known results, because the particular way of reasoning used for the

focal and the image plane, through Eq. (131) and Eq. (132), will be widely used in the following parts of this paper too. The Statistical Optics method conjugated to Fourier Optics results allows us to predict, by manipulations of Eq. (142), the cross-spectral density (and, therefore, the intensity and the absolute value of the spectral degree of coherence) on the focal and on the image plane. In order to use Eq. (131) and Eq. (132) we must take advantage of the expressions for  $\hat{\mathcal{G}}$  and  $\hat{G}$  at the virtual source position, Eq. (145) and Eq. (146) respectively.

With the help of Eq. (131) and Eq. (145), on the focal plane we obtain

$$\hat{G}(\hat{z}_f, \vec{r}_f, \Delta\vec{r}_f) = \exp\left[\frac{i2(\hat{f} - \hat{z}_1)}{\hat{f}^2} \vec{r}_f \Delta\hat{r}_f\right] \exp\left[-\frac{2\hat{N}\Delta\hat{r}_f^2}{\hat{f}^2}\right] \exp\left[-\frac{\vec{r}_f^2}{2\hat{D}\hat{f}^2}\right]. \quad (153)$$

For *any* value of  $\hat{z}_1$  we have a relative intensity on the focal plane given by

$$\hat{I} = \exp\left[-\frac{\vec{r}_f^2}{2\hat{D}\hat{f}^2}\right], \quad (154)$$

while the modulus of the spectral degree of coherence (again, for any position  $\hat{z}_1$  of the lens<sup>10</sup>) is

$$|g(\hat{z}_f, \vec{r}_f, \Delta\hat{r}_f)| = \exp\left[-\frac{2\hat{N}\Delta\hat{r}_f^2}{\hat{f}^2}\right]. \quad (155)$$

These results are intuitively sound. In Section 2 we explained that we expect to find, on the focal plane, the spatial Fourier transform of the wavefront on the object plane (except for a phase and a proportionality factor). Therefore, it is intuitive that the intensity on the focal plane must depend on the electron beam divergence only and that the modulus of the spectral degree of coherence must depend on the electron beam size only. In fact, the exchange of roles of  $\hat{N}$  and  $\hat{D}$  passing from the virtual source plane to the the focal plane is related to the operation of Fourier transform. Also note that the Fourier transform of the field depends on  $\hat{z}_1$  through a phase factor only, and free space basically acts as a Fourier transform itself (see Section 2): what we find on the focal plane in terms of intensity and modulus of the spectral degree of coherence we

---

<sup>10</sup> Note that the *modulus* of the spectral degree of coherence in Eq. (155) is independent of  $\vec{r}_f$ . However, the spectral degree of coherence depends on  $\vec{r}_f$  through a phase factor. This situation corresponds, according to a definition given by us in [2], to a *weakly quasi-homogeneous wavefront*. This remark is valid for many expressions of the modulus of the cross-spectral density given in this work.

must also find in the far field after propagation in free space. The reader may check that, after substitution  $\bar{r}_f/\hat{f} \rightarrow \bar{\theta}$  and  $\Delta\hat{r}_f/\hat{f} \rightarrow \Delta\hat{\theta}$ , Eq. (154) and Eq. (155) can be found from Eq. (54) and Eq. (61) in [2] in the limit  $\hat{z}_o \gg 1$ , which describe propagation in free space, as it should be.

A similar simplified reasoning can be applied for the cross-spectral density on the image plane. With the help of Eq. (132) and Eq. (146), describing the cross-spectral density of the virtual source we obtain:

$$\begin{aligned} \hat{G}(\hat{z}_i, \bar{r}_i, \Delta\hat{r}_i) = & \exp \left[ \frac{2im(m+1)\bar{r}_i\Delta\hat{r}_i}{\hat{z}_1} \right] \exp \left[ -\frac{m^2\bar{r}_i^2}{2\hat{N}} \right] \\ & \times \exp \left[ -2\hat{D}m^2(\Delta\hat{r}_i)^2 \right] . \end{aligned} \quad (156)$$

The relative intensity on the image plane is given by

$$\hat{I} = \exp \left[ -\frac{m^2\bar{r}_i^2}{2\hat{N}} \right] , \quad (157)$$

while the modulus of the spectral degree of coherence is

$$|g(\hat{z}_i, \bar{r}_i, \Delta\hat{r}_i)| = \exp \left[ -2m^2\hat{D}(\Delta\hat{r}_i)^2 \right] . \quad (158)$$

These results are very natural. By definition of image plane, when we image an object with an ideal lens with a large non-limiting pupil aperture, we obtain a magnified version of the object (virtual, in this case).

We remarked before that the intensity and the modulus of the spectral degree of coherence on the image plane can be obtained from that on the focal plane exchanging  $\hat{A}$  with  $\hat{D}$ . This symmetry though is not evident from the expressions in Eq. (154), Eq. (157), Eq. (155) and Eq. (158): to display it one has to express these equations in terms of  $\hat{z}_2$  and  $\hat{z}_1$ .

## 6 Imaging of quasi-homogeneous non-Gaussian undulator sources by a lens with large non-limiting aperture

In the previous Section 5 we treated the case for  $\hat{N} \gg 1$  and  $\hat{D} \gg 1$ . In the present Section 6 we will deal with other quasi-homogeneous cases, always assuming  $\hat{N}_x \gg 1$  and  $\hat{D}_x \gg 1$ . The quasi-homogeneous situations that remain to be treated under this assumption are for either  $\hat{N}_y \gg 1$  or  $\hat{D}_y \gg 1$ . In fact, the situation for both  $\hat{N}_y \gg 1$  and  $\hat{D}_y \gg 1$  is automatically included in Section 5. Moreover, in all quasi-homogeneous cases, the cross-spectral density in the

horizontal direction obeys Eq. (150). Therefore, we will focus our attention on the cross-spectral density in the vertical direction only.

### 6.1 Source with non-Gaussian angular distribution in the vertical direction

Let us use of our Statistical Optics approach to solve a somewhat complicated image formation problem. After assuming separability of the horizontal and vertical directions ( $\hat{N}_x \gg 1$ ,  $\hat{D}_x \gg 1$ ) we suppose that the electron beam has a vertical transverse size much larger than the diffraction size,  $\hat{N}_y \gg 1$ , and a finite divergence  $\hat{D}_y > 0$ . As usual, we will first neglect the influence of the pupil function. The difference with respect to the case treated in the previous Section 5 is that Eq. (133) cannot be explicitly calculated for any value of  $\hat{z}_1$  and  $\hat{z}_2$ . However, as said before, the Statistical Optics method conjugated to Fourier Optics results allows us to predict, for any value of  $\hat{z}_1$ , the cross-spectral density on the focal ( $\hat{z}_2 = \hat{z}_f$ ) and on the image ( $\hat{z}_2 = \hat{z}_i$ ) plane by means of Eq. (131) and Eq. (132). In order to use these equations we must first calculate  $\hat{G}$  and  $\hat{\mathcal{G}}$  at the virtual source at position  $\hat{z}_o = 0$ . This can be done taking the limit  $\hat{z}_o^2 \gg \hat{N}/\hat{D}$  of Eq. (141), i.e. calculating the far zone limit of Eq. (141), and using Eq. (127). First, under the assumption  $\hat{N}_y \gg 1$  we can neglect  $\Delta\hat{\theta}_y$  in the  $S$  functions in Eq. (141), thus obtaining the vertical cross-spectral density function in the far field limit

$$\hat{G} = \exp [i2\bar{\theta}_y \hat{z}_o \Delta\hat{\theta}_y] \exp [-2\hat{N}_y \Delta\hat{\theta}_y^2] \int_{-\infty}^{\infty} d\hat{\phi}_y \exp \left[ -\frac{(\hat{\phi}_y + \bar{\theta}_y)^2}{2\hat{D}_y} \right] \hat{I}_S(\hat{\phi}_y) , \quad (159)$$

where

$$\hat{I}_S(\hat{\phi}_y) = \frac{3}{8\sqrt{\pi}} \int_{-\infty}^{\infty} d\hat{\phi}_x \operatorname{sinc}^2 \left[ (\hat{\phi}_x^2 + \hat{\phi}_y^2) / 4 \right] \quad (160)$$

is a universal function related to undulator radiation. A plot of  $\hat{I}_S$  is given in Fig. 13. Eq. (159), substituted into Eq. (127), gives the Fourier transform of the cross-spectral density at  $\hat{z}_o = 0$ , i.e. at the virtual-source position:

$$\hat{\mathcal{G}}(0, \bar{u}, \Delta\hat{u}) = \exp [-2\hat{N}_y \Delta\hat{u}^2] \int_{-\infty}^{\infty} d\hat{\phi}_y \exp \left[ -\frac{(\hat{\phi}_y + \bar{u})^2}{2\hat{D}_y} \right] \hat{I}_S(\hat{\phi}_y) . \quad (161)$$

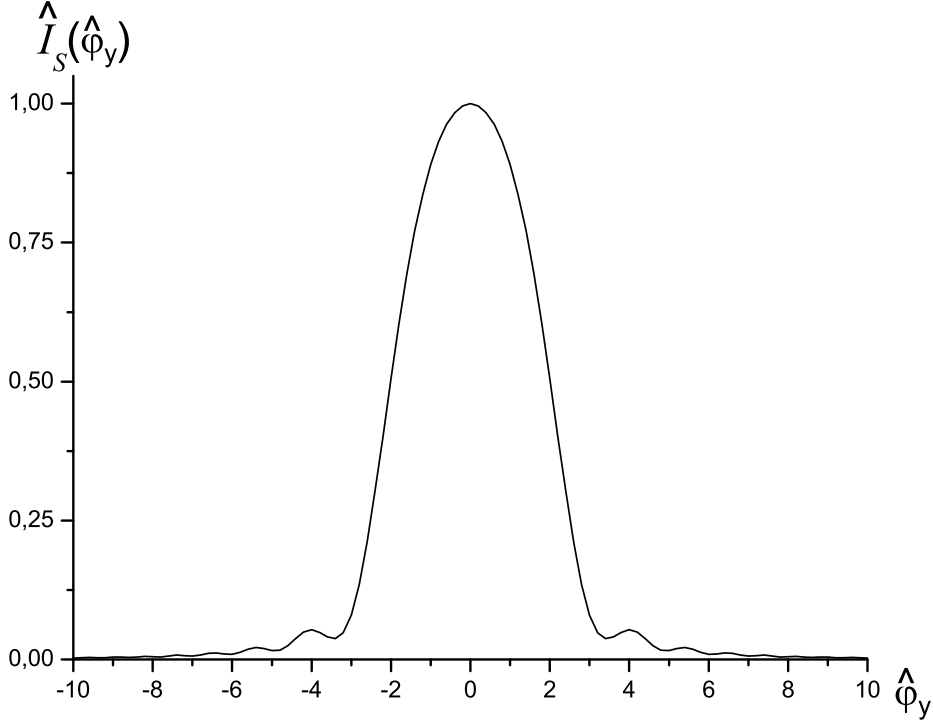


Fig. 13. The universal function  $\hat{I}_S$ , used to calculate the focal intensity of a quasi-homogeneous source at  $\hat{N}_x \gg 1$ ,  $\hat{D}_x \gg 1$  and  $\hat{N}_y \gg 1$ .

Inverse transforming Eq. (161) according to the definition in Eq. (126), we obtain the cross spectral density at the virtual source position

$$\hat{G}(0, \bar{y}, \Delta\hat{y}) = \exp\left[-\frac{\bar{y}^2}{2\hat{N}_y}\right] \exp\left[-2\hat{D}_y\Delta\hat{y}^2\right] \gamma(\Delta\hat{y}), \quad (162)$$

where function  $\gamma(\Delta\hat{y})$  is an inverse Fourier transform, normalized to unity, of  $\hat{I}_S$ , defined as from Eq. (93) in [2]:

$$\gamma(\Delta\hat{y}) = \frac{1}{2\pi^2} \int_{-\infty}^{\infty} d\hat{\phi}_y \exp\left[i(-2\Delta\hat{y})\hat{\phi}_y\right] \hat{I}_S(\hat{\phi}_y). \quad (163)$$

It has been shown in [2] that  $\gamma$  can be expressed in terms of the sine integral function  $\text{Si}(\cdot)$  and of the cosine integral function  $\text{Ci}(\cdot)$ . One has

$$\gamma(\Delta\hat{y}) = \frac{2}{\pi} \left[ \frac{\pi}{2} + 2\Delta\hat{y}^2 \text{Ci}(2\Delta\hat{y}^2) - \sin(2\Delta\hat{y}^2) - \text{Si}(2\Delta\hat{y}^2) \right]. \quad (164)$$

This means that  $\gamma$  is a real function. Moreover, in Eq. (162),  $\Delta\hat{y}$  and  $\bar{y}$  are separated and, since  $\hat{N}_y \gg 1$ , the typical correlation length is much smaller than the radiation spot, independently of the value of  $\hat{D}_y$ . This shows that Eq. (162) models a quasi-homogeneous source. From Eq. (131) and Eq. (161) we obtain the cross-spectral density on the focal plane

$$\begin{aligned} \hat{G}(\hat{z}_f, \bar{y}_f, \Delta\hat{y}_f) &= \exp \left[ \frac{2i}{\hat{f}^2} (\hat{f} - \hat{z}_1) \bar{y}_f \Delta\hat{y}_f \right] \exp \left[ -\frac{2\hat{N}_y \Delta\hat{y}_f^2}{\hat{f}^2} \right] \\ &\times \int_{-\infty}^{\infty} d\hat{\phi}_y \exp \left[ -\frac{(\bar{y}_f/\hat{f} + \hat{\phi}_y)^2}{2\hat{D}_y} \right] \hat{I}_S(\hat{\phi}_y) . \end{aligned} \quad (165)$$

The relative intensity on the focal plane is therefore given by

$$\begin{aligned} \hat{I}(\hat{z}_f, \bar{y}_f) &= \int_{-\infty}^{\infty} d\hat{\phi}_y \exp \left[ -\frac{(\bar{y}_f/\hat{f} + \hat{\phi}_y)^2}{2\hat{D}_y} \right] \hat{I}_S(\hat{\phi}_y) \\ &\times \left\{ \int_{-\infty}^{\infty} d\hat{\phi}_y \exp \left[ -\frac{\hat{\phi}_y^2}{2\hat{D}_y} \right] \hat{I}_S(\hat{\phi}_y) \right\}^{-1} , \end{aligned} \quad (166)$$

while the modulus of the spectral degree of coherence reads

$$|g(\hat{z}_f, \bar{y}_f, \Delta\hat{y}_f)| = \exp \left[ -2\frac{\hat{N}_y \Delta\hat{y}_f^2}{\hat{f}^2} \right] . \quad (167)$$

For the image plane, Eq. (132) and Eq. (162) give the following cross-spectral density:

$$\begin{aligned} \hat{G}(\hat{z}_i, \bar{y}_i, \Delta\hat{y}_i) &= \exp \left[ \frac{im(m+1)\bar{y}_i \Delta\hat{y}_i}{2\hat{z}_1} \right] \\ &\times \exp \left[ -\frac{m^2 \bar{y}_i^2}{2\hat{N}_y} \right] \exp \left[ -2\hat{D}_y m^2 \Delta\hat{y}_i^2 \right] \gamma(m\Delta\hat{y}_i) , \end{aligned} \quad (168)$$

corresponding to a relative intensity on the image plane

$$\hat{I}(\hat{z}_i, \bar{y}_i) = \exp \left[ -\frac{m^2 \bar{y}_i^2}{2\hat{N}_y} \right] . \quad (169)$$

Eq. (169) is the (magnified) image of the electron beam in the object plane  $\hat{z} = 0$ . The modulus of the spectral degree of coherence is:

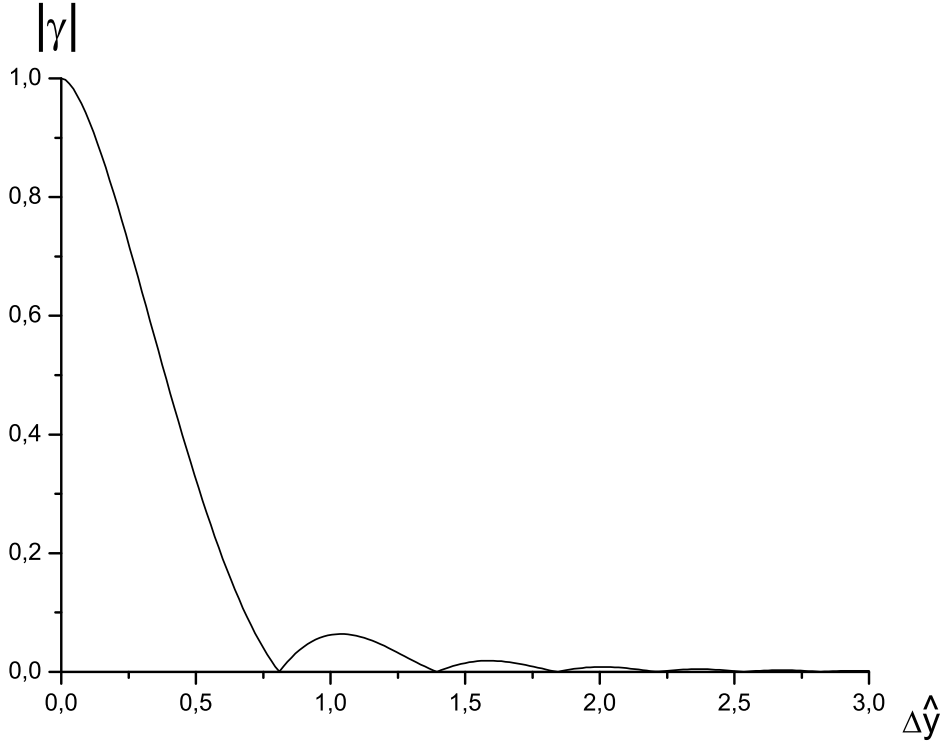


Fig. 14. Absolute value of the universal function  $\gamma$ , used to calculate, on the image plane, the spectral degree of coherence of a quasi-homogeneous undulator source when  $\hat{N}_x \gg 1$ ,  $\hat{D}_x \gg 1$  and  $\hat{N}_y \gg 1$ .

$$|g(\hat{z}_i, \bar{y}_i, \Delta\hat{y}_i)| = \exp \left[ -2\hat{D}_y m^2 \Delta\hat{y}_i^2 \right] |\gamma(m\Delta\hat{y}_i)| . \quad (170)$$

A plot of  $|\gamma(\Delta\hat{y})|$  is given in Fig. 14.

## 6.2 Source with non-Gaussian intensity distribution in the vertical direction

Let us now consider the case when  $\hat{D}_y \gg 1$  and  $\hat{N}_y$  assumes arbitrary values. In this case, Eq. (115) and Eq. (125) of [2] allow reconstruction of the cross-spectral density in the far zone, that is

$$\hat{G} = \exp \left[ 2i\bar{\theta}_y \hat{z}_o \Delta\hat{\theta}_y \right] \exp \left[ -2\hat{N}_y \Delta\hat{\theta}_y^2 \right] \exp \left[ -\frac{\bar{\theta}_y^2}{2\hat{D}_y} \right] \beta(\Delta\hat{\theta}_y) , \quad (171)$$

where the function  $\beta(\Delta\hat{y})$  is defined in Eq. (113) of [2] and reads:

$$\beta(\Delta\hat{\theta}_y) = \frac{1}{2\pi^2} \int_{-\infty}^{\infty} d\hat{\phi}_y \int_{-\infty}^{\infty} d\hat{\phi}_x \times \text{sinc} \left[ \frac{\hat{\phi}_x^2 + (\hat{\phi}_y - \Delta\hat{\theta}_y)^2}{4} \right] \text{sinc} \left[ \frac{\hat{\phi}_x^2 + (\hat{\phi}_y + \Delta\hat{\theta}_y)^2}{4} \right]. \quad (172)$$

Eq. (171) may be obtained directly from Eq. (141) in the limit  $\hat{z}_o^2 \gg \hat{N}_y/\hat{D}_y$ , i.e. in the far zone. Note that if  $\hat{N}_y/\hat{D}_y \ll 1$  ( $\hat{N}_y \lesssim 1$  is our main case of interest since we have already treated the case when both  $\hat{N}_y \gg 1$  and  $\hat{D}_y \gg 1$ ) the far zone begins already at the exit of the undulator, when  $\hat{z}_1 \sim 1$  (see also [2] for details). Let us introduce, in analogy with Eq. (163) the following (inverse) Fourier transform of the function  $\beta$ :

$$\hat{\mathcal{B}}(\bar{y}) = \frac{1}{\mathcal{K}} \int_{-\infty}^{\infty} d\hat{\phi}_y \exp [i(-2\bar{y})\hat{\phi}_y] \beta(\hat{\phi}_y). \quad (173)$$

Here  $\mathcal{K}$  is the normalization factor

$$\mathcal{K} = \int_{-\infty}^{\infty} d\hat{\phi}_y \beta(\hat{\phi}_y) \simeq 2.200, \quad (174)$$

and has been calculated numerically.

Both  $\beta(\Delta\hat{\theta}_y)$  and  $\hat{\mathcal{B}}(\bar{y})$  admit representations in terms of a one-dimensional integral (note that the representation for  $\beta(\Delta\hat{\theta}_y)$  has been already introduced in [2]). In order to see this, let us first consider the function:

$$\tilde{f}(\Delta\hat{\theta}'_x, \Delta\hat{\theta}'_y) = \frac{1}{2\pi^2} \int_{-\infty}^{\infty} d\hat{\phi}_y \int_{-\infty}^{\infty} d\hat{\phi}_x \times \text{sinc} \left[ \frac{(\hat{\phi}_x - \Delta\hat{\theta}'_x/2)^2 + (\hat{\phi}_y - \Delta\hat{\theta}'_y/2)^2}{4} \right] \times \text{sinc} \left[ \frac{(\hat{\phi}_x + \Delta\hat{\theta}'_x/2)^2 + (\hat{\phi}_y + \Delta\hat{\theta}'_y/2)^2}{4} \right]. \quad (175)$$

The function  $\tilde{f}$  is circularly symmetric. This can be seen switching to polar coordinates:

$$\begin{aligned} \hat{\phi}_x &= \hat{r}_\phi \cos(\hat{\eta}_\phi) \\ \hat{\phi}_y &= \hat{r}_\phi \sin(\hat{\eta}_\phi) \end{aligned} \quad (176)$$

and

$$\begin{aligned}
\Delta\hat{\theta}'_x/2 &= \hat{r}_\theta \cos(\hat{\eta}_\theta) \\
\Delta\hat{\theta}'_y/2 &= \hat{r}_\theta \sin(\hat{\eta}_\theta) .
\end{aligned} \tag{177}$$

Then, Eq. (175) can be rewritten as

$$\begin{aligned}
\tilde{f}(\hat{r}_\theta) &= \frac{1}{2\pi^2} \int_0^\infty d\hat{r}_\phi \int_0^{2\pi} d\hat{\eta}_\phi \\
&\times \text{sinc} \left[ \frac{\hat{r}_\phi^2 + \hat{r}_\theta^2 - 2\hat{r}_\phi\hat{r}_\theta \cos(\hat{\eta}_\phi - \hat{\eta}_\theta)}{4} \right] \\
&\times \text{sinc} \left[ \frac{\hat{r}_\phi^2 + \hat{r}_\theta^2 + 2\hat{r}_\phi\hat{r}_\theta \cos(\hat{\eta}_\phi - \hat{\eta}_\theta)}{4} \right] ,
\end{aligned} \tag{178}$$

which does not depend on  $\hat{\eta}_\theta$ , as can be seen switching to the integration variable  $\hat{\eta}' = \hat{\eta}_\phi - \hat{\eta}_\theta$ . The following relation follows:

$$\beta(\Delta\theta_y) = \tilde{f}(\Delta\hat{\theta}'_x, \Delta\hat{\theta}'_y) \tag{179}$$

for any  $(\Delta\hat{\theta}'_x, \Delta\hat{\theta}'_y)$  such that

$$\Delta\hat{\theta}_y = \sqrt{(\Delta\hat{\theta}'_x/2)^2 + (\Delta\hat{\theta}'_y/2)^2} . \tag{180}$$

The function  $\beta$  can be seen as a restriction of the function  $\tilde{f}$ . The reason why  $\tilde{f}$  has been introduced is that it allows the use the autocorrelation theorem to obtain the following relation:

$$\begin{aligned}
&\int_{-\infty}^\infty d\Delta\hat{\theta}'_x \int_{-\infty}^\infty d\Delta\hat{\theta}'_y \exp [i(\alpha_x\Delta\hat{\theta}'_x + \alpha_y\Delta\hat{\theta}'_y)] \tilde{f}(\Delta\hat{\theta}'_x, \Delta\hat{\theta}'_y) = \\
&\frac{1}{2\pi^2} \left| \int_{-\infty}^\infty d\hat{\phi}_x \int_{-\infty}^\infty d\hat{\phi}_y \exp [i(\alpha_x\hat{\phi}_x + \alpha_y\hat{\phi}_y)] \text{sinc} \left[ \frac{\hat{\phi}_x^2 + \hat{\phi}_y^2}{4} \right] \right|^2 .
\end{aligned} \tag{181}$$

The integral in the right hand side of Eq. (181) has been already calculated, in practice, in Eq. (93), and it can be expressed in terms of the universal function  $\Psi$  defined in Eq. (95). It follows that

$$\begin{aligned}
&\int_{-\infty}^\infty d\Delta\hat{\theta}'_x \int_{-\infty}^\infty d\Delta\hat{\theta}'_y \exp [i(\alpha_x\Delta\hat{\theta}'_x + \alpha_y\Delta\hat{\theta}'_y)] \tilde{f}(\Delta\hat{\theta}'_x, \Delta\hat{\theta}'_y) = \\
&2 \left[ \pi - 2\text{Si}(\alpha_x^2 + \alpha_y^2) \right]^2 = 2\pi^2 \Psi \left( \sqrt{\alpha_x^2 + \alpha_y^2} \right) .
\end{aligned} \tag{182}$$

We can now inverse transform Eq. (182) using the Fourier-Bessel formula, thus obtaining

$$\tilde{f}(\Delta\hat{\theta}'_x, \Delta\hat{\theta}'_y) = \pi \int_0^\infty d\alpha \alpha J_o \left( \alpha \sqrt{(\Delta\hat{\theta}'_x)^2 + (\Delta\hat{\theta}'_y)^2} \right) \Psi(\alpha) . \quad (183)$$

Letting  $\Delta\hat{\theta}'_x = 0$  and using Eq. (179) and Eq. (180) we obtain the following representation for  $\beta$ :

$$\beta(\Delta\hat{\theta}_y) = \pi \int_0^\infty d\alpha \alpha J_o (2\alpha\Delta\hat{\theta}_y) \Psi(\alpha) . \quad (184)$$

Applying the definition of  $\hat{\mathcal{B}}$  in Eq. (174) we obtain

$$\hat{\mathcal{B}}(\bar{y}) = \frac{\pi}{\mathcal{K}} \int_0^\infty d\alpha \alpha \Psi(\alpha) \int_{-\infty}^\infty d\Delta\hat{\theta}_y \exp [i(-2\bar{y})\Delta\hat{\theta}_y] J_o (2\alpha\Delta\hat{\theta}_y) . \quad (185)$$

The Fourier integral in  $\Delta\hat{\theta}_y$  can be performed analytically (see [8], Appendix A.3.), thus giving the following representation of  $\hat{\mathcal{B}}$ :

$$\hat{\mathcal{B}}(\bar{y}) = \frac{\pi}{\mathcal{K}} \int_0^\infty d\alpha \frac{\text{rect} [\bar{y}/(2\alpha)]}{[1 - (\bar{y}/\alpha)^2]^{1/2}} \Psi(\alpha) , \quad (186)$$

where the function  $\text{rect}(x)$  is defined, following [8], to be unity for  $|x| \leq 1/2$  and zero otherwise. A plot of the universal  $\hat{\mathcal{B}}$  is given in Fig. 15.

Using Eq. (127) and Eq. (171) we obtain the Fourier transform of the cross-spectral density at the virtual-source position

$$\hat{\mathcal{G}}(0, \bar{u}, \Delta\hat{u}) = \exp [-2\hat{N}_y\Delta\hat{u}^2] \exp \left[ -\frac{\bar{u}^2}{2\hat{D}_y} \right] \beta(\Delta\hat{u}) . \quad (187)$$

Inverse transforming Eq. (187) we can write the cross-spectral density at the virtual-source position

$$\hat{G}(0, \bar{y}, \Delta\hat{y}) = \exp [-2\hat{D}_y\Delta\hat{y}^2] \int_{-\infty}^\infty d\eta \exp \left[ -\frac{(\eta + \bar{y})^2}{2\hat{N}_y} \right] \hat{\mathcal{B}}(\eta) . \quad (188)$$

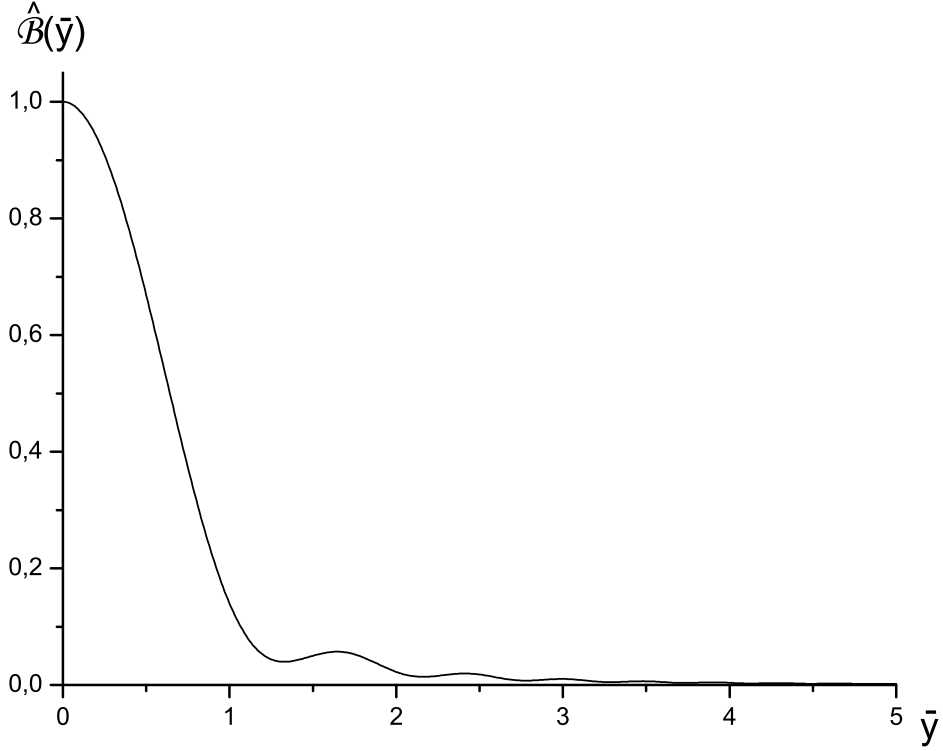


Fig. 15. The universal function  $\hat{\mathcal{B}}$ , used to calculate intensity on the image plane of a quasi-homogeneous undulator source when  $\hat{N}_x \gg 1$ ,  $\hat{D}_x \gg 1$  and  $\hat{D}_y \gg 1$ .

Then, from Eq. (131) and Eq. (187) we obtain the cross-spectral density on the focal plane

$$\begin{aligned} \hat{G}(\hat{z}_f, \bar{y}_f, \Delta\hat{y}_f) &= \exp \left[ \frac{2i}{\hat{f}^2} (\hat{f} - \hat{z}_1) \bar{y}_f \Delta\hat{y}_f \right] \exp \left[ -\frac{2\hat{N}_y \Delta\hat{y}_f^2}{\hat{f}^2} \right] \\ &\times \exp \left[ -\frac{\bar{y}_f^2}{2\hat{D}_y \hat{f}^2} \right] \beta \left( \frac{\Delta\hat{y}_f}{\hat{f}} \right). \end{aligned} \quad (189)$$

The relative intensity on the focal plane is therefore given by

$$\hat{I}(\hat{z}_f, \bar{y}_f) = \exp \left[ -\frac{\bar{y}_f^2}{2\hat{D}_y \hat{f}^2} \right], \quad (190)$$

while the modulus of the spectral degree of coherence reads

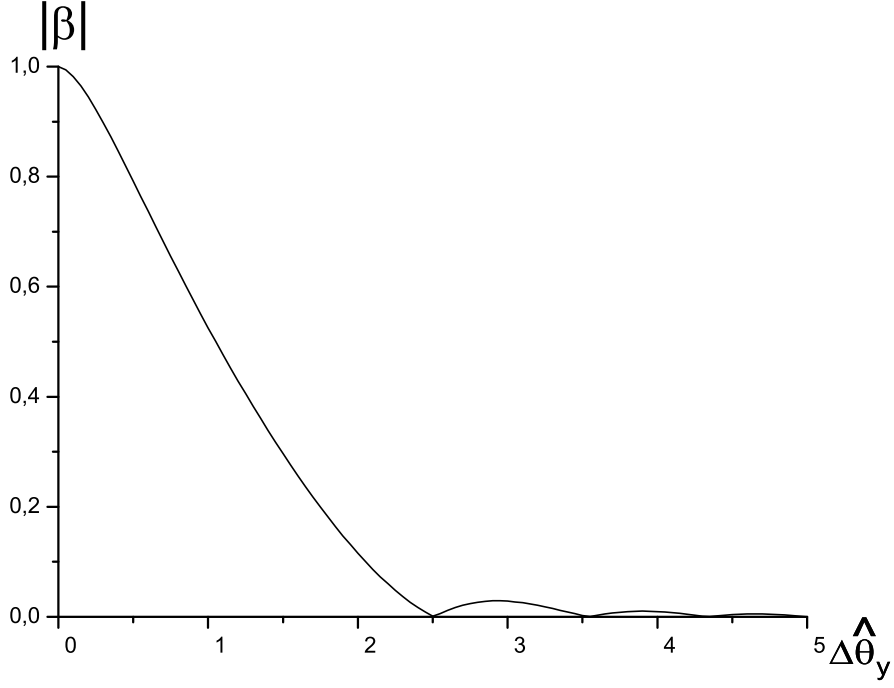


Fig. 16. Absolute value of the universal function  $\beta$ , used to calculate coherence on the focal plane of a quasi-homogeneous undulator source when  $\hat{N}_x \gg 1$ ,  $\hat{D}_x \gg 1$  and  $\hat{D}_y \gg 1$ .

$$|g(\hat{z}_f, \bar{y}_f, \Delta \hat{y}_f)| = \exp \left[ -\frac{2\hat{N}_y \Delta \hat{y}_f^2}{\hat{f}^2} \right] \left| \beta \left( \frac{\Delta \hat{y}_f}{\hat{f}} \right) \right|. \quad (191)$$

A plot of  $|\beta(\Delta \hat{\theta}_y)|$  is given in Fig. 16. For the image plane, Eq. (132) and Eq. (188) give the following cross-spectral density:

$$\begin{aligned} \hat{G}(\hat{z}_i, \bar{y}_i, \Delta \hat{y}_i) &= \exp \left[ \frac{i m(m+1) \bar{y}_i \Delta \hat{y}_i}{2 \hat{z}_1} \right] \\ &\times \exp \left[ -2 \hat{D}_y m^2 \Delta \hat{y}_i^2 \right] \int_{-\infty}^{\infty} d\eta \exp \left[ -\frac{(\eta + m \bar{y}_i)^2}{2 \hat{N}_y} \right] \hat{\mathcal{B}}(\eta), \end{aligned} \quad (192)$$

corresponding to a relative intensity on the image plane

$$\hat{I}(\hat{z}_i, \bar{y}_i) = \int_{-\infty}^{\infty} d\eta \exp \left[ -\frac{(\eta + m \bar{y}_i)^2}{2 \hat{N}_y} \right] \hat{\mathcal{B}}(\eta) / \left\{ \int_{-\infty}^{\infty} d\eta \exp \left[ -\frac{\eta^2}{2 \hat{N}_y} \right] \hat{\mathcal{B}}(\eta) \right\}.$$

(193)

The modulus of the spectral degree of coherence is

$$|g(\hat{z}_i, \bar{y}_i, \Delta\hat{y}_i)| = \exp \left[ -2\hat{D}_y m^2 \Delta\hat{y}_i^2 \right] . \quad (194)$$

Finally, in the particular case for  $\hat{N}_y \ll 1$ , Eq. (193) reduces to

$$\hat{I}(\hat{z}_i, \bar{y}_i) = \hat{\mathcal{B}}(m\bar{y}_i) . \quad (195)$$

## 7 Analysis of the image formation mechanism for quasi-homogeneous undulator sources in terms of Geometrical Optics

In the Introduction we have stressed that the image formation problem is twofold: one should be able to provide a characterization of the virtual source as well as to track the cross-spectral density of the source through the optical beamline.

Let us first analyze the problem of source characterization. In Section 1 we have seen that, in the asymptotic limit for a large electron beam emittance  $\epsilon_{x,y} \gg \lambda/(2\pi)$ , Geometrical Optics may be used equally well as Statistical Optics to fulfill this task. Here we will discuss more in detail the relation between the Statistical Optics approach and the Geometrical Optics approach with particular attention to the applicability region of the latter.

Let us start with a remark, which applies not only to undulator radiation sources but also to sources of other kind (e.g. bending magnets). In the Introduction, in order to decide whether Geometrical Optics or Wave Optics is applicable, we compared the *electron beam* emittance with the radiation wavelength. This is acceptable in many cases when undulator radiation is involved but not, for instance, when bending magnet radiation is considered. In all generality one should separately compare the *photon beam* size and divergence with the radiation diffraction size and diffraction angle, which are quantities pertaining the single electron radiation. Let us fix a given direction  $x$  or  $y$ . The square of the diffraction angle is defined by  $(\sigma'_d)^2 \sim \lambda/(2\pi L_f)$ ,  $L_f$  being the formation length of the radiation at wavelength  $\lambda$  as defined in [1]. The diffraction size of the source is given by  $\sigma_d \sim \sigma'_d L_f$ . In calculating the photon beam size and divergence one should always include diffraction effects. As a result, if  $\sigma^2$  and  $(\sigma')^2$  indicate the square of the electron beam size and divergence, the corresponding square of the photon beam size and divergence will be respectively of order  $\max[\sigma^2, \sigma_d^2]$  and  $\max[(\sigma')^2, (\sigma'_d)^2]$ . These quantities can be rewritten in terms of the electron beam emittance as  $\max[\epsilon\beta, \sigma_d^2]$  and

$\max[\epsilon/\beta, (\sigma'_d)^2]$ ,  $\beta$  being the minimal beta function value, defining the virtual source position for the radiator (undulator, bending magnet, or other). Dividing these two quantities respectively by  $\sigma_d^2$  and  $(\sigma'_d)^2$  give natural values, normalized to unity, for the photon beam size  $\max[2\pi\epsilon\beta/(L_f\lambda), 1]$  and divergence  $\max[2\pi\epsilon L_f/(\beta\lambda), 1]$ . When the product between these two quantities is much larger than unity one can use a Geometrical Optics approach. In this case, this product represents the normalized *photon beam* emittance. When  $\beta \sim L_f$ , as in many undulator cases, one may compare, for rough estimations, the electron beam emittance and the radiation wavelength as we have done before. However, in the case of a bending magnet one may typically have  $\beta$  of order 10 m and  $L_f$  of order  $10^{-3} \div 10^{-2}$  m. The ratio  $\beta/L_f \gg 1$  now constitutes an extra large parameter of the problem. In this case, even if the electron beam emittance is two order of magnitude smaller than the wavelength, due to diffraction effects one can still apply a Geometrical Optics approach, because  $\max[2\pi\epsilon\beta/(L_f\lambda), 1] \cdot \max[2\pi\epsilon L_f/(\beta\lambda), 1] \gg 1$ , i.e. the photon beam emittance is much larger than the wavelength. As a result, dimensional analysis suggests that bending magnet radiation may be treated exhaustively in the framework of Geometrical Optics even for third generation light sources.

As discussed above, when  $\beta \sim L_f$  a large electron beam emittance (compared with the radiation wavelength) is a necessary and sufficient condition for the Geometrical Optic approach to apply. In spite of that, when  $\beta \gg L_f$  or  $\beta \ll L_f$ , a large electron beam emittance is a sufficient, but not necessary condition for the Geometrical Optic approach to be possibly used for source characterization. Let us prove this statement with undulator sources in mind<sup>11</sup>. It is enough to prove that the wider class of quasi-homogeneous sources, which includes situations when the electron beam emittance is not larger than the wavelength, can be described in terms of Geometrical Optics.

Let us then consider the class of quasi-homogeneous virtual sources for undulator devices. The cross-spectral density of the virtual source (positioned at  $z = 0$ , i.e. at the virtual source plane) can be written as in Eq. (2), that we rewrite here for convenience in terms of coordinates  $\bar{r}_{x,y}$  and  $\Delta\hat{r}_{x,y}$ :

$$\hat{G}_o(\bar{r}_x, \bar{r}_y, \Delta\hat{r}_x, \Delta\hat{r}_y) = \hat{I}(\bar{r}_x, \bar{r}_y) g(\Delta\hat{r}_x, \Delta\hat{r}_y) . \quad (196)$$

As usual, the Fourier transform of Eq. (196) with respect to all variables will be indicated with

---

<sup>11</sup> Note that, even though in the case of undulator sources one often has  $\beta \sim L_f$ , there are situations when  $\beta \gg L_f$  or  $\beta \ll L_f$  and when the electron emittance is of order of the wavelength. However, in the undulator case, very large values of the ratio  $\beta/L_f$  of order  $10^3 \div 10^4$ , typical of the bending magnet case, are unrealistic.

$$\begin{aligned} \hat{\mathcal{G}}_o(\bar{\theta}_x, \bar{\theta}_y, \Delta\hat{\theta}_x, \Delta\hat{\theta}_y) &= \int_{-\infty}^{\infty} d\Delta\hat{r}'_x \int_{-\infty}^{\infty} d\Delta\hat{r}'_y \int_{-\infty}^{\infty} d\bar{r}'_x \int_{-\infty}^{\infty} d\bar{r}'_y \hat{G}_o(\bar{r}'_x, \bar{r}'_y, \Delta\hat{r}'_x, \Delta\hat{r}'_y) \\ &\quad \times \exp[2i(\bar{\theta}_x\Delta\hat{r}'_x + \bar{\theta}_y\Delta\hat{r}'_y)] \exp[2i(\Delta\hat{\theta}_x\bar{r}'_x + \Delta\hat{\theta}_y\bar{r}'_y)] . \end{aligned} \quad (197)$$

The two quantities  $\hat{I}(\bar{r}_x, \bar{r}_y) = \hat{G}_o(\bar{r}_x, \bar{r}_y, 0, 0)$  and  $\hat{\Gamma}(\bar{\theta}_x, \bar{\theta}_y) = \hat{\mathcal{G}}_o(\bar{\theta}_x, \bar{\theta}_y, 0, 0)$  are always positive, because, by definition of  $\hat{G}_o$ , they are ensemble averages of quantities under square modulus.

Let us now introduce the Fourier transform of Eq. (196) with respect to  $\Delta\hat{r}_{x,y}$ :

$$\begin{aligned} \hat{\Phi}_o(\bar{r}_x, \bar{r}_y, \bar{\theta}_x, \bar{\theta}_y) &= \int_{-\infty}^{\infty} d\Delta\hat{r}'_x \int_{-\infty}^{\infty} d\Delta\hat{r}'_y \hat{G}_o(\bar{r}_x, \bar{r}_y, \Delta\hat{r}'_x, \Delta\hat{r}'_y) \\ &\quad \times \exp[2i(\bar{\theta}_x\Delta\hat{r}'_x + \bar{\theta}_y\Delta\hat{r}'_y)] . \end{aligned} \quad (198)$$

Accounting for Eq. (196), i.e. in the particular case of a (virtual) quasi-homogeneous source, Eq. (198) can be written as

$$\hat{\Phi}_o(\bar{r}_x, \bar{r}_y, \bar{\theta}_x, \bar{\theta}_y) = \hat{I}(\bar{r}_x, \bar{r}_y) \hat{\Gamma}(\bar{\theta}_x, \bar{\theta}_y) , \quad (199)$$

having recognized that  $\hat{\Gamma}(\bar{\theta}_x, \bar{\theta}_y) = \hat{\mathcal{G}}_o(\bar{\theta}_x, \bar{\theta}_y, 0, 0)$  is the Fourier transform of the spectral degree of coherence  $g$ . The distribution  $\hat{\Phi}_o$ , being the product of two positive quantities, never assumes negative values. Therefore it may always be interpreted as a phase space distribution<sup>12</sup>. This analysis shows that quasi-homogeneous sources can always be characterized in terms of Geometrical Optics. It also shows that, in this particular case, the coordinates in the phase space,  $\bar{r}_{x,y}$  and  $\bar{\theta}_{x,y}$ , are separable.

Eq. (198) is the definition of a Wigner distribution. In the case of quasi-homogeneous sources, as we have just seen, the Wigner distribution is never negative and, therefore, can always be interpreted as a phase space distribution. In the case of non quasi-homogeneous sources one may still define a

<sup>12</sup> It should be remarked that this result has been obtained only on the ground of mathematical basis, i.e. without ascribing to  $\hat{I}$  and  $\hat{\Gamma}$  any physical meaning. In other words, we simply considered the cross-spectral density  $\hat{G}_o$  as the ensemble-averaged product of  $\hat{E}(\hat{r}'_1)$  and  $\hat{E}^*(\hat{r}'_2)$  without ascribing to the function  $\hat{E}$  any physical meaning. Physically, as has been said in the Introduction, in the quasi-homogeneous case  $\hat{\Gamma}$  can be identified with the radiant intensity of the virtual source (compare with Eq. (6)). This follows from a statement similar to the van Cittert-Zernike theorem for quasi-homogeneous sources (see [3]). Note that the intensity and the Fourier transform of the spectral degree of coherence are obtained back from the phase space distribution, Eq. (199), by integration over coordinates  $\bar{\theta}_{x,y}$  and  $\bar{r}_{x,y}$  respectively.

Wigner distribution using Eq. (198). The integral of the Wigner function over its coordinates must still be finite<sup>13</sup>. However the Wigner function itself is not always a positive function. As a consequence it cannot always be interpreted as a phase space distribution. On the one hand, quasi-homogeneity is a sufficient condition for the Geometrical Optics approach to be possibly used in the representation of the source. On the other hand though, necessary and sufficient conditions for  $\hat{\Phi}_o$  to be a positive function are more difficult to find.

One may observe that Bochner's theorem<sup>14</sup> may be used to investigate whether the Wigner function can be interpreted as a phase space distribution in the case of non-homogeneous sources. In particular, it is necessary and sufficient to look for non-negative definite cross-spectral density functions. However, in general, it is not trivial to investigate whether a function is non-negative definite (see footnote 14) and therefore this observation does not seem to constitute a simplification. We will simply leave the search for necessary and sufficient condition for  $\hat{\Phi}_o$  to be a positive function as an open question. We did not rule out, for undulator setups, the possibility of having a positive Wigner distribution in the non quasi-homogeneous case. At first glance it may look like such a

---

<sup>13</sup> This ensures that  $\hat{\Phi}_o$  has finite integral over its variables.  $\hat{\Phi}_o$  is the Fourier transform of a correlation function (the cross-spectral density) of electromagnetic fields. The fields being physical quantities can carry only a finite amount of energy and they are limited in spatial extent. As a result the cross-spectral density must be an integrable function over its variables and so must be, by definition,  $\hat{\Phi}_o$ .

<sup>14</sup> Bochner's theorem "in its elementary form asserts that every non-negative definite function of a broad class has a non-negative Fourier transform and, conversely, that the Fourier transform of every non-negative function of a broad class is non-negative definite. This class includes functions which fall off sufficiently rapidly to infinity to ensure that their Fourier transforms are continuous functions" [cited from paragraph 1.4.2. of reference [3]]. It should hereby be stressed the difference in the mathematical language between a positive function  $f(\xi) \geq 0$  for every real value  $\xi$  and a *non-negative definite* function. The function  $h$  is said to be non-negative definite when "for an arbitrary set of  $N$  real numbers  $\xi_1, \xi_2, \dots, \xi_N$  and  $N$  arbitrary complex numbers  $a_1, a_2, \dots, a_N$ ,  $\sum_{i=1}^N \sum_{j=1}^N a_i^* a_j h(\xi_j - \xi_i) \geq 0$ ." [cited from paragraph 1.4.2. of reference [3]]. Based on the assumption of a quasi-homogeneous source authors of [3] use Bochner's theorem instead of our previous discussion to demonstrate that the spectral degree of coherence  $g$  in Eq. (196) is necessarily non-negative definite. In fact, since the intensity  $\hat{I}$  is a positive function, the sign of  $\sum_{i=1}^N \sum_{j=1}^N a_i^* a_j g(\Delta\hat{r}_x ij, \Delta\hat{r}_y ij)$  is the same of the sign of  $\sum_{i=1}^N \sum_{j=1}^N a_i^* a_j \hat{I}(\bar{r}_x ij, \bar{r}_y ij) g(\Delta\hat{r}_x ij, \Delta\hat{r}_y ij) = \sum_{i=1}^N \sum_{j=1}^N a_i^* a_j \langle E(\hat{r}_j) E^*(\hat{r}_i) \rangle = \left\langle \left| \sum_{i=1}^N a_i E(\hat{r}_i) \right|^2 \right\rangle \geq 0$ , *quantum erat demonstrandum*. This demonstration is more involved than ours, even though it is based, as the ours, on the positivity of the square modulus of quantities. The reason for this complexity is that it uses a more general theorem, i.e. Bochner's theorem. However, as we have seen, it is not necessary to invoke Bochner's theorem in the quasi-homogeneous case.

case brings advantages in the formulation of the imaging theory, because the source can be described in terms of Geometrical Optics. On the one hand, in the case the Wigner distribution is positive, the evolution of the radiation in free space can be described by a ray-tracing approach, as the Wigner distribution can be interpreted as a phase space distribution. On the other hand though, such fact is almost irrelevant because it is not of help when optical elements are considered. As we will see later on, there are two particular conditions at the basis of a simplified formulation of the imaging theory based on the incoherent point spread function of the optical system. The first is the separability of the cross-spectral density is the product of a factor depending on  $\vec{r}$  and a factor depending on  $\Delta\vec{r}$ . The second is a transverse dimension of the source much larger than the transverse coherence length. As we have already seen these two conditions, together, define a quasi-homogeneous source. Quasi-homogeneous sources are necessarily characterized by a positive Wigner function. However, the positivity of the Wigner function alone is not sufficient to obtain a simplified formulation of the imaging theory in terms of incoherent point-spread function. A similar remark holds for a particular kind of sources often considered in literature also in connection with undulator radiation (see [14, 15]). These sources, characterized by a cross-spectral density  $G = \sqrt{I(r_1)}\sqrt{I(r_2)}g(r_1 - r_2)$  are called Shell sources (in particular, in [14, 15] Gaussian-Shell sources are discussed which assume gaussian a profile for both  $I$  and  $g$ ). They exhibit separability of the cross-spectral density, but are not quasi-homogeneous because the transverse dimension of the source fails to be much larger than the transverse coherence length: a simplified formulation of the imaging theory does not hold in this case either. Moreover, as it will be more extensively discussed here below and in Section 15, the Shell model (and, in particular, the Gaussian-Shell model) may be useful for describing light sources other than undulator-based or for educational purposes, but does not describe any practical realization of an undulator source.

We are now interested to find, in particular, equivalent conditions for quasi-homogeneity in terms of the electron beam sizes  $\hat{N}_{x,y}$  and divergences  $\hat{D}_{x,y}$  that apply to our case of interest, i.e. third generation light sources. In order to do so we start deriving an expression  $\hat{\mathcal{G}}$  for the Fourier transform of the cross-spectral density at the virtual source position. This is given by calculating the limit of Eq. (124) for  $\hat{z}_o \gg 1$  and taking advantage of Eq. (127). Aside for an inessential multiplicative constant we obtain:

$$\begin{aligned} \hat{\mathcal{G}}(0, \bar{\theta}_x, \bar{\theta}_y, \Delta\hat{\theta}_x, \Delta\hat{\theta}_y) &= \exp[-2\hat{N}_x\Delta\hat{\theta}_x^2] \exp[-2\hat{N}_y\Delta\hat{\theta}_y^2] \int_{-\infty}^{\infty} d\hat{\phi}_x \int_{-\infty}^{\infty} d\hat{\phi}_y \\ &\times \exp\left[-\frac{(\hat{\phi}_x + \bar{\theta}_x)^2}{2\hat{D}_x}\right] \exp\left[-\frac{(\hat{\phi}_y + \bar{\theta}_y)^2}{2\hat{D}_y}\right] \end{aligned}$$

$$\begin{aligned}
& \times \text{sinc} \left[ \frac{(\hat{\phi}_x - \Delta\hat{\theta}_x)^2 + (\hat{\phi}_y - \Delta\hat{\theta}_y)^2}{4} \right] \\
& \times \text{sinc} \left[ \frac{(\hat{\phi}_x + \Delta\hat{\theta}_x)^2 + (\hat{\phi}_y + \Delta\hat{\theta}_y)^2}{4} \right].
\end{aligned} \tag{200}$$

We have said that the quasi-homogeneity of the virtual source is equivalent to (i) separability of the cross-spectral density  $\hat{G}$  in the product of two factors respectively depending on  $\bar{\theta}_{x,y}$  and  $\Delta\hat{\theta}_{x,y}$  and (ii) a large characteristic scale of  $\bar{\theta}_{x,y}$  with respect to the characteristic scale of  $\Delta\hat{\theta}_{x,y}$ . From condition (i) follows that the virtual source is quasi-homogeneous *only if* it is possible to factorize the Fourier transform of the cross-spectral density,  $\hat{G}$  in Eq. (200), in the product of two factors separately depending on  $\bar{\theta}_{x,y}$  and  $\Delta\hat{\theta}_{x,y}$ . Such factorization, for third generation light sources, is equivalent to a particular choice of the region of parameters for the electron beam:  $\hat{N}_x \gg 1$ ,  $\hat{D}_x \gg 1$  and either (or both)  $\hat{N}_y \gg 1$  and  $\hat{D}_y \gg 1$ <sup>15</sup>. In this case, the second condition (ii) is automatically verified as one can verify inspecting Eq. (200).

An intuitive picture in the real space is given by a (virtual) quasi-homogeneous source with characteristic (normalized) square sizes  $\max(\hat{N}_{x,y}, 1)$  and characteristic (normalized) correlation length square of order  $\min(1/\hat{D}_{x,y}, 1)$ . As already remarked before, in the quasi-homogeneous situation the horizontal and the vertical directions can be treated separately, because Eq. (200) factorizes in the product of factors separately depending on the horizontal and on the vertical coordinates. This corresponds to a large number of independently radiating sources given by the product

$$M_{x,y} = \max(\hat{N}_{x,y}, 1) \max(\hat{D}_{x,y}, 1). \tag{201}$$

The number  $M_{x,y}$  is, in other words, an estimation of the number of coherent modes in the horizontal and in the vertical direction<sup>16</sup>. The number  $M_{x,y}^{-1}$

<sup>15</sup> It should be remarked here, that these conditions describe the totality of third generation quasi-homogeneous sources. In fact, while a purely mathematical analysis indicates that factorization of Eq. (200) is equivalent to more generic conditions ( $\hat{N}_x \gg 1$  and  $\hat{N}_y \gg 1$ , or  $\hat{D}_x \gg 1$  and  $\hat{D}_y \gg 1$ ), comparison with third generation source parameters reduces such conditions to the already mentioned ones.

<sup>16</sup> This is in agreement with an intuitive picture where the photon-beam phase space reproduces the electron-beam phase space up to the limit imposed by the intrinsic diffraction of undulator radiation. Imagine to start from a situation with  $\hat{N}_{x,y} \gg 1$  and  $\hat{D}_{x,y} \gg 1$  and to "squeeze" the electron-beam phase space by diminishing  $\hat{N}_{x,y}$  and  $\hat{D}_{x,y}$ . On the one hand the characteristic sizes of the phase space of the electron beam are always of order  $\hat{N}_{x,y}$  and  $\hat{D}_{x,y}$ . On the other hand the characteristic sizes of the phase space of the photon beam are of order  $\max(\hat{N}_{x,y}, 1)$  and  $\max(\hat{D}_{x,y}, 1)$ : diffraction effects limit the "squeezing" of the phase space of the photon beam.

is the accuracy of Geometrical Optics results compared with Statistical Optics results or, better, the accuracy of the quasi-homogeneous assumption. It should be noted that, as  $M_{x,y}$  approaches unity, the accuracy of the quasi-homogeneous assumption becomes worse and worse and  $M_{x,y}$  cannot be taken anymore as a meaningful estimation of the number of modes: it should be replaced by a more accurate concept based on Statistical Optics. To complete the previous statement we should add that  $M_{x,y}$  completely loses the meaning of "number of modes" when Geometrical Optics cannot be applied. For instance when both  $\hat{N}_y$  and  $\hat{D}_y$  are of order unity (or smaller), one can state that the Geometrical Optics approach fails in the vertical direction because the phase space area is getting near to the uncertainty limit. In this case it is not possible to ascribe the meaning of "number of modes" to the number  $M_y$  simply because the Geometrical Optics approach in the vertical direction fails. However, when  $\hat{N}_y$  and  $\hat{D}_y$  are of order unity (or smaller), but both  $\hat{N}_x \gg 1$  and  $\hat{D}_x \gg 1$ , the cross-spectral density admits factorization in the horizontal and in the vertical direction and the source in the horizontal direction can be still described, independently, with the help of Geometrical Optics.

Up to now we discussed about the roles of Geometrical and Statistical optics in the characterization of the source only. However, as already remarked, the specification of the source constitutes only part of the solution of the imaging problem. One has, in fact, to track information regarding the source through the optical beamline up to the observation plane. Depending on the situation Geometrical Optics may be used or not. For instance, a quasi-homogeneous source may well be described in terms of a phase space distribution, but if diffraction effects dominate the photon beam transport to the observation plane, one cannot use ray-tracing techniques to calculate the intensity profile at the observation plane. However, as we will see in the next Section, if the virtual source is quasi-homogeneous, the intensity at the observation plane can always be expressed as a convolution product between the impulse response of the optical system and the intensity which would be recovered at the observation plane in the case of an ideal optical system (i.e. one with no aberration and non-limiting pupil apertures). In this case, the entire line may be studied with the help of ray-tracing programs if and only if the impulse response of the system can be recovered by means of Geometrical Optics techniques.

In Geometrical Optics, a Hamiltonian description of the optical system holds so that interaction with optical media (i.e. the system evolution) is conveniently modelled in terms of symplectic transformations. A given symplectic transformation  $\mathcal{S}$  acts on point  $\tilde{\rho}_o = (\bar{r}_{ox}, \bar{\theta}_{ox}, \bar{r}_{oy}, \bar{\theta}_{oy})$  of the phase space  $\hat{\Phi}_o$  at  $\hat{z}_o = 0$  and maps it to a point  $\tilde{\rho} = (\bar{r}_x, \bar{\theta}_x, \bar{r}_y, \bar{\theta}_y)$ , of the phase space  $\hat{\Phi}_z$  at  $\hat{z}_o = \hat{z}$  according to

$$\tilde{\rho} = \mathcal{S}(\tilde{\rho}_o) . \tag{202}$$

The phase space distribution is therefore transformed according to

$$\hat{\Phi}_z(\tilde{\rho}) = \hat{\Phi}_o[\mathcal{S}^{-1}(\tilde{\rho})] . \quad (203)$$

According to Liouville's theorem, the area of the phase space is conserved during this process. In the particular case of linear transformations, one can use a matrix formalism. N successive linear transformations are represented by N matrices  $L_1 \dots L_N$  and the resulting transformation is represented by N successive matrix multiplications, which give the matrix  $L = L_N \cdot \dots \cdot L_1$ . The action of L on an element of the phase space is then naturally represented by multiplication. The variables  $\tilde{\rho}$  in phase space characterize a ray with a certain direction and offset with respect to the optical axis. The task of calculating the phase space distribution after a given number of optical elements through

$$\hat{\Phi}_z(\tilde{\rho}) = \hat{\Phi}_o[L^{-1} \cdot (\tilde{\rho})^t] , \quad (204)$$

where t indicates transposition, or through the more general Eq. (203) can be solved by ray-tracing programs. Once  $\hat{\Phi}_z$  is known, these codes usually integrate it over the variable  $\bar{\theta}_x$  and  $\bar{\theta}_y$  to give the intensity distribution

$$\hat{I}(\hat{z}, \bar{r}_x, \bar{r}_y) = \int_{-\infty}^{\infty} d\bar{\theta}_x \int_{-\infty}^{\infty} d\bar{\theta}_y \hat{\Phi}_z(\bar{r}_x, \bar{\theta}_x, \bar{r}_y, \bar{\theta}_y) . \quad (205)$$

However, the same programs may also be used to calculate the Fourier transform of the spectral degree of coherence through

$$\hat{\Gamma}(\hat{z}, \bar{\theta}_x, \bar{\theta}_y) = \int_{-\infty}^{\infty} d\bar{r}_x \int_{-\infty}^{\infty} d\bar{r}_y \hat{\Phi}_z(\bar{r}_x, \bar{\theta}_x, \bar{r}_y, \bar{\theta}_y) . \quad (206)$$

In particular, in free space, Eq. (204) becomes

$$\hat{\Phi}_z(\bar{r}_x, \bar{\theta}_x, \bar{r}_y, \bar{\theta}_y) = \hat{I}(0, \bar{r}_x - \hat{z}\bar{\theta}_x, \bar{r}_y - \hat{z}\bar{\theta}_y) \hat{\Gamma}(0, \bar{\theta}_x, \bar{\theta}_y) , \quad (207)$$

while Eq. (205) and Eq. (206) reduce to convolutions:

$$\hat{I}(\hat{z}, \bar{r}_x, \bar{r}_y) = \int_{-\infty}^{\infty} d\bar{\theta}_x \int_{-\infty}^{\infty} d\bar{\theta}_y \hat{I}(0, \bar{r}_x - \hat{z}\bar{\theta}_x, \bar{r}_y - \hat{z}\bar{\theta}_y) \hat{\Gamma}(0, \bar{\theta}_x, \bar{\theta}_y) \quad (208)$$

and

$$\begin{aligned}\hat{\Gamma}(\hat{z}, \bar{\theta}_x, \bar{\theta}_y) &= \int_{-\infty}^{\infty} d\bar{r}_x \int_{-\infty}^{\infty} d\bar{r}_y \hat{I}(0, \bar{r}_x - \hat{z}\bar{\theta}_x, \bar{r}_y - \hat{z}\bar{\theta}_y) \hat{\Gamma}(0, \bar{\theta}_x, \bar{\theta}_y) \\ &= \hat{\Gamma}(0, \bar{\theta}_x, \bar{\theta}_y) .\end{aligned}\tag{209}$$

Note that  $\hat{\Gamma}$  calculated at  $\hat{z} = 0$  has direct physical sense as the intensity distribution in the far zone, i.e. the angular spectrum. Then, Eq. (209) tells that, at arbitrary distance  $\hat{z}$ , the angular spectrum does not vary.

The intensity recovered at the image plane in the case of an ideal optical system is a scaled copy of that at the virtual source, regardless of the source. Generally, although as we will see exceptions apply, such correspondence between the intensity of the source and the observed intensity is only true in the case the observation plane is the image plane. In the case of a quasi-homogeneous virtual source, Geometrical Optics as well as Statistical Optics techniques can be employed to recover the intensity at the observation plane. Results from the Geometrical Optics and from the Statistical Optics approach must then coincide. Let us prove this fact considering the particular case  $\hat{N} \gg 1$  and  $\hat{D} \gg 1$  in a given direction and showing that we are able to recover Eq. (151) by means of Geometrical Optics techniques, namely by means of the matrix formalism employed in ray-tracing codes.

In this particular situation, the photon beam can be modelled as if a Gaussian photon beam was present at  $\hat{z} = 0$  with the same horizontal phase space of the electron beam. This is an *ansatz* on the virtual quasi-homogeneous source based on the phase space picture described above since strictly speaking it does not make sense to talk about a Gaussian photon beam inside the undulator, i.e. within the radiation formation length. If, however, this *ansatz* is made, we can describe the optical equivalent of the Twiss matrix at  $\hat{z} = 0$ . Let us first introduce the notion of normalized Twiss parameters as:

$$\begin{aligned}\hat{\alpha}_T &= \alpha_T , \\ \hat{\beta}_T &= L_w^{-1} \beta_T , \\ \hat{\gamma}_T &= L_w \gamma_T , \\ \hat{\epsilon} &= (\omega/c) \epsilon ,\end{aligned}\tag{210}$$

where  $\alpha_T$ ,  $\beta_T$  and  $\gamma_T$  are the Twiss parameters and  $\epsilon$  is the emittance pertaining the photon beam<sup>17</sup>. In the case under study they are identical to the analogous electron beam parameters. We have

$$\sigma_{|\hat{z}=0} \equiv \hat{\epsilon} \begin{pmatrix} \hat{\beta}_T(0) & -\hat{\alpha}_T(0) \\ -\hat{\alpha}_T(0) & \hat{\gamma}_T(0) \end{pmatrix} = \begin{pmatrix} \hat{N} & 0 \\ 0 & \hat{D} \end{pmatrix} ,\tag{211}$$

<sup>17</sup>The Twiss parameters are the second moments of the phase space distribution of the photons divided by the emittance.

For this exemplification we will assume a non-limiting pupil aperture. Then, the linear transformation mapping a phase-space point in  $\hat{z} = 0$  to a phase-space point in  $\hat{z} = \hat{z}_2$  is represented by the matrix  $L$ . In our particular case of interest we have

$$\begin{aligned} L &= \begin{pmatrix} 1 & \hat{z}_2 - \hat{z}_1 \\ 0 & 1 \end{pmatrix} \cdot \begin{pmatrix} 1 & 0 \\ -1/\hat{f} & 1 \end{pmatrix} \cdot \begin{pmatrix} 1 & \hat{z}_1 \\ 0 & 1 \end{pmatrix} \\ &= \begin{pmatrix} -\hat{z}_2/\hat{z}_1 + 1 & 0 \\ \hat{z}_2/(\hat{z}_1^2 - \hat{z}_1\hat{z}_2) & \hat{z}_1/(\hat{z}_1 - \hat{z}_2) \end{pmatrix}. \end{aligned} \quad (212)$$

As one can see from Eq. (42),  $L$  describes a free-space flight followed by a focusing element and a second free-space flight. A point  $(\hat{l}_o, \hat{\eta}_o)$  of the photon beam phase space at  $\hat{z} = 0$  is transformed, at  $\hat{z} = \hat{z}_2$  into

$$\begin{pmatrix} \hat{l}_1 \\ \hat{\eta}_1 \end{pmatrix} = L \begin{pmatrix} \hat{l}_o \\ \hat{\eta}_o \end{pmatrix}, \quad (213)$$

while the Twiss parameters for the photon beam at  $\hat{z} = \hat{z}_2$  are described by the matrix

$$\sigma_{|\hat{z}=\hat{z}_2} = L \cdot \sigma_{|\hat{z}=0} \cdot L^t = \hat{\epsilon} \begin{pmatrix} \hat{\beta}_T(\hat{z}_2) & -\hat{\alpha}_T(\hat{z}_2) \\ -\hat{\alpha}_T(\hat{z}_2) & \hat{\gamma}_T(\hat{z}_2) \end{pmatrix} \quad (214)$$

with

$$\begin{aligned} \hat{\epsilon}\hat{\alpha}_T(\hat{z}_2) &= \frac{1}{(\hat{A} + \hat{D})} \left\{ \hat{z}_1 [\hat{A} + (\hat{A} + \hat{D}) Q \hat{z}_1] [\hat{D} + (\hat{A} + \hat{D}) Q \hat{z}_1] \right. \\ &\quad \left. - [\hat{A}\hat{D} + (\hat{A} + \hat{D})^2 Q^2 \hat{z}_1^2] \hat{z}_2 \right\}, \end{aligned} \quad (215)$$

$$\hat{\epsilon}\hat{\beta}_T(\hat{z}_2) = \frac{[\hat{A}\hat{D} + (\hat{A} + \hat{D})^2 Q^2 \hat{z}_1^2] (\hat{z}_1 - \hat{z}_2)^2}{\hat{A} + \hat{D}} \quad (216)$$

and

$$\hat{\epsilon}\hat{\gamma}_T(\hat{z}_2) = \frac{\hat{A}\hat{D}}{\hat{A} + \hat{D}} + (\hat{A} + \hat{D}) Q^2 \hat{z}_1^2 + \frac{(\hat{A} + \hat{D}) \hat{z}_1^2}{(\hat{z}_1 - \hat{z}_2)^2} + \frac{2(\hat{A} + \hat{D}) Q \hat{z}_1^2}{\hat{z}_1 - \hat{z}_2}. \quad (217)$$

It should be recalled that parameters  $Q$  and  $\hat{A}$  have been defined in Eq. (148) and Eq. (149).

The photon phase space distribution at  $\hat{z} = \hat{z}_2$  is described by

$$f_{|z=\hat{z}_2} = \frac{1}{2\pi\hat{\epsilon}} \exp \left[ -\frac{\hat{\gamma}_T(\hat{z}_2)\hat{l}_1^2 + 2\hat{\alpha}_T(\hat{z}_2)\hat{l}_1\hat{\eta}_1 + \hat{\beta}_T(\hat{z}_2)\hat{\eta}_1^2}{2\hat{\epsilon}} \right]. \quad (218)$$

The relative intensity is derived from Eq. (218) integrating over the  $\hat{\eta}_1$ -coordinate, which gives

$$I(\hat{z}_2) = \exp \left[ -\frac{2\hat{l}_1^2}{2\hat{\epsilon}\hat{\beta}_T(\hat{z}_2)} \right]. \quad (219)$$

Finally, substitution of the expression for  $\hat{\epsilon}\hat{\beta}_T(\hat{z}_2)$  obtained in Eq. (216), yields back Eq. (151), as it should be. Similar conclusions may be obtained for the spectral degree of coherence integrating over the  $\hat{l}_1$ -coordinate and inverse Fourier transforming the result.

In spite of these results, we should stress again that Statistical Optics is the only mean to deal with the stochastic nature of Synchrotron Radiation in general. Only in particular cases Synchrotron Radiation can be treated in terms of Geometrical Optics. As we have just discussed, one of these cases is constituted by second generation light sources, when  $\hat{N}_{x,y} \gg 1$  and  $\hat{D}_{x,y} \gg 1$ . Experiments in this region of parameters can take advantage of ray-tracing code techniques.

To conclude this Section, we would like to make a much stronger statement: there are practical cases of interest when the Statistical Optics approach must be used even for second generation light sources. This should not sound too awkward since, as we have stated before, the impulse response of an optical line may not be treatable in terms of Geometrical Optics. Consider, for instance, the setup illustrated in Fig. 17. This consists of an entrance slit, a grating and an exit slit, that is a grating monochromator. The grating equation, which describes how the monochromator works, relies on the principle of interference applied to the light coming from adjacent grooves. Such principle though, can only be applied when phase and amplitude variations of the electromagnetic field are well defined across the grating, that is when the field is perfectly transversely coherent. If the transversely coherent spot of the radiation is smaller than the grating, not all the grating is taken advantage of, resulting

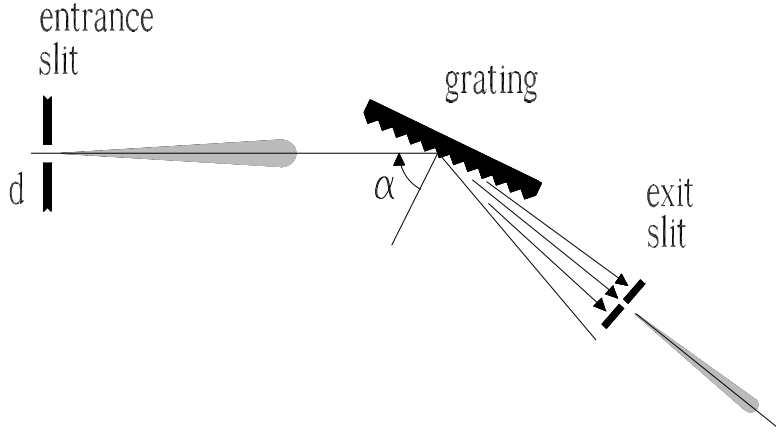


Fig. 17. Illustration of a grating monochromator.

in a decrease of resolution in wavelength. To better explain this point, with reference to Fig. 17, let us indicate the width of the entrance slit with  $d$  and the angle of incidence of the incoming radiation with  $\alpha$ . Moreover, let  $D_g$  be the typical dimension of the grating,  $N_g$  the total groove number,  $m$  the order of diffraction and  $z$  the distance between the entrance slit and the grating. The maximal (relative) resolution which can be obtained with a particular grating is given by  $(mN_g)^{-1}$ . Qualitatively, to obtain such maximal resolution we must have a transverse coherence area of at least the size  $D_g \cos(\alpha)$ . If it is smaller, not all the grating is used. We now need to transform this qualitative requirement into a quantitative requirement.

In practical situations, the grating is placed in the far zone with respect to the entrance slit. This is because the radiation spot size at the grating should be at least of order  $D_g \cos(\alpha)$ , which is much larger than the slit aperture  $d$ . If we assume the slit uniformly illuminated, we can consider the slit itself like a quasi-homogeneous source with rectangular profile. Then, the van Cittert-Zernike theorem applies at the grating position in the far zone. As a result, the modulus of the spectral degree of coherence  $|g|$  in the far zone is equal to the modulus of the Fourier transform of the intensity profile at the slit, which is a rectangular profile. The following expression for  $|g|$  is found in the dispersion direction:

$$|g(\Delta r)| = \left| \text{sinc} \left( \frac{\pi d \Delta r}{\lambda z} \right) \right|. \quad (220)$$

A quantitative requirement for the coherence property of the radiation at the grating can be given imposing that  $|g|$  varies within a fixed interval. For instance, one may require  $0.8 < |g(\Delta r)| < 1$ . This requirement may be changed, and is somewhat subjective. However it corresponds to a quantification of the transverse coherence properties of the radiation on the grating. In particular, if the criterium  $0.8 < |g(\Delta r)| < 1$  is chosen, the argument of the sinc func-

tion in Eq. (220) is allowed to vary a certain range  $[-X, X]$  with  $X \simeq 1.13$ . Moreover, the maximal value for  $\Delta r$  is  $D_g \cos(\alpha)$ , i.e. the grating dimension. Putting all together we obtain the following condition for the monochromator setup parameters:

$$\frac{\pi d D_g \cos(\alpha)}{\lambda z} = X \simeq 1.13 . \quad (221)$$

The same calculation may be repeated with a different choice for the minimal allowed value of  $|g(\Delta r)|$ . This would lead to a different value of  $X$ .

Our result is in agreement with the conclusion that one may draw considering the following relation [16]:

$$\frac{\Delta \lambda}{\lambda} = \left( \frac{d D_g \cos(\alpha)}{\lambda z} \right) \frac{1}{m N_g} . \quad (222)$$

Eq. (222) describes how the entrance slit width limits the resolution in wavelength according to. The second factor on the right hand side of Eq. (222), i.e.  $(m N_g)^{-1}$  is, again, the maximal relative resolution. This resolution can be obtained by setting the first factor to unity. This yields a result in parametrical agreement with Eq. (221). The right parametric dependence in the condition for the maximal resolution can also be obtained in another way. If the radiation sent through the slit has, at the grating, a spot size equal to  $D_g \cos(\alpha)$ , the condition for transverse coherence is given by the space-angle product:

$$d \cdot \theta = \frac{d D_g \cos(\alpha)}{2z} \simeq \frac{\lambda}{2\pi} . \quad (223)$$

Again, the qualitative estimation in Eq. (223) is in parametrical agreement with the quantitative calculation in Eq. (220).

The grating works with a resolution near to the theoretical limit  $(m N_g)^{-1}$  only with transversely coherent radiation. We may say that the purpose of the entrance slit is to supply a transversely coherent radiation spot at the grating in order to allow the monochromator to work with a certain resolution. This fact must hold for any light source, and in particular for second generation light sources. The bottom line is that this monochromator setup cannot be described in terms of Geometrical Optics even in the case of a second generation light source: transversely coherent radiation means that the image on the exit slit is close to the diffraction limit. Therefore, in this case, Geometrical Optics can only be used for approximate estimations, while a correct treatment must involve the application of Statistical Optics techniques.

## 8 Imaging of quasi-homogeneous undulator sources: effect of aperture size

We will now consider, with the help of Eq. (135), the effects of a pupil in the one-dimensional case (that can be practically realized with the help of a slit aperture and a cylindrical lens) when aberrations are not present. First, in Section 8.1, we will consider Gaussian quasi-homogeneous sources. Then, in Section 8.2 we will see that the arguments for Gaussian sources can be generalized without modifying their substance with the help of some notational change to treat the case of non-Gaussian quasi-homogeneous sources as well.

### 8.1 Quasi-homogeneous Gaussian undulator sources

In the case for  $\hat{N}_x \gg 1$  and  $\hat{D}_x \gg 1$  we can treat the horizontal and the vertical direction separately. Then, also the function  $P$  and  $\hat{P}$  can be expressed as the product of factors in the horizontal and in the vertical direction. In particular we may consider the pupil function

$$P(\hat{r}) = \begin{cases} 1 & \text{if } |\hat{r}| < \hat{a} \\ 0 & \text{otherwise} \end{cases}, \quad (224)$$

where  $\hat{r}$  may represent either the variable  $\hat{x}$  or the variable  $\hat{y}$ . According to the definition in Eq. (101) this gives:

$$\hat{P}(\hat{u}) = 2\hat{a}\text{sinc}(\hat{a}\hat{u}) . \quad (225)$$

We can use Eq. (135) and Eq. (156) to describe the case when the lens is in the far zone, that is when condition (136) is satisfied. From Eq. (146) we can estimate the characteristic size of the source, that is of order  $\sqrt{\hat{N}}$ , and of the correlation length at the source, that is of order  $1/\sqrt{\hat{D}}$ . According to condition (136), the lens is in the far zone when  $\sqrt{\hat{N}}/\hat{z}_1 \ll \sqrt{\hat{D}}$ , in agreement with the far zone limit of Eq. (142), which is obtained for  $\hat{A} \ll \hat{D}$ <sup>18</sup>. In this limit, Eq. (135) and Eq. (156) give

<sup>18</sup> Condition (136) is usually not discussed in textbooks describing thermal sources. In fact, for perfectly incoherent thermal sources, the far zone is defined by  $\hat{z} \gg \hat{\sigma}_o$ ,  $\hat{\sigma}_o$  being the source transverse size, i.e. when the paraxial approximation is valid. Therefore, in this case, the pupil is always in the far zone.

$$\begin{aligned}
\hat{G}_P(\hat{z}_i, \bar{r}_i, \Delta\hat{r}_i) &= 4\hat{a}^2 \exp\left[\frac{2im}{\hat{z}_1}\bar{r}_i\Delta\hat{r}_i\right] \\
&\times \int d\bar{u} d\Delta\hat{u} \exp\left[-\frac{\hat{z}_1^2\bar{u}^2}{2\hat{N}}\right] \exp\left[-2\hat{D}\hat{z}_1^2(\Delta\hat{u})^2\right] \\
&\times \text{sinc}\left\{\hat{a}\left[\frac{m}{\hat{z}_1}(\bar{r}_i + \Delta\hat{r}_i) - \bar{u} - \Delta\hat{u}\right]\right\} \\
&\times \text{sinc}\left\{\hat{a}\left[\frac{m}{\hat{z}_1}(\bar{r}_i - \Delta\hat{r}_i) - \bar{u} + \Delta\hat{u}\right]\right\}. \tag{226}
\end{aligned}$$

According to the far field limit of Eq. (142), the quantity  $\hat{D}\hat{z}_1^2$  is the square of the radiation spot size on the pupil, while  $\hat{z}_1^2/\hat{N}$  is essentially the square of the coherence length on the pupil. Two interesting limiting cases of Eq. (226) can be obtained comparing these two characteristic scales with  $\hat{a}^2$ , that is the square of the pupil size.

First, let us consider the case  $\hat{z}_1^2/\hat{N} \lesssim \hat{a}^2 \ll \hat{D}\hat{z}_1^2$ . As we will demonstrate later on, in all situations when the quasi-homogeneous assumption is verified, the exponential function in  $\Delta\hat{u}$  inside the integral in Eq. (226) behaves like a  $\delta$ -Dirac distribution, and one obtains

$$\begin{aligned}
\hat{G}_P(\hat{z}_i, \bar{r}_i, \Delta\hat{r}_i) &= 4\hat{a}^2 \exp\left[\frac{2im}{\hat{z}_1}\bar{r}_i\Delta\hat{r}_i\right] \int_{-\infty}^{\infty} d\bar{u} \exp\left[-\frac{\hat{z}_1^2\bar{u}^2}{2\hat{N}}\right] \\
&\times \text{sinc}\left\{\hat{a}\left[\frac{m}{\hat{z}_1}(\bar{r}_i + \Delta\hat{r}_i) - \bar{u}\right]\right\} \\
&\times \text{sinc}\left\{\hat{a}\left[\frac{m}{\hat{z}_1}(\bar{r}_i - \Delta\hat{r}_i) - \bar{u}\right]\right\}. \tag{227}
\end{aligned}$$

This corresponds to a relative intensity

$$\hat{I}_P(\hat{z}_i, \bar{r}_i) = \frac{1}{\mathcal{C}} \int_{-\infty}^{\infty} d\bar{u} \exp\left[-\frac{\hat{z}_1^2\bar{u}^2}{2\hat{N}}\right] \left| \text{sinc}\left[\hat{a}\left(\frac{\bar{r}_i}{\hat{d}_i} - \bar{u}\right)\right] \right|^2, \tag{228}$$

where the normalization constant  $\mathcal{C}$  is given by

$$\mathcal{C} = \int_{-\infty}^{\infty} d\bar{u} \exp\left[-\frac{\hat{z}_1^2\bar{u}^2}{2\hat{N}}\right] |\text{sinc}(\hat{a}\bar{u})|^2. \tag{229}$$

Eq. (228) expresses the image as a convolution of the geometrical image with the slit diffraction pattern (in two dimensions this would be the Airy pattern). It is valid for values  $\hat{z}_1^2/\hat{N} \lesssim \hat{a}^2 \ll \hat{D}\hat{z}_1^2$  and also for  $\hat{z}_1^2/\hat{N} \ll \hat{a}^2 \ll \hat{D}\hat{z}_1^2$ : the difference between these two cases is that in the first the pupil influence is significant, while in the second it is not. Inspection of Eq. (228) and use of Eq. (31) yields the ratio between the size of the diffraction pattern and

the geometrical image:  $\left(|M|\sqrt{\hat{N}}\hat{a}/\hat{d}_i\right)^{-1} = \left(\hat{a}\sqrt{\hat{N}}/\hat{z}_1\right)^{-1}$ . When  $\hat{z}_1^2/\hat{N} \lesssim \hat{a}^2$  such ratio is comparable with unity, i.e. the diffraction pattern significantly influences the image formation process. When,  $\hat{z}_1^2/\hat{N} \ll \hat{a}^2$ , this ratio is much smaller than unity. As a result, the pupil influence is not significant and the image is given by the geometrical image. The ratio between the size of the diffraction pattern and the geometrical image,  $\hat{z}_1/\hat{a}\sqrt{\hat{N}}$ , gives the resolution of the image due to diffraction effects. It is also interesting to note that in the limiting case when  $\hat{z}_1^2/\hat{N} \ll \hat{a}^2 \ll \hat{D}\hat{z}_1^2$ , Eq. (227) presents the asymptotic behavior

$$\begin{aligned} \hat{G}_P(\hat{z}_i, \bar{r}_i, \Delta\hat{r}_i) &= 4\hat{a}^2 \exp\left[\frac{2im}{\hat{z}_1}\bar{r}_i\Delta\hat{r}_i\right] \exp\left[-\frac{m^2\bar{r}_i^2}{2\hat{N}}\right] \\ &\times \int_{-\infty}^{\infty} d\bar{u} \operatorname{sinc}\left\{\hat{a}\left[\frac{m}{\hat{z}_1}\Delta\hat{r}_i - \bar{u}\right]\right\} \operatorname{sinc}\left\{\hat{a}\left[\frac{m}{\hat{z}_1}\Delta\hat{r}_i + \bar{u}\right]\right\} . \end{aligned} \quad (230)$$

The convolution theorem yields the following expression for the spectral degree of coherence:

$$g_P(\hat{z}_i, \Delta\hat{r}_i) = \frac{1}{\mathcal{D}} \int_{-\infty}^{\infty} d\hat{r}' |P(\hat{r}')|^2 \exp\left[-2i\frac{\hat{r}'\Delta\hat{r}_i}{\hat{d}_i}\right] , \quad (231)$$

the normalization factor  $\mathcal{D}$  being given by

$$\mathcal{D} = \int_{-\infty}^{\infty} d\hat{r}' |P(\hat{r}')|^2 . \quad (232)$$

After the substitution  $\bar{u} \rightarrow \bar{u}'\sqrt{\hat{N}}/\hat{z}_1$  we may rewrite Eq. (228) as a function of  $\xi = \hat{a}m\bar{r}_i/\hat{z}_1$  with the help of the only parameter  $p = \hat{a}\sqrt{\hat{N}}/\hat{z}_1$ , that is easier to plot

$$\hat{I}_P(\xi) = \frac{1}{\mathcal{C}} \int_{-\infty}^{\infty} d\bar{u}' \exp\left[-\frac{\bar{u}'^2}{2}\right] |\operatorname{sinc}(\xi - p\bar{u}')|^2 , \quad (233)$$

where  $\mathcal{C}$  can explicitly be calculated as:

$$\mathcal{C} = \sqrt{\frac{\pi}{2}} \frac{1}{p^2} \left\{-1 + \exp[-2p^2]\right\} + \frac{\pi}{p} \operatorname{erf}[\sqrt{2}p] . \quad (234)$$

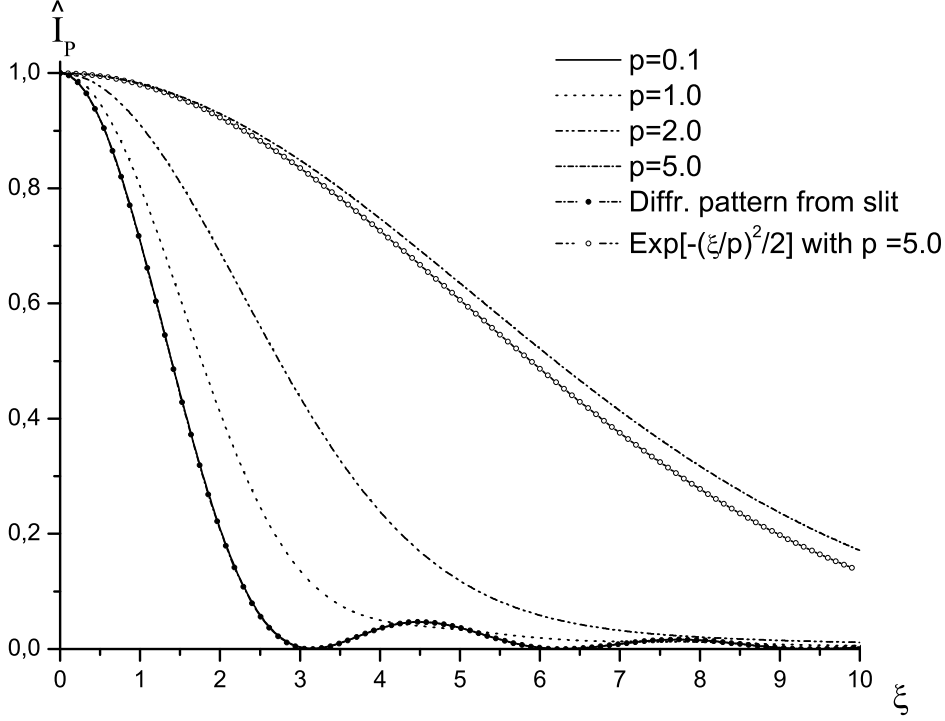


Fig. 18. Image intensity for a quasi-homogeneous source,  $\hat{I}_P$ , as a function of  $\xi = \hat{a}m\bar{r}_i/\hat{z}_1$ , calculated with Eq. (233), for different values of the parameter  $p = \hat{a}\sqrt{\hat{N}}/\hat{z}_1$ . The plot illustrates the one-dimensional image formation problem (slit aperture, cylindrical lens).

The function  $\text{erf}(\cdot)$  in Eq. (234) indicates the error function. Note that the variable  $\xi = \hat{a}m\bar{r}_i/\hat{z}_1$  may also be written as  $\xi = (\hat{a}/\hat{d}_i)\bar{r}_i$ , where  $\hat{d}_i = \hat{z}_i - \hat{z}_1$  and  $|M| = \hat{d}_i/\hat{z}_1 = m^{-1}$ . It is interesting to remark that the ratio  $\hat{d}_i/\hat{a}$  is the dimensionless characteristic size of the Fresnel zone, i.e.  $\lambda d_i/(2\pi a)$ .  $\hat{I}_P$  is plotted in Fig. 18 for several values of the parameter  $p$ . In Fig. 18 we also plot the asymptotic behaviors of  $\hat{I}_p$  for small values of  $p$ , i.e.  $\hat{I}_p = \text{sinc}^2(\xi)$ , that is the diffraction pattern from a slit, and for large values of  $p$ , i.e.  $\exp[-(\xi/p)^2/2]$ .

On the one hand, the integral in  $d\bar{u}$  in Eq. (228) is a convolution. On the other hand, aside for numerical factors, the Fourier transform of  $|\hat{\mathcal{P}}(\hat{u})|^2 = |2\hat{a}\text{sinc}(\hat{a}\hat{u})|^2$  can be given in terms of the triangular function  $\text{tri}(\cdot)$ , defined as<sup>19</sup>

<sup>19</sup> It should be noted that  $\chi = 2\Delta\hat{r}$ . The reason why we introduced the new variable  $\chi$  is to keep a certain homogeneity of notation when comparing with reference [8]. Since our definition of  $\Delta\hat{r}$  differs for a factor 2 with respect to that in [8], it is somewhat convenient to introduce  $\chi = 2\Delta\hat{r}$ .

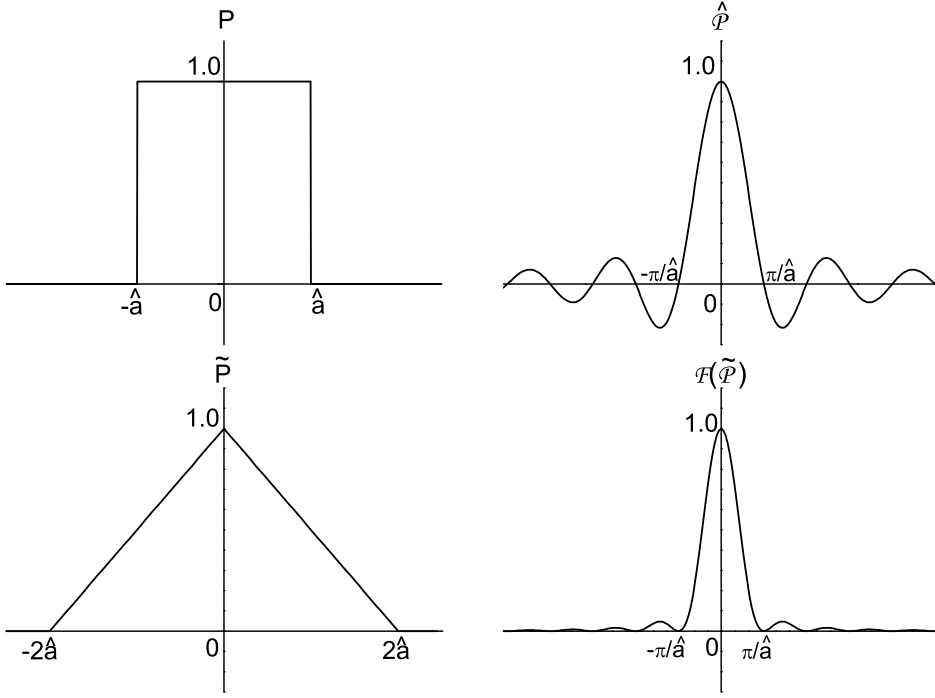


Fig. 19. Upper plots: profile of the pupil function  $P$  (slit aperture), together with  $\hat{P}$ . Lower plots: autocorrelation function of the pupil,  $\tilde{P}$ , together with  $\mathcal{F}(\tilde{P})$ .

$$\text{tri}\left(\frac{\chi}{2\hat{a}}\right) = \begin{cases} 1 + \chi/(2\hat{a}) & \text{if } -2\hat{a} < \chi < 0 \\ 1 - \chi/(2\hat{a}) & \text{if } 0 < \chi < 2\hat{a} \\ 0 & \text{otherwise .} \end{cases} \quad (235)$$

By means of the convolution theorem, Eq. (228) can be written as

$$\hat{I}_P(\hat{z}_i, \bar{r}_i) = \frac{1}{\mathcal{N}} \int_{-\infty}^{\infty} d\chi \exp\left[-\frac{\hat{N}\chi^2}{2\hat{z}_1^2}\right] \text{tri}\left(\frac{\chi}{2\hat{a}}\right) \exp\left[-i\chi\frac{m}{\hat{z}_1}\bar{r}_i\right] . \quad (236)$$

The normalization factor  $\mathcal{N}$  is given by

$$\mathcal{N} = \int_{-\infty}^{\infty} d\chi \exp\left[-\frac{\hat{N}\chi^2}{2\hat{z}_1^2}\right] \text{tri}\left(\frac{\chi}{2\hat{a}}\right) = \frac{\hat{z}_1}{2\hat{a}\hat{N}} \left\{ (1 + \hat{a}^2) \left[ -1 + \exp\left(-2\frac{\hat{a}^2\hat{N}}{\hat{z}_1^2}\right) \right] \hat{z}_1 + 2\hat{a}\sqrt{2\pi\hat{N}} \text{erf}\left[\frac{\sqrt{2\hat{N}}\hat{a}}{\hat{z}_1}\right] \right\} . \quad (237)$$

Eq. (236) can be written as an analogous of Eq. (5.7-10) of [8], that sometimes goes under the name of Shell's theorem. Let us define the autocorrelation function of the pupil as

$$\tilde{P}(\chi) = \int_{-\infty}^{\infty} du P\left(u + \frac{\chi}{2}\right) P^*\left(u - \frac{\chi}{2}\right) . \quad (238)$$

In Fig. 19 we plot the profile of the pupil function  $P$ , together with  $\hat{\mathcal{P}}$  and the autocorrelation function of the pupil  $\tilde{P}$ , together with its Fourier transform  $\mathcal{F}(\tilde{P})$ . With the help of Eq. (238), Eq. (236) can be written as

$$\hat{I}_P(\hat{z}_i, \bar{r}_i) = \frac{1}{\mathcal{N}} \int_{-\infty}^{\infty} d\chi \exp\left[-\frac{\hat{N}\chi^2}{2\hat{z}_1^2}\right] \tilde{P}(\chi) \exp\left[-i\chi\frac{\mathbf{m}}{\hat{z}_1}\bar{r}_i\right] , \quad (239)$$

that is Eq. (5.7-10) of reference [8].

A second limiting case of interest is found when  $\hat{a}^2 \ll \hat{z}_1^2/\hat{N} \ll \hat{D}\hat{z}_1^2$ . The pupil is coherently and uniformly illuminated. In this case both the exponential functions inside the integral in Eq. (226) behave like  $\delta$ -Dirac functions yielding

$$\begin{aligned} \hat{G}_P(\hat{z}_i, \bar{r}_i, \Delta\hat{r}_i) &= 4\hat{a}^2 \exp\left[\frac{2i\mathbf{m}}{\hat{z}_1}\bar{r}_i\Delta\hat{r}_i\right] \text{sinc}\left\{\hat{a}\left[\frac{\mathbf{m}}{\hat{z}_1}(\bar{r}_i + \Delta\hat{r}_i)\right]\right\} \\ &\quad \times \text{sinc}\left\{\hat{a}\left[\frac{\mathbf{m}}{\hat{z}_1}(\bar{r}_i - \Delta\hat{r}_i)\right]\right\} . \end{aligned} \quad (240)$$

corresponding to a relative intensity

$$\hat{I}_P(\hat{z}_i, \bar{r}_i) = \text{sinc}^2\left[\frac{\hat{a}\mathbf{m}}{\hat{z}_1}\bar{r}_i\right] = \frac{1}{4\hat{a}^2} \left|\hat{\mathcal{P}}\left(\frac{\mathbf{m}}{\hat{z}_1}\bar{r}_i\right)\right|^2 . \quad (241)$$

Also, using the definition of the spectral degree of coherence given in Eq. (129) one sees that  $|g| = 1$ , i.e. the pupil is coherently illuminated. Eq. (241) is the analogous of Eq. (5.7-14) in [8].

Results obtained here deal both with the cross-spectral density  $\hat{G}_P$  and the relative intensity  $\hat{I}_P$  in the presence of the pupil. We classified these results comparing the square of the extent of the pupil  $\hat{a}^2$  with the square of the radiation spot size  $\hat{D}\hat{z}_1^2$  and of the coherence length  $\hat{z}_1^2/\hat{N}$  at the pupil location.

Let us now consider the intensity  $\hat{I}_P$  only. In the case of quasi-homogeneous sources, there is a more general method taken from the theory of linear systems to account for the pupil presence. This method can be extended to account for aberrations as well, and allows a more compact treatment of the pupil

effects because it does not depend on how the extent of the pupil scales with respect to the coherence length and to the radiation spot size. It is based on the concept of line spread function. A linear time-invariant system in two dimensions can be characterized by the knowledge of the point spread function (or impulse response)  $h(x, y)$ . Given a certain input  $f(x_1, y_1)$ , the output at any point  $(x, y)$  is given by the convolution of the point-spread function  $h$  and the input  $f$ . The point spread function  $h(x, y)$  is the response to a  $\delta$ -Dirac signal at position  $(0, 0)$ , i.e.  $\delta(x_1, y_1)$ . The line spread  $l(x)$  is, instead, the response obtained from a line input  $\delta(x_1)$ , which is independent of  $y_1$ , and can be calculated by integrating the point spread function  $h(x, y)$  with respect to the  $y$ -variable (see, for instance, [17] Sec 6.2.).

In the quasi-homogeneous case, the intensity  $\hat{I}_P$  can be written as a convolution between a suitable line spread function  $l$ <sup>20</sup> and the intensity  $\hat{I}$  which does not account for the pupil presence, that is

$$\hat{I}_P(\hat{z}_i, \bar{r}_i) = [\hat{I} * l](\hat{z}_i, \bar{r}_i) \quad (242)$$

The line spread function  $l$  acts as the passport of the imaging system, and depends on the properties of the lens only. In this case we are only considering the effect of a finite pupil dimension, i.e. we are accounting for diffraction effects from the pupil. More in general,  $l$  may depend on lens apodization or aberrations too.

In the case under study here, the line spread function of the system is given by

$$l(\bar{r}_i) = \text{sinc}^2\left(\frac{\hat{a}}{\hat{d}_i}\bar{r}_i\right) . \quad (243)$$

For instance, it is straightforward to see that substitution of the (magnified) input signal  $\hat{I} = \exp[-\bar{u}^2/(2|M|^2\hat{N})]$  with the input signal  $\hat{I} = \delta(\bar{u}/|M|)$ , that is a line input, in Eq. (228) gives back Eq. (243).

It should be emphasized that the resolution due to diffraction effects is of order  $\hat{z}_1/(\hat{a}\sqrt{\hat{N}})$ . In all cases when this resolution is better than (i.e.  $\hat{z}_1/(\hat{a}\sqrt{\hat{N}})$  is

<sup>20</sup> Here we are treating a two-dimensional system, but we are considering the case when we have separability properties for both the source and the pupil. For the source this means that  $\hat{N}_x \gg 1$  and  $\hat{D}_x \gg 1$ , while for the pupil it means that the pupil is rectangular. This case is practically realized with the help of slit apertures and cylindrical optics. The line spread function  $l$  is, then, the proper tool to consider. If one wants to consider the situation when no separability property for the pupil is present, one should take advantage of an approach based on the point spread function.

smaller than) the resolution of the ideal image (which does not account for the pupil presence) the pupil does not play any role and, with the accuracy of the calculation of the ideal intensity (see Section 15), the  $l$  function in Eq. (243) cannot be distinguished from a  $\delta$ -Dirac. In our study case, the ideal intensity  $\hat{I} = \exp[-\hat{z}_1^2 \bar{u}^2 / (2\hat{N})]$  is calculated with an accuracy which is much worse than the quasi-homogenous accuracy (see Section 15 for details) and is of order  $\max(1/\sqrt{\hat{D}}, 1/\sqrt{\hat{N}})$ . In general, it is important to compare the resolution due to diffraction effects with the accuracy of the calculation of the ideal intensity. For example, on the basis of such comparison, one may conclude that the case for  $\hat{z}_1^2 / \hat{N} \ll \hat{a}^2 \lesssim \hat{D} \hat{z}_1^2$  can be calculated assuming that the line spread function in Eq. (243) is a  $\delta$ -Dirac. In fact  $\hat{z}_1 / (\hat{a} \sqrt{\hat{N}}) \sim 1/\sqrt{\hat{N} \hat{D}}$  since  $\hat{a}^2 \lesssim \hat{D} \hat{z}_1^2$  and therefore  $\hat{z}_1 / (\hat{a} \sqrt{\hat{N}}) \ll \max(1/\sqrt{\hat{D}}, 1/\sqrt{\hat{N}})$ . This kind of reasoning can be used to treat any quasi-homogeneous case, and the  $l$  function can be modified to include aberrations and apodization effects as well. In the most general case, accounting for the effects of the pupil in one dimension, Eq. (135) yields the relative intensity

$$\begin{aligned} \hat{I}_P(\hat{z}_i, \bar{r}_i) = \frac{1}{\mathcal{S}} \int d\bar{u} d\Delta\hat{u} \exp \left[ -\frac{2i\hat{z}_1}{m} \bar{u} \cdot \Delta\hat{u} \right] \hat{G} \left( \hat{z}_i, \frac{\hat{z}_1}{m} \bar{u}, \frac{\hat{z}_1}{m} \Delta\hat{u} \right) \\ \times \hat{\mathcal{P}} \left[ \frac{m}{\hat{z}_1} \bar{r}_i - \bar{u} - \Delta\hat{u} \right] \hat{\mathcal{P}}^* \left[ \frac{m}{\hat{z}_1} \bar{r}_i - \bar{u} + \Delta\hat{u} \right] , \end{aligned} \quad (244)$$

where the normalization factor  $\mathcal{S}$  is given by

$$\begin{aligned} \mathcal{S} = \int d\bar{u} d\Delta\hat{u} \exp \left[ -\frac{2i\hat{z}_1}{m} \bar{u} \cdot \Delta\hat{u} \right] \hat{G} \left( \hat{z}_i, \frac{\hat{z}_1}{m} \bar{u}, \frac{\hat{z}_1}{m} \Delta\hat{u} \right) \\ \times \hat{\mathcal{P}} [-\bar{u} - \Delta\hat{u}] \hat{\mathcal{P}}^* [-\bar{u} + \Delta\hat{u}] . \end{aligned} \quad (245)$$

In the quasi-homogeneous case (including cases when the source is not Gaussian, see Section 6), if the lens is in the far field, one can write

$$\hat{G} \left( \hat{z}_i, \frac{\hat{z}_1}{m} \bar{u}, \frac{\hat{z}_1}{m} \Delta\hat{u} \right) = \hat{I} \left( \hat{z}_i, \frac{\hat{z}_1}{m} \bar{u} \right) g \left( \hat{z}_i, \frac{\hat{z}_1}{m} \Delta\hat{u} \right) \exp \left[ \frac{2i\hat{z}_1}{m} \bar{u} \cdot \Delta\hat{u} \right] . \quad (246)$$

Further on, within the accuracy of the quasi-homogeneous approximation, the spectral degree of coherence  $g$  behaves like a Dirac  $\delta$ -function in the calculation of both the intensity and the cross-spectral density. In fact, the accuracy of the incoherent impulse response  $|\hat{\mathcal{P}}|^2$  is also the accuracy of the quasi-homogenous assumption, and this is the accuracy with which we can substitute  $g$  with a Dirac  $\delta$ -function on the image plane. As a result, in analogy with Eq. (227) one has

$$\hat{G}_P(\hat{z}_i, \bar{r}_i, \Delta\hat{r}_i) = \int_{-\infty}^{\infty} d\bar{u} \hat{I}\left(\hat{z}_i, \frac{\hat{z}_1}{m}\bar{u}\right) \times \hat{\mathcal{P}}\left[\frac{m}{\hat{z}_1}(\bar{r}_i + \Delta\hat{r}_i) - \bar{u}\right] \hat{\mathcal{P}}^*\left[\frac{m}{\hat{z}_1}(\bar{r}_i - \Delta\hat{r}_i) - \bar{u}\right], \quad (247)$$

while the relative intensity can be written as

$$\hat{I}_P(\hat{z}_i, \bar{r}_i) = \frac{1}{\mathcal{D}} \int_{-\infty}^{\infty} d\bar{u} \left| \hat{\mathcal{P}}\left(\frac{m}{\hat{z}_1}\bar{r}_i - \bar{u}\right) \right|^2 \hat{I}\left(\hat{z}_i, \frac{\hat{z}_1}{m}\bar{u}\right), \quad (248)$$

$\mathcal{D}$  being defined in Eq. (232). The line input response is obtained by setting  $\hat{I}(\hat{z}_i, \hat{z}_1\bar{u}/m)$  to a Dirac  $\delta$ -function, thus obtaining the line spread function:

$$l(\bar{r}_i) = \left| \hat{\mathcal{P}}\left[\frac{m}{\hat{z}_1}\bar{r}_i\right] \right|^2 = \mathcal{F}^{-1}(\tilde{P}). \quad (249)$$

The line spread function is therefore the inverse Fourier transform of the autocorrelation function of the pupil. The autocorrelation function of the pupil, i.e. the Fourier transform of the line spread function, is also known as the Optical Transfer Function (OTF). Other relevant quantities introduced in linear system theory are the phase of the Optical Transfer Function and its modulus, which is known as the Modulation Transfer Function (MTF) [17].

Eq. (248) and, consequently, the line spread function approach, constitutes a universal description of the intensity in all quasi-homogeneous cases. In literature the line spread function is used to describe perfectly incoherent sources only. Note that, in general, radiation produced by an electron beam in an undulator is similar to an incoherent sum of many independent laser-like beams. Yet, it cannot be considered as an incoherent sum of point sources because, as we have seen in Section 3, a single electron cannot be considered as a point-like radiation source. Radiation produced by a single electron is similar to a laser beam. If no influence of focusing is present in the undulator, this laser-like beam has a waist located in the center of the undulator. At the waist the radiation wavefront is plane and the radiation spot size is much larger than the wavelength. We extended the use of the line spread function approach to the realm of quasi-homogeneous sources.

In the case of third generation light sources the line spread function method can almost always be applied in the horizontal direction. However, it fails in the vertical direction, where third generation light sources are seldom quasi-homogeneous. If the source is not quasi-homogeneous, the cross-spectral density cannot be factorized in the product of the intensity and of the spectral degree of coherence, or the coherence length is not short (compared with the size of the source). As a result, the incoherent line spread function  $l$  cannot

be used to describe the system. The function  $\hat{\mathcal{P}}$  is known as the coherent line spread function and must be used in its place. In fact, when the source starts to exhibit a high degree of transverse coherence (i.e. in the non quasi-homogeneous case), the coherent line spread function,  $\hat{\mathcal{P}}$  acts on the field at the image plane analogously to the way the incoherent line spread function acts on the intensity at the image plane. To see this, it is sufficient to inspect Eq. (100).

It is interesting to compare this viewpoint with what can be found in literature. For instance, in [6], where a condenser system is discussed, one may read: "The intrinsic divergence of the extreme ultraviolet (EUV) undulator considered here is  $\theta_{\text{cen}} = 80\mu\text{rad}$ , which is larger than the beamline acceptance  $\theta_{\text{accept}}$  of  $48\mu\text{rad}$ . Therefore it is evident that the incoherent source approximation holds here and the term incoherence source is used accordingly in this paper". In the following Sections of their work, authors of [6] use a point-spread function approach to account for aberration effects: in their paper, the intensity at the source is used, instead of the cross-spectral density, in order to evaluate both the intensity and the degree of coherence at the image plane. Such an approach is justified in the passage above, where they state that the source is incoherent.

The statement in [6] about the incoherence of the source is a misconception. According to such statement, *perfectly coherent* undulator radiation produced by an electron beam with zero emittance should exhibit *incoherent* properties when the radiation divergence is larger than the acceptance of the optical system. In contrast with the assertion made in [6], the coherence properties of the source are independent of the beamline elements which follow. In order to discuss about the coherence properties of the source one has to refer to the radiation field at the virtual plane location only. In particular, the fact that the source is coherent (or not) does not depend on how the beam acceptance angle scales with the intrinsic (single particle) divergence of the undulator radiation. Our conclusion is that the only parameters which describe whether a source is quasi-homogeneous or not are (in the vertical direction)  $\hat{N}_y$  and  $\hat{D}_y$ . If the source is quasi-homogeneous, a point-spread function approach can be used. If not, the more general results described in Section 14.1 should be considered. In particular, in the case of [6], the vertical rms dimension of the source is  $\sigma_y = 16 \mu\text{m}$  and the radiation wavelength is  $\lambda = 13.4 \text{ nm}$ , while the undulator (see [7]) is composed of 55 periods, each one 8 cm long. This means  $L_w = 4.4 \text{ m}$ . Moreover, the vertical emittance at ALS is  $\epsilon_y \simeq 0.1 \text{ nm}$ , while the vertical beta function for beamline 12 is  $\beta_y = 4.2 \text{ m} \simeq L_w$ . As a result both  $\hat{N}_y \sim 0.1$  and  $\hat{D}_y \sim 0.1$  and the source is non-homogeneous. We conclude that, in this case, approximations like Eq. (247) or Eq. (248) cannot be used. Eq. (376) in Section 14 should be considered instead.

As a final remark we should stress that, even in cases when the virtual source is quasi-homogeneous, one should verify the assumption that the lens is in the far zone, before applying a point spread function formalism. In contrast to this, note that in the usual framework of Statistical Optics, the radiant intensity from thermal sources is distributed over a solid angle of order  $2\pi$ , and optical elements can always be considered in the far zone.

## 8.2 *Quasi-homogeneous non-Gaussian undulator sources*

In the present Section 8.2 we will extend results obtained in Section 6. Results obtained in the previous Section 8.1 apply for a quasi-homogeneous Gaussian undulator source only. In particular, under the assumptions  $\hat{N}_x \gg 1$  and  $\hat{D}_x \gg 1$  the cross-spectral density can be factorized in a horizontal and in a vertical contribution, and results in Section 8.1 can be applied in the horizontal direction. Note that, if  $\hat{N}_y \gg 1$  and  $\hat{D}_y \gg 1$ , one has, automatically,  $\hat{D}_x \gg 1$  and  $\hat{D}_x \gg 1$  and the same results in Section 8.1 can be separately applied in both the horizontal and the vertical directions. Here, with the help of Eq. (135), we will include the effects of a pupil in the one-dimensional case when the source is still quasi-homogeneous, but non-Gaussian. In particular, we will still assume  $\hat{N}_x \gg 1$  and  $\hat{D}_x \gg 1$  and concentrate our attention on the vertical direction. First we will study the case when  $\hat{N}_y \gg 1$  and  $\hat{D}_y$  is arbitrary and, then, the case when  $\hat{N}_y$  is arbitrary and  $\hat{D}_y \gg 1$ . We will see that the reasoning applied in the case of quasi-homogeneous Gaussian sources also holds in the case for quasi-homogeneous non-Gaussian sources as it relies on the separability of the cross-spectral density only. As a result we will present practical examples of how, with minor substitutions, we can extend our analysis of the pupil effects to the case of non-Gaussian sources.

### 8.2.1 *Source with non-Gaussian angular distribution in the vertical direction*

Let us start considering the case when  $\hat{D}_y$  is arbitrary and  $\hat{N}_y \gg 1$ . The pupil function and  $\hat{\mathcal{P}}$  are given by Eq. (224) and Eq. (225). The  $r$ -direction should be now substituted with the  $y$ -direction.

We can use Eq. (135) and an asymptotic expression of Eq. (168) to describe the case when the lens is in the far zone, that is when condition (136) is satisfied. From Eq. (162) we can estimate the typical size of the source that is of order  $\sqrt{\hat{N}_y}$ , and of the correlation length at the source, that is of order  $\min[1/\sqrt{\hat{D}_y}, 1]$ . According to Eq. (136), the lens is in the far zone when  $\sqrt{\hat{N}_y}/\hat{z}_1 \ll \max[\sqrt{\hat{D}_y}, 1]$ . In this limit, Eq. (135) and Eq. (168) give

$$\begin{aligned}
\hat{G}_P(\hat{z}_i, \bar{y}_i, \Delta\hat{y}_i) &= 4\hat{a}^2 \exp\left[\frac{2im}{\hat{z}_1}\bar{y}_i\Delta\hat{y}_i\right] \\
&\times \int d\bar{u} d\Delta\hat{u} \exp\left[-\frac{\hat{z}_1^2\bar{u}^2}{2\hat{N}_y}\right] \exp\left[-2\hat{D}_y\hat{z}_1^2(\Delta\hat{u})^2\right] \gamma(\hat{z}_1\Delta\hat{u}) \\
&\times \text{sinc}\left\{\hat{a}\left[\frac{m}{\hat{z}_1}(\bar{y}_i + \Delta\hat{y}_i) - \bar{u} - \Delta\hat{u}\right]\right\} \\
&\times \text{sinc}\left\{\hat{a}\left[\frac{m}{\hat{z}_1}(\bar{y}_i - \Delta\hat{y}_i) - \bar{u} + \Delta\hat{u}\right]\right\}. \tag{250}
\end{aligned}$$

From Eq. (159), one sees that  $\hat{z}_1^2 \max[\hat{D}_y, 1]$  is of the order of the square of the radiation spot size on the pupil, while  $\hat{z}_1^2/\hat{N}_y$  is of the order of the square of the coherence length on the pupil. Note that the limiting expression obtained from Eq. (250) for  $\hat{D}_y \gg 1$  is Eq. (226). As before, two interesting limiting cases of Eq. (226) can be obtained comparing these two scales with  $\hat{a}^2$ , that is the square of the pupil size.

First, let us consider the case  $\hat{z}_1^2/\hat{N}_y \lesssim \hat{a}^2 \ll \hat{z}_1^2 \max[1, \hat{D}_y]$ . As we have already discussed, in all situations when the quasi-homogeneous assumption is verified, the exponential function in  $\Delta\hat{u}$  inside the integral in Eq. (250) behaves like a  $\delta$ -Dirac distribution. As in Eq. (227) one obtains

$$\begin{aligned}
\hat{G}_P(\hat{z}_i, \bar{y}_i, \Delta\hat{y}_i) &= 4\hat{a}^2 \exp\left[\frac{2im}{\hat{z}_1}\bar{y}_i\Delta\hat{y}_i\right] \int_{-\infty}^{\infty} d\bar{u} \exp\left[-\frac{\hat{z}_1^2\bar{u}^2}{2\hat{N}_y}\right] \\
&\times \text{sinc}\left\{\hat{a}\left[\frac{m}{\hat{z}_1}(\bar{y}_i + \Delta\hat{y}_i) - \bar{u}\right]\right\} \\
&\times \text{sinc}\left\{\hat{a}\left[\frac{m}{\hat{z}_1}(\bar{y}_i - \Delta\hat{y}_i) - \bar{u}\right]\right\}. \tag{251}
\end{aligned}$$

Setting  $\Delta\hat{y}_i = 0$  one yields the intensity

$$\hat{I}_P(\hat{z}_i, \bar{y}_i) = \frac{1}{\mathcal{C}} \int_{-\infty}^{\infty} d\bar{u} \exp\left[-\frac{\hat{z}_1^2\bar{u}^2}{2\hat{N}_y}\right] \left| \text{sinc}\left[\hat{a}\left(\frac{m}{\hat{z}_1}\bar{y}_i - \bar{u}\right)\right] \right|^2, \tag{252}$$

where the normalization constant  $\mathcal{C}$  has already been defined in Eq. (229). The result in Eq. (252) is equivalent to the intensity already given in Eq. (228). It can also be written as in Eq. (236), that is

$$\hat{I}_P(\hat{z}_i, \bar{y}_i) = \frac{1}{\mathcal{N}} \int_{-\infty}^{\infty} d\chi \exp\left[-\frac{\hat{N}\chi^2}{2\hat{z}_1^2}\right] \text{tri}\left(\frac{\chi}{2\hat{a}}\right) \exp\left[-i\chi\frac{m}{\hat{z}_1}\bar{y}_i\right], \tag{253}$$

where  $\mathcal{N}$  is defined in Eq. (237). After introduction of  $\tilde{P}$  as in Eq. (238), Eq. (253) can be rewritten as Eq. (239),

$$\hat{I}_P(\hat{z}_i, \bar{y}_i) = \frac{1}{\mathcal{N}} \int_{-\infty}^{\infty} d\chi \exp \left[ -\frac{\hat{N}\chi^2}{2\hat{z}_1^2} \right] \tilde{P}(\chi) \exp \left[ -i\chi \frac{\mathfrak{m}}{\hat{z}_1} \bar{y}_i \right]. \quad (254)$$

In this case, the expression for the intensity is the same as in the case  $\hat{D}_y \gg 1$ . Also note that the results obtained for the case  $\hat{z}_1^2/\hat{N}_y \lesssim \hat{a}^2 \ll \hat{z}_1^2 \max[1, \hat{D}_y]$  are valid in the limit  $\hat{z}_1^2/\hat{N}_y \ll \hat{a}^2 \ll \hat{z}_1^2 \max[1, \hat{D}_y]$  as well. In this case Eq. (252) can be simplified to

$$\hat{I}_P(\hat{z}_i, \bar{y}_i) = \exp \left[ -\frac{\mathfrak{m}^2 \bar{y}_i^2}{2\hat{N}} \right]. \quad (255)$$

The second limiting case that we can mention here for comparison with what has been done in the Gaussian case is when  $\hat{a}^2 \ll \hat{z}_1^2/\hat{N} \ll \max[\hat{D}_y, 1]\hat{z}_1^2$  the pupil is coherently and uniformly illuminated. In this case one recovers the same results in Eq. (240) and Eq. (241).

To sum up, we obtain, in all situations, the same intensity as in the case  $\hat{D}_y \gg 1$ .

### 8.2.2 Source with non-Gaussian intensity distribution in the vertical direction

Let us now study the case when  $\hat{N}_y$  is arbitrary and  $\hat{D}_y \gg 1$ .

We can use Eq. (135) and an asymptotic expression of Eq. (192) to describe the case when the lens is in the far zone, that is when condition (136) is satisfied. From Eq. (188) we can estimate the typical size of the source that is of order  $\max[\sqrt{\hat{N}_y}, 1]$ , and of the correlation length at the source, that is of order  $1/\sqrt{\hat{D}_y}$ . According to Eq. (136), the lens is in the far zone when  $\max[\sqrt{\hat{N}_y}, 1]/\hat{z}_1 \ll \sqrt{\hat{D}_y}$ . In this limit, Eq. (135) and Eq. (192) give

$$\begin{aligned} \hat{G}_P(\hat{z}_i, \bar{y}_i, \Delta\hat{y}_i) &= 4\hat{a}^2 \exp \left[ \frac{2i\mathfrak{m}}{\hat{z}_1} \bar{y}_i \Delta\hat{y}_i \right] \int d\bar{u} d\Delta\hat{u} \\ &\times \int_{-\infty}^{\infty} d\hat{\phi}_y \exp \left[ -\frac{(\hat{\phi}_y + \hat{z}_1 \bar{u})^2}{2\hat{N}_y} \right] \hat{\mathcal{B}}(\hat{\phi}_y) \exp \left[ -2\hat{D}_y \hat{z}_1^2 (\Delta\hat{u})^2 \right] \\ &\times \text{sinc} \left\{ \hat{a} \left[ \frac{\mathfrak{m}}{\hat{z}_1} (\bar{y}_i + \Delta\hat{y}_i) - \bar{u} - \Delta\hat{u} \right] \right\} \\ &\times \text{sinc} \left\{ \hat{a} \left[ \frac{\mathfrak{m}}{\hat{z}_1} (\bar{y}_i - \Delta\hat{y}_i) - \bar{u} + \Delta\hat{u} \right] \right\}. \end{aligned} \quad (256)$$

According to Eq. (171), the quantity  $\hat{z}_1^2 \hat{D}_y$  is of the order of the square of the

radiation spot size on the pupil, while  $\hat{z}_1^2/\max[\hat{N}_y, 1]$  is of the order of the square of the coherence length on the pupil. Note that the limiting expression obtained from Eq. (256) for  $\hat{D}_y \gg 1$  is Eq. (226). We will study again two limiting cases of Eq. (256), which can be obtained comparing these two scales with  $\hat{a}^2$ , that is the square of the pupil size.

First, let us consider the case  $\hat{z}_1^2/\max[\hat{N}_y, 1] \lesssim \hat{a}^2 \ll \hat{z}_1^2 \hat{D}$ . As before, because of the quasi-homogeneous assumption is verified, the exponential function in  $\Delta\hat{u}$  inside the integral in Eq. (256) behaves like a  $\delta$ -Dirac distribution. One obtains

$$\begin{aligned} \hat{G}_P(\hat{z}_i, \bar{y}_i, \Delta\hat{y}_i) &= 4\hat{a}^2 \exp\left[\frac{2im}{\hat{z}_1}\bar{y}_i\Delta\hat{y}_i\right] \\ &\times \int_{-\infty}^{\infty} d\bar{u} \int_{-\infty}^{\infty} d\hat{\phi}_y \exp\left[-\frac{(\hat{\phi}_y + \hat{z}_1\bar{u})^2}{2\hat{N}_y}\right] \hat{\mathcal{B}}(\hat{\phi}_y) \\ &\times \text{sinc}\left\{\hat{a}\left[\frac{m}{\hat{z}_1}(\bar{y}_i + \Delta\hat{y}_i) - \bar{u}\right]\right\} \\ &\times \text{sinc}\left\{\hat{a}\left[\frac{m}{\hat{z}_1}(\bar{y}_i - \Delta\hat{y}_i) - \bar{u}\right]\right\}. \end{aligned} \quad (257)$$

This corresponds to the intensity

$$\begin{aligned} \hat{I}_P(\hat{z}_i, \bar{y}_i) &= \frac{1}{\tilde{\mathcal{C}}} \int_{-\infty}^{\infty} d\bar{u} \int_{-\infty}^{\infty} d\hat{\phi}_y \exp\left[-\frac{(\hat{\phi}_y + \hat{z}_1\bar{u})^2}{2\hat{N}_y}\right] \hat{\mathcal{B}}(\hat{\phi}_y) \\ &\times \left|\text{sinc}\left[\hat{a}\left(\frac{m}{\hat{z}_1}\bar{y}_i - \bar{u}\right)\right]\right|^2, \end{aligned} \quad (258)$$

where

$$\tilde{\mathcal{C}} = \int_{-\infty}^{\infty} d\bar{u} \int_{-\infty}^{\infty} d\hat{\phi}_y \exp\left[-\frac{(\hat{\phi}_y + \hat{z}_1\bar{u})^2}{2\hat{N}_y}\right] \hat{\mathcal{B}}(\hat{\phi}_y) |\text{sinc}(\hat{a}\bar{u})|^2. \quad (259)$$

In analogy with Eq. (239), Eq. (258) can also be written as:

$$\hat{I}_P(\hat{z}_i, \bar{y}_i) = \frac{1}{\tilde{\mathcal{N}}} \int_{-\infty}^{\infty} d\chi \left\{ \exp\left[-\frac{\hat{N}_y\chi^2}{2\hat{z}_1^2}\right] \beta\left(\frac{\chi}{2\hat{z}_1}\right) \right\} \tilde{P}(\chi) \exp\left[-i\chi\frac{m}{\hat{z}_1}\bar{y}_i\right], \quad (260)$$

where the normalization factor  $\tilde{\mathcal{N}}$  is defined as

$$\tilde{\mathcal{N}} = \int_{-\infty}^{\infty} d\chi \left\{ \exp \left[ -\frac{\hat{N}_y \chi^2}{2\hat{z}_1^2} \right] \beta \left( \frac{\chi}{2\hat{z}_1} \right) \right\} \tilde{P}(\chi) . \quad (261)$$

Note that results obtained in the case  $\hat{z}_1^2 / \max[\hat{N}_y, 1] \lesssim \hat{a}^2 \ll \hat{z}_1^2 \hat{D}$  are also valid in the asymptote for  $\hat{z}_1^2 / \max[\hat{N}_y, 1] \ll \hat{a}^2 \ll \hat{z}_1^2 \hat{D}$ . In this case, Eq. (258) is simplified to

$$\hat{I}_P(\hat{z}_i, \bar{y}_i) = \frac{1}{\tilde{\mathcal{S}}} \int_{-\infty}^{\infty} d\hat{\phi}_y \exp \left[ -\frac{(\hat{\phi}_y + m\bar{y}_i)^2}{2\hat{N}_y} \right] \hat{\mathcal{B}}(\hat{\phi}_y) , \quad (262)$$

where

$$\tilde{\mathcal{S}} = \int_{-\infty}^{\infty} d\hat{\phi}_y \exp \left[ -\frac{\hat{\phi}_y^2}{2\hat{N}_y} \right] \hat{\mathcal{B}}(\hat{\phi}_y) . \quad (263)$$

The second limiting case that we will mention here for comparison with what has been done in the Gaussian case is for  $\hat{a}^2 \ll \hat{z}_1^2 / \max(\hat{N}_y, 1) \ll \hat{D}_y \hat{z}_1^2$  the pupil is coherently and uniformly illuminated. In this case one recover the same results in Eq. (240) and Eq. (241).

However, in general, the expression for the intensity is different from that for  $\hat{N}_y \gg 1$ .

## 9 Aberrations and imaging of quasi-homogeneous sources

Up to now we have discussed cases when no aberrations are present. Although there are widespread treatments of Aberration Theory in literature, we will introduce our own here, so that this work is self-consistent. In particular, we will focus on the one-dimensional case, which has not been treated widely in books and monographies, aside for some exception (see [18]). In the present Section 9 we will assume that the virtual undulator source is quasi-homogeneous. Although we will begin introducing the Optical Transfer Function (OTF) for the system, we will mainly be concerned with the line spread function of the system. In addition to that we will discuss the case of severe aberrations, presenting new analytical results for this asymptote and comparison with numerical calculations. Finally, we will intensively discuss defocusing aberrations and present general analytical results for this case too. Our particular consideration of the defocusing case is justified by the fact that this is a privileged kind of aberration in the framework of Fourier Optics. In fact it shows a quadratic

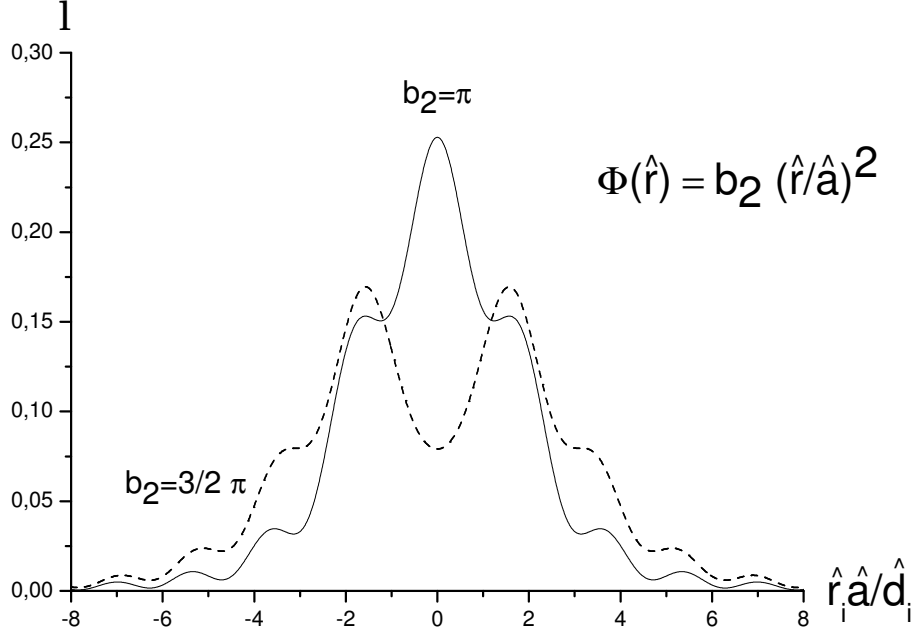


Fig. 20. The line spread  $l$  function in the presence of defocusing aberration.

dependence of the phase error along the pupil aperture, that is quite a natural dependence in the Fourier Optics approach. Quadratic phase factors, which can be interpreted as defocusing aberrations, are present even in the case of a pinhole camera setup (that will be treated in the next Section 10) and of imaging from ideal lenses in an arbitrary plane of interest behind the lens (as it will be seen in Section 11 and 12).

### 9.1 Aberrations and the effect of aperture size

In general, aberrations may be accounted for substituting the pupil function  $P$ , the coherent line spread function  $\hat{P}$ , the autocorrelation function  $\tilde{P}$  and the Fourier transform of the autocorrelation function  $\mathcal{F}(\tilde{P})$  with new functions, respectively  $P_a, \hat{P}_a, \tilde{P}_a$  and  $\mathcal{F}(\tilde{P}_a)$ , that account for aberrations. Since from the very beginning of the present Section 9 we considered only the one-dimensional case, we will consider one-dimensional aberration theory only. Generalization is possible, although calculations would become more cumbersome.

Mathematically, the presence of aberrations in one-dimension modifies the pupil function by means of a phase error  $\Phi(\hat{r})$  leading to

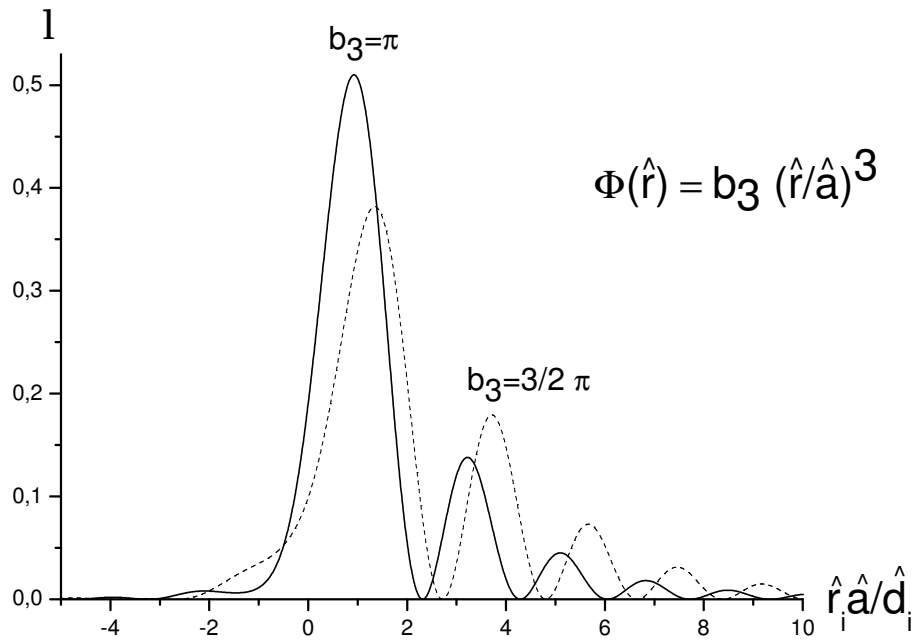


Fig. 21. The line spread  $l$  function in the presence of coma aberration.

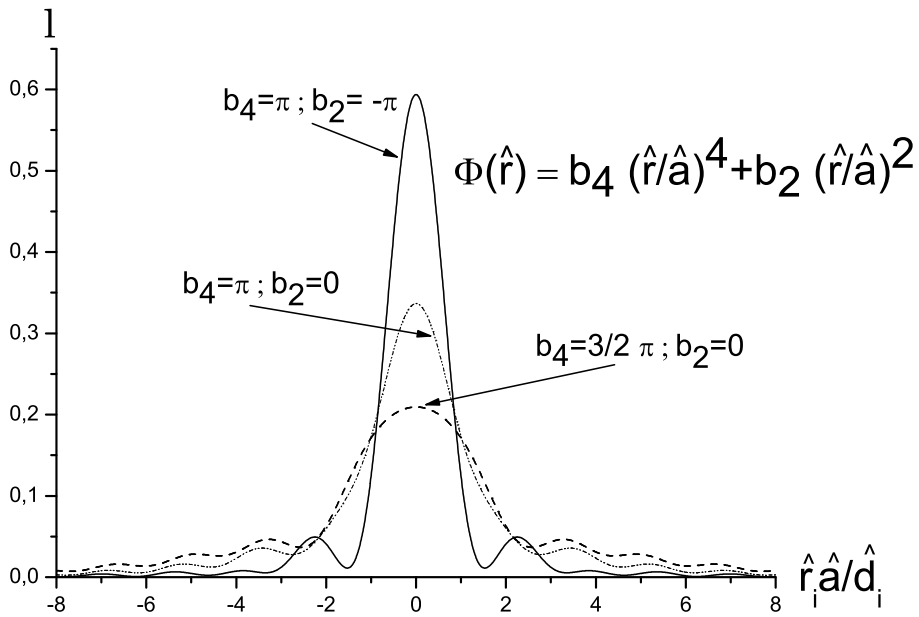


Fig. 22. The line spread  $l$  function in the presence of both spherical and defocusing aberrations.

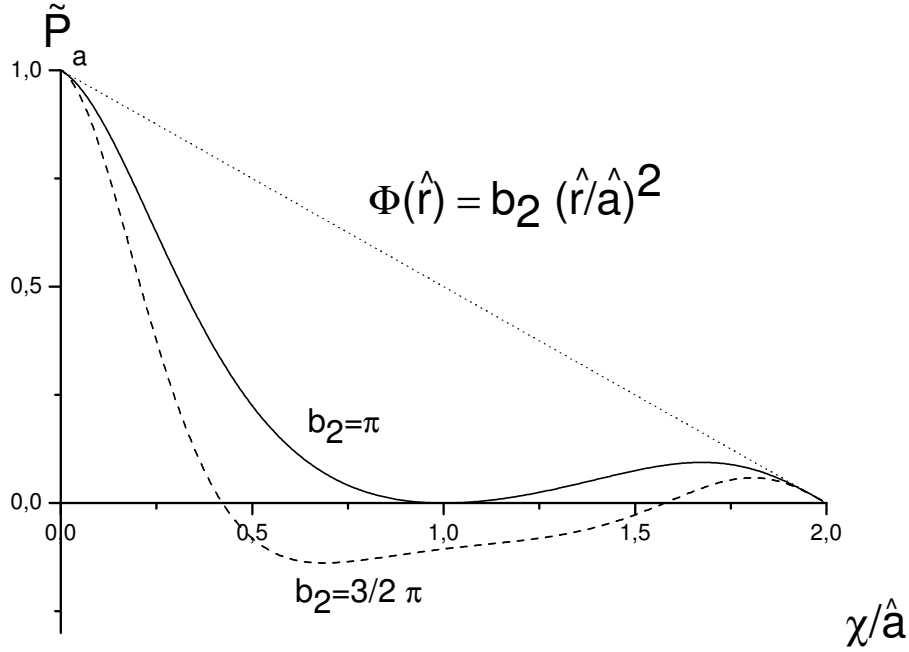


Fig. 23. The transfer function in the presence of defocusing aberration.

$$P_a(\hat{r}) = P(\hat{r}) \exp [i\Phi(\hat{r})] . \quad (264)$$

It is customary (see, for instance, [18]) to consider phase errors of the form:

$$\Phi(\hat{r}) = b_n \left( \frac{\hat{r}}{\hat{a}} \right)^n , \quad (265)$$

$n$  being an integer number, and  $b_n$  being the maximum phase error at the edge of the aperture. The value  $n = 0$  corresponds to a constant phase error and has no effects, as it cancels out when one calculates the pupil autocorrelation function. The value  $n = 1$  contributes to the autocorrelation function for a phase term linearly varying with the position. Its only effect is to shift the image position. We will not deal with the cases  $n = 0$  and  $n = 1$ . We will focus instead on the values  $n = 2$  corresponding to defocusing,  $n = 3$  corresponding to coma and  $n = 4$  corresponding to spherical aberrations.

As we have seen in Section 8, the presence of the pupil can be dealt with independently of how the pupil extension  $\hat{a}$  scales with respect to the radiation spot size and coherence length at the pupil location. Every quasi-homogeneous imaging system can be described by means of a line spread function that depends on the physical characteristics of the pupil only. As has been shown in Section 8, the knowledge of the line spread function  $l$  and of the inten-

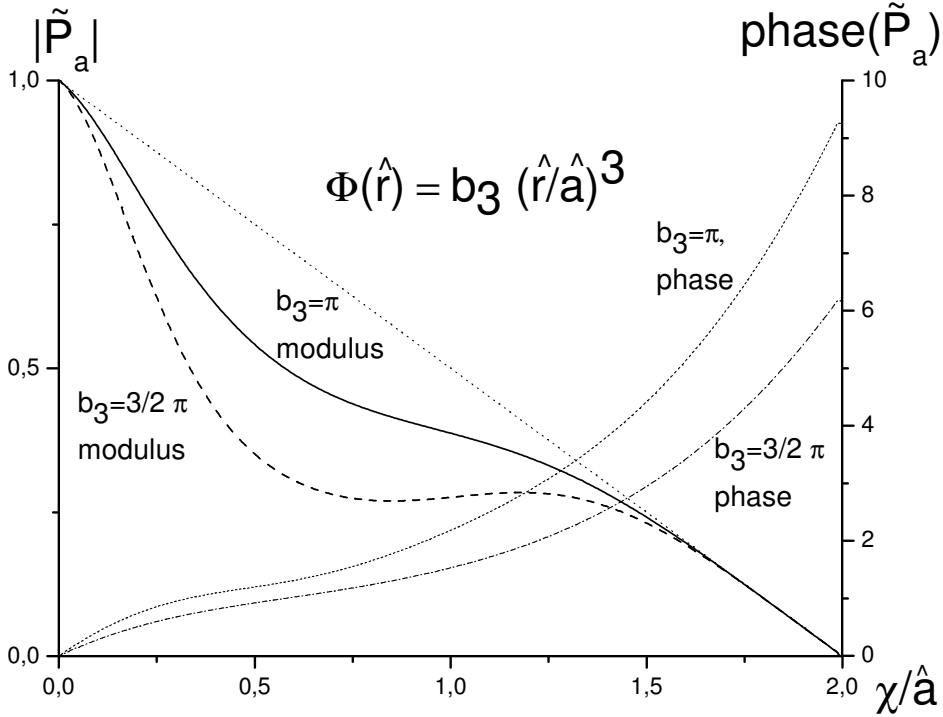


Fig. 24. The transfer function in the presence of coma aberration.

sity at the image plane without the pupil influence allows one to reconstruct the actual image by means of a convolution operation. In the present case of interest, the line spread function must be calculated accounting for the presence of aberrations. With in mind the purpose of calculating the line spread function in presence of aberrations, and with the only assumption of a quasi-homogeneous source, we start considering Eq. (137). The quasi-homogeneous assumption allows to represent the cross-spectral density at the virtual source plane as  $\hat{G}(0, -\hat{z}_1 \bar{u}, -z_1 \Delta \hat{u}) = \hat{I}(0, -\hat{z}_1 \bar{u}) g(0, -\hat{z}_1 \Delta \hat{u})$ . By definition of quasi-homogeneity, and with the accuracy of the quasi-homogeneous assumption  $(\max[1, \hat{N}_y] \cdot \max[1, \hat{D}_y])^{-1/2}$ , the spectral degree of coherence  $g$  plays the role of a Dirac  $\delta$ -function in the calculation of the intensity. Such calculation begins from Eq. (137). Accounting for the pupil influence, the following expression for the intensity at the image plane is therefore found:

$$\hat{I}_P(\hat{z}_i, \bar{r}_i) = \frac{1}{\mathcal{D}} \int_{-\infty}^{\infty} d\bar{u} \left| \hat{\mathcal{P}}_a \left( \frac{m}{\hat{z}_1} \bar{r}_i - \bar{u} \right) \right|^2 \hat{I}(0, -\hat{z}_1 \bar{u}), \quad (266)$$

where we recall that  $\mathcal{D}$  is defined in Eq. (232). Note that Eq. (266) is obtained from Eq. (137) under the only assumption of quasi-homogeneity. Also, when

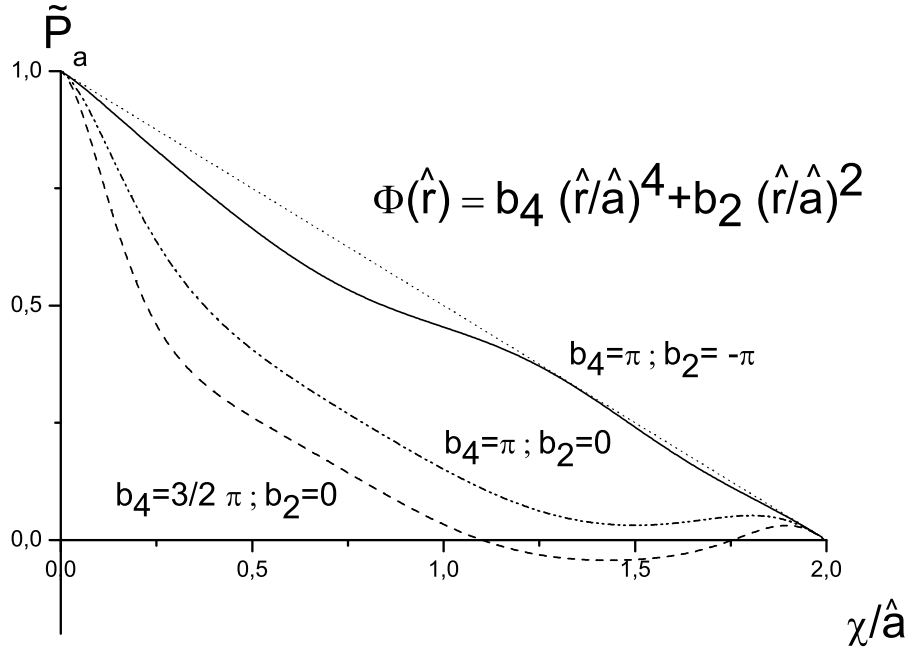


Fig. 25. The transfer function in the presence of both spherical and defocusing aberrations.

$|\hat{\mathcal{P}}_a|^2(\cdot) \rightarrow \delta(\cdot)$  we obtain back an ideal lens and  $\hat{I}_P(\hat{z}_i, \bar{r}_i) = \hat{I}(0, -m\bar{r}_i)$ .

By definition, the line spread function can be obtained by letting  $\hat{I}(0, \hat{r}) \rightarrow \delta(\hat{r})$  in Eq. (266). As a result we have

$$l(\bar{r}_i) = \left| \hat{\mathcal{P}}_a \left( \frac{m}{\hat{z}_1} \bar{r}_i \right) \right|^2 = \int_{-\infty}^{\infty} d\chi \tilde{P}_a(\chi) \exp \left[ -i \frac{\chi}{\hat{d}_i} \bar{r}_i \right]. \quad (267)$$

The proof of the last equality in Eq. (267) is based on the autocorrelation theorem, which states that if the (two-dimensional) Fourier transform of a function  $w(x, y)$  with respect to variables  $\alpha_x$  and  $\alpha_y$  is indicated by  $\bar{w}(\alpha_x, \alpha_y)$ , then the Fourier transform of the two-dimensional autocorrelation function of  $w(x, y)$  with respect to the same variables  $\alpha_x$  and  $\alpha_y$  is given by  $|\bar{w}(\alpha_x, \alpha_y)|^2$ . In formulas, after definition of the autocorrelation function

$$\mathcal{A}[w](x, y) = \int_{-\infty}^{\infty} d\eta \int_{-\infty}^{\infty} d\xi w(\eta + x, \xi + y) w^*(\eta, \xi), \quad (268)$$

which is equivalent to

$$\mathcal{A}[w](x, y) = \int_{-\infty}^{\infty} d\eta \int_{-\infty}^{\infty} d\xi w(\eta + x/2, \xi + y/2) w^*(\eta - x/2, \xi - y/2) , \quad (269)$$

the autocorrelation theorem states that

$$\int_{-\infty}^{\infty} dx \int_{-\infty}^{\infty} dy \exp [i(\alpha_x x + \alpha_y y)] \mathcal{A}[w](x, y) = |\bar{w}(\alpha_x, \alpha_y)|^2 . \quad (270)$$

Eq. (267) could have been written down immediately just recalling that the line spread function is the Fourier transform of the pupil autocorrelation function.

It is convenient to make the change of variable  $\chi \longrightarrow \Delta x \hat{a}$ . In fact, because of the definition of  $b_n$  in Eq. (265), only the ratio  $\Delta \hat{r} / \hat{a}$ , or  $\chi / \hat{a} = 2\Delta \hat{r} / \hat{a}$  is important. Aside for an unimportant factor  $\hat{a}$ , the line spread function becomes

$$l(\bar{r}_i) = \int_{-\infty}^{\infty} d\Delta x \tilde{P}_a(\hat{a}\Delta x) \exp \left[ -i \frac{\hat{a}}{\hat{d}_i} \Delta x \bar{r}_i \right] . \quad (271)$$

The autocorrelation function of the pupil  $\tilde{P}_a$ , which is the Fourier transform of  $l$ , is known under the name of Optical Transfer Function (OTF) of the system. The Optical Transfer Function and the line spread function are obviously equivalent and their knowledge solves the problem of accounting for aberrations. The Optical Transfer Function can be written explicitly modifying Eq. (238) to include a phase error in the expression for the pupil function, that is

$$\begin{aligned} \tilde{P}_a(\hat{a}\Delta x) = & \int d\bar{x} P \left[ \hat{a} \left( \bar{x} + \frac{\Delta x}{2} \right) \right] P \left[ \hat{a} \left( \bar{x} - \frac{\Delta x}{2} \right) \right] \\ & \times \exp \left\{ i\Phi \left[ \hat{a} \left( \bar{x} + \frac{\Delta x}{2} \right) \right] - i\Phi \left[ \hat{a} \left( \bar{x} - \frac{\Delta x}{2} \right) \right] \right\} . \end{aligned} \quad (272)$$

Accounting for the definition of the phase error  $\Phi$  in Eq. (265) one obtains from Eq. (272) the following expression for the Optical Transfer Function:

$$\begin{aligned} \tilde{P}_a(\hat{a}\Delta x) = & \int_{-\infty}^{\infty} d\bar{x} P \left[ \hat{a} \left( \bar{x} + \frac{\Delta x}{2} \right) \right] P \left[ \hat{a} \left( \bar{x} - \frac{\Delta x}{2} \right) \right] \\ & \times \exp \left\{ i b_n \left[ \left( \bar{x} + \frac{\Delta x}{2} \right)^n - \left( \bar{x} - \frac{\Delta x}{2} \right)^n \right] \right\} . \end{aligned} \quad (273)$$

Here  $P$  is the pupil function with no aberrations or apodizations and only an aberration term of order  $n$  has been considered. If  $\bar{x}$  is outside the interval  $[-1, 1]$ , at least one of the  $P$  functions in the integral gives zero value. As a result we may substitute the integration limits in Eq. (273) to obtain the following expression for the Optical Transfer Function:

$$\begin{aligned} \tilde{P}_a(\hat{a}\Delta x) = & \int_{-1}^1 d\bar{x} P \left[ \hat{a} \left( \bar{x} + \frac{\Delta x}{2} \right) \right] P \left[ \hat{a} \left( \bar{x} - \frac{\Delta x}{2} \right) \right] \\ & \times \exp \left\{ ib_n \left[ \left( \bar{x} + \frac{\Delta x}{2} \right)^n - \left( \bar{x} - \frac{\Delta x}{2} \right)^n \right] \right\} . \end{aligned} \quad (274)$$

With the help of Eq. (265) it is possible to directly calculate how different aberrations modify the expression for the autocorrelation function and its Fourier transform. These computations can be carried out by means of numerical techniques for any value of  $n$  and  $b_n$ , in analogy with what has been done in [18].

For completeness we will now calculate the Optical Transfer Function in several situations, which may also be found in [18]. In addition, we will also present the line spread function typical of these situation, which cannot be easily found in textbooks. Other kind of aberrations can be treated in the same fashion, and pupils with different shape may be selected. We are interested in the case when the influence of the phase error is comparable with the influence of diffraction effects on the pupil, i.e. when  $|b_n| \sim 1$ . Here we will consider several cases for defocusing ( $n = 2$ ), coma ( $n = 3$ ), spherical aberrations ( $n = 4$ ) and a combination of defocusing and spherical aberrations as well. This last situation is *per se* interesting, because it illustrates how it is possible to improve the quality of a lens with spherical aberration by further introducing a defocusing aberration (in the case under study, i.e. for  $|b_n| \sim 1$ ). In Fig. 20, Fig. 21 and Fig. 22 we plot the line spread functions describing these aberration cases. As an aside it is worth to anticipate here that Fig. 20 is strictly related with the resolution of a pinhole camera setup. This will be demonstrated in the next Section 10. As has been already said, the knowledge of the line spread function is completely equivalent to the knowledge of the transfer function (OTF) of the system. In Fig. 23, Fig. 24, and Fig. 25 we plot the transfer functions relative to the same cases treated in Fig. 20, Fig. 21 and Fig. 22.

In closing, it is interesting to deal with the limit when  $\hat{z}_1^2/\hat{N} \ll \hat{a}^2 \ll \hat{D}\hat{z}_1^2$ . In this case the coherence length at the pupil is much smaller than the characteristic pupil size, or, equivalently,  $P_a(\hat{r}_1)P_a^*(\hat{r}_2) \simeq |P_a(\hat{r}_1)|^2 \simeq |P_a(\hat{r}_2)|^2$ , as presented in Eq. (7.2-15b) of [8]. In order to retain this last simplification when aberrations are present, we must require that the phase of the pupil function  $P_a$  (that is now a complex object) is not appreciably different when  $\hat{r}_1$  and

$\hat{r}_2$  are separated by a distance of order of the coherence length or smaller. This is equivalent to the requirement that the characteristic scale of the lens imperfections is much larger than the coherence length. Mathematically, this means that  $|b_n| \lesssim 1$ . Under this assumption, aberrations cannot affect the cross-spectral density in the limit  $\hat{z}_1^2/\hat{N} \ll \hat{a}^2 \ll \hat{D}\hat{z}_1^2$ . This fact is known from a long time and, as reported in [8], it was first discovered by Zernike [19]. The same limiting case can be presented in the line spread function formalism. One should recall that the resolution due to diffraction effects is of order  $\hat{z}_1/(\hat{a}\sqrt{\hat{N}})$ , as has already been seen in the previous Section 8. This means that in the limit  $\hat{z}_1^2/\hat{N} \ll \hat{a}^2 \ll \hat{D}\hat{z}_1^2$  it makes sense to account for diffraction effects from the pupil, because in this case the resolution due to diffraction effects is worse than that related with the quasi-homogeneous approximation ( $\hat{z}_1/(\hat{a}\sqrt{\hat{N}}) \gg 1/\sqrt{\hat{N}\hat{D}}$ ). However, one may choose to worsen the resolution of the calculations from  $1/\sqrt{\hat{N}\hat{D}}$  to the resolution due to diffraction effects,  $\hat{z}_1/(\hat{a}\sqrt{\hat{N}}) \ll 1$ . This is equivalent to neglect diffraction effects. In this case, since  $|b_n| \lesssim 1$ , the autocorrelation function of the pupil can be substituted with unity or, equivalently, the line spread function  $l$  plays the role of a Dirac  $\delta$ -function in the calculation of the intensity. Therefore, aberrations cannot affect the intensity distribution at the image plane. Moreover, the expression for the spectral degree of coherence Eq. (231), remains valid for  $|b_n| \lesssim 1$  because, as already discussed,  $P_a(\hat{r}_1)P_a^*(\hat{r}_2) \simeq |P_a(\hat{r}_1)|^2 \simeq |P_a(\hat{r}_2)|^2$ . One concludes that in this limit, and with resolution  $\hat{z}_1/(\hat{a}\sqrt{\hat{N}}) \ll 1$ , aberrations cannot affect the coherence properties on the image plane.

## 9.2 Severe aberrations

It is now interesting to discuss an analytical treatment valid in the case for  $|b_n| \gg 1$ , which exploits the simplifications arising from the large parameter  $|b_n|$ . Under this constraint, aberrations will be considered severe.

### 9.2.1 Physical Optics prediction of the line spread function

Under the approximation  $|b_n| \gg 1$ , it is possible to present an analytical calculation for the line spread function  $l$  which characterizes the imaging system in the case of quasi-homogeneous sources. Then, once the line spread function is known, one obtains the intensity at the image plane by convolving the line spread function and the intensity from an ideal system (i.e. without accounting for the pupil influence).

Let us now focus on that term in the phase factor of Eq. (274) which is linear in  $\Delta x$ , i.e. on  $nb_n\Delta x\bar{x}^{n-1}$ . We will assume that the integrand contributes to

the integral for all values of  $\bar{x}$  inside the interval  $[-1, 1]$ , otherwise the autocorrelation function would be suppressed, as the effective integration range would be smaller than  $[-1, 1]$ . Then, a typical scale of the autocorrelation function is obtained in terms of  $\Delta x$  by imposing  $n|b_n|\Delta x\bar{x}^{n-1} \sim 1$ . In fact, as  $n|b_n|\Delta x\bar{x}^{n-1} > 1$  the integrand starts to exhibit fast oscillatory behavior, thus suppressing the integral. Thus, the characteristic scale  $\Delta x_{typ} \sim 1/(n|b_n|)$  is found. Since we assumed  $|b_n| \gg 1$ , we can state that, with accuracy  $1/|b_n|$ , the functions  $P$  inside the integrand can be substituted with unity and the nonlinear phase factors in  $\Delta x^k$  with  $k = 2, 3, \dots$  can be neglected, at least for reasonable orders of  $n$ , as they would give rise to typical scales of order  $1/|b_n|^{1/k} \gg 1/|b_n|$ . As a result we obtain the following major simplification:

$$\tilde{P}_a(\hat{a}\Delta x) = \int_{-1}^1 d\bar{x} \exp \left[ inb_n\Delta x\bar{x}^{n-1} \right] . \quad (275)$$

Eq. (275) can be integrated analytically for all values of  $n$  (therefore including defocusing, coma, spherical or higher order aberrations). After definition of

$$\mathcal{T}(n, b_n, \Delta x) = \frac{2}{(n-1) [-inb_n\Delta x]^{\frac{1}{n-1}}} \times \left[ (n-1)\Gamma \left( 0, \frac{n}{n-1} \right) - \Gamma \left( \frac{1}{n-1}, -inb_n\Delta x \right) \right] , \quad (276)$$

$\Gamma(s, z)$  being the incomplete Euler gamma function

$$\Gamma(s, z) = \int_z^\infty dt t^{s-1} \exp[-t] , \quad (277)$$

we have the following result:

$$\tilde{P}_a(\hat{a}\Delta x) = \text{Re} [\mathcal{T}(n, b_n, \Delta x)] + \Pi(n) \cdot \text{Im} [\mathcal{T}(n, b_n, \Delta x)] , \quad (278)$$

where  $\Pi(n)$  is the parity of  $n$ , i.e.  $\Pi(n) = 0$  if  $n$  is even and  $\Pi(n) = 1$  if  $n$  is odd. Eq. (278) is valid for any value of  $n > 1$ .

It is interesting to compare the shape of the autocorrelation function obtained in the limiting case  $|b_n| \gg 1$  with that obtained with numerical calculations which do not exploit the simplification based on the large value of the parameter  $|b_n|$ . They rely, instead, on the exact formula for the autocorrelation function, Eq. (274). This gives a visual idea of the accuracy of the asymptotic. Fixing  $b_n = 9\pi$  we plot the autocorrelation function for defocusing aberrations, with  $n = 2$ , in Fig. 26 and Fig. 27. For coma aberrations, with  $n = 3$ , we plot

the real part of the autocorrelation function in Fig. 28 and Fig. 29, while the imaginary part is plotted in Fig. 30 and Fig. 31. The function  $\mathcal{T}$  should be truncated as  $\Delta x > 2$ .

Explicit substitution of Eq. (275) in Eq. (271) gives

$$l(\bar{r}_i) = \int_{-\infty}^{\infty} d\Delta x \int_{-1}^1 d\bar{x} \exp[inb_n \Delta x \bar{x}^{n-1}] \exp\left[-i \frac{\hat{a}}{\hat{d}_i} \Delta x \bar{r}_i\right]. \quad (279)$$

Finally, exchange of the integration order and calculation of the integral in  $d\Delta x$  yields the following expression for the line spread function, provided that  $|b_n| \gg 1$ :

$$l(\bar{r}_i) = \int_{-1}^1 d\bar{x} \delta\left(nb_n \bar{x}^{n-1} - \frac{\hat{a}}{\hat{d}_i} \bar{r}_i\right). \quad (280)$$

Eq. (280) may be explicitly evaluated with the help of the new integration variable  $y = nb_n \bar{x}^{n-1}$ . Care must be taken in separating the cases when  $n$  is even and when  $n$  is odd.

When  $n$  is even we obtain

$$\begin{aligned} l(\bar{r}_i) &= \frac{1}{2(n-1)} \int_{-nb_n}^{nb_n} dy \delta\left(y - \frac{\hat{a}}{\hat{d}_i} \bar{r}_i\right) \left(\frac{\text{abs}(y)}{nb_n}\right)^{-\frac{n-2}{n-1}} \\ &= \frac{1}{2(n-1)} \text{rect}\left(\frac{\hat{a}\bar{r}_i}{2\hat{d}_i nb_n}\right) \cdot \left(\frac{\hat{a} \text{abs}(\bar{r}_i)}{\hat{d}_i nb_n}\right)^{-\frac{n-2}{n-1}}. \end{aligned} \quad (281)$$

Here the function  $\text{rect}(x)$  is defined, as before, following [8], and is equal to unity for  $|x| \leq 1/2$  and zero otherwise. When  $n$  is odd we have

$$\begin{aligned} l(\bar{r}_i) &= \frac{1}{n-1} \int_0^{nb_n} dy \delta\left(y - \frac{\hat{a}}{\hat{d}_i} \bar{r}_i\right) \left(\frac{y}{nb_n}\right)^{-\frac{n-2}{n-1}} \\ &= \frac{1}{n-1} \text{rect}\left(\frac{\hat{a}\bar{r}_i}{\hat{d}_i nb_n} - \frac{1}{2}\right) \cdot \left(\frac{\hat{a}\bar{r}_i}{\hat{d}_i nb_n}\right)^{-\frac{n-2}{n-1}}. \end{aligned} \quad (282)$$

Introduction of the new variable  $\bar{r}'' = \hat{a}\bar{r}_i/(\hat{d}_i nb_n)$  allows to write Eq. (281) and Eq. (282) in a more compact way,

$$l(\bar{r}'') = \frac{1}{2(n-1)} \text{rect}\left(\frac{\bar{r}''}{2}\right) \cdot (\text{abs}(\bar{r}''))^{-\frac{n-2}{n-1}} \quad (283)$$

when  $n$  is even, and

$$l(\bar{r}'') = \frac{1}{n-1} \text{rect}\left(\bar{r}'' - \frac{1}{2}\right) \cdot (\bar{r}'')^{-\frac{n-2}{n-1}} \quad (284)$$

when  $n$  is odd. Note that we have normalized Eq. (283) and Eq. (284) in such a way that integration of  $l$  in  $d\bar{r}''$  over the real field gives unity.

As we will see later on, Eq. (283) and Eq. (284) can be found with the help of Geometrical Optics alone. We will refer to such derivation as the Geometrical Optics prediction of the line spread function. We plotted Eq. (283) or Eq. (284) as a function of  $\bar{r}''$  for different aberrations. In Fig. 32 we plotted the case of defocusing aberration, in Fig. 33 the case of coma and in Fig. 34 the case of spherical aberrations. Also, in these figures, comparison with numerical calculations is shown for the severe aberration cases  $b_2 = 9\pi$ ,  $b_3 = 9\pi$  and  $b_4 = 9\pi$ . Note that Eq. (283) is symmetric in  $\bar{r}''$  (when  $n$  is even  $l$  is symmetric), while Eq. (284) is not (when  $n$  is odd  $l$  is not symmetric). This is consistent with the fact that the Optical transfer function is real in the case  $n$  is even, while it has a non-zero imaginary part in the case  $n$  is odd (see, for instance, Fig. 23, Fig. 24 and Fig. 25 and, later on, Fig. 26, Fig. 28 and Fig. 30). The same behavior is also found in Fig. 20, Fig. 21 and Fig. 22. Furthermore it should be noted that the line spread functions in Fig. 33 and Fig. 34 are not convergent for values of  $\bar{r}''$  near zero. However, the meaning of the line spread function is that of the imaged intensity from a line input, but a line input is not physical, and must be represented in terms of a generalized function, a  $\delta$ -Dirac function. It is not surprising that such an object may lead to a singular result.

### 9.2.2 Physical Optics and Geometrical Optics

In the previous Section 9.2.1 we presented a calculation of the line spread function  $l$  for the case  $|b_n| \gg 1$  based on Physical Optics. This gave us Eq. (280) for the line spread function or, equivalently, Eq. (281) and Eq. (282), that are an explicit evaluation of Eq. (280) in the case  $n$  is even or odd. We have seen that the analytical treatment in Section 9.2.1 follows mathematically from a major simplification of Eq. (274), arising from the large parameter  $|b_n| \gg 1$ . Physically, this condition means that effects of diffraction from the pupil can be neglected. Consider the expression for the pupil autocorrelation function, Eq. (272). On the one hand, when  $\bar{x} \sim 1/b_n$  the phase term due to aberration effects in Eq. (272) becomes comparable to unity, thus leading to oscillatory behavior of the integrand. On the other hand, the pupil finite aperture limits the integration in Eq. (272) for  $\bar{x} \sim 1$ . Therefore,  $|b_n| \gg 1$  diffraction effects can be neglected, while they start to become important when  $|b_n| \lesssim 1$ . It follows that it must be possible to obtain results in Section 9.2.1, which have

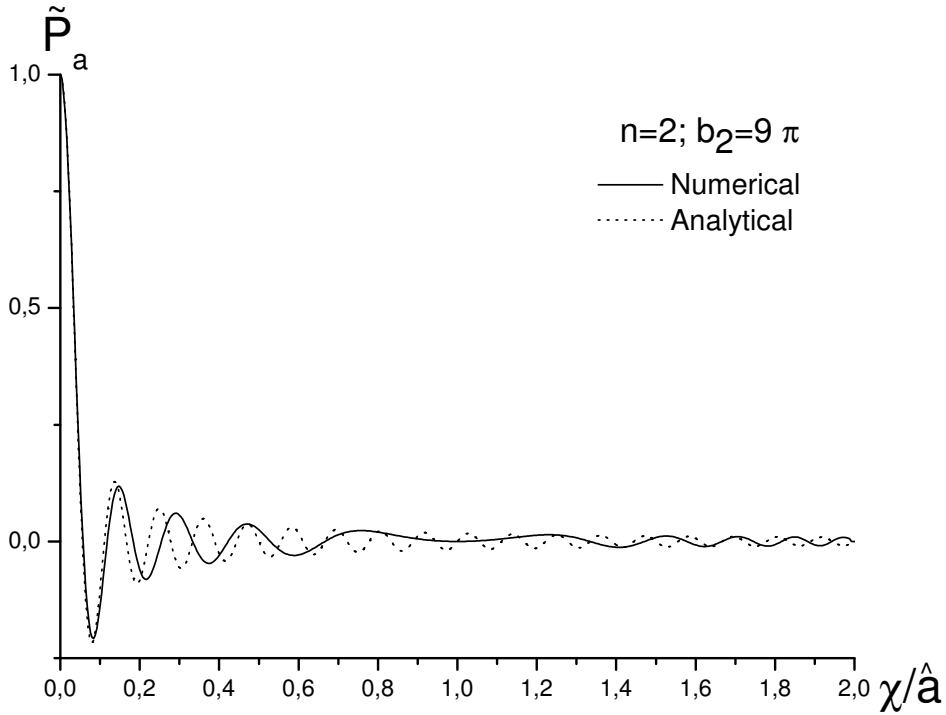


Fig. 26. The transfer function in the presence of defocusing aberration ( $n = 2$ ,  $b_2 = 9\pi$ ). Numerical techniques have been used to calculate the exact autocorrelation function that is compared to the analytical evaluation of the autocorrelation function in the severe aberration asymptote.

been derived with the help of physical Optics, with the help of Geometrical Optics only. In the next Section 9.2.3 we discuss how this can be done.

Before doing that it is worth to discuss the relationship between Geometrical and Physical Optics, which may otherwise be misleading. We should make clear that when we discuss about Geometrical or Physical Optics we are talking about possible ways of calculating the line spread function of the system  $l$ .

In Section 8 we have introduced the concept of line spread function  $l$  and we have demonstrated that, under the assumption that the virtual source is quasi-homogeneous,  $l$  constitutes a sort of passport for a given lens. It relates the intensity from any quasi-homogeneous source imaged with a perfect lens and the intensity obtained by using a particular non-ideal lens. The intensity from a specific optical system can be recovered as a convolution of the intensity obtained in the case of an ideal optical system and the line spread function. The intensity from an ideal system at the image plane is, by definition, the intensity at the virtual source. Therefore, when the quasi-homogeneous approximation is applicable, it is always possible to break the imaging problem

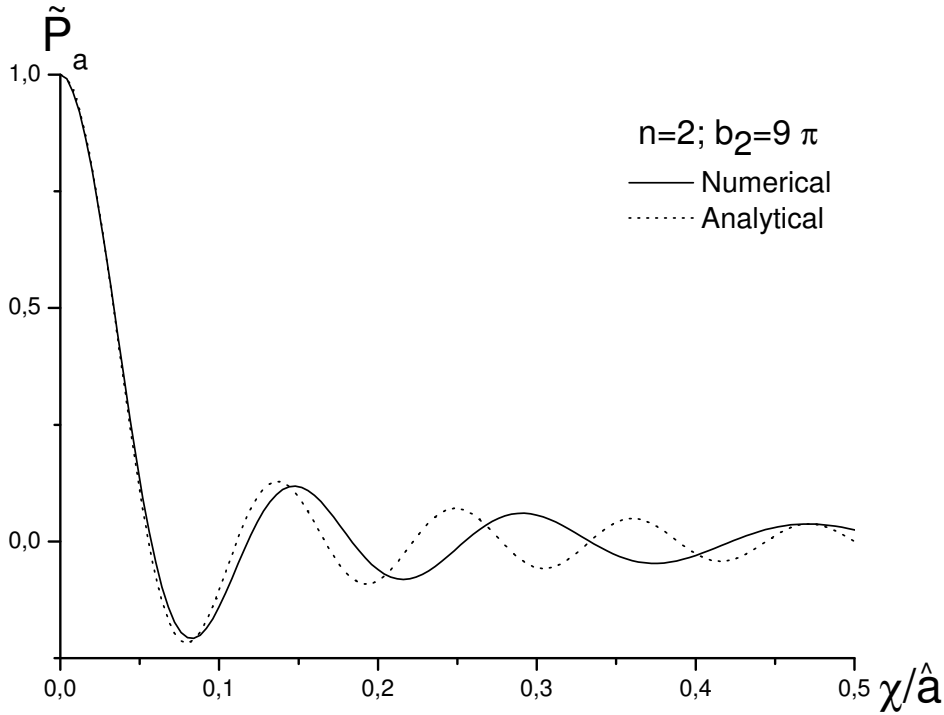


Fig. 27. An enlarged version of Fig. 26. Numerical techniques have been used to calculate the exact autocorrelation function that is compared to the analytical evaluation of the autocorrelation function in the severe aberration asymptote.

into two separate problems. First, specify the intensity distribution of the source. Second, specify the optical system through the  $l$  function.

When diffraction effects are negligible with respect to aberration effects, i.e. when  $|b_n| \gg 1$ , the line spread function of the lens can be calculated by both Physical Optics considerations (as in Section 9.2.1) and Geometrical Optics considerations, as in the next Section 9.2.3. In this case, a finite aperture size does not influence the calculation of the line spread function. It is responsible for the quantity of the total energy transmitted only. Once the source characteristics are specified, one may use a ray-tracing code to get the image intensity from a non-ideal system or, equivalently, one may calculate the  $l$  function and convolve with a scaled version of the intensity on the virtual source. When diffraction effects are not negligible anymore,  $l$  can be evaluated with the help of Physical Optics considerations only. In this case, use of ray-tracing codes to solve the imaging problem makes no sense. Yet, the quasi-homogeneous approximation allows one to use a line spread function approach. Convolution of  $l$  with a scaled version of the intensity on the virtual source solves the imaging problem. From this viewpoint the quasi-homogeneity of the source is an *a priori* condition with respect to the possibility of applying Geometrical

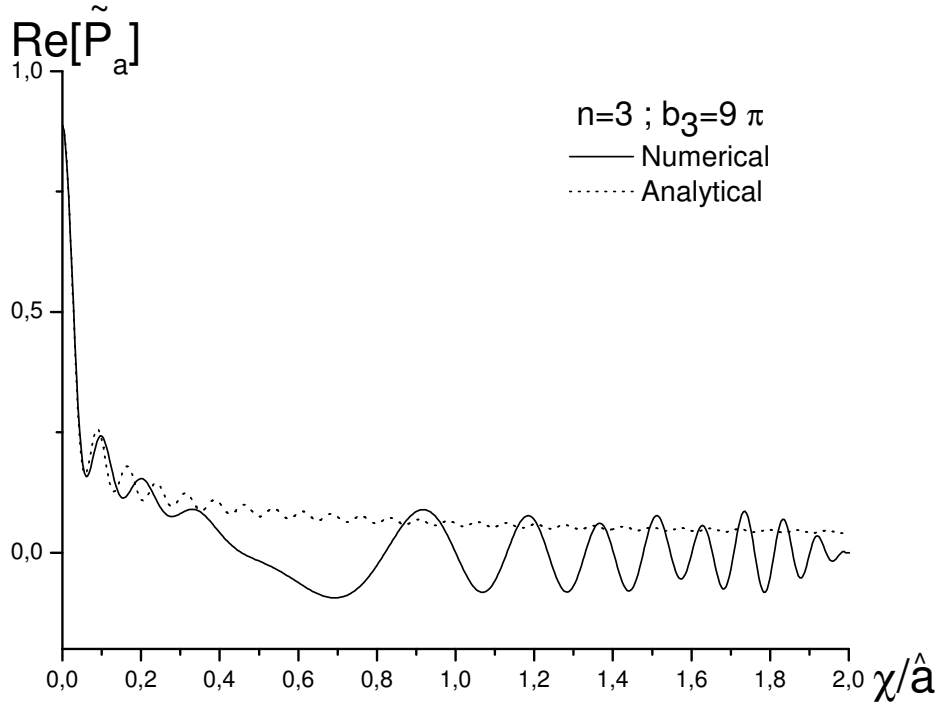


Fig. 28. The real part of the transfer function in the presence of coma aberration ( $n = 3$ ,  $b_3 = 9\pi$ ). Numerical techniques have been used to calculate the exact autocorrelation function that is compared to the analytical evaluation of the autocorrelation function in the severe aberration asymptote.

Optics for the solution of imaging problems from a non-ideal setup.

A final word of caution should be spent regarding notations historically used to represent aberrations (see, for instance, [20]). On the one hand, the knowledge of the phase error  $\Phi(\hat{r}) = b_n(\hat{r}/\hat{a})^n$  is equivalent to the knowledge of the surfaces of equal phase, i.e. of the wavefronts of the electromagnetic field. In this case one usually talks about "wave aberration". On the other hand, the knowledge of the derivative  $d\Phi(\hat{r})/d\hat{r}$  (or, in more dimensions, of the gradient  $\vec{\nabla}\Phi(\vec{r})$ ) is equivalent to the knowledge of the vector field orthogonal to the wavefronts of the electromagnetic field. In the case diffraction effects are not present, one may identify  $d\Phi(\hat{r})/d\hat{r}$  with the extra angular displacement of a ray and recover the deviation of the transverse coordinate of a ray on the image plane. In this case, usually, one talks about "Geometrical aberration" [20]<sup>21</sup>. It should be clear though, that the presentations in terms of "Wave aberration" and "Geometrical aberration" are completely equivalent from a mathematical

<sup>21</sup> In reference [21] the term "Rays aberration" is used in place of "Geometrical aberration"

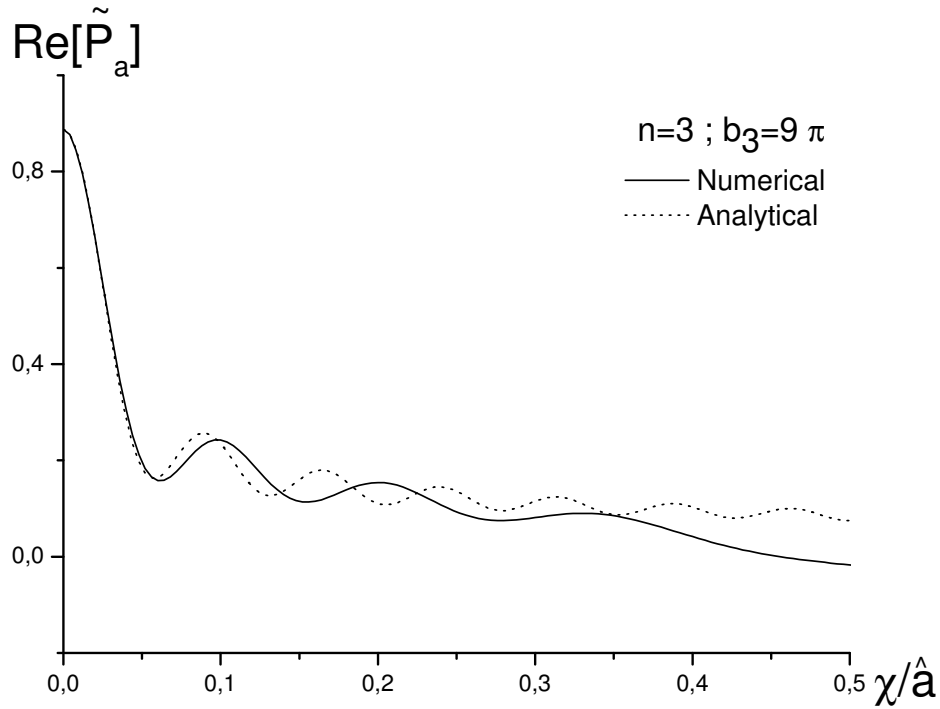


Fig. 29. An enlarged version of Fig. 28. Numerical techniques have been used to calculate the exact autocorrelation function that is compared to the analytical evaluation of the autocorrelation function in the severe aberration asymptote.

viewpoint, regardless the value assumed by the parameter  $|b_n|$  with respect to unity. Therefore, one needs to clearly distinguish between the language used (Geometrical or Wave aberration) and the possibility of applying Geometrical Optics to calculate the line spread function. When  $|b_n| \lesssim 1$  this is not possible, and one has to rely on Wave Optics predictions for the line spread function  $l$  only. When  $|b_n| \gg 1$  one may rely both on Wave Optics predictions (see Section 9.2.1) or Geometrical Optics predictions (see Section 9.2.3), and the two predictions must coincide.

### 9.2.3 Geometrical Optics prediction of the line spread function

As has been already said in Section 9.2.2, when diffraction effects are negligible with respect to aberration effects, i.e. when  $|b_n| \gg 1$ , the line spread function of the lens can be calculated by both Physical Optics considerations (as in Section 9.2.1) and Geometrical Optics considerations. In this case, a finite aperture size does not influence the calculation of the line spread function, and is responsible for the quantity of the total energy transmitted only.

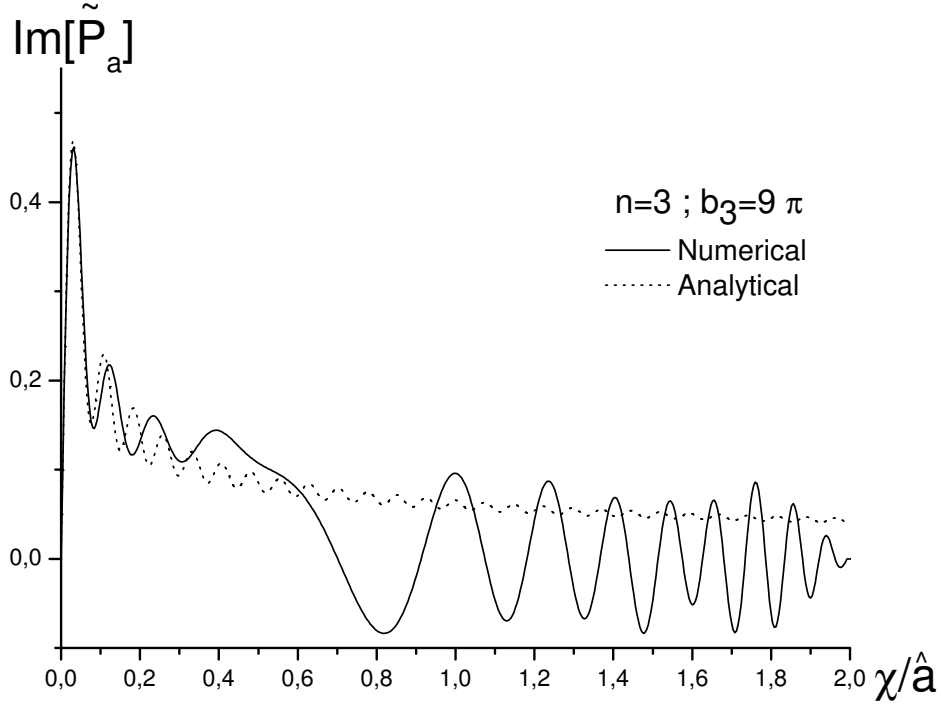


Fig. 30. The imaginary part of the transfer function in the presence of coma aberration ( $n = 3$ ,  $b_3 = 9\pi$ ). Numerical techniques have been used to calculate the exact autocorrelation function that is compared to the analytical evaluation of the autocorrelation function in the severe aberration asymptote.

In the Geometrical Optics limit, Maxwell equations can be replaced by the simpler Eikonal equation, which should be solved for surfaces of equal phase. In our one-dimensional case of study, these surfaces are indeed lines on the plane  $\hat{r} - \hat{z}$  and may be indicated with the family  $\phi_p(\hat{r}, \hat{z})$ , where  $p$  identifies a particular value of the phase. Once the functions  $\phi_p$  are known, one can recover the usual ray-tracing techniques remembering that rays are, at any point, normal to surfaces with equal phase. The following ray equation holds:

$$\vec{s}(\hat{r}, \hat{z}) = \vec{\nabla} \phi_p(\hat{r}, \hat{z}) , \quad (285)$$

where  $\vec{s}$  indicates a vector field tangent to the rays expressed in normalized units. If the lens is ideal one recovers, at the image plane, the intensity profile of the source reversed and magnified. In particular, a line input would be mapped to a line on the image plane. However, aberrations modify the surfaces of equal phase in Eq. (285), because a phase error is to be added to  $\phi_p$ . As a result, when calculating  $\vec{s}$  by means of Eq. (285), one obtains an extra angular displacement in normalized units for each ray dependent on the transverse position of the ray, that is

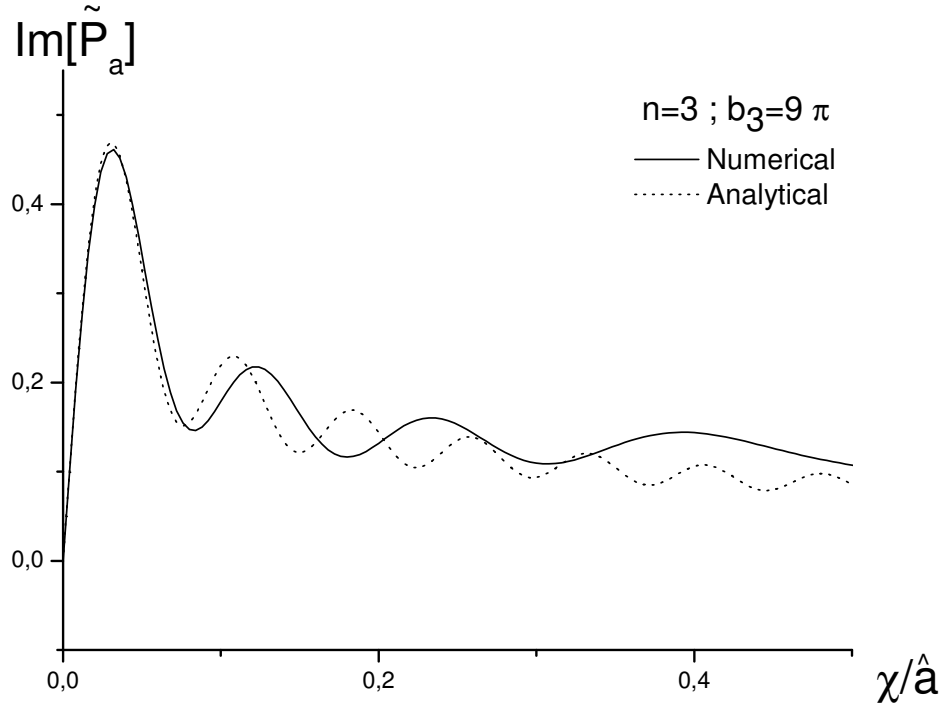


Fig. 31. An enlarged version of Fig. 30. Numerical techniques have been used to calculate the exact autocorrelation function that is compared to the analytical evaluation of the autocorrelation function in the severe aberration asymptote.

$$\alpha(\hat{r}) = \frac{d\Phi(\hat{r})}{d\hat{r}} = \frac{n}{\hat{a}} b_n \left( \frac{\hat{r}}{\hat{a}} \right)^{n-1} . \quad (286)$$

It follows that the coordinate of the ray going through the lens at transverse position  $\hat{r}$  has a transverse position, at the image plane, given by

$$\bar{r}_i(\hat{r}) = \frac{n\hat{d}_i}{\hat{a}} b_n \left( \frac{\hat{r}}{\hat{a}} \right)^{n-1} . \quad (287)$$

The relation between the coordinate of a ray at the pupil and its transverse position at the image plane for  $n = 2$  (defocusing),  $n = 3$  (coma), and  $n = 4$  (spherical aberration) is plotted in Fig. 35.

If the lens is hit by a finite number of rays, the output of the system at the image plane is constituted by a finite sum of Dirac- $\delta$  functions. Each of these can be represented in the implicit form  $\delta \left[ \bar{r}_i - \frac{n\hat{d}_i}{\hat{a}} b_n \left( \frac{\hat{r}}{\hat{a}} \right)^{n-1} \right]$ . Therefore, if the lens is homogeneously illuminated by an infinite number of rays from the input

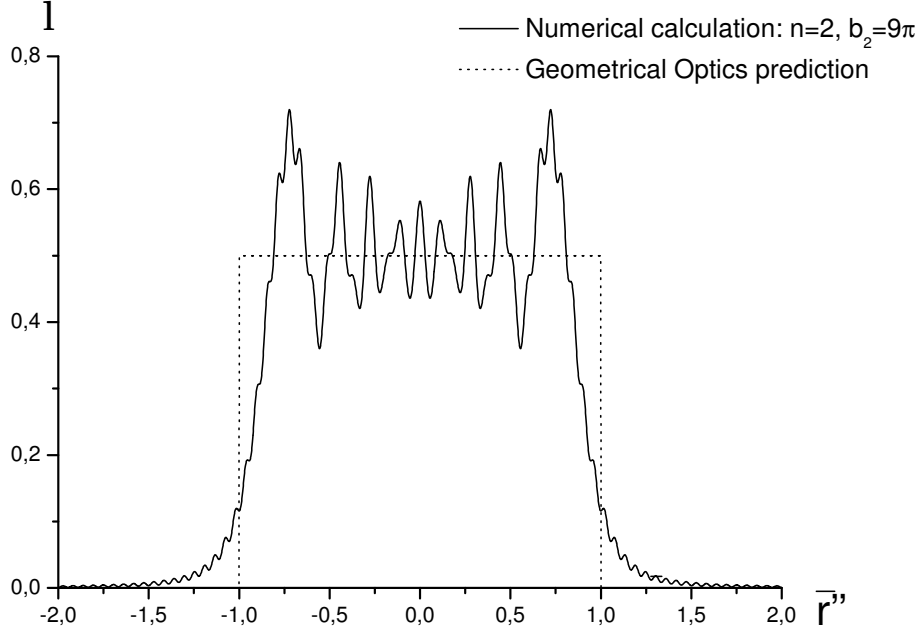


Fig. 32. The line spread function versus the reduced coordinate on the image plane  $\bar{r}'' = \hat{a}\bar{r}_i/(\hat{d}_i n b_n)$  in the case of severe defocusing aberration ( $n = 2$ ,  $b_2 = 9\pi$ ) and comparison with the geometrical optics prediction.

line source, we obtain the line spread function

$$l(\bar{r}_i) = \int_{-a}^a d\hat{r} \delta \left[ \bar{r}_i - \frac{n\hat{d}_i}{\hat{a}} b_n \left( \frac{\hat{r}}{\hat{a}} \right)^{n-1} \right]. \quad (288)$$

Finally, using the new integration variable  $\bar{x} = \hat{r}/\hat{a}$  and normalizing  $l$  so that the integral of  $l$  gives unity yields

$$l(\bar{r}_i) = \int_{-1}^1 d\bar{x} \delta \left( \bar{r}_i - \frac{n\hat{d}_i}{\hat{a}} b_n \bar{x}^{n-1} \right), \quad (289)$$

that is equivalent to Eq. (280). From a ray-tracing viewpoint, the problem of calculating the line spread function reduces to the problem of transforming a uniform distribution of rays into a non-uniform distribution related to the non-linear transformation Eq. (287). When  $|b_n| \lesssim 1$  instead, Geometrical Optics cannot be used to calculate the  $l$  function, and the Eikonal approximation fails. As we have seen in Section 9.2.1 this is equivalent, in the language of Physical Optics, to a situation when the simplification in Eq. (275) does not

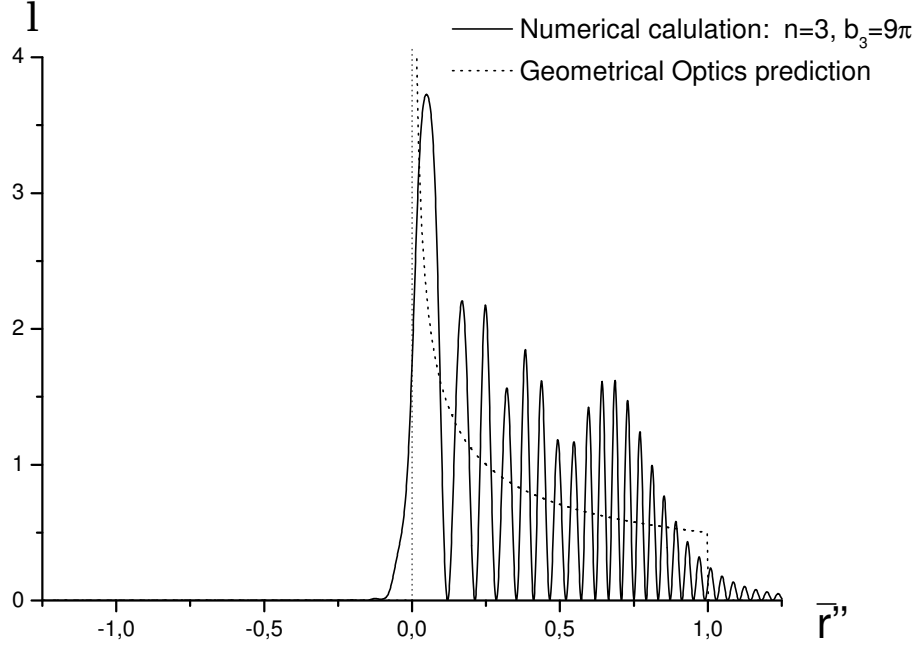


Fig. 33. The line spread function versus the reduced coordinate on the image plane  $\bar{r}'' = \hat{a}\bar{r}_i/(\hat{d}_i n b_n)$  in the case of severe coma aberration ( $n = 3$ ,  $b_3 = 9\pi$ ) and comparison with the geometrical optics prediction.

hold.

## 10 Pinhole optics

Taking advantage of Eq. (133), we will now study the case when images of a virtual source can be obtained with the help of a pinhole (i.e. a pupil without a lens), without further lenses or mirrors. When a pinhole can be treated as an imaging system, people refer to it as an (X-ray) pinhole camera. Here we will consider the geometry in Fig. 36. The study of this relatively simple setup will be helpful to reach a better understanding of Section 11, dedicated to imaging in the focal plane, Section 12, where we will describe imaging in any plane behind the lens, and Section 13, that will deal with the depth of focus of an imaging system. Moreover, it will also suggestively show how a problem apparently not related with the theory of aberrations (in the pinhole camera setup there is not even a lens) can formally be treated like a defocusing aberration problem. This is due to the appearance of a quadratic phase factor in the equation for the intensity at the image plane.

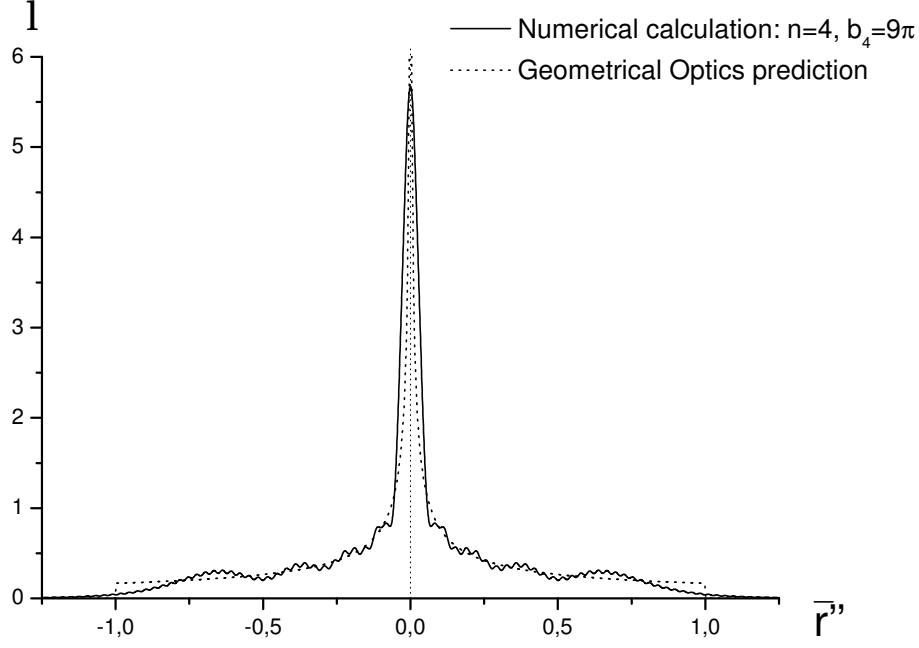


Fig. 34. The line spread function versus the reduced coordinate on the image plane  $\bar{r}'' = \hat{a}\bar{r}_i/(\hat{d}_i n b_n)$  in the case of severe spherical aberration ( $n = 4$ ,  $b_4 = 9\pi$ ) and comparison with the geometrical optics prediction.

An X-ray pinhole camera has the same properties as the more familiar visible light pinhole-camera. The main advantage of such a lensless imaging system is that a pinhole is easier to fabricate than a lens. Pinhole cameras can be combined with X-ray Synchrotron Radiation sources and detectors for a number of relatively specialized applications [22].

The conditions under which the pinhole can be treated as an imaging system are non-trivial, and are not always satisfied. With the help of Eq. (133) we can investigate the properties of the image in the limiting case for  $\hat{f} \rightarrow \infty$ , i.e. when there is no lens. We will restrict ourselves to the one-dimensional case, thus simplifying the vectorial notation in Eq. (133) to scalar notation. The assumption of separability of the cross-spectral density in the horizontal and in the vertical direction ( $\hat{N}_x \gg 1$  and  $\hat{D}_x \gg 1$ ) suggests, in fact, to discuss horizontal and vertical directions separately. In general, one can see that the following conditions must be satisfied in order to form an image of the source (in one dimension):

1. The pinhole must be in the far field. In this case, using Eq. (127), the cross-spectral density on the pupil plane is given by

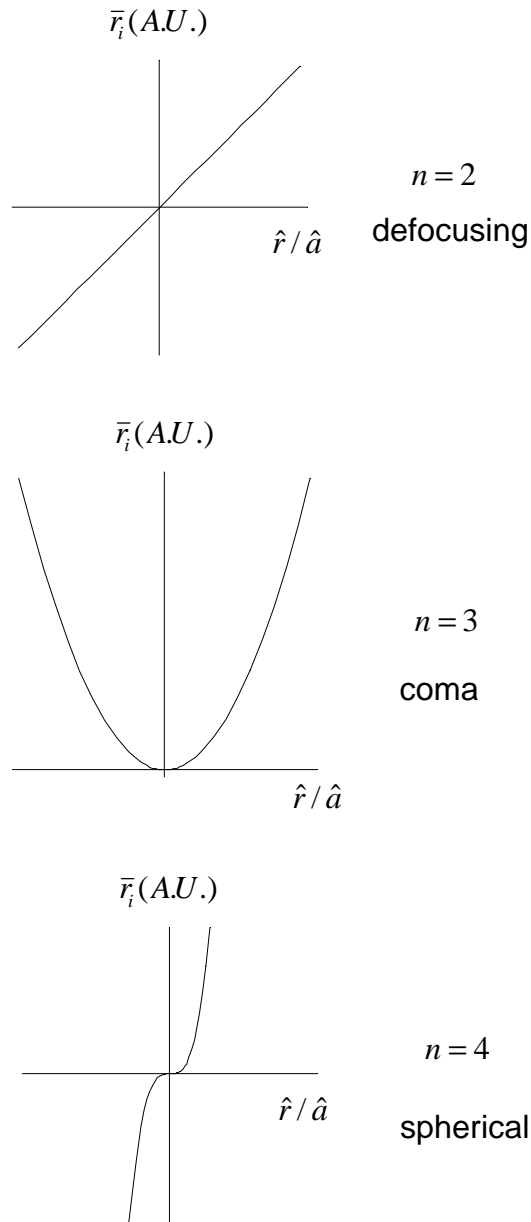


Fig. 35. Amount by which a geometrically traced ray departs from a desired location in the image formed by an optical system. The ordinate for each curve is the height at which the ray intersects the image plane. The abscissa is the coordinate of the ray at the pupil plane.  $n = 2$  represents defocusing,  $n = 3$  represents coma, and  $n = 4$  represents spherical aberration cases according to Eq. (287).

$$\hat{G}(\hat{z}_1, \bar{r}, \Delta\hat{r}) = \frac{1}{4\pi^2 \hat{z}_1^2} \exp[2i\bar{r} \cdot \Delta\hat{r}/\hat{z}_1] \hat{\mathcal{G}}(0, -\bar{r}, -\Delta\hat{r}) . \quad (290)$$

2. In the integrand of Eq. (133) two specific phase factors appear. These are  $\exp[2i\bar{r}' \cdot \Delta\hat{r}'/(\hat{z}_2 - \hat{z}_1)]$  and  $\exp[2i\bar{r}' \cdot \Delta\hat{r}'/\hat{z}_1]$ , the latter appearing through Eq. (290). Both must be negligible.

3. The pinhole size must be larger than the coherence length on the pinhole plane, or the pupil functions  $P$  in Eq. (133) will modify the dependence of  $\hat{G}(\hat{z}_2)$  on  $\bar{r}$  (i.e. the image will not have a good resolution).

If conditions from 1. to 3. above are satisfied, the pinhole camera works as an imaging system forming an inverted image of the source. From Eq. (133) one may see that the image is magnified of a quantity  $|M| = \hat{z}_2/\hat{z}_1$ , because of the same reason as the lens.

We will now give a physical interpretation of conditions 1. through 3. stated above. We begin considering the limiting case when  $\hat{N} \gg 1$  and  $\hat{D} \gg 1$ , i.e. a Gaussian quasi-homogeneous virtual source. Further on we will see up to what extent this assumption can be relaxed. We assume a large magnification constant  $|M| \simeq \hat{d}/\hat{z}_1 \gg 1$ , where  $\hat{d} = \hat{z}_2 - \hat{z}_1$ . Here this assumption will be accepted for simplicity and relaxed, later on, to an arbitrary value of  $|M|$ .

The second condition requires that two distinct phase factors in Eq. (133) may be neglected. The assumption  $\hat{d} \gg \hat{z}_1$  leads to the single requirement  $\bar{r}\Delta\hat{r}/\hat{z}_1 \ll 1$ . On the one hand,  $\bar{r}$  is limited by the presence of the pinhole, i.e. we must impose  $\bar{r} \lesssim \hat{a}$ . On the other hand,  $\Delta\hat{r}$  is limited by the coherence length at the pinhole, i.e.  $\Delta\hat{r} \lesssim \hat{z}_1/\sqrt{\hat{N}}$ , because otherwise the cross-spectral density  $\hat{G}$  in Eq. (133) drops to zero. As a result we obtain that the second condition given above can be expressed in mathematical terms by

$$\hat{a} \ll \sqrt{\hat{N}} . \quad (291)$$

It is possible to give a clear interpretation of condition (291) in terms of Geometrical Optics. In fact, on the one hand, the minimal geometrical spot size from a line source is given, at the image plane, by  $|M|\hat{a}$ . On the other hand, the size of the image is of order  $|M|\sqrt{\hat{N}}$ , by definition of magnification  $|M|$ . Then, in order to have a good resolution, we must require that the image size of a point source be much smaller than the image size of the object, i.e.  $\sqrt{\hat{N}}/\hat{a} \gg 1$ , that is condition (291).

The third condition given above requires that the pinhole size be larger than the coherence length on the pinhole plane, otherwise the pupil functions  $P$  in

Eq. (133) would modify the dependence of  $\hat{G}(\hat{z}_2)$  on  $\vec{r}$  (i.e. the image would be influenced by the pupil). This can be mathematically stated by requiring that

$$\hat{a} \gg \frac{\hat{z}_1}{\sqrt{\hat{N}}} . \quad (292)$$

Condition (292) has a natural explanation in terms of diffraction theory. In fact, the diffraction spot due to the presence of the pupil can be estimated as  $\hat{d}/\hat{a}$ . In order to have a good resolution, we should impose that the diffraction spot be much smaller than the image size of the object, i.e.  $|\mathbf{M}|\sqrt{\hat{N}}/(\hat{d}/\hat{a}) \gg 1$ , that is condition (292).

Finally, the first condition given above requires that the cross-spectral density at the pinhole position be Eq. (290), i.e. the pinhole must be in the far zone region. This fact can be alternatively stated by requiring that the radiation spot size at the pupil be dominated by the angular divergence  $\hat{D}$ , i.e.  $\hat{z}_1\sqrt{\hat{D}} \gg \sqrt{\hat{N}}$ . In the case  $\hat{N} < \hat{D}$ , one should require in any case that  $\hat{z}_1 \gg 1$ . This can be mathematically expressed by the requirement

$$\hat{z}_1 \gg \max \left[ \sqrt{\frac{\hat{N}}{\hat{D}}}, 1 \right] . \quad (293)$$

Note that condition (293) and the initial assumption of a quasi-homogeneous source are equivalent to the requirement that the pinhole be far enough for the van Cittert-Zernike theorem to apply. In the case of a perfectly incoherent object (e.g. thermal light), the source radiates over an angle  $2\pi$ . Then, the validity of the van Cittert-Zernike theorem (i.e. the requirement that the radiation spot size at the pupil be dominated by the angular divergence) is equivalent to the condition that the transverse dimension of the source be much smaller than the distance between the source and the pupil. This is the same condition for the paraxial approximation to be applicable. As a result, condition (293) is always considered satisfied in usual treatments describing pinhole setups in the presence of incoherent objects.

The three conditions (291), (292) and (293) can be summed up in the following:

$$\sqrt{\hat{N}} \gg \hat{a} \gg \frac{\hat{z}_1}{\sqrt{\hat{N}}} \gg \max \left[ \frac{1}{\sqrt{\hat{D}}}, \frac{1}{\sqrt{\hat{N}}} \right] . \quad (294)$$

Let us now discuss about the resolution of the pinhole camera. Consistency of

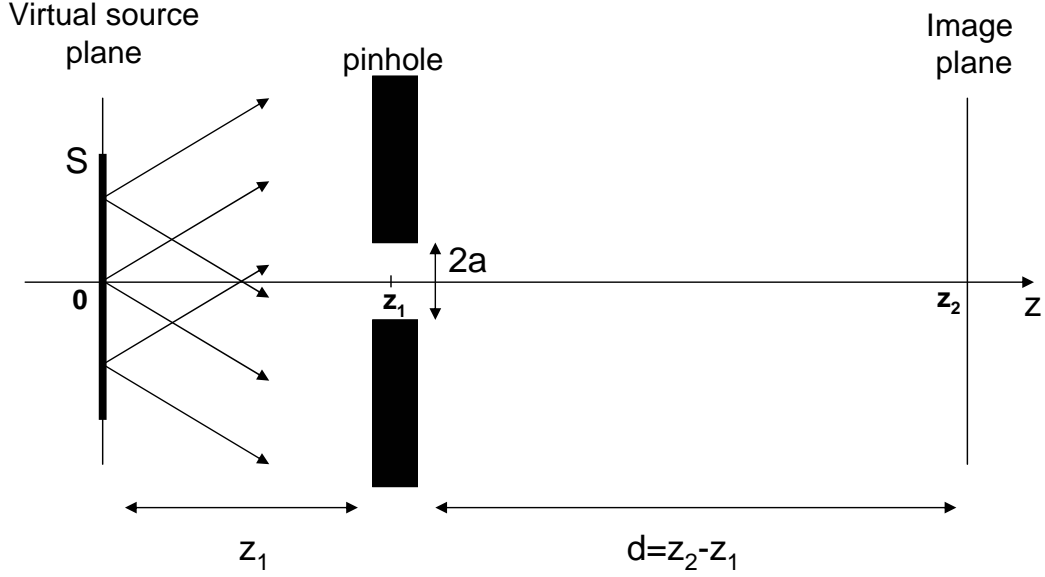


Fig. 36. Geometry for a pinhole camera setup. S indicates the virtual source plane. condition (294) requires that

$$\hat{N} \gg \hat{z}_1 . \quad (295)$$

Although condition (294) requires that condition (295) be satisfied, it does not pose any constraint on the relative magnitude of  $\hat{a}^2$  with respect to  $\hat{z}_1$ . This observation suggests the presence of another characteristic scale of the problem,  $\hat{a}^2/\hat{z}_1$ . This scale is linked with the resolution of the system. When  $\hat{a}^2/\hat{z}_1 \gg 1$  or  $\hat{a}^2/\hat{z}_1 \ll 1$  we are in the presence of an extra large or small parameter and, thus, we have two asymptotic regimes. In order to systematically consider this issue we start writing the expression for the intensity profile for the pinhole camera image with the help of Eq. (133) and Eq. (290), that is

$$\begin{aligned} \hat{I}(\hat{z}_2, \bar{r}) = \frac{1}{\mathcal{Z}} \int d\bar{r}' d\Delta\hat{r}' \left\{ \hat{\mathcal{G}}(0, -\bar{r}', -\Delta\hat{r}') \exp \left[ i \left( \frac{2}{\hat{z}_1} + \frac{2}{\hat{d}} \right) \bar{r}' \Delta\hat{r}' \right] \right. \\ \left. \times P(\bar{r}' + \Delta\hat{r}') P(\bar{r}' - \Delta\hat{r}') \right\} \exp \left[ -\frac{2i}{\hat{d}} \bar{r} \Delta\hat{r}' \right] . \end{aligned} \quad (296)$$

As usual, the normalization factor  $\mathcal{Z}$  is chosen in such a way that  $\hat{I}(\hat{z}_2, 0) = 1$ . The phase in parenthesis  $\{ \dots \}$  must be negligible under condition (291), and the influence of the pupil function  $P$  must also be negligible under condition (292). Here we retain both these factors, because we are interested in studying the resolution of the pinhole camera, i.e. the accuracy of our calculations.

The phase contribution in  $2/\hat{d}$  is always much smaller than the phase contri-

bution in  $2/\hat{z}_1$ , since we assumed  $|M| \gg 1$ . The integrand contributes to the integration results only for those values of  $\bar{r}'$  and  $\Delta\hat{r}'$  for which the phase factor is not much larger than unity, otherwise the integrand exhibits fast oscillatory behavior and it effectively averages to zero. As a result we may neglect, with some accuracy over the accuracy of the integral, the phase term in  $1/\hat{d}$ , that will start oscillating for higher values of  $\bar{r}'$  and  $\Delta\hat{r}'$ .

Note that, under the accepted assumptions  $\hat{N} \gg 1$  and  $\hat{D} \gg 1$ , the expression for the Fourier transform of the cross-spectral density at the virtual source position is given by

$$\hat{\mathcal{G}}(0, \bar{r}', \Delta\hat{r}') = \exp\left[-\frac{2\hat{N}\Delta\hat{r}'^2}{\hat{z}_1^2}\right] \exp\left[-\frac{\bar{r}'^2}{2\hat{z}_1^2\hat{D}}\right], \quad (297)$$

in agreement with Eq. (145).

Analysis of Eq. (297) shows that the exponential function in  $\bar{r}'$  exhibits a characteristic scale of order  $\hat{z}_1\sqrt{\hat{D}}$ . Conditions (291) and (293) require  $\hat{z}_1\sqrt{\hat{D}} \gg \sqrt{\hat{N}} \gg \hat{a}$ . As a result, since  $\hat{z}_1\sqrt{\hat{D}} \gg \hat{a}$ , we can approximate the exponential function in  $\bar{r}'$  in Eq. (297) with unity to obtain an equation still suitable for investigating the resolution of the pinhole camera, that is

$$\begin{aligned} \hat{I}(\hat{z}_2, \bar{r}) &= \frac{1}{\mathcal{Z}} \int_{-\infty}^{\infty} d\Delta\hat{r}' \exp\left[-\frac{2\hat{N}\Delta\hat{r}'^2}{\hat{z}_1^2}\right] \exp\left[-\frac{2i}{\hat{d}}\bar{r}\Delta\hat{r}'\right] \\ &\quad \times \left\{ \int_{-\infty}^{\infty} d\bar{r}' \exp\left[i\left(\frac{2}{\hat{z}_1}\right)\bar{r}'\Delta\hat{r}'\right] P(\bar{r}' + \Delta\hat{r}')P(\bar{r}' - \Delta\hat{r}') \right\}. \end{aligned} \quad (298)$$

The quantity in parenthesis  $\{...\}$  in Eq. (298) is the autocorrelation function of the pupil. It accounts for a phase error, exactly as in the case of aberrations of the second order (defocus). Condition (292) states that the characteristic scale of  $\Delta\hat{r}'$  in Eq. (297) is small compared to  $\hat{a}$ , that is the characteristic scale of the pupil function  $P$ . If also  $\hat{a}^2/\hat{z}_1 \gg 1$  we see that the characteristic scale of  $P$  is large compared with the scale imposed by the phase in parenthesis  $\{...\}$  in Eq. (298), because  $\bar{r}'\Delta\hat{r}'/\hat{z}_1 \gg 1$  at  $\Delta\hat{r}' \sim \hat{a}$  and  $\bar{r}' \sim \hat{a}$ . Therefore, under the assumption  $\hat{a}^2/\hat{z}_1 \gg 1$  we may neglect the dependence of  $P$  on  $\Delta\hat{r}'$  in Eq. (298) and obtain

$$\hat{I}(\hat{z}_2, \bar{r}) = \frac{1}{\mathcal{Z}} \int_{-\infty}^{\infty} d\Delta\hat{r}' \tilde{P}(\Delta\hat{r}') \exp\left[-\frac{2\hat{N}\Delta\hat{r}'^2}{\hat{z}_1^2}\right] \exp\left[-\frac{2i}{\hat{d}}\bar{r}\Delta\hat{r}'\right], \quad (299)$$

where

$$\tilde{P}(\Delta\hat{r}') = \int_{-\infty}^{\infty} d\bar{r}' |P(\bar{r}')|^2 \exp \left[ i \frac{2}{\hat{z}_1} \bar{r}' \Delta\hat{r}' \right] , \quad (300)$$

or, equivalently<sup>22</sup> :

$$\tilde{P}(\Delta\hat{r}') = \int_{-\hat{a}}^{\hat{a}} d\bar{r}' \exp \left[ i \frac{2}{\hat{z}_1} \bar{r}' \Delta\hat{r}' \right] . \quad (301)$$

Except for an unessential multiplicative factor  $\hat{a}$ , Eq. (301) is formally equivalent<sup>23</sup> to Eq. (275) with  $n = 2$  and

$$b_2 = \frac{\hat{a}^2}{2\hat{z}_1} \gg 1 . \quad (302)$$

This means that we may study the problem of the resolution of the pinhole camera as an aberration problem: in particular, a defocusing aberration. The parameter range when  $\hat{a}^2/\hat{z}_1 \gg 1$  leads to equations similar to the case of severe aberrations when  $|b_n| \gg 1$ , treated in Section 9.2. The autocorrelation function of the pupil, that is the Optical Transfer Function of the system, is then obtained by integration of Eq. (301) and reads:

$$\tilde{P}(\Delta\hat{r}') = \text{sinc} \left( \frac{2\hat{a}}{\hat{z}_1} \Delta\hat{r}' \right) , \quad (303)$$

where Eq. (301) has been used and an unessential multiplicative factor  $2\hat{a}$  has been neglected. Substitution of Eq. (303) in Eq. (299) yields

$$\hat{I}(\hat{z}_2, \bar{r}) = \frac{1}{\mathcal{Z}} \int_{-\infty}^{\infty} d\Delta\hat{r}' \text{sinc} \left( \frac{2\hat{a}}{\hat{z}_1} \Delta\hat{r}' \right) \exp \left[ -\frac{2\hat{N}\Delta\hat{r}'^2}{\hat{z}_1^2} \right] \exp \left[ -\frac{2i}{\hat{d}} \bar{r} \Delta\hat{r}' \right] . \quad (304)$$

Eq. (304) allows an estimation of the resolution by taking the ratio of the width of the sinc and of the exponential function in  $\Delta\hat{r}'$ . On the one hand,

<sup>22</sup> We assume, as done before, that no apodization is present.

<sup>23</sup> It should be noted that we switched back from notations  $\bar{x}$  and  $\Delta x$ , used in Section 9, to our usual notation  $\bar{r}'$  and  $\Delta\hat{r}'$ , with  $\bar{r}' = \bar{x}$  and  $2\Delta\hat{r}' = \hat{a}\Delta x$ . We remind that the reason why we used notations  $\bar{x}$  and  $\Delta x$  in Section 9 was for the reader's convenience, as these notations allow direct comparison with aberration theory developed in standard textbooks.

the width of the exponential function is of order  $\hat{z}_1/(2\sqrt{\hat{N}})$ . On the other hand, the width of the sinc function is of order  $\hat{z}_1/(2\hat{a})$ . As a result, when  $\hat{a}^2/\hat{z}_1 \gg 1$  the resolution of the camera is of order  $\hat{a}/\sqrt{\hat{N}}$ . This procedure is justified by the fact that Eq. (304) can be interpreted as a convolution of a rectangular profile with a (new) Gaussian function, and that the width of these two functions can be obtained by taking the inverse widths of the sinc function and the Gaussian function in Eq. (296) and by multiplying them by the factor  $\hat{d}$ .

Let us now deal with the case when  $\hat{a}^2/\hat{z}_1 \ll 1$ . Going back to Eq. (298), we see that  $\hat{a}$  is narrow compared with the scale imposed by the phase in parenthesis  $\{\dots\}$  in Eq. (298), because  $\bar{r}'\Delta\hat{r}'/\hat{z}_1 \ll 1$  at  $\Delta\hat{r}' \sim \hat{a}$  and  $\bar{r}' \sim \hat{a}$ . Therefore we can neglect the phase factor in parenthesis  $\{\dots\}$ , which corresponds to a case with no aberrations. The autocorrelation function of the pupil can now be written as a triangle function

$$\tilde{P}(\Delta\hat{r}') = \text{tri}\left(\frac{\Delta\hat{r}'}{\hat{a}}\right), \quad (305)$$

that should be substituted into Eq. (299) to give the analogous of Eq. (304) in the limit  $\hat{a}^2/\hat{z}_1 \ll 1$ , that is

$$\hat{I}(\hat{z}_2, \bar{r}) = \frac{1}{\mathcal{Z}} \int_{-\infty}^{\infty} d\Delta\hat{r}' \text{tri}\left(\frac{\Delta\hat{r}'}{\hat{a}}\right) \exp\left[-\frac{2\hat{N}\Delta\hat{r}'^2}{\hat{z}_1^2}\right] \exp\left[-\frac{2i}{\hat{d}}\bar{r}\Delta\hat{r}'\right]. \quad (306)$$

Eq. (306) can also be interpreted as a convolution of a  $\text{sinc}^2(\cdot)$  profile with a Gaussian profile.

Similarly to Eq. (304), Eq. (306) allows an estimation of the resolution by taking the ratio of the width of the triangular function and of the exponential function in  $\Delta\hat{r}'$ . As before, on the one hand the width of the exponential function is of order  $\hat{z}_1/(2\sqrt{\hat{N}})$ . On the other hand, the width of the triangular function is of order  $2\hat{a}$ . As a result, when  $\hat{a}^2/\hat{z}_1 \ll 1$  the resolution of the camera is of order  $\hat{z}_1/(\hat{a}\sqrt{\hat{N}})$ .

When  $\hat{a}^2/\hat{z}_1 \gg 1$  the resolution of the camera is of order  $\hat{a}/\sqrt{\hat{N}}$ . One has better resolution as the pupil becomes smaller and smaller, but the condition  $\hat{a}^2/\hat{z}_1 \gg 1$  becomes less and less satisfied. When  $\hat{a}^2/\hat{z}_1 \ll 1$  the resolution of the camera is of order  $\hat{z}_1/(\hat{a}\sqrt{\hat{N}})$ . In this case one has better resolution as the pupil becomes larger and larger, but the condition  $\hat{a}^2/\hat{z}_1 \ll 1$  becomes less and less satisfied. As a result there must be an optimum for pupil apertures of order

$\hat{a}^2 \sim \hat{z}_1$ . This optimum depends on the object considered (in this discussion, for instance, we assumed a Gaussian source) and on the definition of the width of a function, that may vary depending on circumstances. However, starting from Eq. (298), we may present an expression for the Optical Transfer Function of the pinhole camera, which is the quantity in parenthesis {...}. Such quantity can be written as

$$\tilde{P}_{\text{pc}}(\Delta\hat{r}', \hat{a}, \hat{z}_1) = \int_{-\hat{a}}^{\hat{a}} d\bar{r}' P(\bar{r}' + \Delta\hat{r}') P(\bar{r}' - \Delta\hat{r}') \exp \left[ i2 \frac{\bar{r}' \Delta\hat{r}'}{\hat{z}_1} \right]. \quad (307)$$

After introduction of  $\xi = \bar{r}'/\hat{a}$  and  $\Omega = \hat{a}^2/\hat{z}_1$  we can write Eq. (307) as

$$\tilde{P}_{\text{pc}} \left( \frac{\Delta\hat{r}'}{\hat{a}}, \Omega \right) = \int_{-1}^1 d\xi P \left( \xi + \frac{\Delta\hat{r}'}{\hat{a}} \right) P \left( \xi - \frac{\Delta\hat{r}'}{\hat{a}} \right) \exp \left[ i2\xi\Omega \frac{\Delta\hat{r}'}{\hat{a}} \right]. \quad (308)$$

Note that the limit  $\Omega \rightarrow \infty$  of Eq. (308) is a sinc( $\cdot$ ) function, while the limit  $\Omega \rightarrow 0$  is a tri( $\cdot$ ) function, as it should be. Eq. (308) enters in the expression for the intensity as the term in {...} in Eq. (298), that can be reinterpreted as a convolution product. Then, the Fourier transform of Eq. (308) with respect to  $\Delta\hat{r}'/\hat{a}$  is one of the factors in this convolution product, and its width is related with the resolution of the pinhole camera. This Fourier transform is the line spread function for the pinhole camera. After introduction of  $y = \hat{a}\bar{r}_i/\hat{d}$  and  $\eta = \Delta\hat{r}'/\hat{a}$  we can write the line spread function for the pinhole camera as

$$l_{\text{pc}}(\Omega, y) = \int_{-1}^1 d\xi \left\{ \int_{-1}^1 d\eta P(\xi + \eta) P(\xi - \eta) \exp [i2\eta(\xi\Omega - y)] \right\}, \quad (309)$$

where we accounted for the fact that the Fourier transform integral in  $d\xi$  is limited by the presence of the pinhole to the range  $[-1, 1]$ . On the one hand, the integral in parenthesis {...} in Eq. (309) is the Fourier transform of  $P(\xi + \eta)P(\xi - \eta)$  calculated with respect to  $\eta$  as a function of  $2(\xi\Omega + y)$ . On the other hand, the function  $P(\xi + \eta)P(\xi - \eta)$  is a window function similar to the pupil function  $P$ . It is equal to unity for values of  $|\eta| < 1 - |\xi|$ , and it is zero elsewhere. Therefore, the quantity in parenthesis {...} in Eq. (309) can be calculated analytically yielding

$$l_{\text{pc}}(\Omega, y) = \int_{-1}^1 d\xi \frac{\sin [2(\xi\Omega + y)(1 - |\xi|)]}{\xi\Omega + y}. \quad (310)$$

Note that if  $\Omega \rightarrow 0$  we have

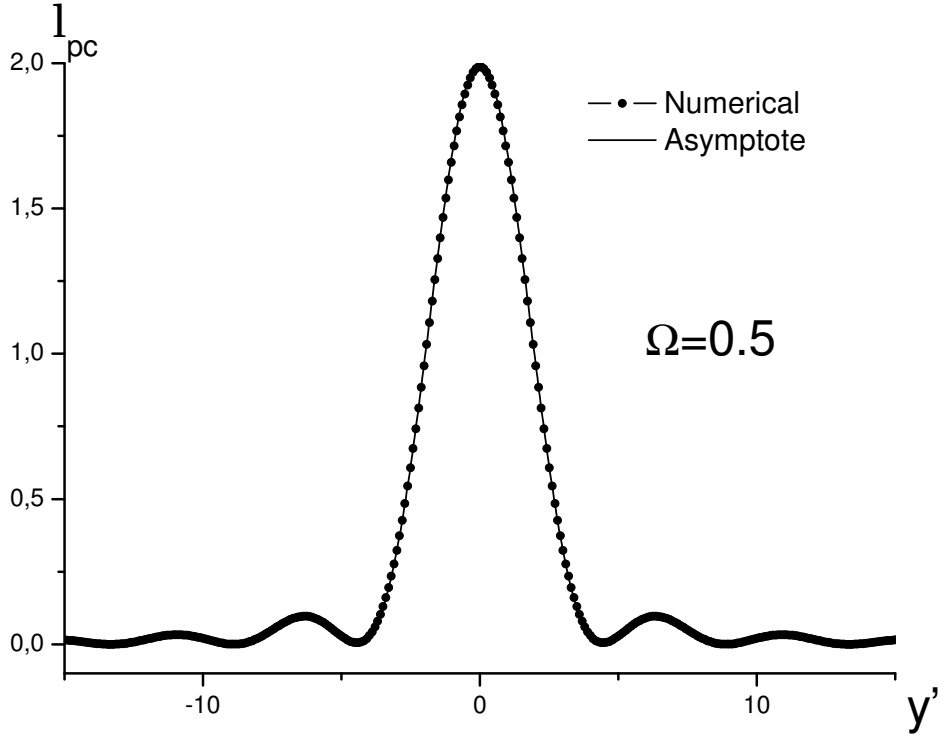


Fig. 37. The line spread function  $l_{\text{pc}}$  with  $\Omega = 0.5$ . In this case the asymptote for  $\Omega \rightarrow 0$ , Eq. (311), is well-matched to the numerical evaluations.

$$l_{\text{pc}}(\Omega, y) \rightarrow \frac{1}{y} \int_{-1}^1 d\xi \sin[2y(1 - |\xi|)] = 2\text{sinc}^2(y) , \quad (311)$$

as it should be, while if  $\Omega \rightarrow \infty$ , after the change of variable  $\xi \rightarrow \xi' = \Omega\xi$  we can rewrite Eq. (310) as

$$\begin{aligned} l_{\text{pc}}(\Omega, y) &\rightarrow \frac{1}{\Omega} \int_{-\Omega}^{\Omega} d\xi' \frac{\sin[2(\xi' + y)]}{\xi' + y} = \frac{1}{\Omega} \text{Si}[2(y + \xi)] \Big|_{-\Omega}^{\Omega} \\ &= \frac{1}{\Omega} \{ \text{Si}[2(y + \Omega)] - \text{Si}[2(y - \Omega)] \} , \end{aligned} \quad (312)$$

where  $\text{Si}(\cdot)$  indicates the sin integral function. It can be seen that, as  $\Omega \rightarrow \infty$ , the function defined by Eq. (312) approximates more and more a rectangular function which is constant for  $-\Omega < y < \Omega$  and equal to zero elsewhere, as it should be.

We may use a new variable  $y' = y/\sqrt{\Omega}$  in Eq. (310), thus obtaining:

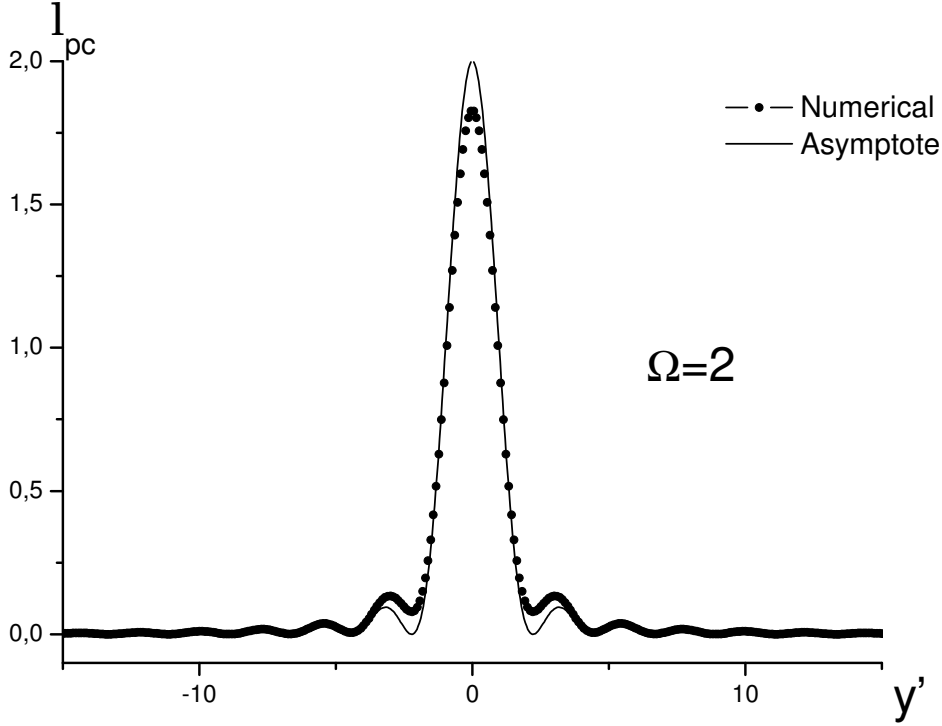


Fig. 38. The line spread function  $l_{\text{pc}}$  with  $\Omega = 2$ . In this case the asymptote for  $\Omega \rightarrow 0$ , Eq. (311), starts to diverge from numerical evaluations. The width of  $l_{\text{pc}}$  is close to its minimum.

$$l_{\text{pc}}(\Omega, y') = \int_{-1}^1 d\xi \frac{\sin [2(\xi\Omega + y'\sqrt{\Omega})(1 - |\xi|)]}{\xi\Omega + y'\sqrt{\Omega}} . \quad (313)$$

The reason for this is that, now, both the asymptotes Eq. (311) for  $\Omega \ll 1$  and Eq. (312) for  $\Omega \gg 1$  present a characteristic width  $1/\sqrt{\Omega}$  and  $\sqrt{\Omega}$  respectively. In Fig. 37, Fig. 38, Fig. 39 and Fig. 40 we present various shapes of the  $l_{\text{pc}}$  function and its asymptotic limit for different values of  $\Omega$ . Once a definition of the width of the function  $l_{\text{pc}}$  is chosen, the optimal operation point for the pinhole camera may be set requiring that the width of  $l_{\text{pc}}$  be minimal. It should be remarked that the definition of the width of  $l_{\text{pc}}$  is somewhat subjective.

One may, for instance, define the width of  $l_{\text{pc}}$  to be the Full Width Half Maximum (FWHM). In Fig. 41 we present different plots for  $l_{\text{pc}}$  normalized to  $l_{\text{pc}}(0)$  for different values of  $\Omega = 1, 2, 3, 4, 5, 6$ . The minimal value of the FWHM of the line spread function for the pinhole camera happens to be located somewhere between  $\Omega = 4$  and  $\Omega = 5$ . It may be estimated to be about 1.5. As a result one concludes that the optimal aperture for the pinhole

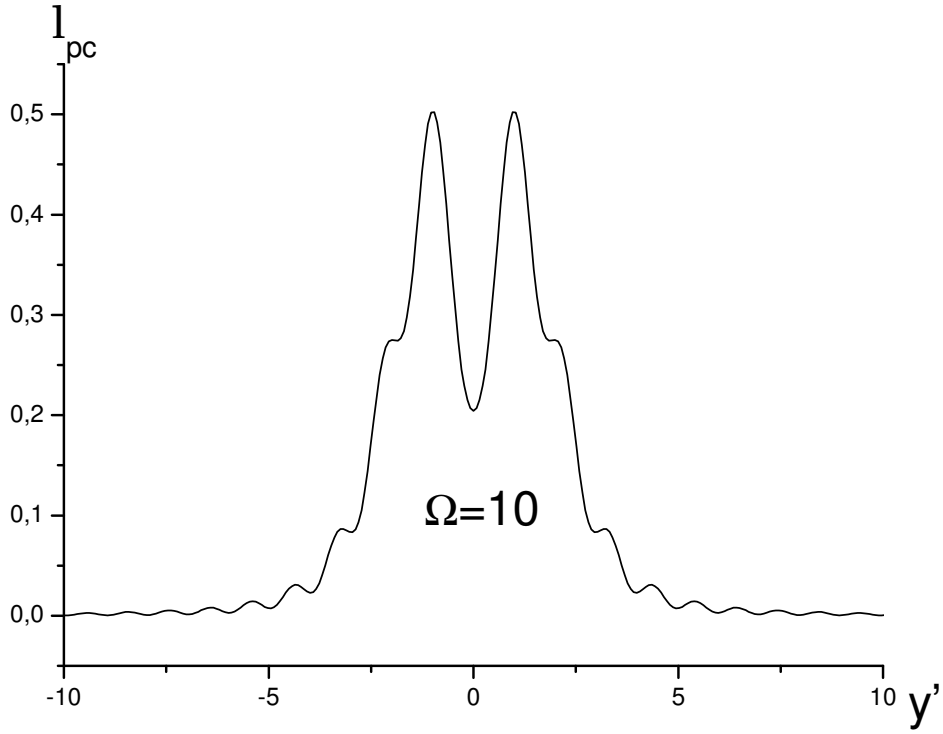


Fig. 39. The line spread function  $l_{\text{pc}}$  with  $\Omega = 10$ . An intermediate situation between the two limits for  $\Omega \rightarrow 0$  and  $\Omega \rightarrow \infty$ .

is given by

$$\hat{a}^2 \simeq 4.5 \hat{z}_1 \quad (314)$$

or, in dimensional units,

$$a^2 \simeq 4.5 \frac{z_1 c}{\omega} . \quad (315)$$

We can estimate the resolution  $\delta r$  of the pinhole camera in dimensional units imposing  $\delta y'$  to be equal to the FWHM of the line spread function, i.e. 1.5, and taking advantage of the definition of  $y'$ . Therefore we obtain

$$\delta r \simeq 1.5 \sqrt{\frac{c}{\omega z_1}} d . \quad (316)$$

Results in this Section have been obtained under the assumption  $|M| \gg 1$ . A

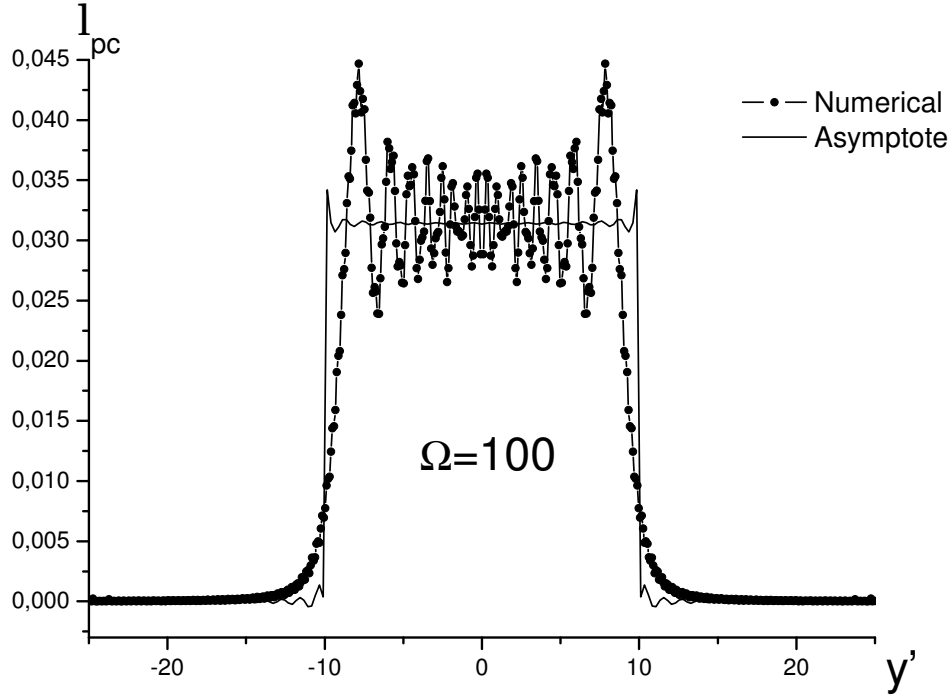


Fig. 40. The line spread function  $l_{pc}$  with  $\Omega = 100$ . The asymptote in Eq. (312) starts to match the numerical calculations. In the limit  $\Omega \rightarrow \infty$  they both merge to a rectangular function.

generalization can be presented introducing

$$\hat{z}_{\text{eff}} = \frac{\hat{z}_1 \hat{d}}{\hat{z}_1 + \hat{d}} \quad (317)$$

and the analogous dimensional value  $z_{\text{eff}} = \hat{z}_{\text{eff}} L_w$  to be used in place of  $\hat{z}_1$  and  $z_1$  in Eq. (314), Eq. (315) and Eq. (316). In dimensional units we have

$$a^2 \simeq 4.5 \frac{z_{\text{eff}} c}{\omega} \quad (318)$$

and

$$\delta r \simeq 1.5 \sqrt{\frac{c}{\omega z_{\text{eff}}}} d. \quad (319)$$

Before proceeding we should discuss about the applicability of Eq. (313). Up to now, in fact, we discussed about a Gaussian quasi-homogeneous undulator source ( $\hat{N} \gg 1$  and  $\hat{D} \gg 1$ ). Eq. (313) can be applied in a wider variety of

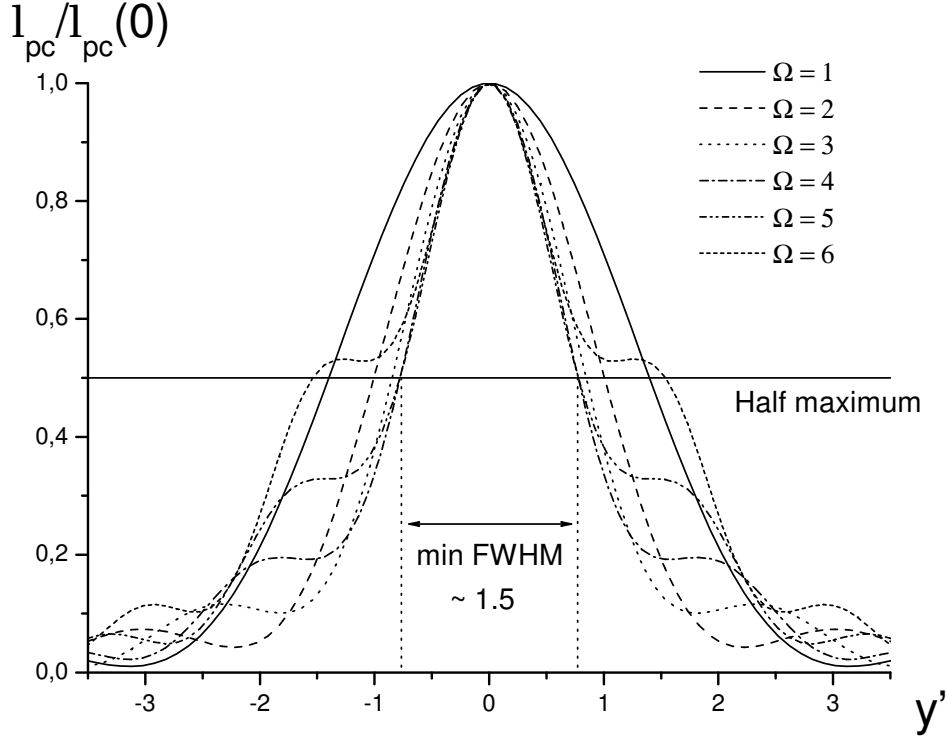


Fig. 41. Relative line spread function  $l_{pc}/l_{pc}(0)$  for different values of  $\Omega$ .

cases. In particular, Eq. (313) can be applied when (a) the virtual source is quasi-homogeneous, (b) the pinhole camera is installed in the far zone and (c)  $\hat{a}^2 \ll \max[1, \hat{D}] \hat{z}_1^2$ . When conditions (a), (b) and (c) are satisfied, the line spread function for the pinhole camera,  $l_{pc}$  can be calculated from Eq. (313). At the beginning of the present Section 10 we stated three conditions in order to have an image of the source, besides the Gaussian quasi-homogeneous assumption (that we relaxed, here, to the more general case (a)). Condition 1. given at the beginning of the present Section 10 can be identified with (b). Condition 1. and 2., together, are responsible for (c). The other requirement was formulated in order to obtain a good quality image of the source. However  $l_{pc}$  can be calculated regardless of it and, in different situations, one may have a good quality or a bad quality of the image, depending on how the width of  $l_{pc}$  scales with the width of the ideal image. The intensity profile at the observation plane located at  $\hat{z} = \hat{z}_2$  is given, in any case, by the convolution product between the line spread function  $l_{pc}$  and the ideal image. In particular, for an undulator source with Gaussian intensity profile at the virtual plane such a product is given by  $l_{pc} * \exp[-\bar{r}^2/(2M^2\hat{N})]$ , where  $|M| = \hat{d}/\hat{z}_1$ . When  $\sqrt{\hat{N}} \gg \hat{a} \gg \hat{z}_1/\sqrt{\hat{N}}$  a good quality image is formed at the observation plane. In other situations instead, the width of  $l_{pc}$  is of order of, or even larger than,

the width of the ideal image, and a bad quality image will be formed. To sum up, in order to calculate the intensity distribution at the observation plane located at position  $\hat{z} = \hat{z}_2$  behind the pinhole, we should first calculate  $\Omega = \hat{a}^2/\hat{z}_{\text{eff}}$ . Then use Eq. (313) to calculate the line spread function  $l_{\text{pc}}$ . Finally, convolve with the ideal image from the source. The minimal width of the line spread function, which correspond to the best accuracy for the image, is for  $\hat{a}^2/\hat{z}_{\text{eff}} \simeq 4.5$ . Note that conditions (a), (b) and (c) above do not require the source to be an undulator source. In particular, (a), (b) and (c) are automatically satisfied for thermal sources, or perfectly incoherent objects. As a result, our theory can be applied for visible light imaging as well.

These remarks simplify our discussion and drastically widen the applicability region of our results. In particular they can describe bending magnet sources. For instance, at ESRF (European Synchrotron Radiation Facility) a pinhole camera setup has been developed for electron beam diagnostics [22]. Synchrotron Radiation from a bending magnet is imaged through an X-ray pinhole camera setup. Subsequent analysis of the pinhole camera image allows one to retrieve the electron beam sizes. In the situation studied in [22] the diffraction angle is of order of  $\gamma^{-1} \sim 10^{-4}$  rad. The system is reported to generate an image of the source when the pinhole is moved at about  $z_1 = 23$  m from the dipole magnet. At this distance, and at the critical wavelength, the spot size due to divergence of the single particle radiation is estimated to be about  $\gamma^{-1}z_1 \simeq 2\text{mm} \gg \sigma_{x,y}$ ,  $\sigma_{x,y}$  being the transverse electron beam sizes. This guarantees that the pinhole is in the far field, i.e. condition (b) is satisfied. The critical wavelength is of order  $\lambda \simeq 3 \cdot 10^{-11}$  m, since one may read, in [22], that "the contribution from diffraction assumes a typical photon energy of 40 keV". The radiation diffraction size can be estimated to be of order  $\lambda\gamma/(2\pi) \simeq 10^{-1}\mu\text{m} \ll \sigma_{x,y}$ , which demonstrates the quasi-homogeneity of the source, i.e. condition (a). In reference [22] one can also find  $d_i = 11.5$  m. We obtain an optimal pinhole aperture of  $a \simeq 12\mu\text{m}$ . Since the pinhole aperture is much smaller than the spot size due to divergence of the single particle radiation, condition (c) is satisfied as well. As a result our theory can be applied to the situation treated in [22]. Our results should be compared with the actual choice in [22]. From Fig. 2 in that reference we can conclude that  $2a \simeq 50\mu\text{m}$  in the horizontal direction. This choice is not optimal, since corresponds to the value  $\Omega \sim 10$ . The line spread function for the pinhole camera in the horizontal direction is illustrated, in this case, in Fig. 39. Estimation of the resolution is not easy because, as already said, is related to the definition of the width of  $l_{\text{pc}}$ , which is quite subjective in the particular case depicted in Fig. 39. However, knowing the profile of the line spread function, we may use it in order to deconvolve experimental results and extract the electron beam size. From the same Fig. 2 in [22] we can also conclude that  $2a \simeq 25\mu\text{m}$  in the vertical direction. Although the definition of the width of  $l_{\text{pc}}$  is somewhat subjective, we can conclude that the choice made in [22] is near the optimal value in the vertical direction. The resolution in the vertical

direction turns out to be, from Eq. (319),  $\delta r \simeq 14\mu\text{m}$ . As a result the resolution in [22], that is about  $26\mu\text{m}$ , is somewhat underestimated. It should be clear from the previous discussion that decreasing the pinhole dimension beyond the optimal size not only will decrease the photon flux, but will also worsen the camera resolution.

## 11 Imaging in the focal plane

In this Section we will investigate the intensity distribution on the focal plane due to a quasi-homogeneous source. We will first consider the case of a Gaussian quasi-homogeneous source ( $\hat{N} \gg 1$ ,  $\hat{D} \gg 1$ ) and subsequently generalize our conclusions, as done before for the more comprehensive case of generic quasi-homogeneous sources. The characteristics of the intensity distribution in the focal plane can be treated in formal analogy with the pinhole camera setup treated in Section 10 and with the physics of aberrations, in particular defocusing aberrations, described in Section 9. This may seem counterintuitive, since, at first glance, we are treating completely different systems from a physical viewpoint. The formal analogy between these situations is a demonstration of the power of the combined Statistical and Fourier Optics approach, which allows one to unify study cases otherwise completely distinct. Such unification can be seen from the expression for the cross-spectral density at any distance from the source in the presence of a pupil, Eq. (133). As usual, we will assume that the lens is in the far field, i.e.  $\hat{D}\hat{z}_1^2 \gg \hat{N}$ . Under this assumption we may use Eq. (127) to characterize the cross-spectral density at the lens position. In the image plane, the far field assumption allows cancellation of all phase factors in the integrand of Eq. (133) and leads to Eq. (226). This cancellation does not hold anymore for the focal plane. Use of the focal plane condition  $\hat{f} = \hat{z}_2 - \hat{z}_1$  and of Eq. (127) yields the intensity ( $\Delta\hat{r}_f = 0$ )

$$\begin{aligned} \hat{I}(\hat{z}_2, \bar{r}_f) = \frac{1}{\mathcal{Z}} \int d\bar{r}' d\Delta\hat{r}' \left\{ \hat{\mathcal{G}}(0, -\bar{r}', -\Delta\hat{r}') \exp \left[ i \frac{2}{\hat{z}_1} \bar{r}' \Delta\hat{r}' \right] \right. \\ \left. \times P(\bar{r}' + \Delta\hat{r}') P(\bar{r}' - \Delta\hat{r}') \right\} \exp \left[ -\frac{2i}{\hat{f}} \bar{r}_f \Delta\hat{r}' \right]. \end{aligned} \quad (320)$$

As one can see, the phase factor in the expression for the cross-spectral density, Eq. (127), survived in Eq. (320) due to the choice of the focal plane as the observation plane. From a formal viewpoint Eq. (320) is identical to Eq. (296). In fact, as the reader will remember, the phase  $\bar{r}'\Delta\hat{r}'/\hat{d}_i$  in Eq. (296) is negligible for  $|M| \gg 1$  and can be retained without change in the formalism in the case  $|M|$  is not much larger than unity by defining  $\hat{z}_{\text{eff}}$  according to Eq. (317). As before, the normalization factor  $\mathcal{Z}$  is chosen in such a way that  $\hat{I}(\hat{z}_2, 0) = 1$ .

Under the (for now) accepted assumptions  $\hat{N} \gg 1$  and  $\hat{D} \gg 1$ , the expression for the Fourier transform of the cross-spectral density at the virtual source position is given by Eq.(297). Substitution of Eq. (297) in Eq. (320) yields

$$\begin{aligned} \hat{I}(\hat{z}_f, \bar{r}_f) &= \frac{1}{\mathcal{Z}} \int_{-\infty}^{\infty} d\Delta\hat{r}' \exp \left[ -\frac{2\hat{N}\Delta\hat{r}'^2}{\hat{z}_1^2} \right] \exp \left[ -\frac{2i}{\hat{f}} \bar{r}_f \Delta\hat{r}' \right] \\ &\times \left\{ \int_{-\infty}^{\infty} d\bar{r}' \exp \left[ i\frac{2}{\hat{z}_1} \bar{r}' \Delta\hat{r}' \right] P(\bar{r}' + \Delta\hat{r}') P(\bar{r}' - \Delta\hat{r}') \right. \\ &\times \left. \exp \left[ -\frac{\bar{r}'^2}{2\hat{z}_1^2 \hat{D}} \right] \right\}. \end{aligned} \quad (321)$$

Note that when the pupil influence is negligible (that is the case when  $\hat{a}^2 \gg \hat{D}\hat{z}_1^2 \gg \hat{z}_1^2/\hat{N}$ ), Eq. (321) reads

$$\begin{aligned} \hat{I}(\hat{z}_f, \bar{r}_f) &= \frac{1}{\mathcal{Z}} \int_{-\infty}^{\infty} d\Delta\hat{r}' \exp \left[ -\frac{2i}{\hat{f}} \bar{r}_f \Delta\hat{r}' \right] \\ &\times \left\{ \int_{-\infty}^{\infty} d\bar{r}' \exp \left[ i\frac{2}{\hat{z}_1} \bar{r}' \Delta\hat{r}' \right] \exp \left[ -\frac{2\hat{N}\Delta\hat{r}'^2}{\hat{z}_1^2} \right] \exp \left[ -\frac{\bar{r}'^2}{2\hat{z}_1^2 \hat{D}} \right] \right\}. \end{aligned} \quad (322)$$

The reader may check that evaluation of Eq. (322) gives back Eq. (190), as it should be. For large non-limiting apertures, the extra phase imposes an extra Fourier transformation of the integrand, which gives the usual result. The intensity in the focal plane is a scaled version of the Fourier transform of the spectral degree of coherence on the virtual source plane. Yet, there are situations when one may recover an image of the virtual source at the focal plane. This happens when parameters are such that the only influence of a final pupil aperture is to make the phase factor in parenthesis  $\{..\}$  in Eq. (321) negligible. Looking for a region in parameter space where this situation is realized is equivalent to what has been done in Section 10. Three conditions were given such that the phase factor in  $\bar{r}'\Delta\hat{r}'$  in Eq. (296) could be neglected. In that case, for a pinhole camera, we had image formation at all positions after the pinhole.

In particular, when  $\hat{D}\hat{z}_1^2 \gg \hat{N} \gg \hat{a}^2 \gg \hat{z}_1^2/\hat{N}$  not only we can neglect the phase factor in Eq. (321) but we can also see that the width of the exponential function in  $\Delta\hat{r}'$  is much narrower than that of the pupil function  $P$ . Therefore, the dependence on  $\Delta\hat{r}'$  in  $P$  can be neglected. Moreover, the width of  $P$  in  $\bar{r}'$  is much narrower than the width of the exponential function in  $\bar{r}'$ , so that the latter can be neglected as well. As a result we simplify Eq. (321) to obtain

$$\hat{I}(\hat{z}_f, \bar{r}_f) = \frac{1}{\mathcal{Z}} \int d\bar{r}' d\Delta \hat{r}' \exp \left[ -\frac{2\hat{N}\Delta \hat{r}'^2}{\hat{z}_1^2} \right] |P(\bar{r}')|^2 \exp \left[ -\frac{2i}{\hat{f}} \bar{r}_f \Delta \hat{r}' \right]. \quad (323)$$

The integral in  $d\bar{r}'$  yields an unessential multiplication constant to be included in  $\mathcal{Z}$ , and one is left with

$$\hat{I}(\hat{z}_f, \bar{r}_f) = \frac{1}{\mathcal{Z}} \int_{-\infty}^{\infty} d\Delta \hat{r}' \exp \left[ -\frac{2\hat{N}\Delta \hat{r}'^2}{\hat{z}_1^2} \right] \exp \left[ -\frac{2i}{\hat{f}} \bar{r}_f \Delta \hat{r}' \right]. \quad (324)$$

Including another unessential constant in the normalization factor  $\mathcal{Z}$ , Eq. (324) can be written as

$$\hat{I}(\hat{z}_f, \bar{r}_f) = \frac{1}{\mathcal{Z}} \exp \left[ -\frac{\hat{z}_1^2 \bar{r}_f^2}{2\hat{f}^2 \hat{N}} \right]. \quad (325)$$

As a result, when  $\hat{D}\hat{z}_1^2 \gg \hat{N} \gg \hat{a}^2 \gg \hat{z}_1^2/\hat{N}$ , we obtain, in the focal plane, a scaled image of the virtual source. This is exactly what a pinhole camera does in the parameter region when conditions 1. to 3. in Section 10 are satisfied. A correspondence between completely different problems has thus been established thanks to the combined power of Statistical Optics and Fourier Optics approach.

Such a correspondence can be pursued further, up to a complete formal identification between the pinhole camera and the focal imaging system. To this purpose we restrict our analysis to the case  $\hat{a}^2 \ll \hat{D}\hat{z}_1^2$ . In the opposite limit we would obtain the already treated result for negligible pupil influence. In this situation we can neglect the exponential function in  $\bar{r}'^2$  in Eq. (321). Eq. (321) can thus be simplified to

$$\begin{aligned} \hat{I}(\hat{z}_f, \bar{r}_f) &= \frac{1}{\mathcal{Z}} \int_{-\infty}^{\infty} d\Delta \hat{r}' \exp \left[ -\frac{2\hat{N}\Delta \hat{r}'^2}{\hat{z}_1^2} \right] \exp \left[ -\frac{2i}{\hat{f}} \bar{r}_f \Delta \hat{r}' \right] \\ &\times \left\{ \int_{-\infty}^{\infty} d\bar{r}' \exp \left[ i\frac{2}{\hat{z}_1} \bar{r}' \Delta \hat{r}' \right] P(\bar{r}' + \Delta \hat{r}') P(\bar{r}' - \Delta \hat{r}') \right\}. \quad (326) \end{aligned}$$

Once the substitutions  $\hat{f} \rightarrow \hat{d}$ ,  $\hat{z}_f \rightarrow \hat{z}_2$  and  $\bar{r}_f \rightarrow \bar{r}$  are made, Eq. (326) is identical to Eq. (298). This means that, in the limit  $\hat{a}^2 \ll \hat{D}\hat{z}_1^2$  studying the pinhole camera setup is completely equivalent to studying the focal imaging setup. As in Eq. (298), the quantity in parenthesis {...} constitutes an Optical Transfer Function, and its Fourier transform yields a line spread function for the system. Note that in the intermediate region for  $\hat{a}^2 \sim \hat{D}\hat{z}_1^2$  one may retain the same formalism: in this case though, the exponential function in  $\bar{r}'^2$  in Eq.

(321) cannot be neglected and results would be different, depending also on the source parameter  $\hat{D}_y$  which introduces a factor formally identical to lens apodization.

However, in the case  $\hat{a}^2 \ll \hat{D}\hat{z}_1^2$ , we can proceed in perfect parallelism with the study of the pinhole camera setup in the previous Section 10. Starting from Eq. (326), we may present an expression for the Optical Transfer Function of the pinhole camera, which is the quantity in parenthesis {...}. This quantity can be written as

$$\tilde{P}_{\text{fp}}(\Delta\hat{r}', \hat{a}, \hat{z}_1) = \int_{-\hat{a}}^{\hat{a}} d\bar{r}' P(\bar{r}' + \Delta\hat{r}') P(\bar{r}' - \Delta\hat{r}') \exp \left[ i2 \frac{\bar{r}' \Delta\hat{r}'}{\hat{z}_1} \right]. \quad (327)$$

After introduction of  $\xi = \bar{r}'/\hat{a}$  and  $\Omega = \hat{a}^2/\hat{z}_1$  we can write Eq. (327) as

$$\tilde{P}_{\text{fp}} \left( \frac{\Delta\hat{r}'}{\hat{a}}, \Omega \right) = \int_{-1}^1 d\xi P \left( \xi + \frac{\Delta\hat{r}'}{\hat{a}} \right) P \left( \xi - \frac{\Delta\hat{r}'}{\hat{a}} \right) \exp \left[ i2\xi\Omega \frac{\Delta\hat{r}'}{\hat{a}} \right]. \quad (328)$$

Similarly as before, the Fourier transform of Eq. (328) with respect to  $\Delta\hat{r}'/\hat{a}$  is the line spread function for the system. Since it refers to the focal plane it will be indicated with  $l_{\text{fp}}$ . After introduction of  $y = \hat{a}\bar{r}_i/\hat{f}$  and  $\eta = \Delta\hat{r}'/\hat{a}$  we can write such Fourier transform exactly as Eq. (309), that is

$$l_{\text{fp}}(\Omega, y) = \int_{-1}^1 d\xi \left\{ \int_{-1}^1 d\eta P(\xi + \eta) P(\xi - \eta) \exp [i2\eta(\xi\Omega - y)] \right\}, \quad (329)$$

where we accounted for the fact that the Fourier transform integral in  $d\xi$  is limited by the presence of the lens to the range  $[-1, 1]$ . On the one hand, the integral in parenthesis {...} is the Fourier transform of  $P(\xi + \eta)P(\xi - \eta)$  calculated with respect to  $\eta$  as a function of  $2(\xi\Omega + y)$ . On the other hand, the function  $P(\xi + \eta)P(\xi - \eta)$  is a window function similar to the pupil function  $P$ . It is equal to unity for values of  $|\eta| < 1 - |\xi|$  and is zero elsewhere. Therefore, as in the previous Section 10, the quantity in parenthesis {...} can be calculated analytically yielding back Eq. (310). Moreover, as in the previous Section 10 we may use a new variable  $y' = y/\sqrt{\Omega}$  in Eq. (329), thus obtaining the following final expression for the line spread function:

$$l_{\text{fp}}(\Omega, y') = \int_{-1}^1 d\xi \frac{\sin [2(\xi\Omega + y'\sqrt{\Omega})(1 - |\xi|)]}{\xi\Omega + y'\sqrt{\Omega}}. \quad (330)$$

Eq. (330) is identical to Eq. (313). Therefore, the shapes of the function  $l_{\text{fp}}$  and of its asymptotic limit for different values of  $\Omega$  are the same as those for  $l_{\text{pc}}$  given in Fig. 37, Fig. 38, Fig. 39 and Fig. 40. As before, once a definition for the width of  $l_{\text{fp}}$  is chosen, the optimal operation point for the pinhole camera may be set requiring that such width be minimal. Defining the width of  $l_{\text{fp}}$  to be the full width half maximum (FWHM) one concludes that the optimal lens aperture for the imaging in the focal plane is given by

$$\hat{a}^2 \simeq 4.5 \hat{z}_1 \quad (331)$$

or, in dimensional units

$$a^2 \simeq 4.5 \frac{z_1 c}{\omega} . \quad (332)$$

We can estimate the best resolution in the focal plane  $\delta r_f$  in dimensional units requiring that  $\delta y'$  be equal to the minimal FWHM of the line spread function, i.e. 1.5, and taking advantage of the definition of  $y'$ , which gives

$$\delta r_f \simeq 1.5 \sqrt{\frac{c}{\omega z_1}} f . \quad (333)$$

Note that results in this Section have not been obtained under the assumption  $|M| \gg 1$  as those in the last Section. Therefore, substitution of  $\hat{z}_1 \rightarrow \hat{z}_{\text{eff}}$  is not required in this case.

Similarly as before, we should now discuss the applicability of Eq. (330). Up to now we discussed about a Gaussian quasi-homogeneous undulator source, but Eq. (330) can be applied in a wider variety of cases. In particular, Eq. (330) can be applied when (a) the source is quasi-homogeneous, (b) the lens is installed in the far zone and (c)  $\hat{a}^2 \ll \max[1, \hat{D}] \hat{z}_1^2$ . When conditions (a), (b) and (c) are satisfied, the line spread function for the lens,  $l_{\text{fp}}$  can be calculated from Eq. (330). Depending on the situation, one may have a good quality or a bad quality of the image. This is related with how the width of  $l_{\text{fp}}$  scales with the width of the ideal image. The intensity profile at the focal plane (located at  $\hat{z} = \hat{z}_1 + \hat{f}$ ) is given, in any case, by the convolution product of the line spread function  $l_{\text{fp}}$  and the ideal image. In particular, for an undulator source with Gaussian intensity profile at the virtual plane, such product is given by  $l_{\text{fp}} * \exp[-\bar{r}^2/(2M^2\hat{N})]$ , where  $|M| = \hat{f}/\hat{z}_1$ . When  $\sqrt{\hat{N}} \gg \hat{a} \gg \hat{z}_1/\sqrt{\hat{N}}$  a good quality image is formed at the observation plane. In other situations instead, the width of  $l_{\text{fp}}$  is of order of the width of the ideal image, and a bad quality image will be formed. To be specific, for values of  $\Omega \gg 1$  the line spread function and, therefore, the intensity distribution at the focal plane tends to a stepped profile, while for values of  $\Omega \ll 1$  one obtains a  $\text{sinc}^2(\cdot)$  profile. To sum

up, in order to calculate the intensity distribution at the focal plane behind the lens, we should first calculate  $\Omega = \hat{a}^2/\hat{z}_1$ . Then use Eq. (330) to calculate the line spread function  $l_{\text{fp}}$ . Finally, convolve with the ideal image from the source. The minimal width of the line spread function, which corresponds to the best image resolution, is when  $\hat{a}^2/\hat{z}_1 \simeq 4.5$ . Note that conditions (a), (b) and (c) above do not require the source to be an undulator source. In particular, (a), (b) and (c) are automatically satisfied for thermal sources, or perfectly incoherent objects. As a result, our theory can be applied for visible light imaging as well. These remarks simplify our discussion and drastically widen the applicability region of our results.

## 12 A unified theory of incoherent imaging by a single lens

In the present Section 12 we will develop a unified theory which is applicable to imaging in an arbitrary plane behind the lens. In the previous Section 11 we discussed the possibility of imaging the source at the focal plane. There we recognized that under conditions (a) the source is quasi-homogeneous (b) the lens is installed in the far zone and (c)  $\hat{a}^2 \ll \max[1, \hat{D}] \hat{z}_1^2$ , the intensity on the focal plane can be calculated as a convolution product of the line spread function of the system and the ideal image, which is a scaled version of the intensity distribution on the source plane. Moreover, it was shown that the characteristics of the intensity distribution in the focal plane can be treated in formal analogy with the pinhole camera setup in Section 10 and with the physics of aberrations, in particular defocusing aberrations, described in Section 9. We have seen that when the lens is in the far field (condition (b)) Eq. (127) can be used to characterize the cross-spectral density at the lens position. In the image plane, this assumption alone allows cancellation of all phase factors in the integrand of Eq. (133) and yields Eq. (226). In the previous Section 11 we showed that this cancellation does not hold anymore for the focal plane. From this viewpoint the focal plane is not privileged in any way with respect to other observation planes. It is this last remark which suggests a generalization of the previous results. For a generic observation plane positioned at  $\hat{z} = \hat{z}_2$  one may use Eq. (127) to get an expression for the intensity ( $\Delta\hat{r} = 0$ ) from Eq. (133), in analogy with Eq. (320) and Eq. (296), that is

$$\begin{aligned} \hat{I}(\hat{z}_2, \bar{r}) = \int d\bar{r}' d\Delta\hat{r}' \left\{ \hat{\mathcal{G}}(0, -\bar{r}', -\Delta\hat{r}') \exp \left[ 2i \left( -\frac{1}{f} + \frac{1}{\hat{z}_1} + \frac{1}{\hat{d}} \right) \bar{r}' \Delta\hat{r}' \right] \right. \\ \left. \times P(\bar{r}' + \Delta\hat{r}') P(\bar{r}' - \Delta\hat{r}') \right\} \exp \left[ -\frac{2i}{\hat{d}} \bar{r} \Delta\hat{r}' \right], \end{aligned} \quad (334)$$

where  $\hat{d} = \hat{z}_2 - \hat{z}_1$ . As one can see, the phase factor in  $\bar{r}' \Delta\hat{r}'$  is more complicated than those Eq. (320) and Eq. (296) due to the complete arbitrariness of the

observation plane. Nevertheless, Eq. (334) can be recast to the same form of Eq. (320) simply with the help of with a new definition of  $\hat{z}_{\text{eff}}$ , that is

$$\frac{1}{\hat{z}_{\text{eff}}} = -\frac{1}{f} + \frac{1}{\hat{z}_1} + \frac{1}{\hat{d}}. \quad (335)$$

Accounting for Eq. (335) we may rewrite Eq. (334) as

$$\begin{aligned} \hat{I}(\hat{z}_2, \bar{r}) = & \int d\bar{r}' d\Delta\hat{r}' \left\{ \hat{\mathcal{G}}(0, -\bar{r}', -\Delta\hat{r}') \exp \left[ i \frac{2}{\hat{z}_{\text{eff}}} \bar{r}' \Delta\hat{r}' \right] \right. \\ & \left. \times P(\bar{r}' + \Delta\hat{r}') P(\bar{r}' - \Delta\hat{r}') \right\} \exp \left[ -\frac{2i}{\hat{d}} \bar{r} \Delta\hat{r}' \right], \end{aligned} \quad (336)$$

which is equivalent to Eq. (320).

All that is left to do is now follow, step by step, the previous Section 11. This leads to the following results. When conditions (a), (b) and (c) are satisfied one may introduce, as before, a line spread function of the system, characteristic of the observation plane  $\hat{z} = \hat{z}_2$ . This line spread function is formally identical to Eq. (330):

$$l_z(\Omega, y') = \int_{-1}^1 d\xi \frac{\sin \left[ 2(\xi\Omega + y'\sqrt{\Omega})(1 - |\xi|) \right]}{\xi\Omega + y'\sqrt{\Omega}}, \quad (337)$$

with  $\Omega = \hat{a}^2/\hat{z}_{\text{eff}}$  and  $y' = y/\sqrt{\Omega}$ ,  $y'$  being defined by  $y = \hat{a}\bar{r}/\hat{d}$ . Here similarity techniques have been employed. The five dimensional parameters  $\lambda$ ,  $a$ ,  $f$ ,  $z_1$  and  $z_2$  have been reduced to the only parameters  $\Omega$  and  $y'$ , so that one is left with the calculation of a dimensionless function in  $y'$  depending on the single parameter  $\Omega$ , Eq. (337). As before, depending on the situation, one may have a good quality or a bad quality of the image. This is related with how the width of  $l_z$  scales with the width of the ideal image. The intensity profile at the observation plane located at  $\hat{z} = \hat{z}_2$  is given by the convolution product of the line spread function  $l_z$  and the ideal image. In particular, for an undulator source with Gaussian intensity profile at the virtual plane, such product is given by  $l_z * \exp[-\bar{r}^2/(2M^2\hat{N})]$ , where  $|M| = \hat{d}/\hat{z}_1$ . When  $\sqrt{\hat{N}} \gg \hat{a} \gg \hat{z}_1/\sqrt{\hat{N}}$  a good quality image is formed at the observation plane. In other situations instead, the width of  $l_z$  is of order of the width of the ideal image, and a bad quality image will be formed. To sum up, we presented here an algorithm to calculate the intensity distribution of radiation at any observation plane located at position  $\hat{z} = \hat{z}_2$  behind the lens, given an arbitrary value of  $\hat{a}$  and a system satisfying conditions (a), (b) and (c). First one should calculate  $\Omega = \hat{a}^2/\hat{z}_{\text{eff}}$ . Then use Eq. (337) to calculate the line spread function  $l_z$ . Finally,

convolve with the ideal image from the source. As before, when  $\Omega \gg 1$  the line spread function tends to a stepped profile and, as a result, the intensity profile reproduces a stepped profile too. Note that,  $\hat{z}_{\text{eff}}$  being arbitrary, we cannot give a relation in terms of  $\hat{a}$  and  $\hat{z}_1$  corresponding to an optimal line spread function. For instance, when  $\hat{z}_2 \rightarrow \hat{z}_i$ , i.e. when we consider the asymptotic limit for the image plane, we obtain from Eq. (335) that  $\hat{z}_{\text{eff}} \rightarrow \infty$  and  $\Omega \rightarrow 0$ . Then, from Eq. (337) one obtains  $l_z \rightarrow \text{sinc}^2(\hat{a}\bar{r}_i/\hat{d})$ , exactly as in Eq. (311). In this case no defocusing aberration is present, quadratic phase term having been cancelled by the particular choice of the observation plane. As a result, we cannot give a criterium for an optimal line spread function: we only have diffraction effects so that the larger the aperture  $\hat{a}$  (always within the constraint imposed by condition (c), i.e.  $\hat{a}^2 \ll \max[1, \hat{D}]\hat{z}_1^2$ ) the better the quality of the image. In closing, it is worth to mention that the asymptote for  $\hat{f} \rightarrow \infty$  corresponds to the pinhole camera setup already discussed in Section 10. As a result, this particular case can be treated in terms of our unified theory as well.

### 13 Depth of focus

According to [23] "the depth of focus of a lens is the permitted displacement, away from the focal or image plane, for which the intensity on axis is diminished by some permissible amount". In particular, when plane wave illumination is considered on a perfect circular lens, the focal plane corresponds to the plane where the radiation assumes the minimal spot size, and the intensity on axis reaches a maximum at that point. It can be shown that, in this case, the on-axis intensity decreases of about 20% when "the observation plane is displaced from the ideal focal plane [...] by an amount" (see [23])

$$|\Delta'z| = \frac{\lambda}{2\text{NA}^2}, \quad (338)$$

where the quantity NA indicates the numerical aperture of the lens.  $\text{NA} = \sin \theta$ ,  $\theta$  being the "half angle measured from the optic axis at the focus back to the lens" [23]. The concept of depth of focus described in Eq. (338), describes a case of coherent illumination of the lens by a plane wave, and the lens is treated, here, as a condenser. The object to be imaged is, in fact, the radiation source itself. Since we are dealing with coherent illumination we may say that, in this case, the depth of focus is diffraction limited.

The depth of focus as described in Eq. (338) is parametrically related to another concept of depth of focus which is used, for example, in Optical Lithography [23, 24]. In this case one needs to illuminate a wafer with a demagnified image of a given pattern on a mask. Here the lens (actually the collection of

lenses) is no more treated as a condenser: its function is to produce the demagnified image of the mask. The mask itself must be illuminated by means of a condenser system instead, and, as remarked in [23], "the ability to print fine, high contrast features is significantly affected by the degree of coherence within the optical system. If there exists a high degree of spatial coherence, diffraction from adjacent mask features will interfere in the image plane, significantly modifying the recorded pattern". The mask should therefore be illuminated by incoherent light and should be considered as a quasi-homogeneous source itself. For a lithography setup, the resolution  $R$  is the width of the diffraction-limited point spread function of the system, while the distance  $X$  over which the image is in proper focus is, more quantitatively, the distance over which  $R$  is increased by some permitted amount. Although a lithography setup constitutes a completely different setup with respect to the condenser system illuminated with coherent plane waves,  $R$  and  $X$  turn out to be respectively [24]:

$$R = k_1 \frac{\lambda}{\text{NA}} ; \quad X = k_2 \frac{\lambda}{\text{NA}^2} . \quad (339)$$

The distance  $X$  is therefore parametrically related to the distance  $|\Delta'z|$  defined in Eq. (338) and even though these two quantities refer to very different setups, involving quite different physics, also  $X$  is named, as  $|\Delta'z|$ , depth of focus.

To complicate the situation further one is frequently interested in the depth of focus  $|\Delta z|$  for a condenser system when the lens is not illuminated by plane waves but by other kind of non quasi-homogeneous or quasi-homogeneous sources, which is a different situation from both cases considered in the previous discussion. In this Section we will treat the case of a condenser lens illuminated by a quasi-homogeneous source characterized by  $\hat{N}_x \gg 1$  and  $\hat{D}_x \gg 1$ . Separate treatments of the  $x$  and  $y$  direction are thus allowed, which simplify to one-dimensional cases. Our study applies to the horizontal direction only. However, if also  $\hat{N}_y \gg 1$  and  $\hat{D}_y \gg 1$  the same results for the horizontal direction can be applied to the vertical direction as well. Our definition of depth of focus will be relative to the plane of smallest spot size of the radiation. Therefore, in the present Section 13, the depth of focus of a lens is defined as the permitted displacement, away from the waist plane, for which the intensity on axis is diminished by some permissible amount.

Before starting to discuss about the depth of focus, it is necessary to derive an expression for the point where the radiation spot size is the smallest. This can be obtained with the help of Eq. (216) in Section 7. In fact, since  $2\sqrt{\hat{\epsilon}\hat{\beta}(\hat{z}_2)}$  is the characteristic width of the Gaussian radiation spot size at the observation plane located at  $\hat{z} = \hat{z}_2$ , it is sufficient to look at the point  $\hat{z}_{2\text{best}}$  where the derivative of  $\hat{\epsilon}\hat{\beta}(\hat{z}_2)$  is zero to obtain the position of the waist plane. With the help of Eq. (216) one finds

$$\hat{z}_{2\text{best}} = \frac{(\hat{f} + \hat{z}_1) \hat{N} - \hat{D} \hat{f} \hat{z}_1^2 + \hat{D} \hat{z}_1^3}{\hat{N} + \hat{D} (\hat{f} - \hat{z}_1)^2} = \frac{(\hat{f} + \hat{z}_1) \hat{A} \hat{z}_1^2 - (\hat{f} - \hat{z}_1) \hat{D} \hat{z}_1^2}{\hat{A} \hat{z}_1^2 + \hat{D} (\hat{f} - \hat{z}_1)^2}. \quad (340)$$

It is interesting to study two limiting cases of Eq. (340) for  $\hat{A} \gg \hat{D}$  and for  $\hat{A} \rightarrow 0$  respectively. Consider first the case when  $\hat{A} \gg \hat{D}$ . From Eq. (340) one may see that, in this first case,  $\hat{z}_{2\text{best}} \rightarrow \hat{z}_f = \hat{f} + \hat{z}_1$ . This means that the waist plane asymptotically goes to the focal plane of the lens. Consider now the case when  $\hat{A} \rightarrow 0$ . Again from Eq. (340) one may see that, in this second case,  $\hat{z}_{2\text{best}} \rightarrow \hat{z}_i = \hat{z}_1^2 / (\hat{z}_1 - \hat{f})$ . This means that the waist plane asymptotically goes to the image plane of the virtual source (located at  $\hat{z} = 0$ ).

From the analysis of the two limiting cases for  $\hat{A} \gg \hat{D}$  and for  $\hat{A} \rightarrow 0$ , we conclude that one always has  $\hat{z}_1 + \hat{f} < \hat{z}_{2\text{best}} < \hat{z}_i$ . In other words, the waist plane is always located between the focal and the image plane. This results may seem counterintuitive. In fact, for our Gaussian virtual source, the waist is located at  $\hat{z}_s = 0$ , which is imaged, reversed and magnified, at the image plane. Therefore, at first glance, the smallest spot size should be located at the image plane. The reason why this is not the case is due to the presence of the magnification factor, which linearly increases with  $\hat{z}_2$ . On the one hand the source has a waist located at  $\hat{z}_s = 0$  and its size increases symmetrically as one moves away from  $\hat{z}_s = 0$  in both the positive and the negative direction. On the other hand the magnification factor increases linearly with  $\hat{z}_2$  and is not characterized by the same symmetric dependence on the displacement from  $\hat{z}_s = 0$ .

In the following Section 13.1 and Section 13.2 we study the problem of the depth of focus in a condenser system with a Gaussian quasi-homogeneous source. Effects from the pupil width will be neglected in Section 13.1, Finite pupil dimensions will be accounted for in Section 13.2.

### 13.1 Large non-limiting aperture

We will discuss, for simplicity, the case when  $|M| = \hat{d}_i / \hat{z}_1 \ll 1$ . In this case, from Eq. (30) we obtain  $\hat{d}_i \simeq \hat{f}$ . Since we assumed as a starting point  $|M| \ll 1$  it follows that  $\hat{f} \ll \hat{z}_1$ , and that the distance between the image and the focal plane is  $\Delta = \hat{d}_i - \hat{f} \simeq \hat{f}^2 / \hat{z}_1 \simeq |M| \hat{f}$ . Moreover, the radiation spot size at the image plane is known to be of order  $|M| \sqrt{\hat{N}}$  from Eq. (157), while the radiation spot size at the focal plane is obtained from Eq. (154) and is of order  $\sqrt{\hat{D}} \hat{f}$ . As has been discussed above, the position of the waist goes from the focal plane to the image plane as we pass from the near to the far zone. This can also be seen by comparing the radiation spot sizes at the image and

at the focal plane in the near and in the far zone. In the near zone  $\hat{A} \gg \hat{D}$ . It follows that  $\sqrt{\hat{D}\hat{f}} \ll \sqrt{\hat{N}\hat{f}/\hat{z}_1}$ , i.e. the radiation spot size at the focal plane is much smaller than that at the image plane. On the contrary in the far zone  $\hat{A} \ll \hat{D}$ . It follows that  $\sqrt{\hat{D}\hat{f}} \gg \sqrt{\hat{N}\hat{f}/\hat{z}_1} \simeq \sqrt{\hat{N}\hat{d}_i/\hat{z}_1}$ , i.e. the radiation spot size at the focal plane is much smaller than that at the image plane. We will analyze these two cases separately.

### 13.1.1 Far zone

In this case  $\hat{A} \ll \hat{D}$  and the waist is near the image. On the one hand, as has been already remarked, the radiation spot size on the image plane is about  $|M|\sqrt{\hat{N}}$  and does not depend on  $\hat{D}$ . On the other hand, the radiation spot size on the non-limiting pupil aperture is defined by the beam divergence and can be estimated as  $\sqrt{\hat{D}\hat{z}_1}$ . This means that the rate of change of the radiation spot size from the lens to the waist can be estimated as  $\sqrt{\hat{D}\hat{z}_1}/\hat{f}$ , since  $\hat{d}_i \simeq \hat{f}$ . The parametric dependence of the depth of focus can be found requiring that the spot size increase due to a displacement  $\Delta\hat{z}$ , that is  $(\sqrt{\hat{D}\hat{z}_1}/\hat{f})\Delta\hat{z}$  be of order of the radiation spot size at the waist, i.e.  $|M|\sqrt{\hat{N}}$ . This yields the following Geometrical Optics prediction for the depth of focus:

$$\Delta\hat{z} \simeq \frac{\hat{f}|M|\sqrt{\hat{N}}}{\sqrt{\hat{D}\hat{z}_1}} \simeq M^2 \sqrt{\frac{\hat{N}}{\hat{D}}} . \quad (341)$$

One may separately estimate the diffraction size related with an aperture of size  $\sqrt{\hat{D}\hat{z}_1}$  (the radiation spot size at the non-limiting pupil aperture) at the observation plane. Such estimation yields a diffraction size  $\hat{d}_i/(\sqrt{\hat{D}\hat{z}_1}) \simeq \hat{f}/(\sqrt{\hat{D}\hat{z}_1})$ . Now, requiring that the spot size increase due to a displacement  $\Delta'\hat{z}$ , that is  $(\sqrt{\hat{D}\hat{z}_1}/\hat{f})\Delta'\hat{z}$ , be of order of the diffraction size  $\hat{f}/(\sqrt{\hat{D}\hat{z}_1})$  one may estimate the diffraction limited depth of focus as

$$\Delta'\hat{z} \simeq \frac{\hat{f}^2}{\hat{D}\hat{z}_1} . \quad (342)$$

The following comparison between the diffraction limited depth of focus  $\Delta'\hat{z}$  and the Geometrical Optics prediction for the depth of focus  $\Delta\hat{z}$  can be pre-

sented:

$$\frac{\Delta' \hat{z}}{\Delta \hat{z}} \simeq \frac{\hat{f}^2}{\hat{D} \hat{z}_1^2} \cdot \frac{1}{M^2} \sqrt{\frac{\hat{D}}{\hat{N}}} \simeq \frac{1}{\sqrt{\hat{N} \hat{D}}} . \quad (343)$$

Eq. (343) allows one to conclude that diffraction effects can be neglected within the accuracy of the quasi-homogeneous approximation, and that Eq. (341) is a correct estimation of the depth of focus in this case. Note that the definition in Eq. (338) has no meaning in the case of a condenser system with a quasi-homogeneous source. Finally, it is interesting to remark that the depth of focus is much shorter than the distance  $\Delta$  between the waist (image) and the focal plane. In fact

$$\frac{\Delta \hat{z}}{\Delta} \simeq M^2 \sqrt{\frac{\hat{N}}{\hat{D}}} \cdot \frac{1}{|M| \hat{f}} \simeq \sqrt{\frac{\hat{N}}{\hat{D} \hat{z}_1^2}} \ll 1 , \quad (344)$$

because of the far zone assumption ( $\hat{A} \ll \hat{D}$ ).

### 13.1.2 Near zone

Similar estimations can be made in the near zone, i.e. assuming  $\hat{A} \gg \hat{D}$ , when the waist is near the focal plane. On the one hand, as has been already remarked, the radiation spot size at the focal plane is about  $\sqrt{\hat{D} \hat{f}}$  and does not depend on  $\hat{N}$ . On the other hand, the radiation spot size on the non-limiting pupil aperture is defined by the electron beam waist and can be estimated as  $\sqrt{\hat{N}}$ . This means that the rate of change of the radiation spot size from the lens to the waist can be estimated as  $\sqrt{\hat{N}}/\hat{f}$  since the waist is near the focal plane. The parametric dependence of the depth of focus can be found imposing that the spot size increase due to a displacement  $\Delta \hat{z}$ , that is  $(\sqrt{\hat{N}}/\hat{f}) \Delta \hat{z}$  be of order of the radiation spot size at the waist, i.e.  $\sqrt{\hat{D} \hat{f}}$ . This yields the following Geometrical Optics prediction for the depth of focus:

$$\Delta \hat{z} \simeq \frac{\sqrt{\hat{D} \hat{f}^2}}{\sqrt{\hat{N}}} . \quad (345)$$

One may separately estimate the diffraction size related with an aperture of size  $\sqrt{\hat{N}}$  (the radiation spot size at the non-limiting pupil aperture) at the observation plane. Such estimation gives a diffraction size  $\hat{d}_i/\sqrt{\hat{N}} \simeq \hat{f}/\sqrt{\hat{N}}$ .

Now, imposing that the spot size increase due to a displacement  $\Delta\hat{z}$ , that is  $(\sqrt{\hat{N}}/\hat{f})\Delta\hat{z}$  be of order of the diffraction size  $\hat{f}/\sqrt{\hat{N}}$  one may estimate the diffraction limited depth of focus as

$$\Delta'\hat{z} \simeq \frac{\hat{f}^2}{\hat{N}}. \quad (346)$$

The following comparison between the diffraction limited depth of focus  $\Delta'\hat{z}$  and the Geometrical Optics prediction of the depth of focus  $\Delta\hat{z}$ :

$$\frac{\Delta'\hat{z}}{\Delta\hat{z}} \simeq \frac{\sqrt{\hat{N}}}{\sqrt{\hat{D}}\hat{f}^2} \frac{\hat{f}^2}{\hat{N}} \simeq \frac{1}{\sqrt{\hat{N}}\hat{D}} \quad (347)$$

Eq. (347) allows one to conclude that diffraction effects can be neglected within the accuracy of the quasi-homogeneous approximation, and that Eq. (345) is a correct estimation for the depth of focus in this case. Finally, it is interesting to remark that the depth of focus is much shorter than the distance  $\Delta$  between the waist (focal plane) and the image plane. In fact

$$\frac{\Delta\hat{z}}{\Delta} \simeq \frac{\sqrt{\hat{D}}\hat{f}^2}{\sqrt{\hat{N}}} \cdot \frac{1}{|\mathbf{M}|\hat{f}} \simeq \sqrt{\frac{\hat{D}\hat{z}_1^2}{\hat{N}}} \ll 1, \quad (348)$$

because of the near zone assumption ( $\hat{A} \gg \hat{D}$ ).

### 13.2 Effect of aperture size

We will now analyze the influence of a finite aperture on our analysis of the depth of focus. For simplicity we will consider the far field case, as all our examples involving effects of finite aperture size have been relying on the far field assumption. At first glance, substitution of the radiation spot size  $\sqrt{\hat{D}}\hat{z}_1$  with the finite aperture size  $\hat{a}$  solves all issues, as it allows estimations of the rate of change of the radiation spot size and of diffraction effects. This would lead to the following equations for the Geometrical Optics prediction of the depth of focus:

$$\Delta\hat{z} \simeq \frac{\hat{f}^2\sqrt{\hat{N}}}{\hat{z}_1\hat{a}}, \quad (349)$$

for the diffraction limited depth of focus:

$$\Delta' \hat{z} \simeq \frac{\hat{f}^2}{\hat{a}^2}, \quad (350)$$

for the ratio between  $\Delta' \hat{z}$  and  $\Delta \hat{z}$ :

$$\frac{\Delta' \hat{z}}{\Delta \hat{z}} \simeq \frac{\hat{f}^2}{\hat{a}^2} \cdot \frac{\hat{z}_1 \hat{a}}{\hat{f}^2 \sqrt{\hat{N}}} \simeq \frac{\hat{z}_1}{\hat{a} \sqrt{\hat{N}}}, \quad (351)$$

and for the ratio between the depth of focus and the distance  $\Delta$ :

$$\frac{\Delta \hat{z}}{\Delta} \simeq \frac{\hat{f}^2 \sqrt{\hat{N}}}{\hat{z}_1 \hat{a}} \cdot \frac{1}{|M| \hat{f}} \simeq \frac{\sqrt{\hat{N}}}{\hat{a}}. \quad (352)$$

We have seen in Section 11 that there exist particular situations when the phase factor in parenthesis  $\{\dots\}$  in Eq. (321) can be neglected.

In one of these cases, when  $\hat{D} \hat{z}_1^2 \gg \hat{N} \gg \hat{a}^2 \gg \hat{z}_1^2 / \hat{N}$  one recovers a scaled image of the virtual source at the focal plane, where the scaling factor  $\hat{f} / \hat{z}_1 \simeq |M|$  (see Eq. (325)). Thus, in this situation, it is not correct to state that the radiation spot size at the image plane is smaller than the radiation spot size at the focal plane, because in both these planes we have the same, identical image of the virtual source with approximatively the same scaling factor. It should be remarked that in this case the depth of focus  $\Delta \hat{z}$  is longer than the distance between focal and image plane,  $\Delta$ , as one may see from Eq. (352) when  $\hat{N} \gg \hat{a}^2$ . Another critical scale to account for is  $\hat{z}_1^2 / \hat{N}$ . As we have seen in Section 11, when  $\hat{a}^2 \ll \hat{z}_1^2 / \hat{N}$  one obtains, at the focal plane, the diffraction pattern of the pupil (aberrated or not, depending on how  $\hat{a}^2$  scales with respect to  $\hat{z}_1$ ). This case corresponds to coherent illumination of the pupil. In this situation, the diffraction limited depth of focus  $\Delta' \hat{z}$  is much longer than the Geometrical Optics prediction of the depth of focus  $\Delta \hat{z}$ , as one may see from Eq. (351). In this case, Eq. (350) should be used instead of Eq. (349) in order to estimate the depth of focus of the system. Summing up, Eq. (349) can be used without any remarks in all the cases when  $\hat{a}^2 \gg \hat{z}_1^2 / \hat{N}$ . When  $\hat{a}^2 \ll \hat{N}$  and  $\hat{a}^2 \gg \hat{z}_1^2 / \hat{N}$  one should remember that the depth of focus becomes longer than the distance between the image and the focal plane, this case corresponding the situation when an image of the virtual source is formed in the focal plane. In all cases when  $\hat{a}^2 \ll \hat{z}_1^2 / \hat{N}$  instead, we have coherent illumination of the pupil. The diffraction limited depth of focus becomes longer than the Geometrical Optics prediction of the depth of focus and, for estimations, one should use Eq. (350) in place of Eq. (349).

## 14 Solutions to the image formation problem for non-homogeneous undulator sources

We will now consider non-homogeneous undulator sources. The next Section 14.1 will deal with the case of a horizontally quasi-homogeneous and vertically non-homogeneous source. Special emphasis will be given to the study of this situation, which is relevant for the majority of Synchrotron Radiation sources of the third generation. In the following Section 14.2 we will discuss, instead, the case of a horizontally non-homogeneous and vertically diffraction limited source. These two cases practically deal with all third generation light sources, from the soft to the hard X-rays.

Our treatment is based on the assumption that the beta functions have minima in the center of the undulator. Placing the virtual source in the center of the undulator, we will obtain a particularly simple expression for the cross-spectral density of the source and its Fourier transform. In particular, calculations will yield real results. Statistical Optics methods conjugated to Fourier Optics will allow us to give explicit presentations of the cross-spectral density and its Fourier transform at the virtual source position. Such presentations will account for all complexities of the source, intrinsic properties of undulator radiation and electron-beam phase space distribution. Based on our previous work [2], we will first calculate the cross-spectral density  $\hat{G}$  in the far zone limit. Then, with the help of Eq. (127), we will be able to recover the Fourier transform of the cross-spectral density  $\hat{\mathcal{G}}$  at the virtual source position. By inverse transforming that expression we will finally recover the cross-spectral density as well.

In general, we cannot give an explicit expression for the cross-spectral density at any observation plane. In other words, as before, Eq. (133) cannot be calculated explicitly for any value of  $\hat{z}_1$  and  $\hat{z}_2$ . However, once the center of the undulator is fixed as the virtual source position, there exists a privileged observation plane. This is the plane where the center of the undulator is imaged and depends on the position  $\hat{z}_1$  chosen for the lens. Throughout this paper we simply called it the image plane. Starting from the expression for the cross-spectral density and its Fourier transform at the virtual source we will be able to calculate, for any choice of  $\hat{z}_1$ , the cross-spectral density on the focal ( $\hat{z}_2 = \hat{z}_f$ ) and on the image ( $\hat{z}_2 = \hat{z}_i$ ) plane. The procedure that we will use to perform these calculations is similar to what has been proposed in the case of homogeneous sources and will take advantage of Eq. (131) and Eq. (132).

As usual, we will begin our investigations neglecting pupil effects. Results for a large non-limiting aperture on the image plane will be generalized to include effects of the pupil with the help of Eq. (135). Finally, in Section 14.3 we will

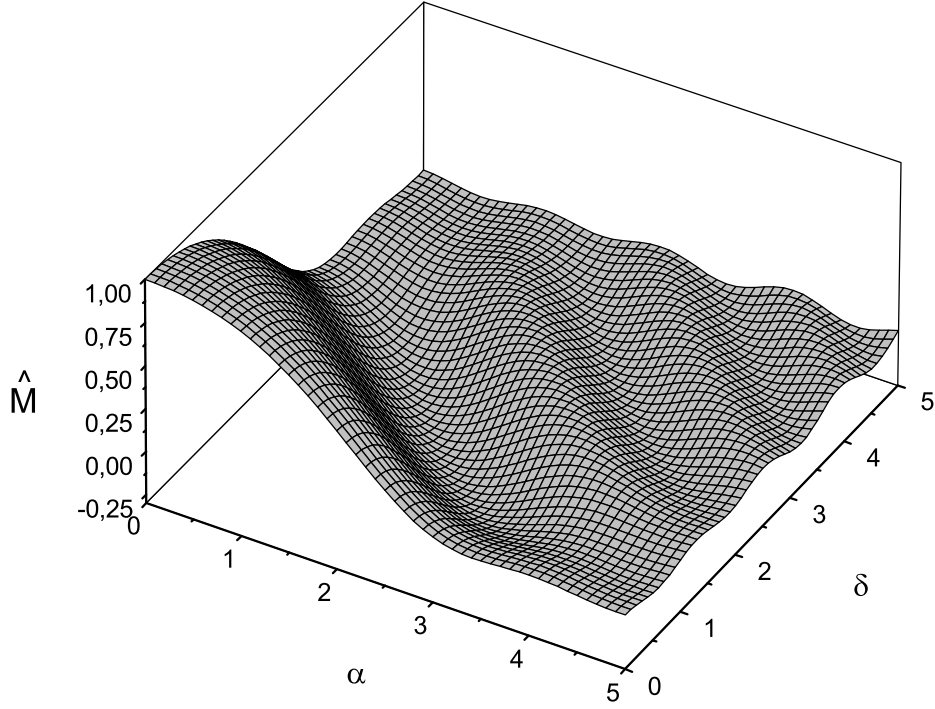


Fig. 42. Plot of the universal function  $\hat{M}$ , used to calculate the cross-spectral density at the focal plane when  $\hat{N}_x \gg 1$ ,  $\hat{D}_x \gg 1$ ,  $\hat{N}_y$  and  $\hat{D}_y$  are arbitrary.

critically discuss the assumptions made throughout this paper and see how and up to what extent they can be relaxed.

#### 14.1 Horizontally quasi-homogeneous and vertically non-homogeneous source

##### 14.1.1 Large non-limiting aperture

Let us first retain the assumption  $\hat{D}_x \gg 1$  and  $\hat{N}_x \gg 1$ , but allow  $\hat{D}_y$  and  $\hat{N}_y$  to assume arbitrary values. Eq. (141) allows the reconstruction of the vertical cross-spectral density in the far zone. Note that, when both  $\hat{N}_y \lesssim 1$  and  $\hat{D}_y \lesssim 1$  the source is non-homogeneous. In this case the far zone limit is for values  $\hat{z}_o \gg 1$ , and one obtains

$$\hat{G}(\hat{z}_o, \bar{\theta}_y, \Delta\hat{\theta}_y) = \exp \left[ i2\bar{\theta}_y \hat{z}_o \Delta\hat{\theta}_y \right] \exp \left[ -2\hat{N}_y \Delta\hat{\theta}_y^2 \right]$$

$$\times \int_{-\infty}^{\infty} d\hat{\phi}_y \exp \left[ -\frac{(\bar{\theta}_y + \hat{\phi}_y)^2}{2\hat{D}_y} \right] M(\hat{\phi}_y, \Delta\hat{\theta}_y) , \quad (353)$$

where the function  $\hat{M}(\alpha, \delta)$  is the normalized version of a universal function first defined in [2] and reads:

$$\hat{M}(\alpha, \delta) = \frac{3}{8\sqrt{\pi}} \int_{-\infty}^{\infty} d\hat{\phi}_x \text{sinc} \left[ \frac{\hat{\phi}_x^2 + (\alpha - \delta)^2}{4} \right] \text{sinc} \left[ \frac{\hat{\phi}_x^2 + (\alpha + \delta)^2}{4} \right] . \quad (354)$$

A plot of the  $\hat{M}$  function is given in Fig. 42. The  $\hat{M}$  function is a real function. Another remarkable property of  $\hat{M}$  is its invariance for exchange of  $\alpha$  with  $\delta$ . Also,  $\hat{M}$  is invariant for exchange of  $\alpha$  with  $-\alpha$  (or  $\delta$  with  $-\delta$ ). The following relations between universal functions hold:

$$\hat{I}_S(\alpha) = \hat{M}(\alpha, 0) , \quad (355)$$

$$\beta(\delta) = \frac{1}{2\pi^2} \int_{-\infty}^{\infty} d\xi \hat{M}(\xi, \delta) \quad (356)$$

and

$$\gamma(x) = \frac{1}{2\pi^2} \int_{-\infty}^{\infty} d\xi \exp[-i2x\xi] \hat{M}(\xi, 0) . \quad (357)$$

Using Eq. (127) and Eq. (353) we obtain the Fourier transform of the cross-spectral density at  $\hat{z}_o = 0$  at the virtual source position

$$\hat{\mathcal{G}}(0, \bar{u}, \Delta\hat{u}) = \exp \left[ -2\hat{N}_y \Delta\hat{u}^2 \right] \int_{-\infty}^{\infty} d\hat{\phi}_y \exp \left[ -\frac{(\bar{u} + \hat{\phi}_y)^2}{2\hat{D}_y} \right] \hat{M}(\hat{\phi}_y, \Delta\hat{u}) . \quad (358)$$

Inverse transforming Eq. (358) we obtain the cross-spectral density at the virtual source position

$$\hat{G}(0, \bar{y}, \Delta\hat{y}) = \exp \left[ -2\hat{D}_y \Delta\hat{y}^2 \right] \int_{-\infty}^{\infty} d\hat{\phi} \exp \left[ -\frac{(\bar{y} + \hat{\phi})^2}{2\hat{N}_y} \right] \hat{\mathcal{M}}(\Delta\hat{y}, \hat{\phi}) . \quad (359)$$

In analogy with Eq. (126), we defined  $\hat{\mathcal{M}}$  as

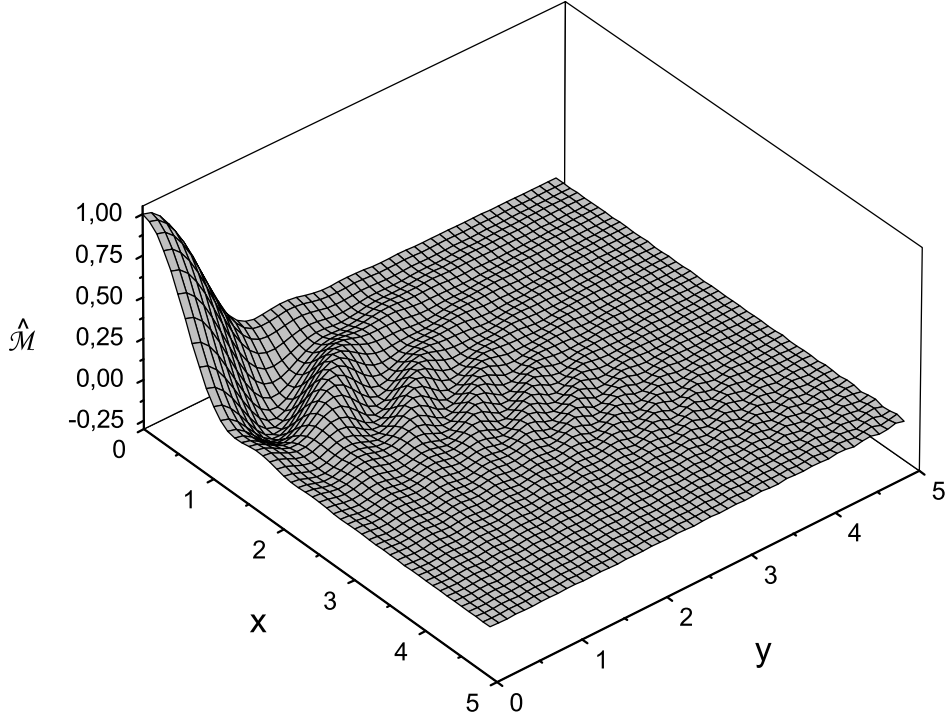


Fig. 43. Plot of the universal function  $\hat{\mathcal{M}}$ , used to calculate the cross-spectral density at the image plane when  $\hat{N}_x \gg 1$ ,  $\hat{D}_x \gg 1$ ,  $\hat{N}_y$  and  $\hat{D}_y$  are arbitrary.

$$\hat{\mathcal{M}}(x, y) = \frac{8\sqrt{\pi}}{3} \frac{1}{2\pi^2\mathcal{K}} \int_{-\infty}^{\infty} d\alpha \int_{-\infty}^{\infty} d\delta \exp[-2i(\alpha x + \delta y)] \hat{M}(\alpha, \delta), \quad (360)$$

where  $\mathcal{K}$  is given in Eq. (174). A plot of  $\hat{\mathcal{M}}$  is presented in Fig. 43. Note that the symmetry of  $\hat{M}$  for exchange of  $\alpha$  with  $-\alpha$  or  $\delta$  with  $-\delta$  implies that  $\hat{\mathcal{M}}$  is a real function. This fact, together with Eq. (359), implies that  $\hat{G}$  at the virtual plane, that is an ensemble-averaged field product, is real as well. This is a consequence of the fact that single particle sources produce a field characterized by a plane wavefront at the virtual source position. It can be seen comparing Eq. (36) with Eq. (94) or, directly, by inspecting Eq. (97). Moreover, note that  $\hat{\mathcal{M}}$  is invariant for the exchange of  $x$  with  $y$ .

From Eq. (131) and Eq. (358) we obtain the cross-spectral density on the focal plane in the vertical direction, that is

$$\begin{aligned} \hat{G}(\hat{z}_f, \bar{y}_f, \Delta\hat{y}_f) &= \exp\left[\frac{2i}{\hat{f}^2}(\hat{f} - \hat{z}_1)\bar{y}_f\Delta\hat{y}_f\right] \exp\left[-\frac{2\hat{N}_y\Delta\hat{y}_f^2}{\hat{f}^2}\right] \\ &\times \int_{-\infty}^{\infty} d\hat{\phi}_y \exp\left[-\frac{(\bar{y}_f/\hat{f} + \hat{\phi}_y)^2}{2\hat{D}_y}\right] \hat{M}\left(\hat{\phi}_y, \frac{\Delta\hat{y}_f}{\hat{f}}\right). \end{aligned} \quad (361)$$

In the vertical direction, the relative intensity on the focal plane is therefore given by

$$\begin{aligned} \hat{I}(\hat{z}_f, \bar{y}_f) &= \int_{-\infty}^{\infty} d\hat{\phi}_y \exp\left[-\frac{(\bar{y}_f/\hat{f} + \hat{\phi}_y)^2}{2\hat{D}_y}\right] \hat{I}_S(\hat{\phi}_y) \\ &\times \left\{ \int_{-\infty}^{\infty} d\hat{\phi}_y \exp\left[-\frac{\hat{\phi}_y^2}{2\hat{D}_y}\right] \hat{I}_S(\hat{\phi}_y) \right\}^{-1}, \end{aligned} \quad (362)$$

because  $\hat{I}_S(\hat{\phi}_y) = \hat{M}(\hat{\phi}_y, 0)$ . In the limit  $\hat{D}_y \ll 1$ , Eq. (362) reduces to

$$\hat{I}(\hat{z}_f, \bar{y}_f) = \hat{I}_S\left(\frac{\bar{y}_f}{\hat{f}}\right). \quad (363)$$

The modulus of the spectral degree of coherence on the focal plane in the vertical direction reads

$$\begin{aligned} |g(\hat{z}_f, \bar{y}_f, \Delta\hat{y}_f)| &= \exp\left[-2\frac{\hat{N}_y}{\hat{f}^2}\Delta\hat{y}_f^2\right] \\ &\times \int_{-\infty}^{\infty} d\hat{\phi}_y \exp\left[-\frac{(\bar{y}_f/\hat{f} + \hat{\phi}_y)^2}{2\hat{D}_y}\right] \hat{M}\left(\hat{\phi}_y, \frac{\Delta\hat{y}_f}{\hat{f}}\right) \\ &\times \left\{ \int_{-\infty}^{\infty} d\hat{\phi}_y \exp\left[-\frac{(\bar{y}_f/\hat{f} + \Delta\hat{y}_f/\hat{f} + \hat{\phi}_y)^2}{2\hat{D}_y}\right] \hat{I}_S(\hat{\phi}_y) \right\}^{-1/2} \\ &\times \left\{ \int_{-\infty}^{\infty} d\hat{\phi}_y \exp\left[-\frac{(\bar{y}_f/\hat{f} - \Delta\hat{y}_f/\hat{f} + \hat{\phi}_y)^2}{2\hat{D}_y}\right] \hat{I}_S(\hat{\phi}_y) \right\}^{-1/2}. \end{aligned} \quad (364)$$

In the limiting case for  $\hat{D}_y \ll 1$  one obtains the simplified expression

$$|g(\hat{z}_f, \bar{y}_f, \Delta\hat{y}_f)| = \exp\left[-2\frac{\hat{N}_y}{\hat{f}^2}\Delta\hat{y}_f^2\right] \chi\left(\frac{\bar{y}_f}{\hat{f}}, \frac{\Delta\hat{y}_f}{\hat{f}}\right), \quad (365)$$

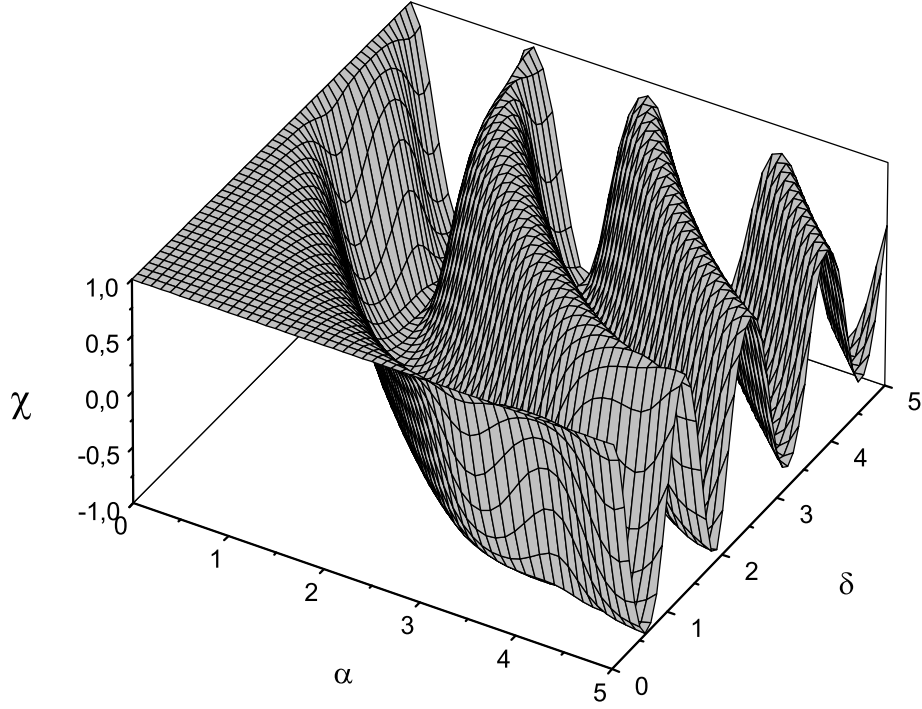


Fig. 44. Plot of the universal function  $\hat{\chi}$ , used to calculate the modulus of the spectral degree of coherence on the focal plane when  $\hat{N}_x \gg 1$ ,  $\hat{D}_x \gg 1$ ,  $\hat{N}_y \ll 1$  and  $\hat{D}_y \ll 1$ .

where, as in Eq. (145) of [2],

$$\chi(\alpha, \delta) = \frac{\hat{M}(\alpha, \delta)}{[\hat{I}_S(\alpha - \delta)]^{1/2} [\hat{I}_S(\alpha + \delta)]^{1/2}}. \quad (366)$$

A plot of  $\chi$  is given in Fig. 44. Eq. (364) reduces even more in the case when both  $\hat{D}_y \ll 1$  and  $\hat{N}_y \ll 1$ . In this case we have

$$|g(\hat{z}_f, \bar{y}_f, \Delta \hat{y}_f)| = \chi\left(\frac{\bar{y}_f}{\hat{f}}, \frac{\Delta \hat{y}_f}{\hat{f}}\right). \quad (367)$$

On the image plane, Eq. (132) and Eq. (359) give the following cross-spectral density in the vertical direction:

$$\begin{aligned} \hat{G}(\hat{z}_i, \bar{y}_i, \Delta\hat{y}_i) &= \exp \left[ \frac{i\mathfrak{m}(\mathfrak{m}+1)\bar{y}_i\Delta\hat{y}_i}{2\hat{z}_1} \right] \int_{-\infty}^{\infty} d\hat{\phi} \exp \left[ -\frac{(\mathfrak{m}\bar{y}_i + \hat{\phi})^2}{2\hat{N}_y} \right] \\ &\quad \times \hat{\mathcal{M}}(\mathfrak{m}\Delta\hat{y}_i, \hat{\phi}) \exp \left[ -2\hat{D}_y\mathfrak{m}^2\Delta\hat{y}_i^2 \right] , \end{aligned} \quad (368)$$

corresponding to a relative intensity on the image plane

$$\begin{aligned} \hat{I}(\hat{z}_i, \bar{y}_i) &= \int_{-\infty}^{\infty} d\hat{\phi} \exp \left[ -\frac{(\mathfrak{m}\bar{y}_i + \hat{\phi})^2}{2\hat{N}_y} \right] \hat{\mathcal{M}}(0, \hat{\phi}) \\ &\quad \times \left\{ \int_{-\infty}^{\infty} d\hat{\phi} \exp \left[ -\frac{\hat{\phi}^2}{2\hat{N}_y} \right] \hat{\mathcal{M}}(0, \hat{\phi}) \right\}^{-1} . \end{aligned} \quad (369)$$

With the help of Eq. (360), Eq. (356) and Eq. (174) one sees that

$$\hat{\mathcal{M}}(0, y) = \frac{1}{2\pi^2\mathcal{K}} \int_{-\infty}^{\infty} d\delta \left[ \exp [i(-2\delta)y] \int_{-\infty}^{\infty} d\alpha \hat{M}(\alpha, \delta) \right] = \hat{\mathcal{B}}(y) . \quad (370)$$

The solution of the image formation problem is thus constituted by a convolution product between a Gaussian function and the universal function  $\hat{\mathcal{B}}$ , which admits the analytical representation given in Eq. (186). The intensity on the image plane is independent of the value of  $\hat{D}_y$ . In the limit  $\hat{N}_y \gg 1$  Eq. (369) gives back Eq. (169). Instead, in the limit  $\hat{N}_y \ll 1$  we obtain

$$\hat{I}(\hat{z}_i, \bar{y}_i) = \hat{\mathcal{M}}(0, \mathfrak{m}\bar{y}_i) = \hat{\mathcal{B}}(\mathfrak{m}\bar{y}_i) . \quad (371)$$

The modulus of the spectral degree of coherence in the vertical direction is given by

$$\begin{aligned} |g(\hat{z}_i, \bar{y}_i, \Delta\hat{y}_i)| &= \int_{-\infty}^{\infty} d\hat{\phi} \exp \left[ -\frac{(\mathfrak{m}\bar{y}_i + \hat{\phi})^2}{2\hat{N}_y} \right] \\ &\quad \times \hat{\mathcal{M}}(\mathfrak{m}\Delta\hat{y}_i, \hat{\phi}) \exp \left[ -2\hat{D}_y\mathfrak{m}^2\Delta\hat{y}_i^2 \right] \\ &\quad \times \left\{ \int_{-\infty}^{\infty} d\hat{\phi} \exp \left[ -\frac{(\mathfrak{m}\bar{y}_i + \mathfrak{m}\Delta\hat{y}_y + \hat{\phi})^2}{2\hat{N}_y} \right] \hat{\mathcal{M}}(0, \hat{\phi}) \right\}^{-1/2} \\ &\quad \times \left\{ \int_{-\infty}^{\infty} d\hat{\phi} \exp \left[ -\frac{(\mathfrak{m}\bar{y}_i - \mathfrak{m}\Delta\hat{y}_y + \hat{\phi})^2}{2\hat{N}_y} \right] \hat{\mathcal{M}}(0, \hat{\phi}) \right\}^{-1/2} . \end{aligned} \quad (372)$$

In the case  $\hat{D}_y \ll 1$  and  $\hat{N}_y \ll 1$  one obtains

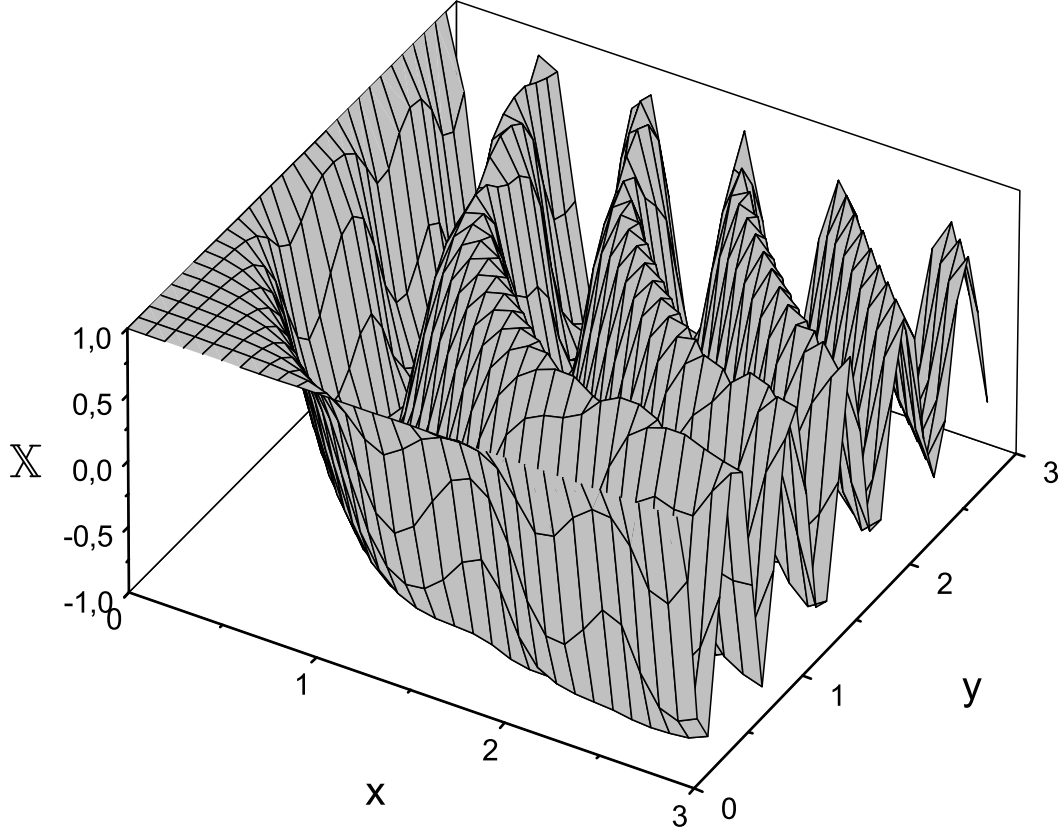


Fig. 45. Plot of the universal function  $\mathbb{X}$ , used to calculate the modulus of the spectral degree of coherence on the image plane when  $\hat{N}_x \gg 1$ ,  $\hat{D}_x \gg 1$ ,  $\hat{N}_y \ll 1$  and  $\hat{D}_y \ll 1$ .

$$|g(\hat{z}_i, \bar{y}_i, \Delta \hat{y}_i)| = \mathbb{X}(m\Delta \hat{y}_i, m\bar{y}_i) \quad (373)$$

where, in analogy with Eq. (366), we define

$$\mathbb{X}(x, y) = \frac{\hat{\mathcal{M}}(x, y)}{[\hat{\mathcal{B}}(x - y)]^{1/2} [\hat{\mathcal{B}}(x + y)]^{1/2}}. \quad (374)$$

Note that when  $\hat{N}_y \gg 1$  and  $\hat{D}_y$  assumes arbitrary values, the modulus of the spectral degree of coherence, Eq. (372), simplifies to Eq. (170). A plot of the universal function  $\mathbb{X}$  is given in Fig. 45.

#### 14.1.2 Effect of aperture size

We will now include, with the help of Eq. (135), the effects of pupil in the one-dimensional case. The pupil function and  $\hat{\mathcal{P}}$  are given by Eq. (224) and Eq. (225). The  $r$ -direction should be now substituted with the  $y$ -direction.

We can use condition (136) and Eq. (368) to describe the case when the lens is in the far zone. From Eq. (368) we can estimate the order of the source dimension, that is  $\max[1, \sqrt{\hat{N}_y}]$ , and the order of the coherence length, that is  $\min[1/\sqrt{\hat{D}_y}, 1]$ . The lens is in the far zone when  $\max[1, \sqrt{\hat{N}_y}]/\hat{z}_1 \ll \max[\sqrt{\hat{D}_y}, 1]$ . Note that several particular cases of interest are automatically included in this condition: the case for  $\hat{D}_y \gg 1$  and  $\hat{N}_y \gg 1$ , that gives  $\hat{z}_1 \gg \sqrt{\hat{N}_y/\hat{D}_y}$ , the case for  $\hat{D}_y \gg 1$  and  $\hat{N}_y \lesssim 1$ , that gives  $\hat{z}_1 \gg 1/\sqrt{\hat{D}_y}$ , as well as the case for  $\hat{D}_y \lesssim 1$  and  $\hat{N}_y \gg 1$ , that gives  $\hat{z}_1 \gg \sqrt{\hat{N}_y}$ . All these situations have been previously discussed in Section 5. The new situation left to consider is for  $\hat{N}_y \sim 1$  and  $\hat{D}_y \sim 1$ . In this case, the lens is in the far field when  $\hat{z}_1 \gg 1$ . From Eq. (135) and Eq. (368) we obtain

$$\begin{aligned}
\hat{G}_P(\hat{z}_i, \bar{y}_i, \Delta\hat{y}_i) &= 4\hat{a}^2 \exp\left[\frac{2im}{\hat{z}_1}\bar{y}_i\Delta\hat{y}_i\right] \int d\bar{u} d\Delta\hat{u} \exp\left[-2\hat{D}_y\hat{z}_1^2\Delta\hat{u}^2\right] \\
&\times \int_{-\infty}^{\infty} d\hat{\phi} \exp\left[-\frac{(\hat{\phi} + \hat{z}_1\bar{u})^2}{2\hat{N}_y}\right] \hat{\mathcal{M}}(\hat{z}_1\Delta\hat{u}, \hat{\phi}) \\
&\times \text{sinc}\left\{\hat{a}\left[\frac{m}{\hat{z}_1}(\bar{y}_i + \Delta\hat{y}_i) - \bar{u} - \Delta\hat{u}\right]\right\} \\
&\times \text{sinc}\left\{\hat{a}\left[\frac{m}{\hat{z}_1}(\bar{y}_i - \Delta\hat{y}_i) - \bar{u} + \Delta\hat{u}\right]\right\}. \tag{375}
\end{aligned}$$

According to Eq. (353),  $\hat{z}_1^2 \max[1, \hat{D}_y]$  is of order of the square of the radiation spot size on the pupil, while  $\hat{z}_1^2/\max[\hat{N}_y, 1]$  is of order of the square of the coherence length on the pupil. It is interesting to see that if  $\hat{D}_y \gg 1$  the exponential function in  $\Delta\hat{u}$  has a very narrow characteristic length with respect to unity, and one can make the substitution  $\hat{\mathcal{M}}(\hat{z}_1\Delta\hat{u}, \hat{\phi}_y) \rightarrow \hat{\mathcal{M}}(0, \hat{\phi}_y) = \hat{\mathcal{B}}(\hat{\phi}_y)$ , thus getting back Eq. (256). If  $\hat{N}_y \gg 1$  instead,  $\hat{\phi}_y$  can be set to zero in the exponential function in  $\hat{\phi}_y + \hat{z}_1\bar{u}$ , and the entire exponential function can be taken out of the integral in  $d\hat{\phi}_y$ . Then, it is possible to show that the surviving integral in  $d\hat{\phi}_y$  is equal to  $\gamma(\hat{z}_1\Delta\hat{u})$ , giving back Eq. (250). Finally, if both  $\hat{N}_y \gg 1$  and  $\hat{D}_y \gg 1$  we get back Eq. (226).

Eq. (375) should be considered as a limiting case when no aberrations are present. More generally, when aberrations and apodization are present, Eq. (375) should be substituted by the following expression:

$$\begin{aligned}
\hat{G}_P(\hat{z}_i, \bar{y}_i, \Delta\hat{y}_i) &= 4\hat{a}^2 \exp\left[\frac{2im}{\hat{z}_1}\bar{y}_i\Delta\hat{y}_i\right] \int d\bar{u} d\Delta\hat{u} \exp\left[-2\hat{D}_y\hat{z}_1^2\Delta\hat{u}^2\right] \\
&\times \int_{-\infty}^{\infty} d\hat{\phi} \exp\left[-\frac{(\hat{\phi} + \hat{z}_1\bar{u})^2}{2\hat{N}_y}\right] \hat{\mathcal{M}}(\hat{z}_1\Delta\hat{u}, \hat{\phi})
\end{aligned}$$

$$\begin{aligned}
& \times \hat{\mathcal{P}}_a \left[ \frac{m}{\hat{z}_1} (\bar{y}_i + \Delta \hat{y}_i) - \bar{u} - \Delta \hat{u} \right] \\
& \times \hat{\mathcal{P}}_a^* \left[ \frac{m}{\hat{z}_1} (\bar{y}_i - \Delta \hat{y}_i) - \bar{u} + \Delta \hat{u} \right] .
\end{aligned} \tag{376}$$

Eq. (376) is very general and is valid under the only assumption that the lens is in the far field region. The use of old coordinates  $\hat{y}_{i1}$  and  $\hat{y}_{i2}$  instead of  $\bar{y}_i$  and  $\Delta \hat{y}_i$  somewhat clarifies the meaning of Eq. (376). Eq. (376) states that the cross-spectral density accounting for the pupil influence (aberrations and diffraction effects) is a double convolution product of Eq. (368), i.e. the cross-spectral density in the ideal case, and  $\hat{\mathcal{P}}_a$ , which can be written as

$$\begin{aligned}
\hat{G}_P(\hat{z}_i, \hat{y}_{i1}, \hat{y}_{i2}) &= \left\langle \left\langle \hat{E}(\hat{u}_1) \hat{E}^*(\hat{u}_2) \right\rangle * \hat{\mathcal{P}}_a(\hat{u}_1) * \hat{\mathcal{P}}_a^*(\hat{u}_2) \right\rangle (\hat{y}_{i1}, \hat{y}_{i2}) \\
&= \left\langle \left[ \hat{E} * \hat{\mathcal{P}}_a \right] (\hat{y}_{i1}) \left[ \hat{E}^* * \hat{\mathcal{P}}_a^* \right] (\hat{y}_{i2}) \right\rangle .
\end{aligned} \tag{377}$$

The intensity at the image plane is found setting  $\hat{y}_{i1} = \hat{y}_{i2} = \hat{y}_i$ , which gives

$$\begin{aligned}
\hat{I}_P(\hat{z}_i, \hat{y}_i) &= \left\langle \left\langle \hat{E}(\hat{u}_1) \hat{E}^*(\hat{u}_2) \right\rangle * \hat{\mathcal{P}}_a(\hat{u}_1) * \hat{\mathcal{P}}_a^*(\hat{u}_2) \right\rangle (\hat{y}_i, \hat{y}_i) \\
&= \left\langle \left| \hat{E} * \hat{\mathcal{P}}_a \right|^2 (\hat{y}_i) \right\rangle .
\end{aligned} \tag{378}$$

In particular, in the case of a completely coherent source, we may neglect the ensemble average.

Note that in order to evaluate the intensity at the image plane, it is no more enough to know the ideal intensity and to convolve with a line spread function. One has to know the cross-spectral density in the ideal case and convolve twice with  $\hat{\mathcal{P}}_a$ , which is known as the amplitude line spread function of the system (or the amplitude point spread function in the two-dimensional case) and is a more general identifier of the system characteristics. Even in the non quasi-homogeneous case one may continue to use, for evaluating the intensity at the image plane, an algorithm based on the calculation of ideal characteristics and further convolution with a function characterizing the system. The difference with respect to the quasi-homogeneous case is that the amplitude line spread function must be used in place of the line spread function, and that the cross-spectral density must be used in place of the intensity.

Note that, in our approach, the Wigner function plays no role, as it constitutes an artificial quantity in the image formation problem, whereas the natural quantity to consider is the cross-spectral density. Even if the virtual source can be characterized by a phase space distribution (i.e. by a positive Wigner function) one has no simplification in the imaging problem. The only simplification of Eq. (378) takes place in the quasi-homogeneous case when, due to the separability of the cross-spectral density variables and to a short

coherence length (compared with the size of the source), one obtains the usual incoherent line spread function formalism.

#### 14.2 Horizontally non-homogeneous and vertically diffraction limited source

We will now relax the assumption of a large horizontal electron beam size and divergence and deal with the non-homogeneous case when  $\hat{N}_x$  assumes arbitrary values, while  $\hat{D}_x \ll 1$ . This is a rather exotic range of parameters, and we will discuss the case for a large non-limiting aperture only. In this case, for third generation light sources we have automatically  $\hat{N}_y \ll 1$  and  $\hat{D}_y \ll 1$  because  $\epsilon_y \ll \epsilon_x$ <sup>24</sup>. In this case, in the limit  $\hat{z}_o \gg 1$ , from Eq. (124) we obtain

$$\begin{aligned} \hat{G} = & \exp\left(i2\bar{\theta}_x\Delta\hat{\theta}_x\hat{z}_o\right) \exp\left[-2\hat{N}_x\Delta\hat{\theta}_x^2\right] \exp\left(i2\bar{\theta}_y\Delta\hat{\theta}_y\hat{z}_o\right) \\ & \times \text{sinc}\left[\frac{(\bar{\theta}_x - \Delta\hat{\theta}_x)^2 + (\bar{\theta}_y - \Delta\hat{\theta}_y)^2}{4}\right] \text{sinc}\left[\frac{(\bar{\theta}_x + \Delta\hat{\theta}_x)^2 + (\bar{\theta}_y + \Delta\hat{\theta}_y)^2}{4}\right]. \end{aligned} \quad (379)$$

Using Eq. (127) and Eq. (379) one obtains the Fourier transform of the cross-spectral density at  $\hat{z}_o = 0$ , i.e. at the virtual-source position, that is given by

$$\begin{aligned} \hat{G}\left(0, \bar{\theta}_x, \Delta\hat{\theta}_x, \bar{\theta}_y, \Delta\hat{\theta}_y\right) = & \exp\left[-2\hat{N}_x\Delta\hat{\theta}_x^2\right] \text{sinc}\left[\frac{(\bar{\theta}_x - \Delta\hat{\theta}_x)^2 + (\bar{\theta}_y - \Delta\hat{\theta}_y)^2}{4}\right] \\ & \times \text{sinc}\left[\frac{(\bar{\theta}_x + \Delta\hat{\theta}_x)^2 + (\bar{\theta}_y + \Delta\hat{\theta}_y)^2}{4}\right]. \end{aligned} \quad (380)$$

Inverse transforming Eq. (380) it is possible to express the cross-spectral density at the virtual source position as

$$\hat{G}(0, \bar{x}, \Delta\hat{x}, \bar{y}, \Delta\hat{y}) = \int_{-\infty}^{\infty} d\bar{\theta}_x d\Delta\hat{\theta}_x d\bar{\theta}_y d\Delta\hat{\theta}_y \exp\left[-2\hat{N}_x\Delta\hat{\theta}_x^2\right]$$

<sup>24</sup>This treatment can be easily generalized to the more exotic situation for  $\hat{N}_x$  arbitrary,  $\hat{D}_x \ll 1$ ,  $\hat{N}_y$  arbitrary and  $\hat{D}_y \ll 1$ . However, here we will be concerned with third generation light sources only. Assuming reasonable values for  $\beta_x \lesssim 10 L_w$  and  $\epsilon_y = \chi\epsilon_x$  with  $\chi \simeq 10^{-2}$  we see that  $\hat{D}_x \ll 1$  implies both  $\hat{N}_y \ll 1$  and  $\hat{D}_y \ll 1$ . Therefore we will avoid to make generalizations which are not pertinent to the case under study, e.g. exotic case for  $\beta_x > 10 L_w$ ,  $\beta_y < 10^{-1} L_w$  or  $\beta_y > 10 L_w$ .

$$\begin{aligned}
& \times \text{sinc} \left[ \frac{(\bar{\theta}_x - \Delta\hat{\theta}_x)^2 + (\bar{\theta}_y - \Delta\hat{\theta}_y)^2}{4} \right] \\
& \times \text{sinc} \left[ \frac{(\bar{\theta}_x + \Delta\hat{\theta}_x)^2 + (\bar{\theta}_y + \Delta\hat{\theta}_y)^2}{4} \right] \\
& \times \exp \left[ 2i(\Delta\hat{\theta}_x \bar{x} + \bar{\theta}_x \Delta\hat{x}) \right] \exp \left[ 2i(\Delta\hat{\theta}_y \bar{y} + i\bar{\theta}_y \Delta\hat{y}) \right].
\end{aligned} \tag{381}$$

From Eq. (131) and Eq. (380) we obtain the cross-spectral density on the focal plane

$$\begin{aligned}
\hat{G}(\hat{z}_f, \bar{x}_f, \Delta\hat{x}_f, \bar{y}_f, \Delta\hat{y}_f) &= \exp \left[ \frac{2i}{\hat{f}^2} (\hat{f} - \hat{z}_1) \bar{x}_f \Delta\hat{x}_f \right] \exp \left[ -\frac{2\hat{N}_x}{\hat{f}^2} \Delta\hat{x}_f^2 \right] \\
& \times \exp \left[ \frac{2i}{\hat{f}^2} (\hat{f} - \hat{z}_1) \bar{y}_f \Delta\hat{y}_f \right] \\
& \times \text{sinc} \left[ \frac{(\bar{x}_f - \Delta\hat{x}_f)^2 + (\bar{y}_f - \Delta\hat{y}_f)^2}{4\hat{f}^2} \right] \\
& \times \text{sinc} \left[ \frac{(\bar{x}_f + \Delta\hat{x}_f)^2 + (\bar{y}_f + \Delta\hat{y}_f)^2}{4\hat{f}^2} \right].
\end{aligned} \tag{382}$$

The relative intensity on the focal plane is therefore given by

$$\hat{I}(\hat{z}_f, \bar{x}_f, \bar{y}_f) = \text{sinc}^2 \left[ \frac{\bar{x}_f^2 + \bar{y}_f^2}{4\hat{f}^2} \right]. \tag{383}$$

This is just the relative intensity on the focal plane from a single electron, i.e. Eq. (91). It is interesting to note that the modulus of the spectral degree of coherence on the focal plane depends on  $\Delta\hat{x}_f$  only, and can be written as

$$|g(\hat{z}_f, \bar{x}_f, \Delta\hat{x}_f, \bar{y}_f, \Delta\hat{y}_f)| = \exp \left[ -\frac{2\hat{N}_x}{\hat{f}^2} \Delta\hat{x}_f^2 \right]. \tag{384}$$

In the limit  $\hat{N}_x \ll 1$  one recovers the deterministic case of a single particle. In this limit  $|g|$  reduces to unity, and the wavefront is perfectly coherent.

As regards the image plane, we should note that Eq. (381) is not easy to manipulate analytically in the most general case. However, when  $\Delta\hat{x} = 0$  and  $\Delta\hat{y} = 0$ , one can calculate the intensity of the virtual source. With the help of Eq. (175) and Eq. (181) one obtains

$$\hat{I}(0, \bar{x}, \bar{y}) = \int_{-\infty}^{\infty} d\hat{\phi}_x \exp \left[ -\frac{(\bar{x} + \hat{\phi}_x)^2}{2\hat{N}_x} \right] \tilde{\Psi}(\hat{\phi}_x, \bar{y}) , \quad (385)$$

where we have set

$$\tilde{\Psi}(x, y) = \Psi \left( \sqrt{x^2 + y^2} \right) . \quad (386)$$

The function  $\Psi$  was already defined in Eq. (95). Using Eq. (132) and Eq. (385) we can now give the following expression for the relative intensity:

$$\begin{aligned} \hat{I}(\hat{z}_i, \bar{x}_i, \bar{y}_i) &= \int_{-\infty}^{\infty} d\hat{\phi}_x \exp \left[ -\frac{(\mathfrak{m}\bar{x}_i + \hat{\phi}_x)^2}{2\hat{N}_x} \right] \tilde{\Psi}(\hat{\phi}_x, \mathfrak{m}\bar{y}_i) \\ &\times \left\{ \int_{-\infty}^{\infty} d\hat{\phi}_x \exp \left[ -\frac{\hat{\phi}_x^2}{2\hat{N}_x} \right] \tilde{\Psi}(\hat{\phi}_x, 0) \right\}^{-1} . \end{aligned} \quad (387)$$

In the limit  $\hat{N}_x \ll 1$  we have

$$\hat{I}(\hat{z}_i, \bar{x}_i, \bar{y}_i) = \mathfrak{m}^2 \tilde{\Psi}(\mathfrak{m}\bar{x}_i, \mathfrak{m}\bar{y}_i) , \quad (388)$$

in agreement with Eq. (96).

### 14.3 General imaging considerations

In the present Section 14.3 we discuss a general algorithm for the solution to the image formation problem for undulator sources based on our Statistical Optics approach.

Eq. (376) is an expression for the cross-spectral density on the image plane in the case of a non-homogeneous undulator source and of a lens with an arbitrary pupil function (i.e. a lens with aberrations, apodization and finite aperture size). However, we assumed that the electron beam has (i) a Gaussian transverse profile and (ii) a large horizontal emittance compared with the radiation wavelength ( $\hat{N}_x \gg 1$  and  $\hat{D}_x \gg 1$ ), that (iii) the radiation frequency is tuned at perfect resonance with the fundamental frequency of the undulator, i.e.  $\hat{C} \ll 1$ <sup>25</sup>, that (iv) the minimal beta functions in both horizontal and

<sup>25</sup> This means that monochromatization is good enough to neglect finite bandwidth of the radiation around the fundamental frequency, as well as electron beam energy spread.

vertical directions are located at  $\hat{z} = 0$ , that (v) there is no influence of focusing inside the undulator, that (vi) the lens is placed in the far zone and, finally, that (vii) the observation plane is located at position  $\hat{z} = \hat{z}_i$ , where the virtual source (that we assume at  $\hat{z} = 0$ ) is imaged. Assumptions (i), (ii), (iii), (iv) and (v) are related to the form of the cross-spectral density at the virtual source plane, Eq. (359). They are very often, but not always verified. Moreover they do not depend on the particular imaging setup related with a given photon beamline. Assumptions (vi) and (vii) instead, are related with the imaging setup i.e. with how the lens and the observation points are positioned.

The majority of the assumptions from (i) to (vii) are often verified for third generation light sources. As a matter of fact, our theory is specifically built to deal with third generation light sources. However, a generalization to include the case of spontaneous undulators installed in XFEL facilities (see e.g. [25], [26]) is certainly desirable. Of all restrictions from (i) to (vii), (v) is the more difficult to be relaxed. In order to do so, one needs to modify the expression for the single particle field to account for the influence of focusing inside the undulator. The other assumptions may be more easily relaxed, to give a more general algorithm for the calculation of the cross-spectral density in the case of arbitrary position of the lens (near or far zone). The case of spontaneous undulators installed in XFEL facilities is a particular one when it is needed to deal with both horizontal and vertical electron beam emittances comparable or smaller than the radiation wavelength. In fact,  $\epsilon_x \simeq \epsilon_y \simeq 0.3\text{\AA}$ . Results based on a Gaussian model of the electron beam with generic  $\hat{N}_{x,y}$  and  $\hat{D}_{x,y}$  may be presented. To this purpose one may use Eq. (124) to calculate the cross-spectral density in free space. As one may see inspecting Eq. (124), it is no more possible to separate the horizontal and the vertical direction. Eq. (124) is still subject to assumptions (i), (iii), (iv) and (v). Our theory is built by exploiting many simplifying assumptions. When some of them fail, one should go back to the point where the invalid simplification is exploited, and use a more generic expression in its place. In particular, while assumption (i) is quite realistic in the case of storage ring sources, it is to be regarded as a conventional assumption when treating sources based on linear accelerators. Our most generic expression, Eq. (114) should be used in place of Eq. (124) if one wishes to relax assumption (i), as well as (iii) and (iv). Once the cross-spectral density in free space is known through Eq. (124) or Eq. (114), one may account for a generic observation plane, thus relaxing assumption (vii). To this purpose one needs to put attention on the fact that any observation plane located at position  $\hat{z} = \hat{z}_2$  is related with a certain plane at position  $\hat{z} = \hat{z}_s$  in front of the lens through the lens-maker equation, Eq. (21). The next step in our algorithm consists in finding the cross-spectral density at  $\hat{z} = \hat{z}_s$ , which will be imaged at our chosen observation plane, located at  $\hat{z} = \hat{z}_2$ . To this purpose, Eq. (128) may be used. In fact, Eq. (128) describes the propagation of the Fourier transform of the cross-spectral density,  $\hat{\mathcal{G}}$ , in free space. As we

have seen, the fact that the lens is placed in the far field allows cancellation of one phase factor in the relation between the cross-spectral density on the image plane and the cross-spectral density on the virtual source plane. This can be seen using condition (136) in Eq. (132). Such phase factor should be retained if the lens is in the near zone (that is when condition (136) is not satisfied). In this way, assumption (vi) can be relaxed as well. At this point, the cross-spectral density  $\hat{G}(\hat{z}_s, \vec{r}, \Delta\vec{r})$  is known. The final step consists in the calculation of the amplitude point spread function  $\hat{\mathcal{P}}_a$  of the system. The cross-spectral density at position  $\hat{z} = \hat{z}_2$  is found convolving twice the product of the cross-spectral density at the source plane and the extra phase-factor due to the failure of condition (136) with the amplitude point spread function. This gives

$$\begin{aligned}
\hat{G}_P(\hat{z}_2, \vec{r}, \Delta\vec{r}) &= 4\hat{a}^2 \exp\left[\frac{2im}{\hat{z}_1} \vec{r} \cdot \Delta\vec{r}\right] \int d\vec{u} d\Delta\vec{u} \\
&\times \exp\left[2i\hat{z}_1 \vec{u} \cdot \Delta\vec{u}\right] \hat{G}\left(\hat{z}_s, -\hat{z}_1 \vec{u}, -\hat{z}_1 \Delta\vec{u}\right) \\
&\times \hat{\mathcal{P}}_a\left[\frac{m}{\hat{z}_1} (\vec{r} + \Delta\vec{r}) - \vec{u} - \Delta\vec{u}\right] \\
&\times \hat{\mathcal{P}}_a^*\left[\frac{m}{\hat{z}_1} (\vec{r} - \Delta\vec{r}) - \vec{u} + \Delta\vec{u}\right], \tag{389}
\end{aligned}$$

where  $m$  is now defined as  $m = (\hat{z}_1 - \hat{z}_s)/(\hat{z}_2 - \hat{z}_1)$ , according to Eq. (22).

It should be noted that, in this paper, together with a theory for third generation light sources we also developed a particular language that can be applied for a wider range of problems. Up to now, research works dealing with transverse coherence properties of Synchrotron Radiation have used the standard language developed to treat Statistical Optics problems. Such a language has a very limited scope because Statistical Optics has mainly dealt with thermal-like sources. As a result, a time domain approach has often been used. Quasi-stationary approximation and ergodicity are usually assumed, so that time averages are used instead of ensemble averages. Then, the concept of cross-spectral purity [3, 8] must be forcefully evoked in order to separate longitudinal and transverse coherence effects, which are described through the mutual intensity function. Such language though, is not suitable to describe Synchrotron Radiation experiments, where many radiation pulses are collected and results are averaged over an ensemble. Our approach starts from the very foundation of Statistical Optics, thus avoiding inconvenient assumptions. A language based on a frequency domain description and on ensemble averages over an ensemble of radiation pulses (each corresponding to a different electron bunch) has been developed. In our paper we aimed at presenting a satisfactory description of the physics involved in the characterization of light sources from a statistical viewpoint, trying to exhaustively explain where the main ideas come from and where they lead to. We restricted our attention

to a quantitative treatment of third-generation light sources but we also laid the foundations to describe other kind of radiation sources, e.g. spontaneous undulator sources installed in XFEL facilities. In fact, many of the features of the relatively specialized setup considered in this work are common in the general theory of undulator sources.

## 15 Supplementary remarks on quasi-homogeneous undulator source asymptotes

In the last Section 14 we presented quite general results for vertically non-homogeneous sources. Under the only assumption of a large horizontal emittance ( $\hat{D}_x \gg 1$  and  $\hat{N}_x \gg 1$ ), Eq. (353) specifies the cross-spectral density of the radiation in the far zone and in the vertical direction without constraints on  $\hat{N}_y$  and  $\hat{D}_y$ . Under the same conditions, Eq. (359) specifies the cross-spectral density of the virtual source in the vertical direction. Note that Eq. (359) is a convolution. When the dependence of  $\hat{G}$  on  $\Delta\hat{y}$  can be isolated in a single factor, the source is forcefully quasi-homogeneous, while there are no cases when it is described by a more generic kind of Shell model (i.e.  $\hat{G} \sim \sqrt{I(y_1)}\sqrt{I(y_2)}g(\Delta\hat{y})$ ). It is important to stress this fact in connection with several research works [14, 15] devoting particular attention to the relation between the Gaussian-Shell model and undulator sources. As we remarked in Section 7, Shell models (and, in particular, Gaussian-Shell models) may certainly be useful for describing light sources other than undulator-based ones and for educational purposes, but they do not describe any practical realization of undulator radiation sources.

From Eq. (353), setting  $\Delta\hat{\theta}_y = 0$ , one obtains the intensity distribution in the far zone

$$\hat{I}(\bar{\theta}_y) = \int_{-\infty}^{\infty} d\hat{\phi}_y \exp \left[ -\frac{(\bar{\theta}_y + \hat{\phi}_y)^2}{2\hat{D}_y} \right] \hat{I}_S(\hat{\phi}_y) , \quad (390)$$

having used Eq. (355). From Eq. (359), setting  $\Delta\hat{y} = 0$ , one gets the intensity distribution of the virtual source in the center of the undulator<sup>26</sup>,

$$\hat{I}(0, \bar{y}) = \int_{-\infty}^{\infty} d\hat{\phi} \exp \left[ -\frac{(\bar{y} + \hat{\phi})^2}{2\hat{N}_y} \right] \hat{\mathcal{B}}(\hat{\phi}) , \quad (391)$$

---

<sup>26</sup>We are always assuming that the minimal beta function of the electron beam is located at the center of the undulator.

having taken advantage of Eq. (370).  $\hat{I}_S$  in Eq. (390) and  $\hat{\mathcal{B}}$  in Eq. (391) are the universal functions given in Eq. (160) and Eq. (186). Both Eq. (390) and Eq. (391) are convolutions, and are valid regardless the values of  $\hat{N}_y$  and  $\hat{D}_y$ , i.e. regardless the fact that the source is quasi-homogeneous or not. In the case of a large non-limiting aperture and an ideal lens, other two exact results can be found in Section 14, which are independent of the values of  $\hat{N}_y$  and  $\hat{D}_y$ . In fact, Eq. (362) and Eq. (369) prove that the exact expression for the intensity distribution is, both on the focal and on the image plane, a convolution between Gaussian and universal functions.

When the source is quasi-homogeneous, with an accuracy scaling as the inverse number of modes,  $1/\sqrt{\max[\hat{N}_y, 1] \max[\hat{D}_y, 1]}$ , we may take the approximation  $\hat{\mathcal{M}}(\Delta\hat{y}, \hat{\phi}) \simeq \gamma(\Delta\hat{y})\mathcal{B}(\hat{\phi})$  in Eq. (359).

This fact may be demonstrated as follows. First, let us introduce a normalized version of the one-dimensional inverse Fourier transform of the function  $M$ , that is

$$\begin{aligned} M'(\Delta\hat{y}, \Delta\hat{\theta}_y) &= \frac{1}{\mathcal{A}} \int_{-\infty}^{\infty} \hat{M}(\bar{\theta}_y, \Delta\hat{\theta}_y) \exp[-2i\Delta\hat{y}\bar{\theta}_y] d\bar{\theta}_y \\ &= \frac{1}{\mathcal{A}} \int_{-\infty}^{\infty} \hat{\mathcal{M}}(\Delta\hat{y}, \bar{y}) \exp[2i\Delta\hat{\theta}_y\bar{y}] d\bar{y}. \end{aligned} \quad (392)$$

The normalization factor  $\mathcal{A}$  in Eq. (392) is defined as

$$\mathcal{A} = \int_{-\infty}^{\infty} \hat{\mathcal{M}}(0, \bar{y}) d\bar{y}, \quad (393)$$

so that  $M'(0, 0) = 1$ . The cross-spectral density in Eq. (359) can therefore be written as

$$\begin{aligned} \hat{G}(0, \bar{y}, \Delta\hat{y}) &= \exp[-2\hat{D}_y\Delta\hat{y}^2] \\ &\times \int_{-\infty}^{\infty} d\hat{u} \exp[-2i\hat{u}\bar{y}] \exp[-2\hat{N}_y\hat{u}^2] M'(\Delta\hat{y}, \hat{u}), \end{aligned} \quad (394)$$

having used the convolution theorem. Under the quasi-homogeneous assumption, we can approximate  $M'(\Delta\hat{y}, \hat{u}) \simeq M'(\Delta\hat{y}, 0)M'(0, \hat{u})$ . To show this, let us represent  $M'(x, y)$  using a Taylor expansion around the point  $(0, 0)$ . One obtains

$$M'(x, y) = 1 + \sum_{k=1}^{\infty} \frac{1}{k!} \left[ x^k \frac{\partial^k M'(x, 0)}{\partial x^k} \Big|_{x=0} + y^k \frac{\partial^k M'(0, y)}{\partial y^k} \Big|_{y=0} \right] + O(xy) , \quad (395)$$

where the normalization relation  $M'(0, 0) = 1$  has been taken advantage of. Similarly, one may consider the following representation of the product  $M'(x, 0) M'(0, y)$  also obtained by means of a Taylor expansion:

$$\begin{aligned} M'(x, 0)M'(0, y) &= \left[ M'(0, 0) + \sum_{k=1}^{\infty} \frac{x^k}{k!} \frac{d^k M'(x, 0)}{dx^k} \Big|_{x=0} \right] \\ &\times \left[ M'(0, 0) + \sum_{j=1}^{\infty} \frac{y^j}{j!} \frac{d^j M'(0, y)}{dy^j} \Big|_{y=0} \right] \\ &= 1 + \sum_{n=1}^{\infty} \frac{1}{n!} \left[ x^n \frac{d^n M'(x, 0)}{dx^n} \Big|_{x=0} \right. \\ &\quad \left. + y^n \frac{d^n M'(0, y)}{dy^n} \Big|_{y=0} \right] + O(xy) , \end{aligned} \quad (396)$$

having used  $M'(0, 0) = 1$ . Comparison of the last equality in (396) with the right hand side of Eq. (395) shows that  $M'(x, y) \simeq M'(x, 0)M'(0, y)$  up to corrections of order  $xy \sim 1/\sqrt{\max[\hat{N}_y, 1] \max[\hat{D}_y, 1]}$ , that is the quasi-homogeneous accuracy. Using this approximation in Eq. (394) yields

$$\begin{aligned} \hat{G}(0, \bar{y}, \Delta\hat{y}) &= \exp \left[ -2\hat{D}_y \Delta\hat{y}^2 \right] M'(\Delta\hat{y}, 0) \\ &\times \int_{-\infty}^{\infty} d\hat{u} \exp \left[ -2i\hat{u}\bar{y} \right] \exp \left[ -2\hat{N}_y \hat{u}^2 \right] M'(0, \hat{u}) . \end{aligned} \quad (397)$$

Finally, recalling the definitions of  $\gamma$  and  $\mathcal{B}$  we can write Eq. (397) as

$$\hat{G}(0, \bar{y}, \Delta\hat{y}) = \exp \left[ -2\hat{D}_y \Delta\hat{y}^2 \right] \gamma(\Delta\hat{y}) \int_{-\infty}^{\infty} d\hat{\phi} \exp \left[ -\frac{(\bar{y} + \hat{\phi})^2}{2\hat{N}_y} \right] \hat{\mathcal{B}}(\hat{\phi}) . \quad (398)$$

Eq. (398) is valid in any quasi-homogeneous case.

Note that Eq. (398) accounts for diffraction effects through the universal functions  $\gamma$  and  $\mathcal{B}$ . This may be traced back to the use of the inhomogeneous wave equation to calculate the cross-spectral density for the virtual source, from which Eq. (398) follows. Deriving Eq. (398), we assume a large number of modes, and this justifies the use of phase space representation as an alternative characterization of the source, in place of the cross-spectral density (i.e. Eq. (398) itself).

Setting  $\Delta\hat{y} = 0$ , Eq. (398) gives the exact intensity distribution at the virtual source, i.e. Eq. (391). The spectral degree of coherence on the virtual source is then recovered using the definition of quasi-homogeneous source  $\hat{G} = \hat{I}(\bar{y})g(\Delta\hat{y})$ . Since the source is quasi-homogeneous, the Fourier transform of the spectral degree of coherence  $g(\Delta\hat{y})$  yields the intensity in the far zone. Remembering that  $\gamma$  and  $I_S$  form a Fourier pair, we conclude that, starting from Eq. (398) it is possible to reproduce the exact result for the intensity in the far zone, Eq. (390). Quite remarkably, Eq. (398), which is derived under the quasi-homogeneous approximation and is related to an accuracy  $1/\sqrt{\max[\hat{N}_y, 1] \max[\hat{D}_y, 1]}$ , yields back two results, Eq. (390) and Eq. (391) which are valid regardless the fact that the source is quasi-homogeneous or not. Moreover, in the case of perfect optics and non-limiting pupil aperture, and independently of the quasi-homogeneous assumption, the intensity profile in the virtual plane reproduces the intensity profile in the image plane, while the intensity profile in the far zone reproduces the intensity profile in the focal plane. Therefore, we can also conclude that Eq. (398) gives both the intensity in the focal and in the image plane for an ideal lens. Note again that also these two results, Eq. (362) and Eq. (369), have perfect accuracy. They are exact and are not subject to the quasi-homogeneous accuracy  $1/\sqrt{\max[\hat{N}_y, 1] \max[\hat{D}_y, 1]}$ .

Let us now consider the particular quasi-homogeneous case when both  $\hat{N}_y \gg 1$  and  $\hat{D}_y \gg 1$ . In this case, the number of modes along the virtual source is of order  $\sqrt{\hat{N}_y \hat{D}_y}$  and the normalized coherence length can be estimated as  $\hat{\xi}_c \sim 1/\sqrt{\hat{D}_y} \ll 1$ . In the case of non-ideal optics, once a line spread function  $l$  for the system is found, one may obtain the intensity distribution of the radiation by convolving  $l$  with the ideal image. The accuracy of these calculations is now the accuracy of the quasi-homogeneous assumption,  $1/\sqrt{\hat{N}_y \hat{D}_y}$ . In the case a pupil with aperture  $\hat{a}$  is present, we concluded in Section 8.1 that it makes sense to account for diffraction effects when  $\hat{a} \ll \sqrt{\hat{D}_y \hat{z}_1}$ . In this case in fact, the ratio between the width of the line spread function and the width of the ideal image is of order  $\hat{z}_1/(\hat{a}\sqrt{\hat{N}_y}) \gg 1/\sqrt{\hat{N}_y \hat{D}_y}$ . As a result, when Eq. (398) is used to calculate the ideal intensity, it makes sense to account for diffraction effects. Worsening the accuracy in the calculation of the cross-spectral density of the source, we may reduce Eq. (398) to

$$\hat{G}(0, \bar{y}, \Delta\hat{y}) = \exp \left[ -2\hat{D}_y \Delta\hat{y}^2 \right] \exp \left[ -\frac{\bar{y}^2}{2\hat{N}_y} \right], \quad (399)$$

that is Eq. (146). Note that neglecting the product with the  $\gamma$  function can be done with an accuracy  $1/\sqrt{\hat{D}_y}$ , while extraction of the exponential function in  $\bar{y}$  from the convolution product with the  $\mathcal{B}$  function can be done with an accuracy  $1/\sqrt{\hat{N}_y}$ . In our study case when  $\hat{D}_y \gg 1$  and  $\hat{N}_y \gg 1$ , the overall

accuracy of Eq. (399) (or Eq. (146)) can be estimated as  $\max(1/\sqrt{\hat{D}_y}, 1/\sqrt{\hat{N}_y})$ , that is the accuracy of the Gaussian approximation. Such accuracy is much worse than that of the quasi-homogeneous assumption in Eq. (398), that is  $1/\sqrt{\hat{N}_y\hat{D}_y}$ . This fact has interesting consequences. In fact, Eq. (399) can first be used to calculate the ideal intensity on the image plane and, then, it may be convolved with the line spread function of the lens to give a characterization of the intensity distribution with a reduced accuracy. If, for instance,  $\hat{a} \ll \sqrt{\hat{D}\hat{z}_1}$  we can have situation when  $\hat{z}_1/(\hat{a}\sqrt{\hat{N}_y}) \gg 1/\sqrt{\hat{N}_y\hat{D}_y}$  but  $\hat{z}_1/(\hat{a}\sqrt{\hat{N}_y}) \ll 1/\sqrt{\hat{N}_y}$  and, as a result, accounting for diffraction effects would not modify the intensity with accuracy  $1/\sqrt{\hat{N}_y}$ . In spite of this, going back to Eq. (398) to calculate the ideal intensity with better accuracy  $1/\sqrt{\hat{N}_y\hat{D}_y}$ , diffraction effects will appreciably modify the intensity within the accuracy  $1/\sqrt{\hat{N}_y\hat{D}_y}$ .

When  $\hat{N}_y \gg 1$  and  $\hat{D}_y \simeq 1$  the accuracy of the quasi-homogeneous approximation becomes  $1/\sqrt{\hat{N}_y \max[1, \hat{D}_y]}$ . When  $\hat{N}_y \simeq 1$  and  $\hat{D}_y \gg 1$  it becomes, instead,  $1/\sqrt{\max[1, \hat{N}_y]\hat{D}_y}$ . In these cases, the accuracy of the quasi-homogeneous approximation is comparable to the accuracy of the Gaussian approximation. To be specific, when  $\hat{N}_y \gg 1$  and  $\hat{D}_y \simeq 1$  the accuracy of the quasi-homogeneous approximation is of order  $1/\sqrt{\hat{N}_y}$  (note that the coherence length at the pupil is  $\hat{\xi}_c \simeq 1$ , that is the diffraction size) and Eq. (398) can be substituted with

$$\hat{G}(0, \bar{y}, \Delta\hat{y}) = \exp\left[-\frac{\bar{y}^2}{2\hat{N}_y}\right] \exp\left[-2\hat{D}_y\Delta\hat{y}^2\right] \gamma(\Delta\hat{y}) \quad (400)$$

without loss of accuracy, because the relative accuracy of the convolution is of order  $1/\sqrt{\hat{N}_y}$  as the accuracy of the quasi-homogeneous approximation. Eq. (400) is just Eq. (162). A similar reasoning can be done when  $\hat{D}_y \gg 1$  and  $\hat{N}_y \simeq 1$ . In this case the accuracy of the quasi-homogeneous approximation is of order  $1/\sqrt{\hat{D}_y}$  (note that the coherence length at the pupil is  $\hat{\xi}_c \ll 1$ , that is much smaller than the diffraction size), and Eq. (398) can be substituted with

$$\hat{G}(0, \bar{y}, \Delta\hat{y}) = \exp\left[-2\hat{D}_y\Delta\hat{y}^2\right] \int_{-\infty}^{\infty} d\hat{\phi} \exp\left[-\frac{(\bar{y} + \hat{\phi})^2}{2\hat{N}_y}\right] \hat{\mathcal{B}}(\hat{\phi}). \quad (401)$$

without loss of accuracy. In fact, neglecting the  $\gamma$  function in Eq. (398) is equivalent to approximate the convolution in Eq. (390) with a Gaussian distribution, which can be done with an accuracy of order  $1/\sqrt{\hat{D}_y}$ , the same of the quasi-homogeneous approximation. Eq. (401) is just Eq. (188).

In closing this Section we should stress that, in the case of ideal lenses, the intensity on the image plane, that is a scaled version of Eq. (391), is exactly given by a convolution of a known universal function and the electron beam profile. In the case the electron beam profile is unknown, one may measure the intensity and deconvolve Eq. (391) in order to find back the electron beam profile. In literature (see, for example, [27]) it is usually accepted that the resolution of any electron beam size  $\sigma$  inferred from the measurement of the radiation intensity distribution on the image plane is limited (in the case of an ideal lens) by the diffraction size of the single particle undulator radiation, i.e. the resolution is of order  $\sqrt{\lambda L_w}/(2\pi\sigma)$ . However, we have seen that Eq. (391) is an exact result. Therefore, any measurement of  $\sigma$  obtained by deconvolution of Eq. (391) is only limited by the finite accuracy of the detector.

## 16 Conclusions

As has been remarked in [28]: "[...] it is very desirable to have a way to model the performance of undulator beamlines with significant partial coherent effects, and such modelling would, naturally, start with the source. The calculation would involve the knowledge of the partial coherence properties of the source itself and of how to propagate partially coherent fields through space and through the optical components used in the beamline. [...] it is important to recognize that, although most of these calculations are, in principle, straightforward applications of conventional coherence theory (Born and Wolf, 1980; Goodman, 1985), there is not much current interest in the visible optics community. [...] For example, even for the rather simple problem of diffraction by an open aperture with partially coherent illumination, we have found published solutions only for circular and slit-shaped apertures and only for sources consisting of an incoherently illuminated aperture of similar shape to the diffracting aperture. Thus, there is no counterpart in these types of Fourier Optics problem to the highly developed art of ray tracing in geometrical optics, not is there anything as simple as a ray to which an exact system response can be calculated." This program of development of Synchrotron Radiation theory was formulated more than ten years ago. Operation of third generation light sources also started in this period. This demonstrates that when third generation light sources were born, it was immediately recognized that the usual theory of Synchrotron Radiation was not adequate to describe them. Yet, up to now, no theoretical progress has been made in that direction. The present paper, as well as our previous work [2] are devoted to the realization of the before mentioned program of development of Synchrotron Radiation theory.

In [2] we described spatial coherence properties of undulator radiation from third-generation light sources in free space. In this paper we aim at an exten-

sion of [2]. Previous scientific works and textbooks postulate that the cross-spectral density at the virtual undulator source can be described in terms of a Gaussian-Shell model or, even more restrictively, that undulator sources are perfectly incoherent. Such assumption is not adequate when treating third generation light sources, because the vertical emittance is comparable or even much smaller than the radiation wavelength (i.e.  $\epsilon_y \ll \lambda/(2\pi)$ ) in a wide spectral interval extending from the Åmstrong wavelength range up to the soft X-rays.

In this work we combined Statistical Optics methods with Fourier Optics techniques in order to describe in an analytical way the propagation of the cross-spectral density of Synchrotron Radiation through a lens. In particular, we focused our attention on the problem of finding both the intensity and the spectral degree of coherence of undulator radiation at the focal and at the image plane of the lens. Although our paper is not limited to this situation alone, our main result deals with the quite generic case of a large normalized horizontal emittance  $\epsilon_x \gg \lambda/(2\pi)$  and an arbitrary vertical emittance  $\epsilon_y$ .

Our paper provides physical understanding of a setup of general interest and we expect it to be useful for practical estimations in almost all range of the parameter space for third generation light sources. We expect that, in the future, numerical codes fully capable of dealing with transverse coherence properties of Synchrotron Radiation will also be developed, and will be capable of providing detailed analysis of particular experimental setups. Our theory will be of help to developers of these codes because it provides both benchmarks and partially manipulated equations for the field correlation, simpler to treat numerically than first principle calculations and still reasonably generic.

Two basic non-restrictive assumptions made in our theory are the paraxial approximation and the resonance approximation. The first is justified by the fact that we are treating an ultra-relativistic system. The second means that we are working with an undulator composed of a large number of period  $N_w \gg 1$  and that we are interested in frequencies near the fundamental. This allows to neglect the vertical polarization component of the field and to treat the field within a scalar theory.

Analytical studies also required the introduction of some restrictive assumptions introduced in our theory, to be relaxed in the future. First, we assumed that the beta functions in both directions have their minima in the center of the undulator. However, beta functions are (or may be) often tuned around the center of the undulator in cases of practical interest. Second, we assumed a single converging thin lens with none or very specific pupil functions. However, other shapes of the lens can be accounted for by means of numerical convolutions between a more complicated complex pupil function and our fundamental results referring to the case when influence of the pupil is negligible. Note that

the situation of a thin lens is often met in practice in the case of X-ray radiation, as grazing incidence reflective optics is quite frequently used for image formation in this spectral range. Third, we assumed that monochromatization is good enough to neglect finite bandwidth of the radiation around the fundamental and also electron beam energy spread. Both these effects may be taken into account by an extension of this theory. However, in practical cases of interest these restrictions are often met. For instance, a monochromator relative bandwidth of  $10^{-3}$  is sufficient to guarantee a reasonably narrow bandwidth for undulators up to about 40 periods. Also, with this number of undulator periods, such a monochromator guarantees small corrections to our results for electron beams with a relative energy spread of  $10^{-3}$  or better.

The three before mentioned assumptions are somewhat restrictive. However, they are often met in practice and our theory can be extended to the case when they are not met. A more restrictive assumption is that radiation frequency is tuned at perfect resonance with the fundamental frequency of the undulator. Although this last assumption is also often met in practice, our theory cannot be easily extended to account for the situation when it is not satisfied because the starting point for the calculation of the cross-spectral density is given by an expression for the electric field around the fundamental frequency.

As a final remark, it should be said that we chose not to deal with bending magnet sources in this paper. This is left for future investigations. However, some estimates based on dimensional analysis suggest that, as discussed in Section 7, Geometrical Optics treatments may be sufficient to describe in a satisfactory way bending magnet radiation from third generation light sources.

To conclude, our paper constitutes, to our knowledge, the first satisfactory theory describing imaging of undulator sources by a single non-ideal lens. We restrict ourselves to the analysis of a single lens for simplicity, the results for more complicated optical systems involving a larger quantity of optical elements being a straightforward extension of the present work.

## Acknowledgements

The authors wish to thank Hermann Franz and Petr Ilinski for many useful discussions, Jochen Schneider and Edgar Weckert for their interest in this work.

## References

- [1] G. Geloni, E. Saldin, E. Schneidmiller and M. Yurkov, Paraxial Green's functions in Synchrotron Radiation theory, DESY 05-032, ISSN 0418-9833 (2005)
- [2] G. Geloni, E. Saldin, E. Schneidmiller and M. Yurkov, "Understanding transverse coherence properties of X-ray beams in third generation Synchrotron Radiation source", DESY 05-109, ISSN 0418-9833 (2005)
- [3] L. Mandel and E. Wolf, Optical Coherence and Quantum Optics, Cambridge University Press, 1995
- [4] C. Welnaek, G.J. Chen, F. Cerrina, Nucl.Instr. Meth. A 347, 344-347 (1994)
- [5] O.Chubar and P.Elleaume, in Proc. of the 6th European Particle Accelerator Conference EPAC-98, 1177-1179 (1998)
- [6] C.Chang, P.Naulleau and D.Attwood, Appl. Opt. 42, 2506-2512 (2003)
- [7] C.Chang, P.Naulleau, E.Anderson and D.Attwood, Opt. Commun. 182, 25-34 (2000)
- [8] J. W. Goodman, Statistical Optics, John Wiley & Sons, Inc., 1985
- [9] J. W. Goodman, Introduction to Fourier Optics, Mc Graw-Hill, 1968
- [10] M. Yabashi, K. Tamasaku and T. Ishikawa, Phys. Rev. A 69, 023813 (2004)
- [11] M. Yabashi, K. Tamasaku S. Goto and T. Ishikawa, J. Phys D: Appl. Phys. 38 (2005) A11-A16
- [12] T. Tanaka and H. Kitamura, J. Synchrotron Radiat. 8, 1221 (2001)
- [13] F. Pfeiffer et al., Phys. Rev. Lett. 94, 164801 (2005)
- [14] R. Coisson, Applied Optics 34, No. 5, 904-908 (1995)
- [15] R. Coisson and S. Marchesini, J. Synchrotron Radiat. 4, 263 (1997)
- [16] J.B. West and H.A. Padmore, "Optical engineering", in Handbook of Synchrotron Radiation, Vol. 2, Elsevier Science Publishers B.V., 1987
- [17] J.C. Dainty and R. Shaw, "Image Science", Academic Press, 1976
- [18] E. L. O'Neill, "Introduction to statistical optics", Dover Publications Inc., 2003
- [19] F. Zernike, Physika, 5, 785-795 (1938)
- [20] Applied Optics and Optical Engineering, edited by R. R. Shannon and J. C. Wyant, Academic Press (1980)

- [21] M. Born and E. Wolf, "Principles of Optics", 2nd rev. ed., MacMillan Company, New York (1968)
- [22] P. Ellaume, C Fortgang, C. Penel and E. Tarazona, *J. Synchrotron Rad.* 2, 209-214 (1995)
- [23] D. Attwood, "Soft X-rays and extreme ultraviolet radiation", Cambridge University Press, 1999
- [24] J. E. Bjorkholm, "EUV Lithography – The Successor of Optical Lithography?", in *Intel Technology Journal Q3'98* (1998)
- [25] P. Audebert et al., "TESLA XFEL: First stage of the X-ray laser laboratory - Technical design report" edited by R. Brinkmann et al., Preprint DESY 2002-167 (2002)
- [26] M. Cornacchia et al., SLAC-PUB-10133 (2003)
- [27] A. Hofmann, "Diagnostics with Synchrotron Radiation", CERN 98-04 (1998)
- [28] M.R. Howells and M.M. Kincaid, "The properties of undulator radiation" in *New Directions in Research with Third-Generation Soft X-Ray Synchrotron Radiation Sources*, Kluwer Academic Publishers, 315-358 (1994)

## List of Figures

1	Single lens imaging system with an undulator source as object.	17
2	Illustration of the undulator geometry and of the observation plane after the undulator.	33
3	Comparison between $f(\zeta) = \text{sinc}(\zeta^2/4)$ (solid line), the real (dashed line) and the imaginary (dash-dotted line) parts of $f(\zeta) = \hat{z}_o S(0, \hat{z}_o, \zeta^2)$ at $\hat{z}_o = 1$ .	36
4	Comparison between $f(\zeta) = \text{sinc}(\zeta^2/4)$ (solid line), the real (dashed line) and the imaginary (dash-dotted line) parts of $f(\zeta) = \hat{z}_o S(0, \hat{z}_o, \zeta^2)$ at $\hat{z}_o = 2$ .	37
5	Comparison between $f(\zeta) = \text{sinc}(\zeta^2/4)$ (solid line), the real (dashed line) and the imaginary (dash-dotted line) parts of $f(\zeta) = \hat{z}_o S(0, \hat{z}_o, \zeta^2)$ at $\hat{z}_o = 5$ .	37
6	Comparison between $f(\zeta) = \text{sinc}(\zeta^2/4)$ (solid line), the real (dashed line) and the imaginary (dash-dotted line) parts of $f(\zeta) = \hat{z}_o S(0, \hat{z}_o, \zeta^2)$ at $\hat{z}_o = 10$ .	38
7	Universal function $\text{sinc}^2(\alpha^2/4)$ used to calculate (according to Eq. (91)) the focal intensity of a single electron at the fundamental harmonic at perfect resonance.	40
8	Universal function $\Psi(\alpha)$ used to calculate (according to Eq. (96)) the intensity distribution on the image plane from a single electron at the fundamental harmonic at perfect resonance.	40
9	Comparison between the relative intensity for a single electron at the image plane $\hat{I}_P$ , Eq. (109), the universal function $\Psi$ , Eq. (96), and the (Airy) diffraction pattern from a circular hole, Eq. (110), as a function of $m\hat{r}_i$ . Here $\hat{a}/\hat{z}_1 = 1$ .	45
10	Comparison between the relative intensity for a single electron at the image plane $\hat{I}_P$ , Eq. (109), the universal function $\Psi$ , Eq. (96), and the (Airy) diffraction pattern from a circular hole, Eq. (110), as a function of $m\hat{r}_i$ . Here $\hat{a}/\hat{z}_1 = 5$ .	46

- 11 Comparison between the relative intensity for a single electron at the image plane  $\hat{I}_P$ , Eq. (109), the universal function  $\Psi$ , Eq. (96), and the (Airy) diffraction pattern from a circular hole, Eq. (110), as a function of  $m\hat{r}_i$ . Here  $\hat{a}/\hat{z}_1 = 10$ . 47
- 12 Measurement of the cross-spectral density of an undulator source. (a) Young's double-pinhole interferometer demonstrating the coherence properties of undulator radiation. Radiation must be spectrally filtered by a monochromator or detector (not shown in figure). (b) In the quasi-homogeneous case the fringe visibility  $V$  of the resultant interference pattern is equal to the absolute value of the spectral degree of coherence:  $V = |g|$ . 53
- 13 The universal function  $\hat{I}_S$ , used to calculate the focal intensity of a quasi-homogeneous source at  $\hat{N}_x \gg 1$ ,  $\hat{D}_x \gg 1$  and  $\hat{N}_y \gg 1$ . 65
- 14 Absolute value of the universal function  $\gamma$ , used to calculate, on the image plane, the spectral degree of coherence of a quasi-homogeneous undulator source when  $\hat{N}_x \gg 1$ ,  $\hat{D}_x \gg 1$  and  $\hat{N}_y \gg 1$ . 67
- 15 The universal function  $\hat{\mathcal{B}}$ , used to calculate intensity on the image plane of a quasi-homogeneous undulator source when  $\hat{N}_x \gg 1$ ,  $\hat{D}_x \gg 1$  and  $\hat{D}_y \gg 1$ . 71
- 16 Absolute value of the universal function  $\beta$ , used to calculate coherence on the focal plane of a quasi-homogeneous undulator source when  $\hat{N}_x \gg 1$ ,  $\hat{D}_x \gg 1$  and  $\hat{D}_y \gg 1$ . 72
- 17 Illustration of a grating monochromator. 84
- 18 Image intensity for a quasi-homogeneous source,  $\hat{I}_P$ , as a function of  $\xi = \hat{a}m\hat{r}_i/\hat{z}_1$ , calculated with Eq. (233), for different values of the parameter  $p = \hat{a}\sqrt{\hat{N}}/\hat{z}_1$ . The plot illustrates the one-dimensional image formation problem (slit aperture, cylindrical lens). 89
- 19 Upper plots: profile of the pupil function  $P$  (slit aperture), together with  $\hat{\mathcal{P}}$ . Lower plots: autocorrelation function of the pupil,  $\tilde{P}$ , together with  $\mathcal{F}(\tilde{\mathcal{P}})$ . 90
- 20 The line spread  $l$  function in the presence of defocusing aberration. 101

21	The line spread $l$ function in the presence of coma aberration.	102
22	The line spread $l$ function in the presence of both spherical and defocusing aberrations.	102
23	The transfer function in the presence of defocusing aberration.	103
24	The transfer function in the presence of coma aberration.	104
25	The transfer function in the presence of both spherical and defocusing aberrations.	105
26	The transfer function in the presence of defocusing aberration ( $n = 2, b_2 = 9\pi$ ). Numerical techniques have been used to calculate the exact autocorrelation function that is compared to the analytical evaluation of the autocorrelation function in the severe aberration asymptote.	112
27	An enlarged version of Fig. 26. Numerical techniques have been used to calculate the exact autocorrelation function that is compared to the analytical evaluation of the autocorrelation function in the severe aberration asymptote.	113
28	The real part of the transfer function in the presence of coma aberration ( $n = 3, b_3 = 9\pi$ ). Numerical techniques have been use to calculate the exact autocorrelation function that is compared to the analytical evaluation of the autocorrelation function in the severe aberration asymptote.	114
29	An enlarged version of Fig. 28. Numerical techniques have been use to calculate the exact autocorrelation function that is compared to the analytical evaluation of the autocorrelation function in the severe aberration asymptote.	115
30	The imaginary part of the transfer function in the presence of coma aberration ( $n = 3, b_3 = 9\pi$ ). Numerical techniques have been use to calculate the exact autocorrelation function that is compared to the analytical evaluation of the autocorrelation function in the severe aberration asymptote.	116
31	An enlarged version of Fig. 30. Numerical techniques have been use to calculate the exact autocorrelation function that is compared to the analytical evaluation of the autocorrelation function in the severe aberration asymptote.	117

- 32 The line spread function versus the reduced coordinate on the image plane  $\bar{r}'' = \hat{a}\bar{r}_i/(\hat{d}_i n b_n)$  in the case of severe defocusing aberration ( $n = 2, b_2 = 9\pi$ ) and comparison with the geometrical optics prediction. 118
- 33 The line spread function versus the reduced coordinate on the image plane  $\bar{r}'' = \hat{a}\bar{r}_i/(\hat{d}_i n b_n)$  in the case of severe coma aberration ( $n = 3, b_3 = 9\pi$ ) and comparison with the geometrical optics prediction. 119
- 34 The line spread function versus the reduced coordinate on the image plane  $\bar{r}'' = \hat{a}\bar{r}_i/(\hat{d}_i n b_n)$  in the case of severe spherical aberration ( $n = 4, b_4 = 9\pi$ ) and comparison with the geometrical optics prediction. 120
- 35 Amount by which a geometrically traced ray departs from a desired location in the image formed by an optical system. The ordinate for each curve is the height at which the ray intersects the image plane. The abscissa is the coordinate of the ray at the pupil plane.  $n = 2$  represents defocusing,  $n = 3$  represents coma, and  $n = 4$  represents spherical aberration cases according to Eq. (287). 121
- 36 Geometry for a pinhole camera setup. S indicates the virtual source plane. 124
- 37 The line spread function  $l_{pc}$  with  $\Omega = 0.5$ . In this case the asymptote for  $\Omega \rightarrow 0$ , Eq. (311), is well-matched to the numerical evaluations. 129
- 38 The line spread function  $l_{pc}$  with  $\Omega = 2$ . In this case the asymptote for  $\Omega \rightarrow 0$ , Eq. (311), starts to diverge from numerical evaluations. The width of  $l_{pc}$  is close to its minimum. 130
- 39 The line spread function  $l_{pc}$  with  $\Omega = 10$ . An intermediate situation between the two limits for  $\Omega \rightarrow 0$  and  $\Omega \rightarrow \infty$ . 131
- 40 The line spread function  $l_{pc}$  with  $\Omega = 100$ . The asymptote in Eq. (312) starts to match the numerical calculations. In the limit  $\Omega \rightarrow \infty$  they both merge to a rectangular function. 132
- 41 Relative line spread function  $l_{pc}/l_{pc}(0)$  for different values of  $\Omega$ . 133

- 42 Plot of the universal function  $\hat{M}$ , used to calculate the cross-spectral density at the focal plane when  $\hat{N}_x \gg 1$ ,  $\hat{D}_x \gg 1$ ,  $\hat{N}_y$  and  $\hat{D}_y$  are arbitrary. 150
- 43 Plot of the universal function  $\hat{\mathcal{M}}$ , used to calculate the cross-spectral density at the image plane when  $\hat{N}_x \gg 1$ ,  $\hat{D}_x \gg 1$ ,  $\hat{N}_y$  and  $\hat{D}_y$  are arbitrary. 152
- 44 Plot of the universal function  $\hat{\chi}$ , used to calculate the modulus of the spectral degree of coherence on the focal plane when  $\hat{N}_x \gg 1$ ,  $\hat{D}_x \gg 1$ ,  $\hat{N}_y \ll 1$  and  $\hat{D}_y \ll 1$ . 154
- 45 Plot of the universal function  $\mathbb{X}$ , used to calculate the modulus of the spectral degree of coherence on the image plane when  $\hat{N}_x \gg 1$ ,  $\hat{D}_x \gg 1$ ,  $\hat{N}_y \ll 1$  and  $\hat{D}_y \ll 1$ . 156